



The
University
Of
Sheffield.

**Tissue engineering approaches to the
treatment of bisphosphonate-related
osteonecrosis of the jaw**

George Bullock

A thesis submitted in partial fulfilment of the requirements for the
degree of Doctor of Philosophy

**The University of Sheffield
Faculty of Engineering
Department of Materials Science and Engineering**

March 2019

Abstract

Bisphosphonate-related osteonecrosis of the jaw (BRONJ) is a disease defined by necrotic jaw bone that has become exposed through the surrounding soft tissue, which affects patients with osteoporosis and bone metastases taking the anti-resorptive bisphosphonate (BP) drugs. Currently this disease is without a specific treatment, in part due to its complex, and not fully understood, pathophysiology.

This research used tissue engineering principles to further investigate the effects of BPs on the soft tissue, both in two and three dimensions, and investigated a potential preventative treatment for the disease *in vitro*. The BPs investigated were pamidronic acid (PA) and zoledronic acid (ZA), two BPs most commonly associated with BRONJ.

We explored the effects of PA and ZA on human oral fibroblasts and keratinocytes at clinically relevant concentrations in 2D. Both PA and ZA caused significant reductions to metabolic activity, and further study indicated an increase in apoptosis in fibroblasts, and apoptosis and necrosis in keratinocytes. PA and ZA led to a significant reduction in proliferation, and ZA reduced the adhesion of keratinocytes. However, BPs did not affect cellular migration.

A 3D oral mucosa model was used to investigate PA and ZA. PA prevented the stratification of newly formed epithelia and reduced the thickness of healthy epithelia. ZA showed the same effects, but at higher concentrations was also toxic. We began the development of a 3D wound healing assay which could be used as an *in vitro* model of BRONJ, and indicated that BPs also inhibit oral mucosa wound healing.

Finally, we examined the ability of hydroxyapatite (HA) to bind BPs. The abilities of a variety of spectroscopic methods to detect BP binding were tested. Biological assays were also performed to examine the ability of HA to prevent BP toxicity. We have successfully demonstrated that HA could be used to reduce PA and ZA toxicity *in vitro*. This indicates a potential mechanism by which BRONJ development could be prevented.

Acknowledgements

I would like to begin this thesis by extending my gratitude and appreciation to my supervisors. Their patience, guidance, support and belief have allowed for me to become the scientist I am today, and I feel privileged to have worked with them. Firstly, thank you to Dr. Vanessa Hearnden, who was always there with ideas, encouragement and understanding. Thanks also go to Dr. Cheryl Miller, who instilled in me the high standards which I now pride myself on. I would also like to thank Mr. Alasdair McKechnie, whose clinical insight was invaluable for this project. And finally, to Dr. Robert Moorehead, for ably stepping up during Cheryl's maternity leave and for his assistance in the DTU and with the FormLabs printer.

This project would not have been possible without funding, and therefore thanks go to the EPSRC for allowing me the opportunity to complete this research. Thanks also go to the Armourers and Brasiers' Company and the University of Sheffield Learned Society for funding me to attend conferences, share my research and gain new ideas. I would also like to thank Ceramisys Limited for the generous gift of hydroxyapatite granules.

I could not have completed this work alone, and I would therefore like to thank those that assisted me throughout this project. Thanks go to Vanessa Singleton, who was always there to take requests and listen to me moan about lab matters, and to Robert Dickinson, whose help made working at Kroto easy. Special thanks go to Sue and Kay from the Flow Cytometry facility for training me, Dr. Toby Holmes for help with the cauteriser, Dr. Joss Atkinson for XRD assistance, Dr. Chris Holland and Dr. Pete Laity for UV-vis and FTIR use and expertise, Dr. Marcela Garcia-Martinez for Raman help, and finally to Dr. Sam Pashneh-Tala and Jonathan Field for assistance in the designing and printing of the cell culture ring.

I would like to acknowledge all the other colleagues I had in both Materials Science and the Dental School for their knowledge and camaraderie, especially on the days where nothing seemed to be going right. In particular, thanks go to Hossein Bahmaee, Mehri Behbehani, Alex Bolger, Liam Boyle, Sarina Chand, Kat Murray, and Rob Owen. And to my friends away from work who helped keep me sane throughout this work, particularly Ed, Ethan, Joey, Lizzie and Matt.

And, finally, I would like to thank my family for all their support. Thank you to my father, Jason, to Mathew and Deryn, to Louis and Georgia, and to Amelia and Oscar, who were always there to brighten my mood when I needed it most. I would especially like to thank my mother, Lisa, and dedicate this work to her, as without her constant support, pride and encouragement, I would not be where I am today.

Outputs

Publications in preparation

“Hydroxyapatite inhibits bisphosphonate toxicity to the oral mucosa in vitro” G Bullock, CA Miller, A McKechnie, V Hearnden

Oral presentations

“Hydroxyapatite granules prevent bisphosphonate toxicity to oral fibroblasts and keratinocytes in 2D and 3D in vitro” G Bullock, CA Miller, A McKechnie, V Hearnden. BiTEG 2018. Sheffield, UK.

“Bisphosphonates prevent the formation and re-epithelialisation of the oral mucosa in vitro in 3D” G Bullock, CA Miller, A McKechnie, V Hearnden. TCES 2018. Keele, UK.

“The development of a 3D in vitro model of bisphosphonate-related osteonecrosis of the jaw” G Bullock, CA Miller, A McKechnie, V Hearnden. BiTEG 2017. Leeds, UK. (*Flash presentation and poster*)

Poster presentations

“Tissue engineering a model of bisphosphonate-related osteonecrosis of the jaw” G Bullock, CA Miller, A McKechnie, V Hearnden. ESB 2018. Maastricht, Netherlands.

“The development of a 3D in vitro model of bisphosphonate-related osteonecrosis of the jaw” G Bullock, CA Miller, A McKechnie, V Hearnden. BiTEG 2017. Leeds, UK.

“The effect of bisphosphonates on the viability and migration of oral keratinocytes and fibroblasts” G Bullock, CA Miller, RD Moorehead, A McKechnie, V Hearnden. TCES 2017. Manchester, UK.

Table of contents

Abstract.....	i
Acknowledgements	iii
Outputs	v
List of abbreviations	xii
List of figures.....	xv
List of tables.....	xxii
List of equations	xxii
1. Introduction.....	1
2. Literature review	3
2.1 Bone.....	3
2.2 Diseases associated with high bone resorption	4
2.2.1 Osteoporosis.....	4
2.2.2 Osteogenesis imperfecta.....	4
2.2.3 Paget's disease of bone.....	5
2.2.4 Bone metastases	5
2.3 Bisphosphonates	7
2.3.1 Chemical structure and mechanism of action	9
2.3.2 Effects of treatment.....	12
2.4 Oral mucosa	15
2.4.1 Oral wound healing	17
2.5 Bisphosphonate-related osteonecrosis of the jaw (BRONJ).....	20
2.6 Pathophysiology of BRONJ	23
2.7 BRONJ treatment	25
2.8 Current position of BRONJ research.....	26
2.8.1 2D effects of BPs	26
2.8.2 3D effects of BPs	36
2.8.3 Models of BRONJ	41
2.8.4 Novel BRONJ treatments	42
2.9 Bone filler materials – a potential BRONJ treatment method?	46

2.9.1	Common bone filler materials	46
2.10	Detection and quantification methods	51
3.	Aims and objectives	55
4.	Materials and methods	57
4.1	Cell culture	57
4.1.1	Cell sources and media	57
4.1.2	Cell maintenance	58
4.1.3	Primary cell isolation	59
4.1.4	Preparation of de-cellularised dermis (DED)	59
4.2	Bisphosphonates	60
4.3	Statistics	60
5.	The effects of bisphosphonates on human oral fibroblasts and keratinocytes in 2D 61	
5.1	Aim	61
5.2	Introduction	61
5.3	Materials and methods	62
5.3.1	MTT assay	62
5.3.2	Apoptosis and necrosis assay	63
5.3.3	Mitomycin C optimisation	63
5.3.4	Proliferation assay	64
5.3.5	Migration assay	65
5.3.6	Adhesion assay	68
5.3.7	120 hour cell viability	69
5.3.8	Cytoskeleton staining	69
5.3.9	Statistics	70
5.4	Results	72
5.4.1	Pamidronic acid and zoledronic acid were toxic to human oral fibroblasts and keratinocytes over 72 hours	72
5.4.2	Pamidronic acid and zoledronic acid led to apoptosis in oral mucosa cells 79	

5.4.3	Mitomycin C prevented proliferation of fibroblasts and immortalised keratinocytes	81
5.4.4	Pamidronic acid and zoledronic acid prevented fibroblast and immortalised keratinocyte proliferation.....	83
5.4.5	Sub-toxic concentrations of pamidronic acid and zoledronic acid did not affect the migration rate of oral mucosa cells.....	85
5.4.6	Pre-treating fibroblasts with pamidronic acid prevented exclusion zone closure through toxicity	97
5.4.7	Zoledronic acid caused a small reduction in immortalised keratinocyte adhesion.....	100
5.4.8	Zoledronic acid did not affect expression of keratinocyte cytoskeleton proteins	102
5.5	Discussion	107
5.6	Summary	117
6.	The development of an <i>in vitro</i> model of the soft tissue component of BRONJ	119
6.1	Aim	119
6.2	Introduction.....	119
6.3	Materials and methods	120
6.3.1	Seeding of 3D oral mucosa model	120
6.3.2	DED model epithelium stratification test.....	120
6.3.3	Resazurin assay	121
6.3.4	Oral mucosa models with bisphosphonates	121
6.3.5	Wounding of oral mucosa models	122
6.3.6	3D printed ring design and manufacture.....	122
6.3.7	3D wound healing assay	123
6.3.8	Histology	124
6.3.9	Statistics	126
6.4	Results	127
6.4.1	DED models with immortalised keratinocytes were cultured to approximate native tissue	127
6.4.2	Bisphosphonates prevented a stratified epithelium from forming.....	129

6.4.3	Bisphosphonates reduced the thickness of healthy, established epithelia	132
6.4.4	Models wounded with biopsy punch showed capacity to regenerate; models wounded with cauteriser and soldering iron did not	138
6.4.5	Seeding with bespoke 3D printed cell culture rings created a 3D wound healing assay	143
6.4.6	Seeding models at air-liquid interface is not reproducible	150
6.4.7	Pamidronic acid prevents re-epithelisation of the oral mucosa wound model	151
6.4.8	Seeding models with an <i>in situ</i> ALI provides a more reproducible wound model	154
6.4.9	Pamidronic acid and zoledronic acid prevented full healing of <i>in situ</i> wound model	156
6.5	Discussion.....	160
6.6	Summary.....	167
7.	Hydroxyapatite granules prevent bisphosphonate toxicity <i>in vitro</i>	169
7.1	Aim.....	169
7.2	Introduction	169
7.3	Materials and methods	170
7.3.1	Preparation of HA	170
7.3.2	Sintering of HA discs.....	170
7.3.3	HA granules.....	170
7.3.4	X-ray diffraction (XRD).....	170
7.3.5	Brunauer–Emmett–Teller (BET) surface area	170
7.3.6	Ultraviolet-visible (UV-vis) spectroscopy	171
7.3.7	Calibration curves	171
7.3.8	Hydroxyapatite binding and release of zoledronic acid.....	171
7.3.9	Fourier-transform infra red spectroscopy - attenuated total reflectance (FTIR-ATR)	172
7.3.10	Raman spectroscopy	172
7.3.11	Biological binding assays.....	172
7.3.12	Statistics	173

7.4	Results	174
7.4.1	Hydroxyapatite retains phase purity when sintered at 1200 °C.....	174
7.4.2	Hydroxyapatite granules have a larger surface area than sintered discs	175
7.4.3	Zoledronic acid concentration was quantified using ultraviolet-visible spectroscopy	176
7.4.4	Unsintered hydroxyapatite effected bisphosphonate signal	177
7.4.5	Sintered hydroxyapatite discs exhibited a potential zoledronic acid binding behaviour	178
7.4.6	Sintered hydroxyapatite may have released previously bound zoledronic acid	179
7.4.7	Sintered hydroxyapatite interfered with the ultraviolet-visible spectroscopy signal at 210 nm	180
7.4.8	FTIR-ATR cannot be used to detect zoledronic acid bound to sintered hydroxyapatite discs	181
7.4.9	Raman spectroscopy indicated some surface binding of zoledronic acid to sintered hydroxyapatite discs, though not quantitatively	182
7.4.10	Hydroxyapatite granules prevented bisphosphonate metabolic activity effects in 2D	184
7.4.11	Hydroxyapatite granules prevented zoledronic acid toxicity to oral mucosa models	188
7.4.12	BP binding was affected by HA surface area.....	192
7.5	Discussion	193
7.6	Summary	197
8.	Conclusions.....	199
9.	Future work	201
10.	Appendices.....	205
10.1	Appendix 1 - Cell seeding densities	205
10.2	Appendix 2 – Migration assay after cell tracing	207
10.3	Appendix 3 – Removal of outliers	208
10.4	Appendix 4 – BET isotherms	209
11.	References	211

List of abbreviations

2D	Two dimensions
3D	Three dimensions
°C	degrees Celsius
μ	micro
AAOMS	American Association of Oral and Maxillofacial Surgeons
ALI	Air-liquid interface
ANOVA	Analysis of variance
ARONJ	Anti-resorptive agent-related osteonecrosis of the jaw
β-TCP	Beta tricalcium phosphate
BET	Brunauer–Emmett–Teller
BP	Bisphosphonate
BRONJ	Bisphosphonate-related osteonecrosis of the jaw
BSA	Bovine serum albumin
DAPI	4',6-diamidino-2-phenylindole
DBBM	Demineralised bovine bone matrix
DED	De-epidermised dermis
DMEM	Dulbecco's modified Eagle medium
DMSO	Dimethyl sulfoxide
DPX	p-Xylene-bis(N-pyridinium bromide)
ECM	Extracellular matrix
EDTA	Ethylenediaminetetraacetic acid
FAK	Focal adhesion kinase
FCS	Foetal calf serum
FDA	Federal Drug Administration
FITC	Fluorescein isothiocyanate
FPP	Farnesyl pyrophosphate
FTIR	Fourier transform infrared spectroscopy
FTIR-ATR	Fourier transform infrared spectroscopy – attenuated total reflectance
GGOH	Geranyl-geraniol
GGPP	Geranylgeranyl pyrophosphate
h	hour
H&E	Haematoxylin and eosin
HA	Hydroxyapatite
HAM	Human amniotic membrane
HCl	Hydrochloric acid
HGF	Human gingival fibroblast

HPLC	High-performance liquid chromatography
i3t3	Irradiated murine fibroblast
I _{plf}	Proliferation index
IC ₅₀	Half maximal inhibitory concentration
IMS	Industrial methylated spirit
IV	Intravenous
JCPDS	Joint Committee on Powder Diffraction Standards
KSFM	Keratinocyte serum free medium
l	litre
LLLT	Low level laser therapy
m	metre
m	milli
M	molar
MMP	Matrix metalloproteinases
MRONJ	Medication-related osteonecrosis of the jaw
MTS	3-(4,5-dimethylthiazol-2-yl)-5-(3-carboxymethoxyphenyl)-2-(4-sulfophenyl)-2H-tetrazolium
MTT	3-(4,5-dimethylthiazol-2-yl)-2,5-diphenyltetrazolium bromide
n	nano
nBP	Nitrogen-containing bisphosphonate
nHA	nanohydroxyapatite
NOK	Normal oral keratinocyte
OI	Osteogenesis Imperfecta
OKF6	Immortalised human oral keratinocyte
ONJ	Osteonecrosis of the jaw
ORN	Osteoradionecrosis
PA	Pamidronic acid
PBS	Phosphate buffered saline
PDF	Powder diffraction files
PDB	Paget's Disease of Bone
PI	Propidium iodide
PPi	Inorganic pyrophosphate
R ₁	First functional group
R ₂	Second functional group
RANKL	Receptor activator of nuclear factor kappa-B ligand
TRITC	Tetramethylrhodamine isothiocyanate
SD	Standard deviation
TCP	Tricalcium phosphate
TGFβ	Transforming growth factor beta

US	United States of America
UV	Ultraviolet
UV-vis	Ultraviolet-visible
VEGF	Vascular endothelial growth factor
XPS	X-ray photoelectron spectroscopy
XRD	X-ray diffraction
ZA	Zoledronic acid

List of figures

Figure 2.1. Diagram of an osteoclast resorbing bone.	4
Figure 2.2. The feedback loop osteolytic tumours and bone.....	6
Figure 2.3. The generic bisphosphonate structure.....	9
Figure 2.4. BP interaction with bone.....	10
Figure 2.5. The mevalonate pathway.	11
Figure 2.6. Proposed anti-tumour effects of bisphosphonates in bone.	14
Figure 2.7. A simplified cross sectional diagram of the oral mucosa.....	16
Figure 2.8. Haematoxylin and eosin stained section of healthy oral mucosa..	16
Figure 2.9. Haematoxylin and eosin stained section of healthy gingiva.	17
Figure 2.10. Diagram representing the healing of an extraction socket.	19
Figure 2.11. Exposed necrotic bone in a zoledronic acid patient.	22
Figure 2.12. One hypothesis for the sequence of BRONJ development following tooth extraction.	24
Figure 2.13. Wound healing of primary human oral fibroblasts treated with 30 μ M zoledronic acid.	33
Figure 2.14 Effect of zoledronic acid on integrin-mediated cell-substratum adhesions of oral fibroblasts.....	35
Figure 2.15. An example of a 3D oral mucosa model.....	37
Figure 2.16. H&E stained sections of a collagen based oral mucosa model with bone component.	38
Figure 5.1. Oris™ migration stoppers, and being placed into a 96 well plate.....	65
Figure 5.2. Cross sectional diagram of the migration assay setup.....	66
Figure 5.3. Human oral fibroblasts seeded in control medium using the Oris™ migration stoppers, imaged over 72 hours.	67
Figure 5.4. A flow diagram of the method for the crystal violet adhesion assay.	69
Figure 5.5. Human oral fibroblast metabolic activity over 72 hours in the presence of pamidronic acid.	72
Figure 5.6. Immortalised human oral keratinocyte (OKF6) metabolic activity over 72 hours in the presence of pamidronic acid.	73
Figure 5.7. Primary human oral keratinocyte metabolic activity over 72 hours in the presence of pamidronic acid.....	74
Figure 5.8. Human oral fibroblast metabolic activity over 72 hours in the presence of zoledronic acid.	75
Figure 5.9. Immortalised human oral keratinocyte (OKF6) metabolic activity over 72 hours in the presence of zoledronic acid.	76

Figure 5.10. Primary human oral keratinocyte metabolic activity over 72 hours in the presence of zoledronic acid.....	77
Figure 5.11. IC ₅₀ graphs for fibroblasts, immortalised and primary keratinocytes when treated with either pamidronic acid or zoledronic acid for 72 hours.	78
Figure 5.12. Proportion of human oral fibroblasts viable, early apoptotic, late apoptotic or necrotic after 72 hours treatment with pamidronic acid or zoledronic acid.	80
Figure 5.13. Proportion of human oral immortalised keratinocytes viable, early apoptotic, late apoptotic or necrotic after 72 hours treatment with pamidronic acid or zoledronic acid..	80
Figure 5.14. Human oral fibroblast cell number over 96 hours in the presence of Mitomycin C.....	82
Figure 5.15. Immortalised human oral keratinocyte (OKF6) cell number over 72 hours in the presence of Mitomycin C.....	82
Figure 5.16. Human oral fibroblast proliferation over 72 hours in the presence of pamidronic acid or zoledronic acid.	84
Figure 5.17. Immortalised human oral keratinocyte (OKF6) proliferation over 72 hours in the presence of pamidronic acid or zoledronic acid.....	84
Figure 5.18. Human oral fibroblast migration over 48 hours in the presence of pamidronic acid.....	86
Figure 5.19. Human oral fibroblast migration over 72 hours in the presence of pamidronic acid.....	87
Figure 5.20. Human oral fibroblast migration over 48 hours in the presence of zoledronic acid.....	89
Figure 5.21. Human oral fibroblast migration over 72 hours in the presence of zoledronic acid.....	90
Figure 5.22. Immortalised human oral keratinocyte (OKF6) migration over 16 hours in the presence of pamidronic acid.	92
Figure 5.23. Immortalised human oral keratinocyte (OKF6) migration over 24 hours in the presence of pamidronic acid..	93
Figure 5.24. Immortalised human oral keratinocyte (OKF6) migration over 16 hours in the presence of zoledronic acid.....	95
Figure 5.25. Immortalised human oral keratinocyte (OKF6) migration over 24 hours in the presence of zoledronic acid.....	96
Figure 5.26. Human oral fibroblast migration over 48 hours in the presence of pamidronic acid, following 72 hours pre-treatment.	98
Figure 5.27. Human oral fibroblasts after 72 hours in the presence of 30 µM pamidronic acid, following 72 hours pre-treatment..	99

Figure 5.28. Human oral fibroblast migration over 72 hours in the presence of pamidronic acid, following 72 hours pre-treatment.....	99
Figure 5.29. Adhesion of immortalised keratinocytes (OKF6) over time measured by crystal violet assay.....	101
Figure 5.30. Adhesion assay results for immortalised keratinocytes (OKF6) treated with zoledronic acid for 24 hours then fixed (control) or detached, re-seeded and allowed to adhere for 2 hours (detached), measured by crystal violet assay.....	101
Figure 5.31. Immortalised human oral keratinocytes (OKF6) after treatment with zoledronic acid for 24 hours, stained for F-actin and vinculin.....	103
Figure 5.32. Immortalised human oral keratinocytes (OKF6) after treatment with zoledronic acid for 48 hours, stained for F-actin and vinculin (green).	104
Figure 5.33. Immortalised human oral keratinocyte (OKF6) cell number after treating with zoledronic acid for 120 hours..	105
Figure 5.34. Immortalised human oral keratinocytes (OKF6) after treatment with zoledronic acid for 120 hours, stained for F-actin, vinculin and nuclei.....	106
Figure 6.1. The general seeding process for oral mucosa models.....	120
Figure 6.2. A flow diagram to show the different treating regimens for oral mucosa models treated with bisphosphonates.....	121
Figure 6.3. The computer-aided design model of a bespoke cell culture ring	123
Figure 6.4. Cross sectional diagram of the process for seeding models at air-liquid interface (ALI) or with an in situ ALI.....	124
Figure 6.5. A diagrammatical representation of sample preparation for histology	125
Figure 6.6. H&E stained sections of oral mucosa models seeded with human oral fibroblasts and immortalised human oral keratinocytes cultured at ALI then fixed after 4 days, 7 days, 10 days or 14 days.	128
Figure 6.7. Metabolic activity of immortalised keratinocyte oral mucosa models when treated with 50, 75 and 100 μ M pamidronic acid and 1, 10 and 30 μ M zoledronic acid immediately after placing at ALI	130
Figure 6.8. H&E stained sections of oral mucosa models seeded with human oral fibroblasts and immortalised human oral keratinocytes cultured at ALI in (A) control medium, (B) 50 μ M, (C) 75 μ M and (D) 100 μ M pamidronic acid, (E) 1 μ M, (F) 10 μ M and (G) 30 μ M zoledronic acid, respectively, for 10 days.	131
Figure 6.9. Metabolic activity of immortalised keratinocyte oral mucosa models when cultured at ALI for 7 days in control medium, then treated with 50, 75 and 100 μ M pamidronic acid and 1, 10 and 30 μ M zoledronic acid for 7 days.....	133
Figure 6.10. H&E stained sections of oral mucosa models seeded with human oral fibroblasts and immortalised human oral keratinocytes cultured at ALI or 7 days in control medium, then treated with (A) control medium, (B) 50 μ M, (C) 75 μ M and (D) 50 μ M	

pamidronic acid, (E) 1 μ M, (F) 10 μ M and (G) 30 μ M zoledronic acid, respectively, for 7 days.....	134
Figure 6.11. Metabolic activity of primary keratinocyte oral mucosa models when cultured at ALI for 7 days in control medium, then treated with 50, 75 and 100 μ M pamidronic acid and 1, 10 and 30 μ M zoledronic acid for 7 days.....	136
Figure 6.12. H&E stained sections of oral mucosa models seeded with human oral fibroblasts and primary human oral keratinocytes culutred at ALI for 7 days in control medium, then treated with (A) control medium, (B) 50 μ M, (C) 75 μ M and (D) 50 μ M pamidronic acid, (E) 1 μ M, (F) 10 μ M and (G) 30 μ M zoledronic acid, respectively, for 7 days.....	137
Figure 6.13. Oral mucosa models immediately after wounding.....	139
Figure 6.14. Metabolic activity of immortalised keratinocyte DED models wounded after 10 days culture by three different methods – damaged with a biopsy punch, burned with a cauteriser or burned with a soldering iron – or unwounded.....	139
Figure 6.15. H&E stained sections of oral mucosa models seeded with human oral fibroblasts and immortalised human oral keratinocytes cultured at ALI for 10 days. Samples were then (A, B) unwounded, (C, D) damaged with a biopsy punch, (E, F) burned with a soldering iron or (G, H) burned with a cauteriser.....	140
Figure 6.16. H&E stained sections of oral mucosa models seeded with human oral fibroblasts and immortalised human oral keratinocytes, cultured for (A) 10 days, then wounded with a biopsy punch and fixed immediately or (B) cultured for 7 days, wounded with a biopsy punch then cultured for a further 10 days.....	142
Figure 6.17. Selectively seeded oral mucosa models, cultured for 7 days in control medium, pamidronic acid and zoledronic acid.....	144
Figure 6.18. Metabolic activity of selectively seeded immortalised keratinocyte DED models cultured for 7 days in pamidronic acid and zoledronic acid.....	145
Figure 6.19. H&E stained sections of oral mucosa model selectively seeded with human oral fibroblasts and immortalised human oral keratinocytes, then placed at ALI in control medium for 1 day.....	145
Figure 6.20. H&E stained sections of oral mucosa models selectively seeded with human oral fibroblasts and immortalised human oral keratinocytes, then placed at ALI in (A) control medium, (B) 50 μ M pamidronic acid, (C) 100 μ M pamidronic acid and (D) 10 μ M zoledronic acid for 7 days.....	146
Figure 6.21. Selectively seeded oral mucosa models, placed at ALI with the culture ring for 0, 4 or 7 days.....	148
Figure 6.22. Selectively seeded oral mucosa models, cultured at ALI for 7 days before the culture ring was removed, then cultured for 1, 4 or 7 days.....	148

Figure 6.23. H&E stained sections of oral mucosa models selectively seeded with human oral fibroblasts and immortalised human oral keratinocytes, then placed at ALI with a 3D printed cell culture ring preventing migration for (A) 4 days and fixed immediately, or for 7 days and fixed (B) immediately, (C) after 1 day, (D) after 4 days or (E) after 7 days further culture	149
Figure 6.24. Oral mucosa models selectively seeded at ALI with human oral fibroblasts and immortalised human oral keratinocytes	150
Figure 6.25. Oral mucosa models selectively seeded at ALI with human oral fibroblasts and immortalised human oral keratinocytes, then cultured for 7 days before removing the cell culture ring, and culturing for 7 days in 50 μ M pamidronic acid or control medium	152
Figure 6.26. H&E stained sections of oral mucosa models selectively seeded at ALI with human oral fibroblasts and immortalised human oral keratinocytes, then treated at ALI with (A, B) 50 μ M pamidronic acid or (C) control medium for 7 days.....	153
Figure 6.27. Oral mucosa models selectively seeded with human oral fibroblasts and immortalised human oral keratinocytes, before creating an in situ ALI and culturing for a further 7 days.	154
Figure 6.28. H&E stained sections of an oral mucosa model selectively seeded with human oral fibroblasts and immortalised human oral keratinocytes, before creating an in situ ALI and culturing for 7 days	155
Figure 6.29. Selectively seeded oral mucosa models, cultured with an in situ ALI for 7 days, before culturing for 7 days in control medium, pamidronic acid or zoledronic acid.....	157
Figure 6.30. Metabolic activity of selectively seeded immortalised keratinocyte DED models using in situ ALI, cultured for 7 days in pamidronic acid and zoledronic acid...	158
Figure 6.31. H&E stained sections of oral mucosa models selectively seeded with human oral fibroblasts and immortalised human oral keratinocytes, before creating an in situ ALI and culturing for 7 days, then placed at ALI in (A) control medium, (B) 50 μ M pamidronic acid, (C) 100 μ M pamidronic acid, (D) 1 μ M zoledronic acid and (E) 10 μ M zoledronic acid for 7 days.	159
Figure 7.1. X-ray diffraction patterns for hydroxyapatite discs pressed and sintered at 1200 $^{\circ}$ C, and standard reference cards of β -tricalcium phosphate and hydroxyapatite.	174
Figure 7.2. BET surface area measurements for hydroxyapatite granules and sintered discs.....	175
Figure 7.3. Ultraviolet-visible spectroscopy calibration curves for aqueous zoledronic acid and pamidronic acid at 210 nm, from 0 to 250 μ M.....	176
Figure 7.4. Ultraviolet-visible spectroscopy readings for water containing a hydroxyapatite disc, 200 μ M zoledronic acid containing a hydroxyapatite disc, and 200 μ M zoledronic acid alone, incubated at 37 $^{\circ}$ C for 1 day	177

Figure 7.5. Ultraviolet-visible spectroscopy readings for water containing a sintered hydroxyapatite disc, 200 μ M zoledronic acid containing a hydroxyapatite disc, and 200 μ M zoledronic acid alone, incubated at 37 $^{\circ}$ C for 14 days.....	178
Figure 7.6. Ultraviolet-visible spectroscopy readings for water containing a sintered hydroxyapatite disc incubated at 37 $^{\circ}$ C for 10 days. Discs had previously been incubated for 14 days in either water or 200 μ M zoledronic acid.....	179
Figure 7.7. Ultraviolet-visible spectroscopy readings for water containing a sintered hydroxyapatite disc incubated at 37 $^{\circ}$ C for 6 days. Discs had previously been incubated for 14 days in either water or 200 μ M zoledronic acid.	180
Figure 7.8. FTIR-ATR spectra for sintered hydroxyapatite discs after three different treatments: 14 days incubation in water, 14 days incubation in 200 μ M zoledronic acid, and 14 days incubation in 200 μ M zoledronic acid followed by 10 days incubation in water. An untreated disc was also measured.....	181
Figure 7.9. Raman spectra for sintered hydroxyapatite discs: untreated as a control, incubated in 200 μ M zoledronic acid for 14 days, or incubated in 200 μ M zoledronic acid for 14 days and then incubated into water for a further 10 days	182
Figure 7.10. Raman spectra for sintered hydroxyapatite discs incubated in 100, 200 or 300 μ M zoledronic acid for 14 days.....	183
Figure 7.11. Human oral fibroblast metabolic activity over 72 hours in the presence of pamidronic acid and zoledronic acid, incubated prior for 72 hours with hydroxyapatite in sintered disc or granule form.....	185
Figure 7.12. Immortalised human oral keratinocyte metabolic activity over 72 hours in the presence of pamidronic acid and zoledronic acid, incubated prior for 72 hours with hydroxyapatite in sintered disc or granule form.....	187
Figure 7.13. Metabolic activity of immortalised keratinocyte oral mucosa models when treated with control medium or 30 μ M zoledronic acid, in the presence of a sintered hydroxyapatite disc or granules, after first culturing at ALI in control medium for 7 days. Models cultured with no HA present as controls.....	189
Figure 7.14. H&E stained sections of oral mucosa models seeded with human oral fibroblasts and primary human oral keratinocytes cultured at ALI for 7 days in control medium, then treated with (A) control medium, (B) control medium and a sintered HA disc, (C) control medium and HA granules, (D) 30 μ M zoledronic acid, (E) 30 μ M zoledronic acid and a sintered HA disc, (F) 30 μ M zoledronic acid and HA granules, respectively, for 7 days, with a full media changing occurring at day 3 and day 10..	191
Figure 7.15. Human oral fibroblast metabolic activity after 72 hours in the presence of 100 μ M pamidronic acid previously incubated for 72 hours with hydroxyapatite granules.	192

Figure 10.1. Human oral fibroblast confluence over 72 hours at different seeding densities.	205
Figure 10.2. Immortalised human oral keratinocyte confluence over 72 hours at different seeding densities.	206
Figure 10.3. Human oral fibroblast migration over 72 hours in the presence of pamidronic acid	207
Figure 10.4. MTT data for human oral fibroblasts treated with pamidronic acid for 72 hours. Grubbs' test for outliers was performed to indicate outliers.....	208
Figure 10.5. Brunauer-Emmett-Teller surface area plots for hydroxyapatite granules, granules and discs.	209

List of tables

Table 2.1. Commonly prescribed bisphosphonates and their primary treatment, delivery method, anti-resorptive potency and functional group	8
Table 2.2. Stage definitions of BRONJ.....	22
Table 2.3. Current treatment methods for BRONJ.....	25
Table 2.4. A summary of the current literature investigating the 2D effects of pamidronic acid (PA) and zoledronic acid (ZA) on fibroblasts.....	27
Table 2.5. A summary of the current literature investigating the 2D effects of pamidronic acid (PA) and zoledronic acid (ZA) on keratinocytes.....	28
Table 2.6. Evaluation of a variety of approved calcium phosphate bone filler materials for use in socket healing.....	48
Table 2.7. Bisphosphonate concentration detection methods.....	53
Table 4.1. Dulbecco's modified Eagle's medium composition	57
Table 4.2. Keratinocyte serum free medium composition.....	58
Table 4.3. Green's medium composition.....	58
Table 5.1. Seeding densities and incubation times for the MTT assay	62
Table 6.1. The tissue processing schedule	125
Table 6.2. The process for histological staining with haematoxylin and eosin.....	126

List of equations

Equation 5.1. An equation to convert median fluorescence intensity to proliferation index.....	65
Equation 10.1. Grubbs' test for outliers.....	208

1. Introduction

Bisphosphonate-related osteonecrosis of the jaw (BRONJ) is a disease defined by necrotic jaw bone that has become exposed through the surrounding soft tissue [1]. As the name suggests, it is suffered by patients receiving bisphosphonate (BP) treatment. BPs are a group of anti-resorptive drugs and are therefore used to treat diseases that present with increased bone resorption. They are primarily used to treat osteoporosis and bone metastases, and are currently the most commonly prescribed anti-resorptive worldwide [1], [2]. BRONJ typically develops following wounding to the jaw, and in the majority of cases follows a tooth extraction [1]. It affects between 1 in 10 and 100 patients prescribed BPs for bone metastases, and 1 in 10,000 and 100,000 of those being treated for osteoporosis [3]–[5].

BPs affect both the bone and surrounding oral mucosa to contribute to the development of the disease. Four main pathways are thought to be involved: osteoclast inhibition, angiogenesis inhibition, soft tissue toxicity, and infection and inflammation. Soft tissue toxicity is the primary clinical feature of BRONJ, and closure of the BRONJ wound has been hypothesised as the key to the treatment of the disease [2]. This complex pathophysiology makes treatment of BRONJ difficult, and, as such, there is currently no definitive treatment for the disease, with treatment based around conservative management [1]. This work in this thesis aimed to use tissue engineering approaches to study the soft tissue component of BRONJ; investigating both the development of the disease and potential solutions.

This thesis reports on a wide variety of BP effects on the oral mucosa in both two and three dimensions. Further understanding of how BPs affect the oral mucosa and lead to the exposure of necrotic bone is an important step in the treatment of the disease. The work in this thesis also examined whether calcium phosphate-containing bone filler materials can be used to locally reduce BP effects, as BPs have a well-documented binding affinity for calcium. These materials are already in use as post-extraction medical devices, and therefore present an attractive method by which to treat the disease.

2. Literature review

This chapter reviews the current literature regarding BRONJ, including introductions to the bone diseases which require BP treatment, an explanation of BP effects and side-effects, and a summary of what is known about BRONJ pathophysiology, incidence and treatment. The field of research regarding BPs and their effects in the development of BRONJ is then summarised. Calcium containing bone filler materials and their BP binding properties are reviewed, before a final summary of methods to detect BPs, with the aim of justifying the research presented in this thesis.

2.1 Bone

Bone is a dynamic organ, constantly remodelling and repairing in response to mechanical stimuli and structural damage [6], [7]. Remodelling mainly involves two cell types – osteoblasts and osteoclasts - which are responsible for formation and resorption, respectively [7]. These processes are usually balanced, and this balance is important for the shape, size and integrity of the bone [8].

Osteoblasts are involved in the formation of bone matrix and contribute to the mineralization of bone. They differentiate from osteogenic progenitor cells, and their number increases in response to stress or fracture, making them key to wound healing [9].

Osteoclasts are polykaryonic macrophages formed through the fusion of stem cells [6], [9] and are the principal cells in bone resorption [10]. They are formed following the stimulation of precursor monocyte/macrophage cells by receptor activator of nuclear factor kappa-B ligand (RANKL) [10]. When stimulated, an osteoclast goes through internal changes in preparation for resorption, before lining up on the surface of its target bone [6]. Once on the bone surface, the osteoclast polarizes, forming a ruffled border, demonstrated in Figure 2.1 [10]. This ruffled border is the resorptive organelle [11]. In resorption, an osteoclast attaches to the target matrix, whereby it secretes hydrogen ions into the local environment, which are followed by chloride ions, creating a lacuna filled with hydrochloric acid (HCl). The lacuna has a pH of around 4.5 [10]. The acidic environment dissolves the bone mineral, before secreted proteases digest the organic component of bone. This leaves trenches within the bone, which are filled with new bone matrix by osteoblasts [12].

The balance between the osteoblast and osteoclast function allows for bone mineral density to be maintained at a constant level [13]. However, several diseases present with excessive or imbalanced resorption levels, which can lead to severe issues.

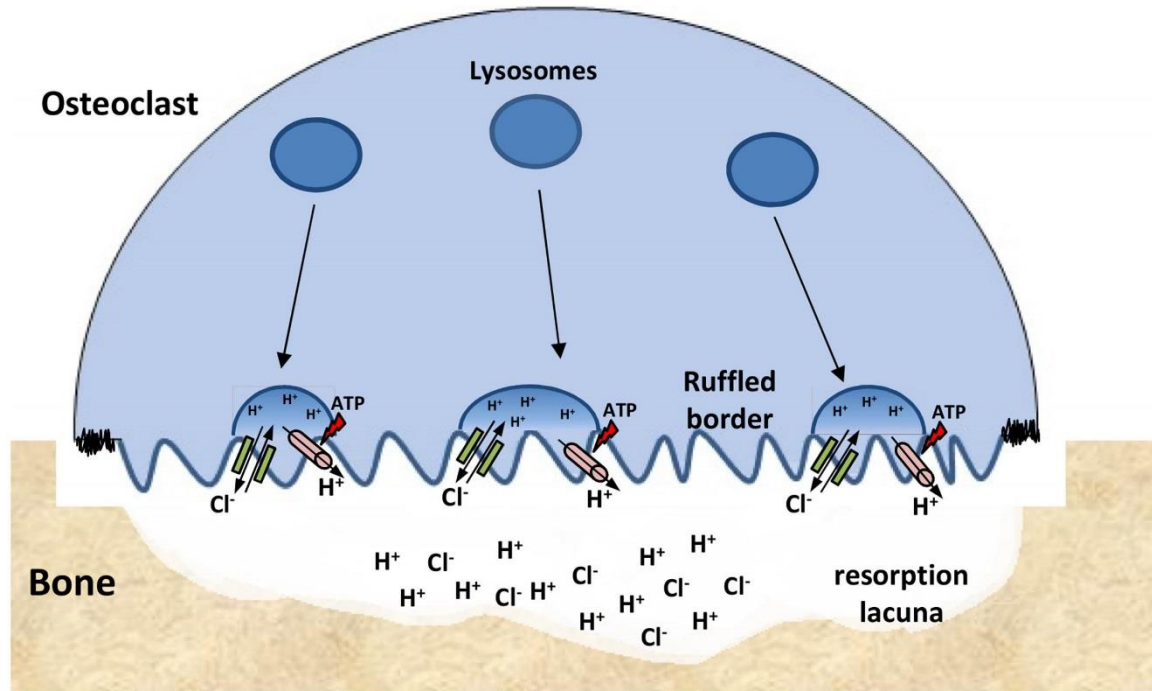


Figure 2.1. Diagram of an osteoclast resorbing bone. Reproduced with permission from Poroca et al. [14] under a Creative Commons license.

2.2 Diseases associated with high bone resorption

2.2.1 Osteoporosis

Osteoporosis occurs when bone remodelling is imbalanced, so that resorption takes place at a greater rate than formation. It is a disease that affects both the quality and quantity of bone in patients, leading to a risk of osteoporotic fractures of vertebrae and long bones. The risk of hip fracture has been reported as high as 1 in 6 [15]. It affects approximately 50 % of women and 20 % of men over the age of 50 in white populations, and treating osteoporotic fractures in the European Union amounts to approximately \$30 billion expenditure per year [15]. Due to the aging population, the number of these fractures is constantly increasing [16]. In patients with osteoporosis, resorption rate is increased as osteoclasts are over-stimulated. This alters the micro- and macro-architecture of the remaining bone, causing it to be weaker, more brittle and to have a lower bone mineral density [15]. Once the mineral density lowers to a clinically significant level, a patient is diagnosed as having osteoporosis.

2.2.2 Osteogenesis imperfecta

Osteogenesis imperfecta (OI), or 'brittle bone disease' [17], is an inherited genetic disease where a mutation in the collagen encoding genes leads to poor collagen formation [18], [19]. It is the most common bone fragility disease, affecting approximately

1 in 150,00 people in the United States of America (US), and as a genetic disorder, it affects people from birth [17]. As collagen makes up most of the organic component of bone, this disease primarily affects bone tissue [18]. The bone formed by OI patients is thinner, with less trabecular bone, and common symptoms of the disease are fractures, bowed long bones, stunted growth and scoliosis [18].

2.2.3 Paget's disease of bone

Osteitis deformans, more commonly known as Paget's disease of bone (PDB) is a chronic bone disorder primarily found in older adults [20]. In this disease, osteoclasts become hypersensitive to RANKL and other factors, leading them to become higher in number and size and hypernucleated, which in turn increases the rate of bone resorption, often in one site alone [20]. In response, osteoblasts are recruited to the site which increases bone formation [21]. The abnormally high rate of both resorption and formation leads to a reduction in bone quality, which leads to fractures, fissures and enlarged bones [20]. Symptoms include pain, arthritis and bone deformity, though around 20 % of cases are asymptomatic [22]. In the United Kingdom, around 5 % of the population have the disease, hypothesised to be due to viral transmission in patients genetically predisposed to its development [21].

2.2.4 Bone metastases

As well as diseases purely related to bone, resorption is also affected by bone metastases of cancer. Metastases occur when tumours from one tissue translocate to another [23]. Breast and prostate cancers are the most likely to metastasise [24], with approximately 70 % of people with advanced forms of these cancers developing metastases [25]. Approximately 90 % of cancer related deaths are due to metastases [23].

The skeleton – and in particular the axial skeleton – is the most common site [24], [25]. The red marrow, high blood flow and immobilised growth factors within the bone cause the preference for skeletal tissue and provide a fertile ground for tumour growth [11]. Metastases are defined by their primary cellular action – those that affect osteoclasts and resorption are osteolytic, while those affecting osteoblasts and formation are osteosclerotic [24], [26]. These differing types of tumours have differing effects on bone.

Osteosclerotic metastases stimulate osteoblast activity to increase bone formation and can cause severe pain [11]. Osteolytic metastases, mostly associated with breast cancer [11], are destructive lesions mediated by osteoclasts, and involve large resorption of bone. They cause severe bone pain, along with poor bone density and hypercalcemia [26], [27]. Osteolytic tumours create a feedback loop with osteoclasts, shown in Figure 2.2 [11]. Once in bone, the tumours release factors that increase osteoclast activity [26], [27].

This increased activity leads to higher resorption rates, causing factors immobilised within bone to be released, which in turn stimulate the tumour growth. As the tumour grows it releases more factors, restarting the loop.

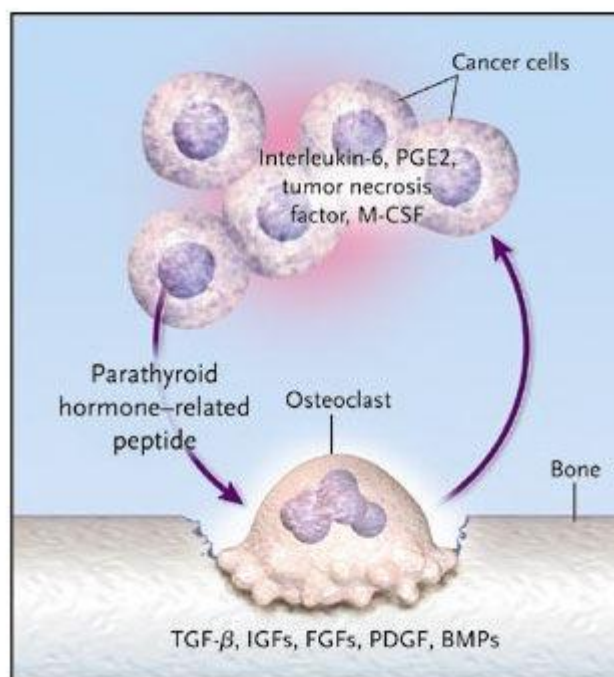


Figure 2.2. The feedback loop osteolytic tumours and bone. Reproduced with permission from Roodman et al. [11] Copyright Massachusetts Medical Society.

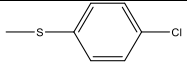
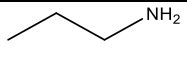
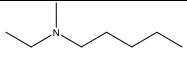
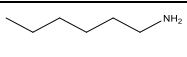
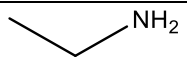
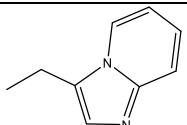
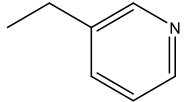
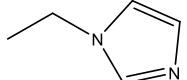
2.3 Bisphosphonates

A key treatment for diseases which present with high resorption are anti-resorptives. Bisphosphonates (BPs) are the most commonly used anti-resorptive treatments for skeletal disorders [28] and one of the most common in the treatment of cancer-related bone resorption [26], [29], [30]. They are taken either orally or intravenously (IV) and bind to the mineral content of bone. During resorption they are released, where they work on a biological and physicochemical level to lower the level of resorption taking place [31]. Due to osteoporosis being an irreversible disease, BP treatment length is long, with a usual initial course of 3 to 5 years, depending on disease severity, before a review. In many patients, BP treatment is a lifelong process [32], [33].

In the US, the market for BPs was reported at \$11-12 billion in 2012 [34] and it is estimated that over 190 million prescriptions for oral BPs have been dispensed worldwide since their first clinical use in 1969 [35]. A study of women in the US noted over 300,000 patients initiating BP treatment for osteoporosis in the first quarter of 2012 [36]. It has been reported that as many as 1 in 7 post-menopausal women in the US have received BP treatment. [37]. However, BP treatment numbers have been decreasing due to concerns regarding their side effects, which is leading to complications associated with osteoporosis to increase [38]–[41].

The properties of some of the more commonly prescribed BPs are summarised in Table 2.1. Throughout this thesis, BPs are referred to by their British Approved Names, i.e. those ending with the –onic acid suffix, rather than the –ate forms, as they match the international non-proprietary names designated by the World Health Organisation.

Table 2.1. Commonly prescribed bisphosphonates and their primary treatment, delivery method (oral or intravenous (IV)), anti-resorptive potency (*relative to etidronic acid) and functional group. Adapted from [4], [31], [42]–[44].

	Chemical name (Commercial name)	Primary treatment	Delivery method	Anti-resorptive potency (*)	Second functional group (R ₂)
1 st Generation	Etidronic acid (Didronel)	Paget's Disease	Oral	1x	—CH ₃
	Clodronic acid (Bonfos, Clasteon, Loron)	Bone Metastases	Oral	10x	—Cl
	Tiludronic acid (Skelid)	Paget's Disease	Oral	10x	
2 nd Generation	Alendronic acid (Fosamax)	Osteoporosis	Oral	>100x	
	Ibandronic acid (Bondronat)	Osteoporosis	Oral/IV	10,000x	
	Neridronic acid (Nerixia)	Osteogenesis Imperfecta	IV	100x	
	Pamidronic acid (Aredia)	Bone Metastases	Oral/IV	100x	
3 rd Generation	Minodronic acid (Bonoton/Recalbon)	Osteoporosis	Oral	>1,000x	
	Risedronic acid (Actonel)	Osteoporosis	Oral	>1,000x	
	Zoledronic acid (Zometa)	Bone Metastases	IV	>10,000x	

2.3.1 Chemical structure and mechanism of action

BPs are synthetic analogues of inorganic pyrophosphate (PPI) [16], [45], a naturally occurring regulator of bone mineralization. Both contain two phosphonate molecules bound to a central atom. BPs differ from PPI in that they contain a non-hydrolysable carbon as their central atom, rather than an oxygen molecule [29]. This prevents the enzymatic breakdown of the drug [46] and reduces the risk of negative effects occurring throughout the body. All BPs have the same generic structure shown in Figure 2.3, and this structure gives the BPs their specific mechanism of action.

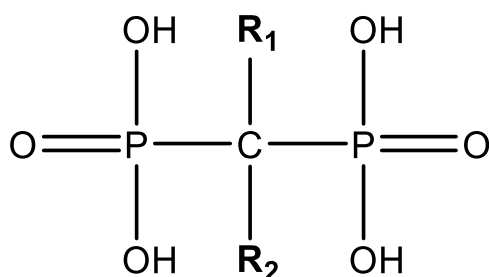


Figure 2.3. The generic bisphosphonate structure.

The BP structure controls two key effects: calcium affinity and anti-resorptive action. The generic structure causes BPs to bind to bone [31], and in particular bones with high turnover rates [47]. BPs readily chelate Ca^{2+} ions [42], [48], and once in the body, they target the calcium in hydroxyapatite (HA) - $\text{Ca}_{10}(\text{PO}_4)_6(\text{OH})_2$ [49] - the mineral component of bone. The two phosphonate molecules work as “bone hooks” to give the BPs their high affinity for bone mineral [31]. The calcium affinity provided by the chemical structure allow for the bone specific effects of BPs.

BPs also contain two functional groups. The first functional group (R_1) is usually a hydroxyl group, which allows for chelation of calcium ions by tridentate bonding, as opposed to bidentate [31], [45], [48], [50]. This further increases the BP ability to bind calcium. The second functional group (R_2) can also cause a slight effect on calcium binding affinity, though this is not its primary function [42], [45]. For example, the primary amine group in pamidronic acid and alendronic acid creates more hydrogen bonds with the surface of the HA, and thus further increases their affinity for the mineral [51]. When BPs bind to HA, they can prevent dissolution, which is thought to contribute slightly to their prevention of resorption [31], [49], [52].

The amount of BP bound by bone is controlled by two factors. Firstly, administration method, which affects bioavailability. This is lower than 1 % for oral administration, but 100 % for IV [16]. Secondly, the affinity for calcium affects the amount of the bioavailable drug that binds to bone. Approximately 50 % of bioavailable BP locates to the bone, with the remaining 50 % quickly leaving via renal excretion [29], [53]. Zoledronic acid (ZA), a

higher affinity BP, has a reported release rate of only 38% [54]. The effects of BP calcium affinity on uptake and resorption are shown in Figure 2.4.

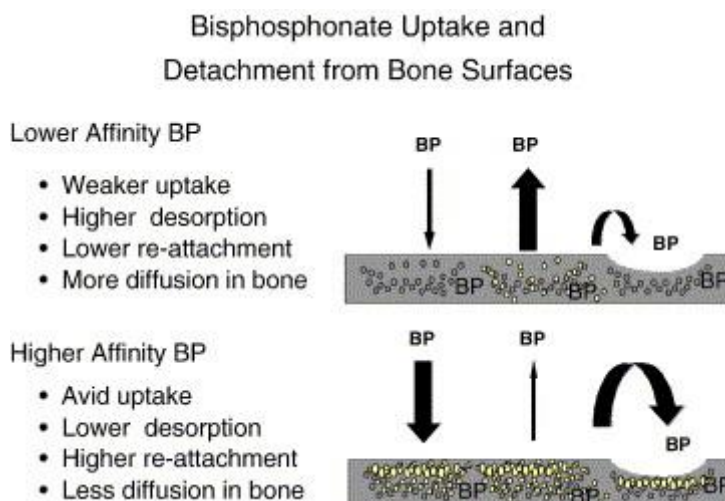


Figure 2.4. BP interaction with bone. Reproduced with permission from Nancollas et al. [45].

Over time, the BP in bone accumulates. Though the blood serum concentration is relatively low (estimated to be 1.47 μM for IV ZA [55]), the high affinity for calcium and prolonged treatment length leads to much higher concentrations within the bone. The dormant bone concentration is thought to lie between 200 and 2000 μM , depending on BP used, treatment method and length [56], [57]. This is thought to be higher still in bones with high turnover rates, such as the jaws [56].

Once bound, the BP remains inactive until it is displaced by other ions, or in the case of resorption, when the structure it is bound to degrades and it is released into the surrounding area [31]. It is hypothesised that the low pH of a resorption lacuna facilitates the release of the BPs into the local environment further, by protonation of the phosphonate groups and reducing chelation [48]. The concentration of BPs in an osteoclast lacuna is estimated to be approximately 1000 μM [26], [31]. After BPs are released into an osteoclast lacuna, they are internalised by the endocytic osteoclasts [31], [58], [59]. Their proximity to osteoclasts, and the tendency of osteoclasts to internalise molecules are thought to be behind BPs specific effect on bone resorption.

On a biological level, BPs reduce resorption by causing apoptosis of osteoclasts. The R_2 group mainly controls the mechanism of action for this, as well as efficacy and potency [29], [45], [48]. The mechanism by which apoptosis is caused varies depending on the generation of the BP. There are currently three BP generations, with each new generation being more potent than the last [50]. First generation BPs are metabolised by the osteoclasts into a cytotoxic analogue of adenosine triphosphate, which accumulates within the cells [58]. Second and third generation BPs are collectively known as

nitrogen containing BPs (nBPs), as their R₂ group contains a nitrogen molecule [48]. In third generation BPs this nitrogen molecule is found in a heterocyclic ring [31], [42]. nBPs have a much more specific mechanism, blocking the production of farnesyl pyrophosphate synthase in the mevalonate pathway [42], [60], [61]. The mevalonate pathway regulates several processes key to the osteoclast, including protein ruffling and cell migration, and is shown in Figure 2.5 [29], [31]. The inhibition of this pathway prevents the ruffled border from forming, removing the osteoclasts' ability to resorb bone [62], and ultimately leads to apoptosis, as the mevalonate pathway effect prevents the formation of proteins key for cellular survival [63].

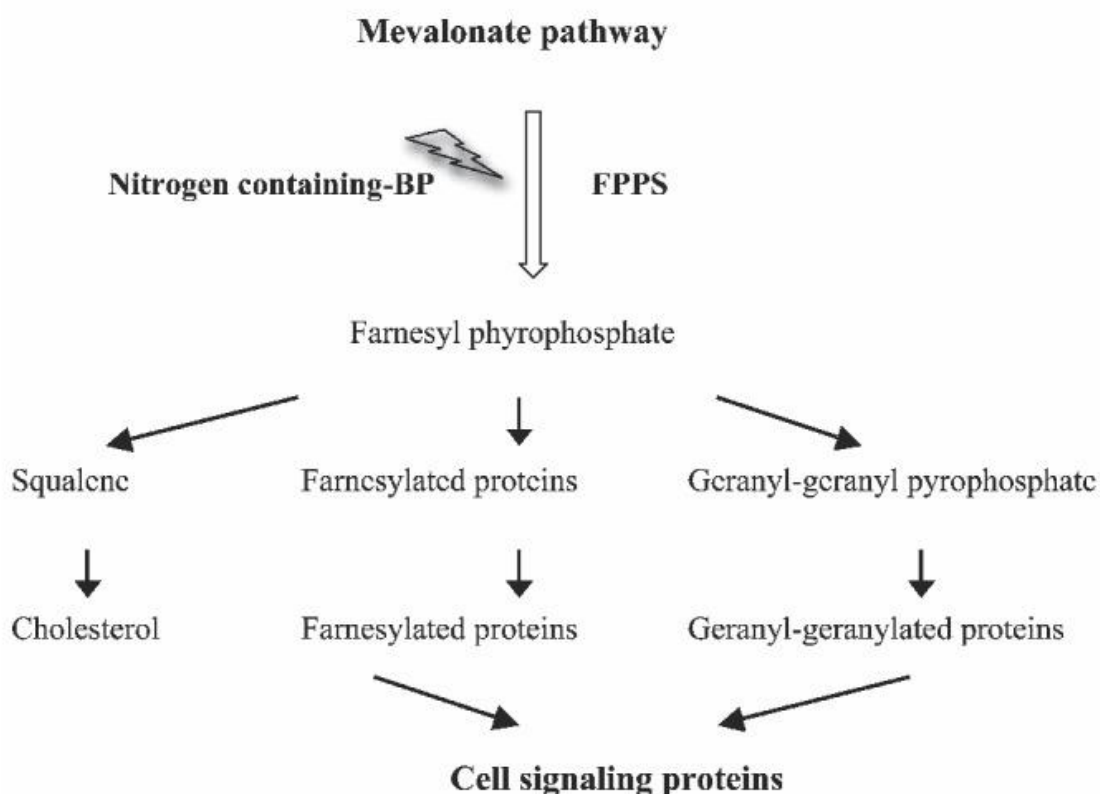


Figure 2.5. The mevalonate pathway. Reproduced with permission from Paulo et al. [48] under a Creative Commons license.

As Table 2.1 indicates, there is a wide range of BP potencies. These potencies are defined related to the first BP, etidronic acid, and are measured by the ability of BPs to increase bone density in rats in the 'Schenk' model [31], [64]. The more potent BPs are used to treat bone metastases, while the less potent are used to treat osteoporosis, or other similar bone related diseases [1], [48], [65]. The BP effect is not limited to preventing resorption through osteoclast apoptosis, however.

Although the primary effect of BPs is on osteoclasts, BPs have also been shown to affect osteoblasts. An *in vitro* study showed that, when cultured in the presence of different BPs, osteoblast proliferation increased [66]. However, differentiation and

mineralisation decreased. These effects could potentially cause an increase in osteoclast number while decreasing maturation. Further work from the same group indicated that transforming growth factor β (TGF β) production increased while RANKL production decreased [67]. These effects were mainly seen with low concentrations of BPs (<1 μ M), while higher concentrations saw less of an effect [66]. These signalling effects may lead to the promotion of matrix production and the reduction of osteoclast formation, contributing to the clinically seen anti-resorptive effects.

Mesenchymal stem cells are a key part of bone tissue regeneration, due to their ability to differentiate into bone cells, and as such, BP effects on these cells have been examined. A study from Park *et al.* investigated the effects of clinically relevant concentrations of ZA on stem cells from bone marrow of four different areas of the mouth, however, they saw no effects on viability, proliferation and morphology [68].

2.3.2 Effects of treatment

BPs prevent osteoclast activity, which lowers bone resorption. During treatment, patient resorption rate lowers to a new steady state level, where it stays approximately constant and does not progress over time [31]. This takes 3 months for oral treatment, and less with IV administration [29]. The new resorption level is vital in the treatment of osteoporosis, allowing for an increase in bone density and a reduction in the risk of fracture [69]. BPs can lower the fracture rates of osteoporosis patients by between 20 and 50 % [70]–[72]. This new steady state resorption level is maintained until the BP has left the body.

The length of time taken to leave the body following the cessation of treatment varies with binding affinity [45]. ZA can inhibit resorption for up to a year from a single 4 mg dose [73]. Several studies have compared patients receiving 10 years of alendronic acid treatment to patients receiving 5 years of alendronic acid followed by 5 years of placebo treatment [74]–[76]. In all cases, a BP effect on resorption was still seen 5 years after the cessation of treatment.

The reduced resorption rate is also beneficial to patients with OI and PDB. In OI patients, bone mass and mineral density increase as resorption rate decreases. This leads to a lower fracture rate, though still higher than a healthy patient [18], [19], [77]. Osteoclast inhibition prevents the high resorption triggered by the hypersensitive osteoclasts in PDB patients, allowing for bone remodelling to return to a normal rate, decreasing fracture rate and reducing pain [20].

Due to the resorption effect seen in bone metastases, BPs are a common treatment. BPs are hypothesised to work both directly and indirectly against tumours, as shown in Figure 2.6 [26], [78]–[81]. The high resorption rate triggered by the tumours is reduced, which helps manage symptoms [31]. Tumour cell invasion is reduced, while apoptosis is increased, reducing tumour burden. BPs also reduce the adhesion of cancer

cells [82]. Lowered osteoclast activity and effects on the immune system indirectly affect tumours. BPs are anti-angiogenic, reducing the level of circulating Vascular Endothelial Growth Factor (VEGF), the most important factor in angiogenesis [83]. This anti-angiogenic effect is hypothesised to contribute to the reduction of tumour burden through the reduction of tumour vascularisation [81].

The reduced resorption rate closes the feedback loop caused by osteolytic metastases, preventing the release of immobilised growth factors and thereby reducing tumour burden [11], [26]. Although osteosclerotic tumours primarily affect osteoblast activity, BPs have been shown to be beneficial in their treatment; helping the management of pain and preventing fracture [11]. It has been demonstrated that osteoclast activation is involved in the formation of osteoblastic metastases [84], and therefore their regulation by BPs is advantageous. This wide range of effects make BPs useful in the treatment of bone metastases, however BPs also come with side effects.

Several adverse effects can come from BP treatment. Oral BP administration causes toxicity to the mucosa of the gastrointestinal tract, which in severe cases can lead to ulceration, and this previously led to a lack of patient adherence [29], [85]–[87]. Advances in the field have reduced these effects. Increased potency BPs allow for reduced treatment frequency, and IV administration avoids contact with the gastrointestinal system entirely. BP treatment has more recently been associated with side effects in the jaw, especially in longer term courses of treatment [1]. Though the bone is affected, BPs also effect the oral mucosa.

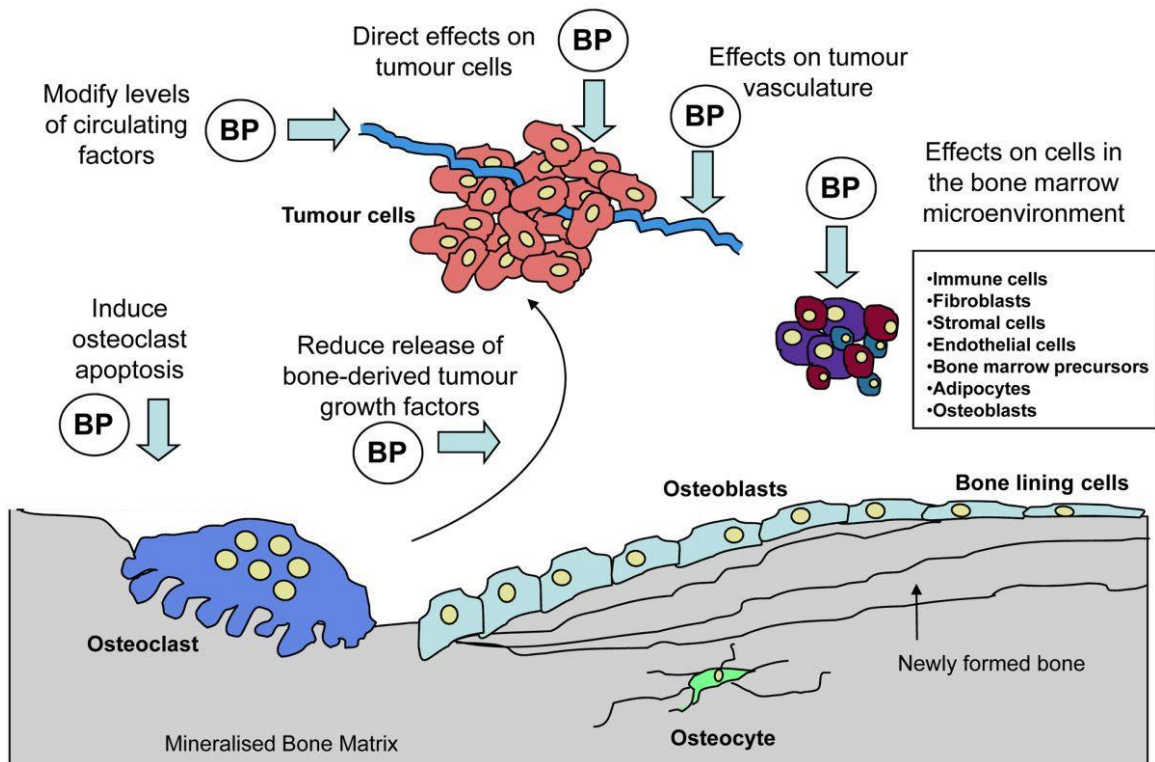


Figure 2.6. Proposed anti-tumour effects of bisphosphonates in bone. Reproduced with permission from Holen et al. [81] under a Creative Commons license.

2.4 Oral mucosa

The oral mucosa is a mucous membrane found in the oral cavity. It provides protection; both from mechanical forces and as a barrier against microorganisms. It also has a role in taste and touch, and is involved in the secretion of saliva [88]. It is made up of a stratified squamous epithelium, a basement membrane, the lamina propria and a submucosal layer containing nerves and blood vessels [89], [90]. A diagram of the oral mucosa is shown in Figure 2.7, with a histological section shown in Figure 2.8.

The epithelium is made up of keratinocytes with four distinct morphologies [91], [92]. The basal layer is a single layer of cells and lies above the basement membrane. The keratinocytes in this layer are cuboidal and the least mature of the epithelium. They are attached to the basement membrane through hemidesmosomes and focal adhesions. The basal keratinocytes are proliferative [89], [93]. Above this are differentiated, squamous cells, forming the prickle cell layer. These two layers make up approximately two thirds of the epithelium. Next is the granular layer, where cells appear longer and flatter. The final layer is the keratinised or cornified layer, where cells are dead and normally contain no organelles [89]. When the epithelium exists in this form it is orthokeratinised, though some oral mucosa is parakeratinised, that is, its keratinised layers still contain nuclei [92]. The epithelial thickness within the mouth varies from approximately 100 μm in the soft palate and floor of the mouth, and 500 μm in the buccal and labial mucosa [91]. At the junction between the epithelium and the connective tissue below, there are downward projections of epithelium – called rete ridges – which increase the surface area of the junction and allows for mechanical forces placed on the epithelium to be spread over a greater area of tissue [91].

Below the epithelium is the basement membrane, which contains laminin 5 and collagen IV [94]. The lamina propria is connective tissue, made of mainly collagen I and III, and contains fibroblasts. The fibroblasts synthesise the majority of molecules found in the extra cellular matrix (ECM). Below the lamina propria usually lies the submucosa. This layer is made up of fatty tissue, blood vessels and nerves, and contains the salivary glands. The blood supply is rich, particularly in regards to other epithelial tissue such as skin, and this is thought to contribute to the fast healing of the oral mucosa [91]. This layer, however, is not found in the gingiva and areas of the soft palate [92].

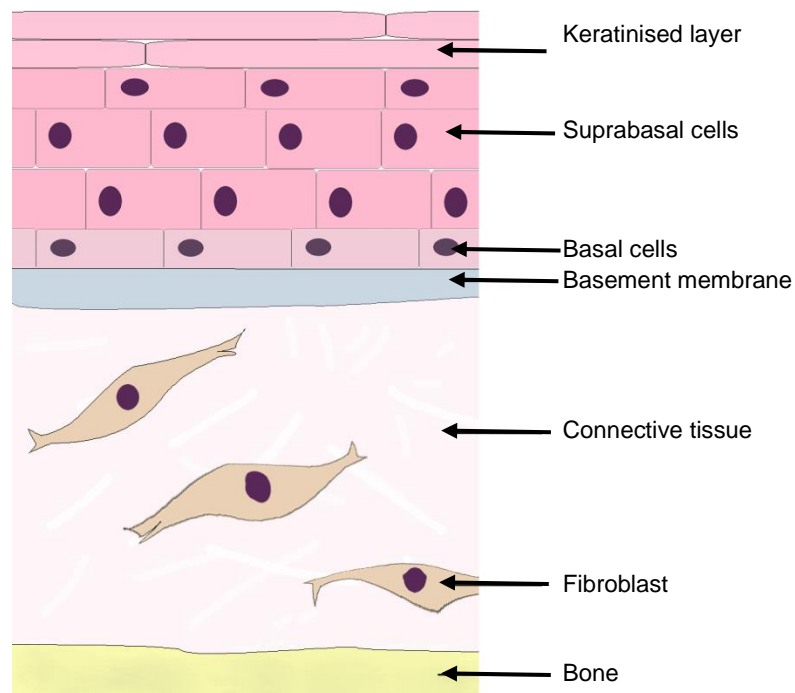


Figure 2.7. A simplified cross sectional diagram of the oral mucosa. Adapted with permission from Glim et al. [89]

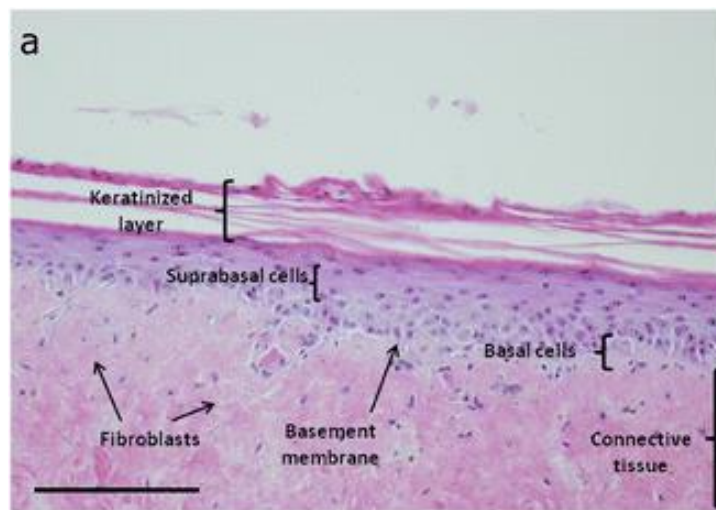


Figure 2.8. Haematoxylin and eosin stained section of healthy oral mucosa. Reproduced with permission from Hearnden et al. [95].

The gingiva is the specific oral mucosa that sits over the jaws, and contains no submucosal layer, with the lamina propria instead attaching directly to the bone [89]. This arrangement is called mucoperiosteum [91]. It is a masticatory mucosa, and contains a relatively thick epithelial layer (approximately 250 μm), as it is subjected to shear forces and abrasion [91]. Its epithelium can be up to 75 % parakeratinised, however this varies from person to person [92]. The lamina propria contains more dense collagen, with less elastin and vascularisation [89], [91], [92]. A histological section of gingiva is shown in Figure 2.9, where a thick parakeratinised epithelium and rete ridges are visible.

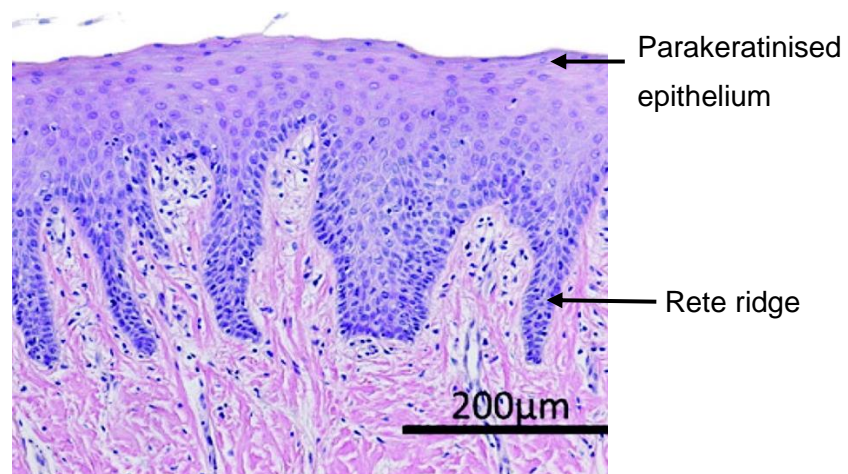


Figure 2.9. Haematoxylin and eosin stained section of healthy gingiva. Reproduced with permission from Buskermolen et al. [94] under a Creative Commons license. Annotations own.

2.4.1 Oral wound healing

The wound healing process in the mouth involves several different cell types from both the hard and soft tissue working in unison to close the wound and generate new tissue. Wound healing follows four phases: the haemostatic phase, the inflammatory phase, the proliferative phase and the remodelling phase [96]. In the first phase, a blood clot seals the wound before a provisional matrix made of fibrin mesh and adhesion proteins is formed, while inflammatory cells are recruited. Within 24 hours of the wound creation, inflammatory cells arrive, secreting proteases and removing bacteria from the wound [96]. In the proliferative phase, ‘granulation tissue’ – highly vascularised tissue made of ECM and fibroblasts – replaces the provisional matrix, while fibroblasts, keratinocytes and endothelial cells from the wound edges proliferate and migrate towards the centre of the wound [96]–[98]. Myofibroblasts – fibroblasts that express high levels of α -smooth muscle actin – contract to close the wound. In the remodelling phase, the newly formed tissue matures, and during this phase scars form [98]. This process leads to a healed wound.

Within the proliferative phase, the soft tissue wound closes. This process is mainly controlled by keratinocytes [99]. When the epithelium is wounded, cells in the basal epithelium loosen their adhesions to allow migration and begin to divide more rapidly [99], [100]. The cells directly at the wound edge migrate across the wound, until cells from both sides meet and contact inhibition prevents further migration [91], [101]. Cells behind the wound edge proliferate in place, and some cells from the layers above the basal layer roll across as the cells below them migrate. Once a single layer of epithelia covers the wound, the keratinocytes proliferate in place to stratify and form a complete, multi-layered epithelium [99]. The proliferation is controlled by growth factors. During this process, keratinocytes release growth factors which in turn stimulate fibroblasts to migrate and deposit new ECM [102]. This new ECM allows for more keratinocyte motility [103]. Throughout this process, both fibroblasts and keratinocytes release TGF β , which stimulates granulation tissue and myofibroblast formation required to complete the proliferative phase [104]. Currently, most of what is known of epithelial wound healing comes from skin [96], however several key differences exist in oral mucosa healing [105], [106].

With the oral mucosa, wounds heal more quickly. Oral mucosa wounds also heal with less scarring. Several theories exist as to why this is. Firstly, more interleukin 1 (IL-1) is found in oral wounds, which increases the immune response to injury [107]. Saliva is known to contain the antimicrobial peptide histatin, which has been demonstrated to speed up the wound healing process [108]. Oral cells are thought to proliferate more quickly in response to injury and close the wound faster [98]. Finally, oral mucosal fibroblasts have been demonstrated to be phenotypically different to those in skin [109].

Several studies have demonstrated the differences between skin and oral mucosal fibroblasts, and how those differences allow for faster, non-scarring wounds in the oral mucosa. Oral fibroblasts are phenotypically closer to foetal cells, and foetal wounds also heal without scarring [110]. A variety of genes relating to this healing phenotype are expressed in greater number in oral fibroblasts, compared to those found in skin [111]. Oral fibroblasts express higher levels of matrix metalloproteinases (MMPs), a facilitator of remodelling, whilst skin fibroblasts express higher levels of tissue inhibitors of MMPs [109]. Oral fibroblasts also have longer telomeres, and therefore a higher proliferative lifespan [112], an increased ability to reorganise and contract collagen [113], and demonstrate a resistance to the myofibroblast formation caused by TGF β [114]. These phenotypic differences allow for a complete, scarless wound healing process.

The wound healing process for a tooth extraction is shown in Figure 2.10. Bone resorption is induced and a blood clot forms [115]. Epithelial cells begin migration 12 hours after surgery. Granulation tissue forms over the first few days [97]. Between days 7 and 10, bone production begins [116]. A provisional matrix is formed, and mineralisation

and the formation of immature bone occur. Re-epithelialisation occurs between days 20 and 40. Within 1 year of extraction, the socket is completely healed, with most of the bone remodelling occurring within 3 months [117]. However, in BP patients, these processes are affected, which may lead to BRONJ, and tooth extraction is the most common BRONJ-preceding event.

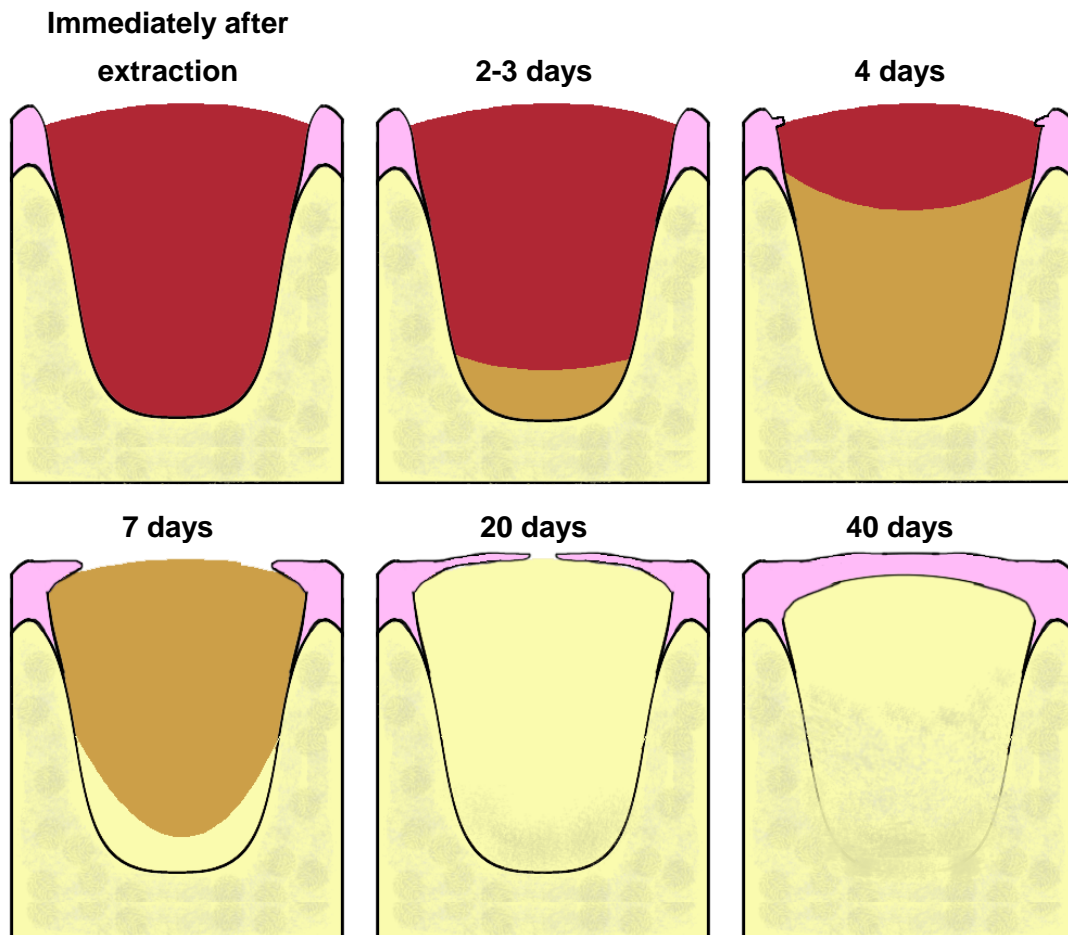


Figure 2.10. Diagram representing the healing of an extraction socket. Immediately after extraction, a blood clot forms. Granulation tissue begins replacing the clot after 2-3 days. At 4 days epithelisation begins. After 7 days, provisional matrix begins to replace granulation tissue, some mineralisation begins. Granulation tissue is replaced by connective tissue after 20 days. Epithelial fusion occurs between 20 and 40 days. Adapted with permission from Amler et al. [97].

2.5 Bisphosphonate-related osteonecrosis of the jaw (BRONJ)

Osteonecrosis of the jaw (ONJ) as a symptom in BP patients was first reported in 2003 [43], and was first recognised by oral and maxillofacial surgeons in 2004 [118]. A photograph of a BRONJ case is shown in Figure 2.11. It usually develops following damage to the jaw, where the BP mechanism has a chain reaction effect, affecting both the bone and surrounding soft tissues and causing the development of a disease that is extremely difficult to treat.

The current BRONJ definition was created by the American Association of Oral and Maxillofacial Surgeons (AAOMS) in 2007 [119]. A patient is defined as having BRONJ when they have “exposed bone or bone that can be probed through a fistula(e) that has persisted for more than eight weeks”, provided they are being or have been treated with BPs, and have no history of radiation therapy to the jaws [1]. Within this definition of BRONJ, there are four stages of increasing severity, shown in Table 2.2. It has been hypothesised that up to 25 % of BRONJ patients may be Stage 0 and as yet undiagnosed [120], [121].

As BRONJ is a recently defined condition, the risk factors associated with its development are not yet fully clear. The specific BP taken, the method of administration and the length of treatment are all thought to influence the risk of BRONJ developing. The incidence of BRONJ has been difficult to determine due to a variety of factors [122] – with differing treatment lengths, doses, administration methods and the various potencies of the different BPs making collating the data difficult. Generally, the risk of developing BRONJ in patients receiving intravenous BPs is between 1 and 10 %, and in patients receiving oral BPs, between 0.01 and 0.001 % [3]–[5]. This risk increases with length of exposure, with a 4 year BP treatment course thought to double the risk of a patient developing BRONJ compared to a 2 year treatment [1], [123]. Due to the risk factors associated with longer term treatment, and the high number of new BP prescriptions, the number of BRONJ cases increases every year [121].

Another risk factor is operative treatment to the jaws. The majority of BRONJ cases are preceded by a ‘dental event’ [5]. Approximately 60 % of BRONJ cases follow a tooth extraction [5], [34], [57], and as such, a tooth extraction is known to increase the risk of BRONJ. Patients taking BPs orally are reported to have a 2 % chance of developing BRONJ following tooth extraction [124], while the risk following extraction in patients receiving IV BPs has been reported higher than 14 % [125]. BRONJ can also be preceded by other oral surgeries, and periodontitis and trauma from poor-fitting dentures have been reported as triggers [126]. Spontaneous cases of BRONJ have been reported, however these are rare and often in areas most susceptible to oral mucosa trauma, and as such it

is hypothesised that these cases are not in fact spontaneous, but the result of undetected trauma [47], [127].

BRONJ affects the two jawbones with differing frequency. The mandible alone is affected in 73 % of cases, while 22.5 % affect only the maxilla [5]. In 4.5 % of BRONJ cases both jaws are affected simultaneously. BPs accumulate in greater concentrations in bone with higher turnover rates. Due to mastication forces often leading to micro fractures and requiring remodelling, the jaws have one of the highest turnover rates in the body [2], [47]. This, in combination of the presence of dental pathology and the proximity of the bone to the oral environment, is thought to contribute the specificity of BRONJ to the jaw.

Age and sex have been reported as risk factors for BRONJ [128], but there is the possibility that this is due to older females being more susceptible to conditions which require BP treatment, and therefore at a higher risk of contracting BRONJ. Both breast cancer and osteoporosis are more common in females, and in particular older females, and hence this group is prescribed BPs at a higher rate than males.

Other medications have also caused ONJ, and these can be grouped with BRONJ under the umbrella term Medication Related Osteonecrosis of the Jaw (MRONJ) [123]. Denosumab prevents bone resorption by inhibiting RANKL, and patients have a comparable risk of ONJ as those prescribed ZA [123]. Anti-angiogenic medications prescribed as cancer treatments, such as sunitinib (a tyrosine kinase inhibitor) and bevacizumab (a VEGF inhibitor), have been shown to cause ONJ [129]. These medications are often prescribed alongside BPs, and can raise the risk of BRONJ by as much as 10% [123].

Some debate over the name of the condition still exists, with AAOMS preferring the term MRONJ, while the International Task Force on Osteonecrosis of the Jaw prefer anti-resorptive agent-related osteonecrosis of the jaw (ARONJ) [130]. These definitions cover ONJ caused by denosumab and anti-angiogenic medications. While denosumab causes an anti-resorptive effect, it does not cause cytotoxicity [131]. As the work in this thesis investigated the cytotoxic effects of BPs, the term BRONJ is used throughout.

Osteonecrosis can also be caused by radiotherapy, termed osteoradionecrosis (ORN), hence the need for the exclusion of radiotherapy patients from the BRONJ diagnostic criteria [98], [132]. ORN also presents with necrotic bone, the formation of fistulae and a dehiscent oral mucosa wound [133], [134]. However, as the source of this issue is radiation, this was not included in the focus of the work in this thesis.



Figure 2.11. Exposed necrotic bone in a zoledronic acid patient. Reproduced with permission from Ruggiero et al. [118].

Table 2.2. Stage definitions of BRONJ. [1]

Stage	Symptoms
Stage 0	No clinical evidence of necrotic bone, but non-specific symptoms or clinical and radiographic findings not attributable to other jaw diseases
Stage 1	Exposed, necrotic bone or necrotic bone that can be probed through a fistula(e) in asymptomatic patients with no evidence of infection
Stage 2	Exposed, necrotic bone or necrotic bone that can be probed through a fistula(e) with evidence of infection
Stage 3	As stage 2, with one or more of: <ul style="list-style-type: none"> • Exposed, necrotic bone extending beyond alveolar bone • Pathologic fracture • Extra-oral fistula • Oral antral/oral nasal communication • Osteolysis extending to the inferior border of the mandible or sinus floor

2.6 Pathophysiology of BRONJ

The mechanisms by which BRONJ develops are yet to be fully determined [135], however, it is hypothesised that several combine to cause the disease to develop following the wounding of the jaw, affecting both the bone and the surrounding mucosa. BP effects on bone remodelling, angiogenesis, inflammation, soft tissue and infection are all thought to contribute to the disease. A diagram showing one hypothesis for the sequence of BRONJ development is shown in Figure 2.12.

When bone is damaged, osteoclast resorption is a key part of the remodelling process during wound healing [136]. BP effects on osteoclasts prevent remodelling from occurring, which thereby prevents full wound healing [137]. This non-healing jaw wound is the beginning of BRONJ. This is similar in MRONJ cases where resorption is prevented, supporting the hypothesis that osteoclast inhibition is involved in the development of BRONJ [138].

Osteonecrosis is considered as the death of bone tissue due to lack of blood supply [1]. Mandibular bone is one of the densest bones in the body and at its thickest part contains few blood vessels, making it a prime target for necrosis [48]. Successful bone healing relies on angiogenesis [139]. BPs' anti-angiogenic properties inhibit the formation of new blood vessels [140], which hinders wound healing and leads to the damaged bone becoming necrotic. Anti-angiogenic medications have led to ONJ, supporting the hypothesis that BP-inhibited angiogenesis is involved in the development of BRONJ [129].

Inflammation has also been linked to the development of BRONJ, with it hypothesised that early, low level inflammation may be a trigger for the condition [141] and BPs shown to be pro-inflammatory [137]. Inflammation is part of the normal healing response in an extraction socket [115], and therefore low level inflammation will exist prior to the development of BRONJ. The number of medullary inflammatory cells has been statistically linked to the onset of BRONJ in patients, suggesting that inflammation may progress to necrosis in some cases [141].

As the damaged bone is exposed to the surrounding environment, BPs are released, and at certain concentrations, become toxic to the surrounding tissues. The full mechanism by which BPs are released into the mouth, and the concentration to which the oral mucosa is exposed are not known, and is difficult to estimate given the variety of BPs, affinities and dosing regimen [56]. A study by Scheper *et al.* measured the ZA concentration in the saliva of BP patients 5 minutes after IV treatment at between 0.4 and 5 μM [142]. In higher affinity BPs, such as ZA, more BP will be present and it will be located close to the surface of the bone [45]. Therefore the concentration of BPs with a lower calcium affinity may be lower. During wound healing and infection, the pH in the

mouth can decrease, which is hypothesised to lead to further and more prolonged release of BPs due to the effect of pH on chelation described in section 2.3.1 [143].

BPs within the expected oral range have been shown to be toxic to both oral keratinocytes and fibroblasts, and negatively affect cell proliferation and migration [57], [140], [144]. Oral mucosa wound healing is known to be more difficult without healthy underlying bone [98]. These combine to prevent the damage soft tissue from healing and maintain bone exposure. This is Stage 1 BRONJ, and this soft tissue toxicity is hypothesised to be key to BRONJ development [2]. As the mucosa of the lower jaw is thinner, it contributes to the mandible being more susceptible to the development of BRONJ [53].

With no oral mucosa surrounding it, the necrotic bone becomes exposed to the inside of the mouth, and therefore to several species of bacteria [47], [145]. Infections both prior to and post-extraction have been hypothesised as risk factors for BRONJ, with bacteria commonly present in biopsied necrotic tissue, and infection thought to occur in 60 % of BRONJ patients [146], [147]. BPs can lead to an increased biofilm formation in the mouth, which increases infection risk [58], [148]. These factors, and the lack of blood flow to the necrotic area, makes BRONJ patients particularly at risk of infection. This infection is Stage 2 BRONJ, with Stage 3 then developing if it goes untreated.

If untreated, the symptoms worsen. The first fatal case of BRONJ was reported in 2018, where a ZA patient developed BRONJ following a routine tooth extraction [149]. This was unable to be treated and progressed to Stage 3 BRONJ, whereby the patient began to bleed from the wound and later died following haemorrhagic shock.

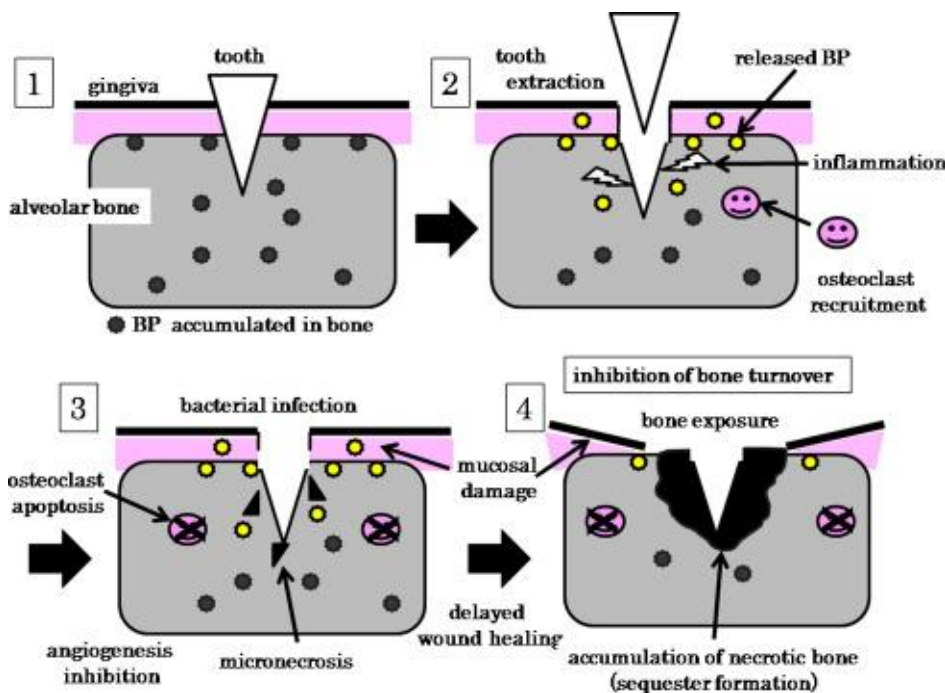


Figure 2.12. One hypothesis for the sequence of BRONJ development following tooth extraction. Reproduced with permission from Ikebe et al. [47].

2.7 BRONJ treatment

There is no specific treatment for BRONJ currently available [150], and management strategies vary depending on the patients other co-morbidities, quality of life, and stage of the disease. The relatively low incidence and incomplete knowledge of its pathogenesis has made devising a definitive treatment challenging [151]. The main treatments are summarised in Table 2.3. These include pain medication, antibiotics and antibacterial rinses, and in more severe cases, the surgical debridement of necrotic tissue [44], [135], [152]. The guideline treatment for BRONJ is to treat conservatively without surgical intervention, however this has a success rate lower than 50 % [153]. Surgical intervention has been demonstrated to have success [154]–[158], however this is not always possible due to patient ineligibility, and can lead to relapse, often due to infection [159]. Surgery to remove the necrotic bone is difficult, as distinguishing between necrotic and healthy bone may be challenging and dependent on surgical skill [159], [160]. Surgery can expose vital bone which has also been subjected to systemic BP treatment and is therefore not ideal [118], [161]. As such, other treatments have been sought.

One treatment suggested is a drug holiday - whereby a patient ceases BP treatment for several months prior to dental extractions. However, in a retrospective study of risk factors, this was shown to be ineffective in the prevention of BRONJ [162]. The calcium binding affinity for BPs, as described in section 2.3.2, gives them an incredibly high bone retention rate for BPs and an extended period of action, and as previously mentioned, studies showing 5 year placebo treatment after 5 years alendronic acid treatment did not completely remove BP effect [74]–[76]. As such, a short term drug holiday is inadvisable. Given the severity of conditions that BPs are used to treat, longer term drug holidays are also likely to be unsuitable for patients.

The need for a more specific BRONJ treatment is clear, and as such current research in the area focusses on two areas: further identification of the pathophysiology of BRONJ and potential novel treatments.

Table 2.3. Current treatment methods for BRONJ. [1]

Stage	Treatment
Stage 0	Systemic treatment, including antibiotics and pain medication
Stage 1	Antibacterial rinse, quarterly clinical follow-up, & patient education and review of indications for continued bisphosphonate therapy
Stage 2	Systemic treatment with oral antibiotics, oral antibacterial rinse, pain control, debridement, and infection control
Stage 3	Antibacterial rinse, antibiotic therapy, pain control, surgical debridement or resection to reduce pain/infection

2.8 Current position of BRONJ research

Due to the severity of BRONJ and the increasing number of BRONJ patients diagnosed every year [121], there is an increasing amount of research focussed in the area, aiming to further understand the causes of BRONJ while also developing a more specific and successful treatment for the disease. In understanding the causes of BRONJ, a key focus is the effects of BPs on the oral mucosa, due to the hypothesis that this is key to the development of the disease [2]. Work in this area focusses on both 2D and 3D cell culture, and a wide variety of BP effects. In order to gain a further understanding of the condition, several *in vivo* models of the disease have been developed in small and large animals. Finally, a variety of novel treatments for the disease have been developed and examined, using 2D and 3D cell culture and *in vivo* BRONJ models to test their efficacy. The work presented in this section mainly covers BRONJ soft tissue research, due to the previously described hypothesis regarding its importance.

2.8.1 2D effects of BPs

Several studies have investigated the effects of BPs on cells of the oral mucosa in 2D, examining a broad variety of effects, including viability, migration, proliferation and adhesion. This section summarises the main findings of these studies. This section only reviews articles which have used either pamidronic acid (PA) or zoledronic acid (ZA), as these BPs are most commonly associated with BRONJ [153], [163]. A summary of the effects seen on fibroblasts is shown in Table 2.4, with the effects on keratinocytes shown in Table 2.5.

Table 2.4. A summary of the current literature investigating the 2D effects of pamidronic acid (PA) and zoledronic acid (ZA) on fibroblasts.

Effect	BP	Effect seen	Concentration of effect	Disadvantages of studies	References
Viability	PA	Decrease	60 μ M – 48 h 25 μ M – 96 h 30 μ M – 168 h	Inconsistency between time points and concentrations used	[144], [164], [165]
	ZA	Decrease	50 μ M – 24 h 3 μ M – 48 h 5 μ M – 72 h 10 μ M – 96 h 2 μ M – 168 h 0.16 μ M – 4 weeks		[35], [55], [144], [166]–[171]
Apoptosis	PA	Increase	10 μ M	Some inconsistency of results	[144], [164], [165]
	ZA	Increase	1 μ M		[35], [167], [169], [171], [172]
Proliferation	PA	Decrease	10 μ M	Few cells sampled; cell counting often used	[165]
	ZA	Decrease	1 μ M		[167], [169], [173]
Migration	PA	Decrease	50 μ M	Toxic concentrations; no control for proliferation	[144], [170], [172]
	ZA	Decrease/ No effect	30 μ M/ 1 μ M		[35], [144], [170], [173]
Adhesion	ZA	Decrease/ Decrease on titanium	30 μ M/ 0.5 μ M	Titanium not representative of BRONJ	[144], [174]

Table 2.5. A summary of the current literature investigating the 2D effects of pamidronic acid (PA) and zoledronic acid (ZA) on keratinocytes.

Effect	BP	Effect seen	Concentration of effect	Disadvantages of studies	References
Viability	PA	Decrease	100 μ M – 24 hr 50 μ M – 72 hr 1 μ M – 96 hr 100 μ M – 1 week	Inconsistency between time points, cell sources and concentrations used	[57], [86], [164], [175]
	ZA	Decrease/ Increase	5 μ M – 24 hr 3 μ M – 48 hr 1 μ M – 72 hr/ 10 μ M – 48 hr		[35], [86], [169], [175]–[178]
Apoptosis	PA	No effect/ Increase	100 μ M/ 5 μ M	Inconsistency of cell sources and results	[57], [86], [164], [175]
	ZA	No effect/ Increase	10 μ M/ 0.25 μ M		[35], [140], [168], [169], [175]
Proliferation	ZA	Decrease	1 μ M	Few cells sampled; cell counting often used; inconsistency of cell sources	[164], [169], [173], [177]
Migration	PA	Decrease	50 μ M	Toxic concentrations; no control for proliferation; inconsistency of cell sources and results	[57], [86], [175]
	ZA	Increase/ No effect/ Decrease	10 nM/ 1 μ M/ 100 nM		[35], [86], [140], [173], [175], [178]
Adhesion	ZA	Decrease on titanium	0.5 μ M	Not representative of BRONJ	[174]

2.8.1.1 Cell viability

The effects of BPs on oral mucosa cell viability have been extensively studied. Investigations have used fibroblasts and keratinocytes from a variety of sources to assess the effects of BPs over time. Both PA and ZA have been reported to be toxic to fibroblasts and keratinocytes at concentrations clinically relevant to BRONJ patients [35], [57], [170]–[172], [175]–[177], [86], [144], [164]–[169].

PA has been demonstrated to be toxic to human oral fibroblasts after 24 hours, 72 hours, 96 hours and 1 week of administration. When studied for 24 hours, a 5 μM concentration was shown to be toxic by Walter *et al.* [170]. However in the longer term studies, this concentration was shown to have no effect. A half-maximal inhibitory concentration (IC_{50}) of 42 μM was generated at 72 hours of treatment [165]. Concentrations above 10 μM were required to significantly reduce viability in the 96 hour study, and 30 μM and above in the 1 week study [144], [164]. In the 24 hour study, Walter *et al.* also tested ZA and found only a 50 μM concentration was toxic, indicating PA is more potent. ZA is known to be more a potent anti-resorptive and has consistently been demonstrated to be more toxic to oral mucosa cells, however, supporting the results of the longer term studies and negating the results seen by Walter *et al.* [86], [144], [170].

Similar studies have been conducted with ZA. A study by Ravosa *et al.* indicated ZA concentrations above 30 μM were toxic to a human gingival fibroblast (HGF) cell line after 48 hours of treatment [35]. Komatsu *et al.* saw toxicity from a 14.7 μM treatment at this time point [55]. Two studies examined HGFs in the presence of ZA over 72 hours, one found concentrations of 30 and 100 μM toxic [167], and the other indicated 50 μM (the only concentration tested) to significantly reduce viability [168]. Jung *et al.* found 5 μM and above ZA was toxic to periodontal ligament fibroblasts at the same time point. Zafar *et al.* demonstrated 10 μM concentrations were toxic to HGFs at 96 hours [171], and the previously referenced study by Cozin *et al.* found a dose dependent effect above 2 μM at 1 week of dosing [144]. The effect of ZA on fibroblast viability has been tested as far as 4 weeks of treatment, where concentrations ranging from 0.15625 to 2.5 μM were shown to have a dose dependent, significant effect on viability [166]. While it is evident that PA and ZA are toxic to fibroblasts, there is a lack of clarity regarding this effect.

Keratinocyte viability in the presence of both drugs has also been examined. Pabst *et al.* cultured human oral keratinocytes in the presence of either PA or ZA in two studies, one over 24 hours [175] and one over 72 hours [86]. It was demonstrated that ZA was twice as toxic as PA at 24 hours, with a 50 μM concentration causing a significant reduction of cell viability, compared to 100 μM for PA, using a calcein viability assay. By 72 hours, 5 μM concentrations of both drugs caused a significant reduction in viability, with ZA leading to a more pronounced effect. Kim *et al.* also demonstrated 5 μM concentrations of PA reduced human oral keratinocyte viability after 72 hours [164]. Although this again was

only a slight reduction, with their data indicating an IC_{50} of approximately 50 μ M. Work by Ohnuki *et al.* indicated 3 and 10 μ M ZA reduced primary oral keratinocyte viability by a small but significant amount after only 48 hours of treatment [177]. Murine oral keratinocytes appeared more resilient in a study by Landesberg *et al.*, where concentrations from 3 to 30 μ M had no effect on cell viability over 1 week, but 100 μ M PA significantly reduced viability after 24 hours [57]. In the previously mentioned study by Ravosa *et al.* [35], human oral keratinocytes immortalised through transduction to prevent telomere shortening (OKF6/TERT-2) [179] were cultured for 48 hours in the presence of ZA, where 10 μ M and above concentrations significantly reduced viability.

However, Renò *et al.* indicated that sub-toxic concentrations had beneficial effects on HaCaT cells (a common immortalised skin keratinocyte line), with 10 nM to 10 μ M ZA concentrations increasing cellular viability, measured through a resazurin reduction based assay [178]. It was suggested this was due to BPs inhibiting farnesyl pyrophosphate (FPP), an intermediate in the mevalonate pathway. This can inhibit wound healing as it acts as an agonist for glucocorticoid receptor. Therefore concentrations low enough to not cause toxicity but high enough to reduce FPP levels could have a positive effect on epithelial cells. This theory, however, is unsupported by the previously mentioned literature using BP concentrations below 1 μ M which demonstrated no effect [165], [166], [169], [177]. Arai *et al.* also treated HaCaT cells with ZA at 10 nM and above concentrations, and showed no beneficial effect of nanomolar BP treatment [176]. They did, however, indicate that local calcium levels could drastically affect the potency of BPs. They theorised that due to the BP binding affinity for calcium, increasing cellular calcium levels would thereby increase the amount of BP acting upon the cell. While these papers are an indication of BP keratinocyte effects, as HaCaT cells are immortalised skin keratinocytes, this data is therefore not particularly relevant to BRONJ patients. Due to this, and the inconsistencies in other viability results, more work to fully examine BP toxicity is required.

2.8.1.2 Apoptosis

As well as confirming that BPs reduce viability to cells of the oral mucosa, the mechanism by which BPs cause cell death has been investigated. Apoptosis is the programmed death of a cell, and can occur in response to certain external triggers, and both PA and ZA have been shown to increase apoptosis in human oral fibroblasts and keratinocytes. Apoptosis is measured *in vitro* through several different techniques, generally through staining for specific apoptosis markers. Caspases are enzymes activated during apoptosis, and cells are often stained with antibodies targeted at specific caspases to identify apoptotic cells. Annexin V binds competitively to phosphatidylserine, a protein expressed during apoptosis. Fluorescently labelled annexin V staining is another commonly used method for measuring apoptotic cells.

Agis *et al.* demonstrated 30 and 50 μM ZA led to HGF apoptosis after 48 hours of treatment through annexin V staining [167]. They also confirmed their results by detecting the presence of cleaved poly (ADP-ribose) polymerase, another apoptosis marker. This work was supported by Zafar *et al.*, who used the same cell type and ZA concentrations, and found increased caspase 3 staining over 96 hours [171]. Jung *et al.* used different oral fibroblasts, taken from the periodontal ligament, and saw a similar effect, as caspase 3 staining indicated apoptosis increased fivefold with 72 hours of ZA treatment [172]. Soydan *et al.* indicated PA also led to HGF apoptosis over 72 hours in a dose dependent manner from 0.1 to 100 μM concentrations through measuring caspase 3 levels [165]. Contrarily, while Cozin *et al.* did observe apoptosis in HGFs with both PA and ZA, they indicated only PA led to increased caspase activity [144].

While fibroblast apoptosis is a fairly consistent effect throughout the literature, there is less clarity regarding keratinocytes. Scheper *et al.* investigated the effects of ZA on both a HGF cell line and HaCaT cells [169]. They indicated apoptosis was triggered at a slightly lower concentration in keratinocytes (0.25 μM to 1 μM), and occurred at a considerably greater rate than in fibroblasts. This contradicts work from both Ravosa *et al.* and Kim *et al.*, who compared apoptosis levels in fibroblasts and keratinocytes when treated with ZA and PA, respectively [35], [164]. In both studies, while apoptosis was high in fibroblasts, there was no significant increase in keratinocyte apoptosis. This is supported by the previously mentioned paper from Landesberg *et al.* who indicated PA did not lead to a significant increase in keratinocyte apoptosis [57]. Kim *et al.* suggested that BPs led to the cell death of keratinocytes by triggering early senescence, rather than apoptosis as in fibroblasts, and successfully stained for markers of senescence to confirm their theory [164].

However, other literature again states keratinocyte apoptosis can be triggered through BP treatment. Both previously mentioned papers by Pabst *et al.* indicated a significant increase in human oral keratinocyte apoptosis in response to both PA and ZA concentrations of 5 and 50 μM , however in one paper indicated ZA led to more apoptosis, while the other saw higher apoptosis in PA treated cells [86], [175]. Kobayashi *et al.* found a slight increase of murine oral epithelial cell apoptosis in response to concentrations of 100 nM to 10 μM , but only a significant increase at 100 μM [140]. Further work is needed to fully elucidate the cytotoxic mechanisms of PA and ZA on keratinocytes.

2.8.1.3 Proliferation

Cell proliferation is a key part of wound healing. Regenerating tissue requires new cells, and proliferation is the process by which they are generated. It has been suggested that a potential mechanism by which BPs prevent oral mucosa wound healing is through decreasing proliferation.

Several papers in this literature review purported to have reported on effects on proliferation, using 3-(4,5-dimethylthiazol-2-yl)-2,5-diphenyltetrazolium bromide (MTT) or similar metabolic activity assays [35], [57], [144], [166], [178]. However, as these assays in fact measure metabolic activity, not proliferation, those results have been discussed in section 2.8.1.1. The review of literature in this section only relates to those papers that have directly measured proliferation.

PA and ZA have both been shown to reduce proliferation of human oral fibroblasts. Soydan *et al.* examined HGF proliferation through staining for Ki67, a cellular proliferation marker [165]. They found PA reduced proliferation in a dose dependent manner with concentrations ranging from 0.1 to 100 μM , however only sampling 100 cells. A similar effect was found in HGFs when treated with ZA [167]. Cells were labelled with ^3H thymidine to track proliferation, and both 30 and 100 μM concentrations caused a significant reduction, in comparison to untreated cells. ZA concentrations as low as 1 and 3 μM were found to reduce proliferation by Scheper *et al.*, who observed proliferation through cell counts [169].

Keratinocyte proliferation has also been found to be affected by ZA. In the previously mentioned study by Scheper *et al.*, HaCaT proliferation was also significantly decreased by 1 and 3 μM concentrations of ZA [169]. McLeod *et al.* found 1 μM ZA had no effect on OKF6 proliferation, but a 5 μM dose significantly reduced proliferation between 2 and 5 days culture [173]. This effect was also observed in foreskin fibroblasts in the same study. Work from Ohnuki *et al.* indicated ZA reduced primary oral keratinocyte proliferation, through fluorescent labelling of DNA [177]. Concentrations ranging from 0.1 to 10 μM caused a dose dependent reduction in DNA over 48 hours. Further analysis indicated that this was due to the cell cycle being arrested in the S phase by damaging DNA and thereby reducing the expression of proteins involved in cell cycle regulation. This effect was also seen in work from Kim *et al.* [164]. Which analysed the cell cycle of both oral fibroblasts and keratinocytes treated with 10 and 50 μM PA. Their data again indicated the arrest of keratinocytes in the S phase of the cell cycle, where fibroblasts treated with 50 μM PA were largely in the sub-G1 phase. This suggests that keratinocytes were prevented from completing their cell cycles while fibroblasts became apoptotic when treated with BPs.

As of yet, no work has directly measured the effect of PA on keratinocyte proliferation, and this presents an area for further study.

2.8.1.4 Migration

In the development of BRONJ, sections of the oral mucosa fail to heal following a dental event. As migration is a key part of oral mucosa wound healing, the effects of BPs on cellular migration have been examined. Migration is often studied *in vitro* with a scratch

assay, whereby cells are cultured to confluence, before a sterile pipette tip is scratched across the cell monolayer to create a gap between the cells [180]. Migration across this 'wound' is then assessed over time.

The effects of BPs on fibroblast migration have been investigated in several studies [35], [144], [170], [172], [173]. Data from these have shown 60 and 100 μM concentrations of PA significantly slowed migration over a 72 hour time period [144], [170]. As with viability and proliferation, the higher potency of ZA is again thought to transfer to migration effects. ZA concentrations of only 10, 30 and 50 μM were variably required to cause a similar effect to 60 and 100 μM PA [35], [144], [172]. As previously with viability, Walter *et al.* found ZA to cause less of an effect than PA, when migration was measured in the presence of both drugs, which is again contradictory to the other data seen with these cells [170].

Keratinocyte migration has also been assessed, however several different effects have been reported. In two studies by Pabst *et al.* 50 μM concentrations of both PA and ZA slowed the rate of migration of human oral keratinocytes over 72 hours in scratch assays [86], [175]. Kobayashi *et al.* demonstrated a similar effect on murine oral keratinocytes, with ZA concentrations ranging from 100 nM to 10 μM slowing migration over 15 hours [140]. However, Landesberg *et al.* reported PA concentrations from 3 to 100 μM had no effect on murine oral keratinocyte migration over 96 hours [57]. Only when cells were pre-treated with 100 μM for 72 hours prior to the experiment was any effect seen, and this concentration was reported to be toxic at this exposure time earlier the paper [57]. Several papers report cellular toxicity and migration effects from the same concentrations at the same time points [86], [144], [170], [172], [175], likely pointing to lack of wound closure through cell toxicity, rather than a separate migration effect. In all except the paper by Cozin *et al.*, images of the cells are not included, and in that paper the cells of the unclosed wounds do not appear to be alive, with either side of the wound no longer well-formed [144], particularly when treated with ZA shown in Figure 2.13.

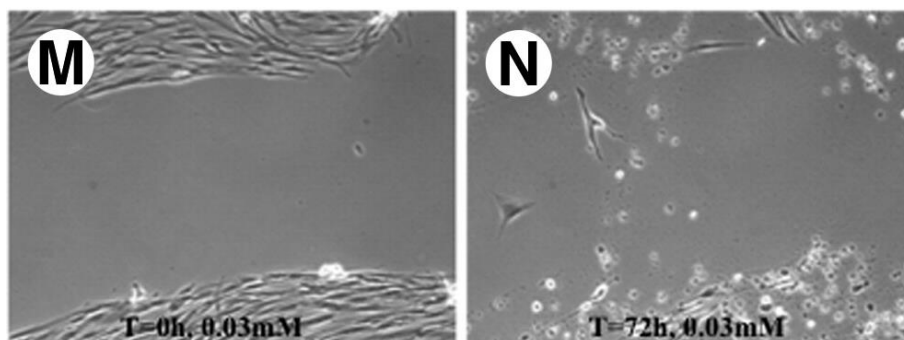


Figure 2.13. Wound healing of primary human oral fibroblasts treated with 30 μM zoledronic acid. M shows fibroblasts immediately after the creation of a scratch. N shows the same cells 72 hours after. Reproduced with permission from Cozin *et al.* [144].

Alternatively, ZA has also been reported to promote migration of keratinocytes. Ravosa *et al.* also investigated migration effects on OKF6 cells, and demonstrated scratch wounds closed faster over 30 hours when treated with 10 μ M ZA [35]. They did not explain this effect. Renò *et al.* again found ZA to promote migration in a human skin cell line (HaCaT) [178]. Concentrations ranging from 10 nM to 10 μ M all decreased wound closure time in a scratch assay.

As previously described, proliferation is a key part of wound healing, and therefore, to truly assess migration effects, proliferation must be prevented. None of the previously mentioned papers appeared to control for proliferation in their assays.

The migration of immortalised human foreskin fibroblasts and OKF6 cells was studied in the presence of sub-toxic levels of ZA by McLeod *et al.* [173]. Using sub-toxic levels of the drug ensures that toxicity will not prevent the wound from closing. Rather than the usual scratch assay, a transwell migration assay was performed, which assesses cellular ability to migrate towards a chemoattractant. This therefore gives a clearer picture of motility effects alone. No effect on the migration of either cell type was observed over a 24 hour time period in this study.

While a range of data exists for the effects of BPs on cellular migration, the methods by which this data has been obtained leave a lot to be desired. A study which controlled for proliferation alone while examining concentrations below the toxic levels of the drug would allow for a much clearer answer as to whether BPs inhibit or promote cellular migration.

2.8.1.5 Adhesion

Nitrogen-containing BPs (nBPs) have been shown to affect the adhesion of a wide variety of cell types including smooth muscle cells [181], endothelial cells [182], [183] and cancer cells [82]. This is hypothesised to be due to the nBP effect on the mevalonate pathway.

The mevalonate pathway is responsible for the prenylation of proteins [31] – the BP effect prevents proteins from acting at the correct location in the cell. This leads to changes in proliferation, survival, cytoskeletal organisation and vesicular trafficking. The main effect is on Guanosine-5'-triphosphatases in the Rho family. These proteins are in a signalling pathway with Focal Adhesion Kinase (FAK) [184]. The phosphorylation of FAK is critical for the assembly and disassembly of focal adhesions [185]. Therefore the mevalonate pathway effect of BPs could theoretically lead to a reduction in adhesion.

ZA has been demonstrated to decrease FAK phosphorylation in several cell types *in vitro* [82], [181], [182], [186], in conjunction with a reduction in adhesion, this further strengthens the theory of a link between BPs and reduced cellular adhesion. Cozin *et al.* demonstrated that 30 μ M concentrations of ZA lowered fibroblast adhesion alongside its toxic effect [144]. Cells were stained to visualise focal adhesions and f-actin bundles in the

cytoskeleton, and these were seen to be reduced when cells were treated with the BP, shown in Figure 2.14.

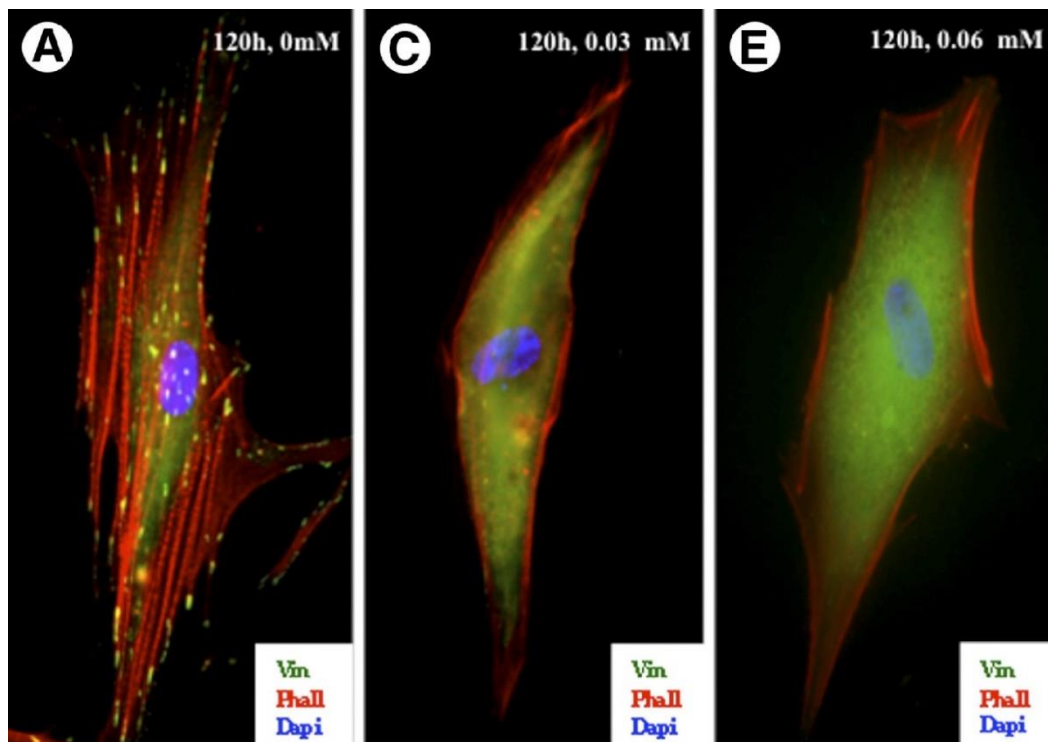


Figure 2.14 Effect of zoledronic acid on integrin-mediated cell-substratum adhesions of oral fibroblasts. Cells were plated on fibronectin-coated coverslips and exposed to 30 or 60 μM zoledronic acid. The cells were fixed after 120 hours and then stained with vinculin and phalloidin to visualize the focal adhesions and actin cytoskeleton. Reproduced with permission from Cozin *et al.* [144].

ZA has also been shown to prevent some integrin-mediated adhesion, specifically $\alpha_v\beta_3$ [82] and $\alpha_v\beta_6$ [187]. However, these integrins are not present in the epithelium of healthy oral mucosa, with $\alpha_v\beta_6$ only expressed in response to wounding [188]. As BRONJ develops following wounding of the epithelium, this pathway would be a likely candidate for any effect that BPs have on oral epithelial adhesion. Alendronic acid has also been linked to a reduction in epithelial adhesion, with biopsies from long term oral BP patients stained for desmoglein-1, a protein involved in the adhesion of keratinocytes in the oral epithelium [189]. In the patients tested, the epithelium was still intact though the outer layers contained less desmoglein. This suggests that in even in BP patients which appear healthy, the epithelium is already weaker and more susceptible to lesions forming, which may play a role in the development of BRONJ.

The effects of ZA on gingival fibroblast and HaCaT adhesion to titanium were tested by Basso *et al.* [174]. In their study 0.5 and 1 μM treatments of ZA led to fewer cell numbers and less actin and homing cell adhesion molecule staining over 48 hours. However, as this was investigating their effects on titanium it is less relevant to BRONJ patients.

2.8.2 3D effects of BPs

2.8.2.1 3D cell culture

While 2D cell culture is a useful tool, it is not fully representative of the true *in vivo* setting. As such, 3D culture systems have been developed to provide a greater understanding of the function of tissues. 3D systems allow for the inclusion of several cell types in an environment analogous to how they would be found *in vivo*, and thereby allow for cell-cell interactions and signalling similar to the native environment, making any studies performed with these tissues more physiologically relevant to the clinical scenario they are approximating.

Originally, 3D culture was performed on *ex vivo* pieces of tissue, maintained in a culture system [190], however due to limited availability, ethical issues, and high variability between samples, tissue engineered models have been developed.

The first full thickness, *in vitro* oral mucosa model was developed by Masuda *et al.* in 1996 [191] and involved contracted collagen gels containing fibroblasts, with keratinocytes seeded on top. A similar model was developed by Rouabhia and Deslauriers [192], involving collagen mixed with oral fibroblasts as an analogue to the lamina propria, with oral epithelial cells seeded four days later. The models were cultured at air-liquid interface (ALI), whereby the epithelial layer was in contact with air which caused stratification to occur. The tissue engineered mucosa was characterised and shown to express several cell markers and integrins involved in the interaction between the two cell types within the model, and cytokine analysis of the supernatants demonstrated the presence of interleukins.

This model was developed further by Dongari-Bagtzoglou and Kashleva [190], who used immortalised keratinocytes to increase the reproducibility of the model and the precision of any results generated, as the donor variability found in primary culture can lead to differences in the behaviour of the epithelium when stratifying [193]. Along with collagen, other natural materials have been used as scaffolds for tissue engineered oral mucosa, including gelatin and fibrin. These models have some disadvantages, primarily in the poor mechanical properties of the scaffold material [194]. In response to this, several compounds have been added to these in an attempt to improve the mechanical properties while also improving biological activity. For example, chitosan, a naturally derived polysaccharide has been added to both collagen and gelatin based scaffolds with good results [195], [196].

As well as modification of the natural materials, scaffolds from other sources have been developed in order to overcome the issues. Scaffolds have been derived from skin, with acellular dermis common, whether from a commercial source (e.g. AlloDerm™) or prepared in the lab (e.g. de-epidermised dermis (DED)). DED is prepared by removing the

epithelium and dermal fibroblasts from split thickness skin [197]. As these models already contain the structural architecture desired in the 3D model, they have the benefit of creating models that more closely represent the native environment, however they rely on the regular sourcing of donor skin. Through the seeding of oral cells, these scaffolds have been used to develop reproducible organotypic oral mucosa models which appear similar to native tissue with histology (Figure 2.15) and immunohistochemistry [198]–[200].

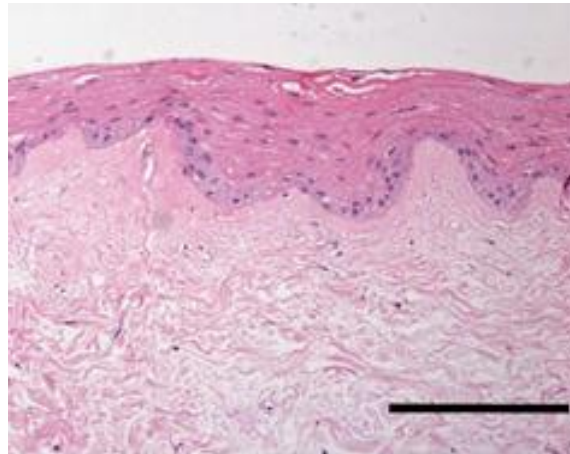


Figure 2.15. An example of a 3D oral mucosa model. Primary oral fibroblasts and keratinocytes cultured on DED for 14 days. Scale bar = 200 μ M. Reproduced with permission from Colley *et al.* [199].

The oral mucosa sits above bone, and as such, the inclusion of a bone component in a 3D organotypic oral mucosa model has also been tested. In a study by Almela *et al.* [201], HA/tricalcium phosphate (TCP) discs were placed in suspension with an osteosarcoma cell line for three months to allow cells to invade and mineralize, creating something similar to human alveolar bone. A collagen based mucosa model was then fixed to the top of the disc with fibrin glue, shown in Figure 2.16. Bae *et al.* [202] placed rat calvariae on an acellular collagen gel, then directly seeded oral fibroblasts in a collagen gel onto the bone component, with keratinocytes seeded on top three days later. While these scaffolds increase the physiological relevance of the model, they introduce another layer of complexity to the seeding process. Differing cell types require different cell culture media, and the bone layer is thought to prevent the delivery of the culture medium to the epithelium [201], [202]. The optimisation of these models is a significant step to overcome before they can be used for further analysis.

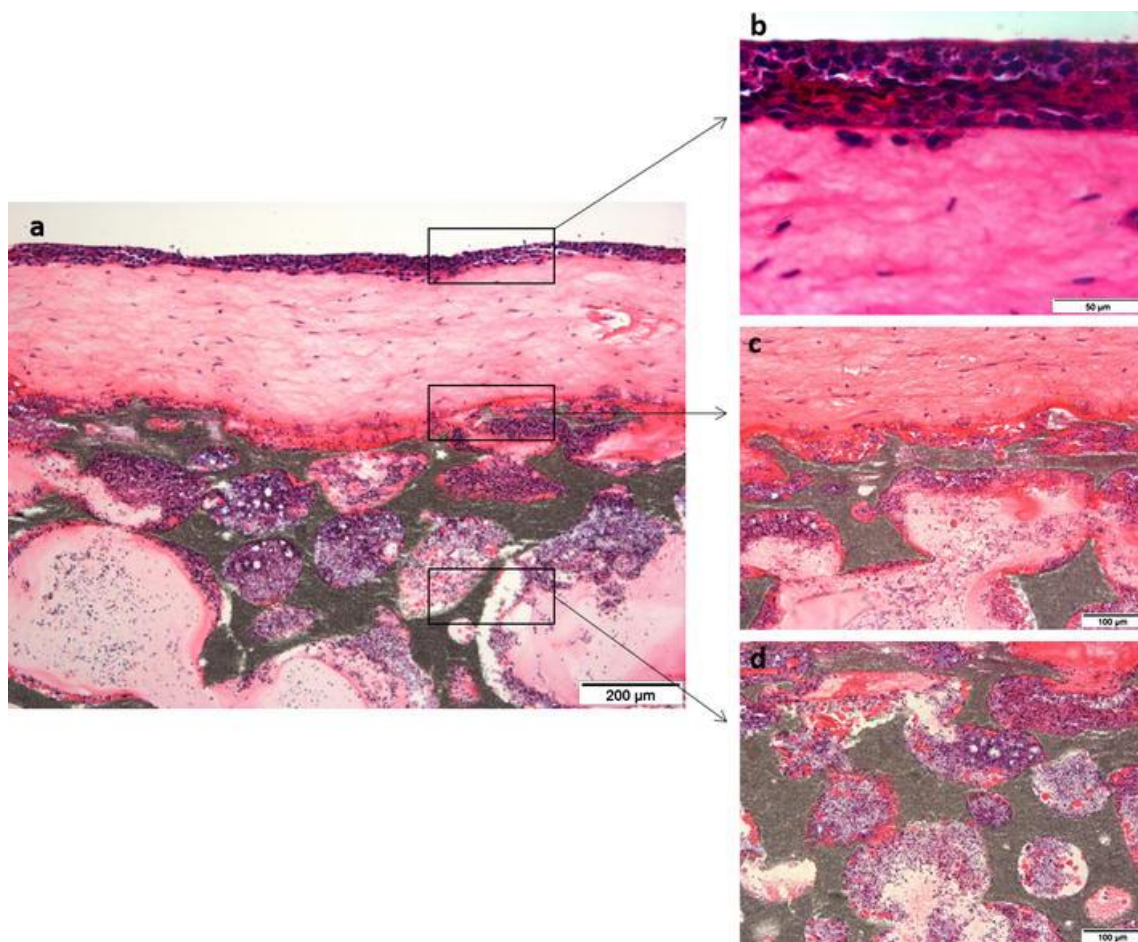


Figure 2.16. H&E stained sections of a collagen based oral mucosa model with bone component. Reproduced with permission from Almela et al. [201] under a Creative Commons license.

2.8.2.2 Use of organotypic 3D wound models

The development of organotypic models allows for the study of tissue response to certain conditions, including wounding. Several different wounding methods have been developed. Both hot and cold burning, whereby a metal rod was heated with an element or cooled in liquid nitrogen, before applying to a model for a set amount of time have been shown to give repeatable healing wounds [94], [203], [204].

Sharps have also been used for the same purpose. Kim *et al.* [164] used a biopsy punch to create a circular wound in the epithelium of an oral mucosa model, and demonstrated the re-epithelialisation of the wound. Scalpels have been used similarly [198], [205]. These wounds, however, have issues with reproducibility and analysis [206], and therefore other methods have been studied. These include modifications to current methods – e.g. an ‘excision tool’ made from two scalpels fixed together [187] – or modifications to the seeding process.

One prospective solution is through selective seeding of cells, creating a space in the epithelium of a known size, and examining how this gap closes over time, similar to a 2D migration assay. This has been done by using a stainless steel ring to create an exclusion zone where cells cannot adhere using both skin, in a model devised by the MacNeil group, and a commercially sourced collagen scaffold [207], [208]. Another method involved placing sterile plastic strips over a collagen model prior to the seeding of keratinocytes, then removing the strip following the formation of an epithelium [209]. These models are not ideal, however. In the model devised by the MacNeil group, large amounts of DED and primary cells are required [207]. When using a collagen model, the dermal equivalent is less representative of the *in vivo* scenario [194]. As such, a more representative model using fewer cells would be ideal.

The use of 3D *in vitro* models also allows for more in depth assessment of tissue response to wounding. Assaying allows for *in situ* analysis of cell response, and histology and immunohistochemistry give a representative sample of the tissue as a whole at specific time points. Several assays have been used in oral mucosa models to assess the cellular response to wounding. These include basic cell viability assays – such as the MTT assay [94] – more complex assays for specific proteins – including VEGF & hepatocyte growth factor [203] and lactate dehydrogenase [209] – and assays looking for specific cytokines thought to be present in the supernatant [94], [164], [203]. These models can also be fixed and processed for histology to allow further analysis.

Histology allows for the staining of specific substances to gain a further understanding of how the wound healing occurs at certain time points. Haematoxylin and eosin (H&E) staining is often used [94], [187], [198], [202], [209] to give a general picture of the tissue by staining nuclei violet and cytoplasm pink, with the contrast provided by this stain showing tissue morphology. Further information can be gained through

immunohistochemistry – the selective binding of a variety of proteins using specific antibodies [210]. This allows for the detection of specific proteins – e.g. different collagen varieties known to be found in various regions within tissues [203] – and also allows markers of specific processes – e.g. Ki67, a proliferation marker [198].

2.8.2.3 3D *in vitro* effects of BPs

To gain a greater understanding of how BPs effect oral tissues, a variety of 3D oral mucosa models have been used to examine BP effects. The effects of BPs on both healthy and healing tissue have been investigated, to examine both general BP effects on the oral mucosa and how BPs may contribute to the development of BRONJ following the introduction of a wound prior to the condition.

The effects of BPs on epithelial development have been investigated. McLeod *et al.* used a collagen/matrigel model with an OKF6 epithelium to study the effects of sub-toxic BP levels on epithelial development [173]. They treated models with 1 μM ZA for 7 days immediately after raising to ALI, and through histology saw no differences between the models. With or without BP treatment, the epithelium was able to stratify as normal. However, as ZA concentration in BRONJ patients is known to rise above 1 μM [142], more study is needed to fully examine the effects of BPs on epithelial development.

BP effects on healthy mucosa equivalents have also been examined. A study by Bae *et al.* [202] introduced a less potent but fluorescently labelled version of ZA on a collagen model with immortalised keratinocytes, including a rat calvariae bone layer, to examine the localisation of the drug. The model was allowed to stratify at ALI for 1 week before treating with the drug for a further week. When examined, BPs were found in both the bone and outer layers of the epithelium, even though the mucosal section of the model was never in direct contact with the drug containing media. The calcium content of the outer epithelial layers is higher than the basal layers [211], which therefore suggests that even within the epithelium, the calcium binding affinity of BPs plays a role in its effects. They also used standard ZA at a 4 μM concentration, and saw a reduction in epithelial thickness due to loss of the keratinised outer layers of the epithelium, where the fluorescent BP had localised. It was theorised that low levels of BPs may localise to the soft tissue prior to the BRONJ-precipitating event, and be released following the damage to the soft tissues, potentially explaining part of the pathway by which BRONJ develops.

A reduction in epithelial thickness was also seen by Ohnuki *et al.* when keratinocytes alone were seeded on AlloDerm® (a commercially available cadaveric dermis) [177]. The model was raised to ALI and allowed to stratify for a week before treating with 10 μM ZA for a further week. However, rather than a reduction in the keratinised outer layers, they saw effects on the basal cells. As mentioned in section 2.8.1.3, further testing showed basal cells proliferated less with BP treatment, due

to the drug arresting cells in the S phase of the cell cycle. The group then took this further, seeding AlloDerm® with both primary oral keratinocytes and fibroblasts, then treating with 10 µM ZA at ALI from day 8 to 19 of culture [187]. Using the 'excision tool' described in section 2.8.2.2, they created a wound in the epithelium of the model, and found ZA slowed the healing significantly. Through further staining, they determined this to be due to a reduction in proliferation, and reduction in expression of the $\alpha_v\beta_6$ integrin, indicating BPs prevent the intracellular signalling mechanisms which promote wound healing.

Kim *et al.* also saw a reduction in epithelial thickness with BP treatment [164]. A collagen model with primary oral cells was treated with 10 µM PA from day 5 of culture to day 14. They saw a thinner basal layer and intact keratinised layers, and suggested that BP treatment may speed up keratinocyte differentiation. To examine wound healing, they created a biopsy punch wound on culture day 7. PA prevented these wounds from healing and further examination again pointed to a lack of proliferation. These studies represent a promising start in examining the effects of BPs on healthy mucosa, but more detail is required.

2.8.3 Models of BRONJ

While *in vitro* testing allows for the study of individual mechanisms within BRONJ pathology, *in vivo* studies give a broader view of the disease. Ethical issues limit the *in vivo* work able to be done in humans, however. Inducing BRONJ in a patient is unethical, and including untreated control groups in studies goes against treatment guidelines [150]. For these reasons, animals have been used in the *in vivo* assessment of BRONJ.

Small animal models (mice, rats and rabbits) are the most common [212]. BRONJ can be induced in rodents with relative ease, with 80 – 100 % of animals developing the disease after short term BP treatment and a tooth extraction [213]. The animals exhibit a wide range of the expected symptoms, including limited mucosal wound healing, decreased vascularisation, and increased inflammation and microbial colony formation. Often these models are of 'high-risk' BRONJ, using high doses of ZA to mimic the more severe cases of the disease [151]. These models are already in use in examining potential BRONJ treatments, with some success [214], [215].

While small animal models have benefits in comparison to large animals, including a lower cost, higher level of reproducibility, ease of handling, and fewer ethical issues, they also come with drawbacks [151], [213], [214]. Mice and rats have faster metabolisms than humans, meaning dosing them in a way that can extrapolate meaningfully in relation to humans is difficult [216]. Their bones also remodel differently to humans, and have differences in the anatomy and structure of the jaws [217]. A potential solution for this is the use of larger animal models, and as such, there has been some development of these

with beagle dogs and minipigs [216]–[218]. Both these animals are closer to humans anatomically and have similar microflora in the mouth.

Allen *et al.* attempted to develop a BRONJ model using beagle dogs [218]. Dogs were treated with ZA for 3 months, using doses comparable to those of metastases patients, with a tooth extraction after 1 month. In all cases, post-surgical healing was impaired, however only in 1 of 6 of the dogs was BRONJ induced, hence this model is unsuitable for further BRONJ investigations.

A more robust large animal BRONJ model has been developed in minipigs. This was first reported in a paper by Pautke *et al.* in 2012 [216] and developed further by the same group in 2017 [217]. In their model, the minipigs were treated with ZA infusions for 20 weeks, with some receiving molar extractions taking place at week 12. This work successfully induced BRONJ in all animals treated with BPs and receiving a tooth extraction, and also in some animals without extractions in areas of infection, confirming the theory that infection plays a key role in BRONJ development. This repeatable model offers a potential mechanism by which to further study the pathophysiology, however was not without drawbacks.

Though animal models are useful, there are ethical implications involved. The 3Rs (replacement, reduction, refinement) advocate for the use of methods which do not require animal studies, the reduction in number of animals per study and the minimisation of the suffering of the animals involved in the studies [219]. As current animal models aim to create a severe version of the disease, this can lead to issues in the welfare of the animals used. Animals in the minipig studies suffered weight loss as their BRONJ became too severe for them to eat sufficient food [217]. An *in vitro* model would hence be a useful tool in the study of BRONJ in its development, bridging the gap between 2D cell culture and *in vitro* models and thereby allowing for a reduced number of animal models.

2.8.4 Novel BRONJ treatments

Due to the lack of consistent success with current BRONJ treatment methods, there has been widespread investigation into potential novel methods to either treat the disease or prevent its development post-extraction. This section covers five areas of research: full reversal of BP effects, drug therapy to counter specific BP effects, reduction of BP concentration, improved surgical intervention, and cell based therapies.

2.8.4.1 Reversal of BP effects

Nitrogen containing BPs (nBPs) are more likely to cause BRONJ than first generation BPs, and as such, research into the prevention and treatment of BRONJ has a nBP focus. As nBPs inhibit the mevalonate pathway, introducing metabolites from the pathway that have

been inhibited has been suggested as a possible therapeutic agent to reverse nBP effects. Geranyl-geraniol (GGOH) is one such molecule. It was first demonstrated in 1999 that GGOH could be introduced as a way of reversing nBPs [220], [221]. Since then GGOH has been used to reverse a wide range of nBP effects including apoptosis [222], proliferation [86], [168], adhesion [144], [183], [222], migration [86], [144], [223] and anti-angiogenic effects [171]. These reports cover a wide variety of cell types, notably including oral fibroblasts and keratinocytes.

Several of the papers reviewed in section 2.8.1 also investigated the potential of GGOH as a method of counteracting nBP effects [86], [144], [164], [168], [171]. Cozin *et al.* demonstrated the ability of GGOH to counteract the effect of both ZA and PA in an *in vitro* study with primary human oral fibroblasts, adding GGOH alongside the BPs [144]. Cell proliferation was restored partially for cells dosed with PA and entirely for those dosed with ZA. This ability to reverse the effects of the nBPs is universal across the literature.

GGOH has also been investigated using *in vivo* models of BRONJ. Nagaoka *et al.* used GGOH in a murine model [215]. In brief, mice were treated with ZA for a total of 6 weeks. After two weeks, a molar was extracted, and GGOH was administered with the BP for the remainder of the study. Micro-computed tomography analysis demonstrated higher mineral density and bone deposition in mice treated with GGOH, in comparison to those treated with ZA alone. Koneski *et al.* examined local GGOH administration in a Wistar rat BRONJ model [214]. Rats were dosed once weekly with ZA for 5 weeks, and a tooth extraction was performed on day 21. A local 5 mM dose of GGOH was administered daily for 14 days after extraction. The GGOH treatment reduced infection rate, inflammation and bone exposure. The formation of new tissue was also increased, however, due to the level of BP already existing in the bone, tissue formation was not complete. Nonetheless, this is a promising avenue for exploration.

2.8.4.2 Drug therapy

Due to the wide range of BP cell effects, several therapies have been tested to reduce some of these in small studies. Dexrazoxane is an FDA approved, cytoprotective drug that can reduce cell apoptosis [34]. It has been investigated as a treatment for BRONJ, both *in vitro* and *in vivo*. Human osteoclasts and gingival fibroblasts were treated with ZA both alone and in conjunction with dexrazoxane. Cell viability improved compared to cells treated with ZA alone. Bio-Oss® (bovine derived HA granules) was loaded with ZA and dexrazoxane before implantation into the tibia of rabbits, and again, dexrazoxane was shown to be beneficial in counteracting ZA effects.

As infection is a key component of BRONJ, antibacterial treatments have been used in trials with some success. Sitaflaxacin is an antibiotic capable of killing quinolone-resistant bacteria. In a study by Ikeda *et al.* [150], 20 patients suffering from

either Stage 2 or 3 BRONJ were administered with the drug, for periods of 2 to 10 weeks, both as a standalone treatment and in conjunction with debridement and sequestration, depending on the severity of the BRONJ. In 19 of the cases, the infection was successfully removed and the BRONJ was either healed or in remission. However, it was not possible to include a control group in this study, due to ethical regulations. These drugs may provide a method of treating BRONJ, either alone or as part of a combination of methods.

2.8.4.3 *Reduction of oral BP concentration*

Prevention of BRONJ has been suggested as the best solution for the disease [159], and methods of reducing the oral concentration of BPs to allow full wound healing have been suggested [40], [131], [224]–[227]. These studies have focussed on the removal or replacement of the bound BP in bone.

BPs bound to bone can be replaced. Ethylenediaminetetraacetic acid (EDTA) is a calcium chelating agent with a higher affinity for calcium than BPs. A study by Elsayed *et al.* investigated using EDTA to prevent BRONJ in a rodent model [40]. They successfully demonstrated that rinsing an extraction socket with EDTA following surgery prevented the development of BRONJ in rats treated with ZA. The previously bound ZA was rinsed away using a saline solution.

Interestingly, less potent BPs have also been suggested as a BRONJ treatment method, replacing the previously bound BPs with a BP less likely to cause BRONJ [131]. In a study by Oizumi *et al.*, etidronic acid was able to expel the previously bound nBPs from bone in mice [226]. It was hypothesised that replacing the bound nBPs with the less potent etidronic acid would reduce the risk of BRONJ development while still maintaining some BP effect. A small clinical trial had success, with etidronic acid promoting the recovery of soft tissues while maintaining some reduction in anti-resorption [227].

BPs can be modified to be fluorescently labelled, which reduces their potency [202]. Two studies have used these fluorescently labelled BPs *in vivo* in rodents, and demonstrated that these BPs lead to reduced BRONJ development, again indicating the success of localised BP concentration reduction [224], [225].

2.8.4.4 *Improved surgical intervention*

As explained in section 2.7, surgical intervention has demonstrated some success in BRONJ treatment but is not without complications. In order to improve the success rate of these treatments, different methods have been suggested, including antimicrobial and laser therapy [228], [229], improved coverage of the wound [151], [230], [231] and fluorescent markers to allow better detection of necrotic bone [160].

Several papers have investigated the use of laser based therapies in BRONJ treatment [228], [229], [232], [233]. Antimicrobial photodynamic therapy (aPDT) is a process whereby a photosensitive dye is applied to an area, then a laser is used to excite the dye and introduce reactive oxygen species to the area, leading to the death of bacterial species [234]. Several case reports have shown the success of aPDT in treating BRONJ, however these are only small studies and further clinical trials are needed [228], [232], [233]. Low level laser therapy (LLLT), where a low energy laser is focussed on a wound, is theorised to be biostimulating, leading to less cell death and improved wound healing, although the mechanism is unclear, and is as yet unproven in wide clinical study [235]. In work by Momesso *et al.*, LLLT was demonstrated as successful in treating BRONJ, however this was also combined with a high dose of antibiotic treatment and removal of the implant that had triggered the BRONJ development, and as such, the specific effect of the LLLT is unclear [229].

Different methods have been demonstrated effective in closing the BRONJ soft tissue wound. Human amniotic membrane (HAM) is a biological dressing with several desirable properties for BRONJ treatment [231]. It is anti-inflammatory, anti-microbial and has low immunogenicity. In two cases where BRONJ was diagnosed after the slow healing of oral wounds, HAM was used as a dressing following a two month drug holiday and the removal of the osteonecrotic tissue. In both cases, the wounds were completely asymptomatic 180 days later. Mucoperiosteal coverage of the damaged jaw has been demonstrated as a preventative measure in Wistar rat BRONJ models [151], [230]. This is thought to be due to an increased blood supply and prevention of bacterial contamination, however this was not successful as a treatment in all cases, and is less likely to be successful in later stages of BRONJ (and potentially not possible) due to the amount of coverage required.

As detecting necrotic bone is difficult, surgical intervention to remove necrotic bone is a complicated procedure and can often effect healthy bone [160]. Tetracycline is a fluorescent compound which can be used as a marker for osteonecrosis [236]. A study by Otto *et al.* used this method during surgical intervention on 54 BRONJ patients and demonstrated an 86 % success rate in treating BRONJ legions [160]. However, 10 % of legions relapsed and 4 % of legions did not heal following this surgery. While this is a relatively high level of success for BRONJ treatment, further improvement is required.

2.8.4.5 Cell-based therapies

Cell-based therapies are an exciting avenue within tissue engineering, and, as such, have also been noted for their potential to treat BRONJ. Stem cells have immunomodulatory properties and secrete growth factors to improve healing [151]. Several studies have indicated mesenchymal stem cells (MSCs) as successful BRONJ treatments in murine

and porcine models, and there are case reports of their successful use in humans [237]–[240]. Barba-Recreo *et al.* used the previously defined ‘high-risk’ BRONJ model to examine the suitability of adipose-derived mesenchymal stem cells (AdMSCs) as a BRONJ treatment method [151]. They placed AdMSCs into the sockets following molar extraction before covering with a mucoperiosteal flap and suturing. The cell therapy significantly reduced the incidence rate of osteonecrosis, and increased the number of osteoclasts found in the sockets and thereby also improving resorption rate. While this is positive, as discussed in section 2.8.3, the limitations of small animal models of BRONJ mean further study is required before this has widespread use in humans.

2.9 Bone filler materials – a potential BRONJ treatment method?

Preventative treatment has been identified as the best solution for BRONJ, due to the potential severity of the condition and the difficulties in treatment [1], [40], [159]. Reduction of the oral concentration of BPs has been demonstrated to reduce the development of BRONJ *in vivo* [40], [131], [224]–[227]. We hypothesise that due to the known BP affinity for calcium, calcium phosphate bone filler materials could reduce local BP concentration.

Calcium phosphate bone fillers would be advantageous in the treatment of BRONJ. Their ability to bind and retain BPs has been demonstrated [241]. They are already approved and in use following the surgeries that make up BRONJ preceding events [242]. This would allow for a combined effect for a BRONJ patient: both reducing the BP concentration to which the oral mucosa is exposed, while also promoting faster healing of the bone wound. Ideally, a solution would also allow vascularisation so as to prevent osteonecrosis, promote soft tissue healing, and prevent infection. However these may be less important if the condition can be prevented from developing, or stopped early.

As tooth extraction is the precipitating event for BRONJ over half the known cases, a treatment that could be implanted following this surgery would have the most impact on the condition, and therefore this review explores the potential of bone filler materials which could be used for BRONJ prevention in tooth extraction sockets.

2.9.1 Common bone filler materials

Though bone has a high regenerative potency, graft materials are often used to enhance bone repair. Autologous bone grafts are currently the gold standard as they are osteoinductive, however they come with certain limitations, such as donor site morbidity and low quantity of available graft material [243]. In BP patients, grafting from another area could lead to more severe complications as the donor site may experience poor healing. Allografts have some use, however they are only osteoconductive, and their regenerative potency varies relating to the age of the donor [244]. There is also the risk of viral

transmission and an immune response [243]. Xenografts are currently the most widely used in dental applications [245], but have a risk of viral transmission, have a costly production process, and lead to religious and ethical objections [246]. Synthetic materials similar to the mineral phase of bone - such as HA and beta tricalcium phosphate (β -TCP) [247] – have thus been developed as alternatives, due to increased availability, lower risk of disease transmission, and easy control over structural properties. Further tailoring of the chemical structure of HA is possible, including the introduction of other ions, which allows for a more application specific material [248].

HA has the benefit of being osteoconductive, non-toxic, not triggering an inflammatory or immune response, and being highly resorbable [52], [249]. Once implanted, it is resorbed and transformed into autologous bone. However, HA implants are often sintered, which reduces their porosity [250]. This lack of porosity can interfere with osteogenesis and angiogenesis, and therefore differing methods of incorporating these materials in implantable forms have been studied, and various commercially available clinical forms exist.

In order to prevent BRONJ, the BP concentration in the mouth should be removed. The calcium containing nature of these materials make them suitable candidates for the binding of BPs, and this has been tested in several studies [251]–[253]. BPs' high affinity for calcium will theoretically lead to a slow release rate once bound [50]. While the ability of these materials to absorb BPs quickly [46] and be used as localised delivery methods for BPs has been confirmed [34], [49], [60], [251]–[253], their binding profile and release rate is largely unreported. A summary of different calcium phosphate bone filler materials is shown in Table 2.6.

Table 2.6. Evaluation of a variety of approved calcium phosphate bone filler materials for use in socket healing.

Material form	Structural properties	BP binding/release	Advantages	Disadvantages	References
Granules (e.g. Bio Oss®, ReproBone®)	Variety of sizes allowing for control of structure	Binding demonstrated though not quantified; release seen at a level toxic to cells	Positive results in comparison studies; animal derived granules current clinical leader	Low mechanical stability	[34], [60], [245], [246], [249], [252]–[260]
Powder (e.g. NanoBone®)	Variety of sizes allowing for control of structure	High level of binding demonstrated; no release studies	Control over structure allows for application specific use	Possible particle mobilisation	[52], [116], [260]–[266]
Paste (e.g. Ostim®)	Contains powder, therefore similar control of properties; highly resorbable	No studies, but contains powder	Shown to promote angiogenesis	First day pain	[116], [267]–[270].
Cement	Hardens after implantation; low porosity	Tested as localised delivery method - low release once set	Can be moulded to fit defects	Limited regenerative potential	[259], [271]

2.9.1.1 Granules

Granules are one of the most common forms of bone filler materials, with demineralised bovine bone matrix being the market leader in dental applications [246]. Porcine variants are also commercially available [245]. Granules are well tolerated, have a low toxicity and inflammatory response, and have been shown to be successful in the treatment of tooth extraction sockets *in vivo* in both human and animal models [249], [254], [258]–[260]. Due to the success of the granules, and the previously mentioned issues with xenografting, synthetic granules are also used clinically.

Various synthetic granules have been produced, including the commercially available ReproBone® (indicated for use in non-load bearing osseous defects), with the structure and composition of them easily tailored to suit the application. Differing sizes and porosities have been shown to have an effect on the substitution of new bone, with lower porosity increasing bone formation [249]. Altering the composition has also been tested [246], [255], with differing ratios of HA and β -TCP giving a control of bone regeneration rate. As β -TCP dissolves faster than HA, it provides areas for new growth while the HA provides structure [255]. Synthetic granules give similar positive *in vivo* bone regeneration results to their animal derived counterparts [245], [246]. However, one study indicated a higher inflammatory response from synthetic granules compared to bovine, although this was hypothesised to be due to the morphology of the granules, which were smooth with a low surface area [245].

Bio-Oss®, bovine derived HA granules, have recently been studied *in vivo* as a localised BP delivery system, confirming the ability to bind BPs [34], [60], [252], [253]. Synthetic granules have been demonstrated as BP loading devices [256]. The success of these studies suggests this binding is not permanent, with the amount released being sufficient to trigger necrosis in one study [252]. As the studies were focussed on determining the ability of the materials to function as localised delivery methods, the binding and release profiles were not reported. However, the binding and release profiles of granules of differing size and surface area were tested chemically in a study by Sørensen *et al*, which indicated that although ZA binding increased with surface area, so did the release of bound ZA [257]. This is an important consideration, as if BPs were released this could lead to BRONJ, rather than prevent it.

2.9.1.2 Powder

HA can be used as powder, such as NanoBone®, a nanocrystalline form. Nanohydroxyapatite (nHA) has been shown to have a similar chemical structure to naturally occurring bone [261] - as 60% of HA in bone is needle like and less than 100 nm on all axes [272] - and has a higher resorption potential than sintered HA [262]. As it is

synthetic it has advantages in both price and disease transmission, and has been demonstrated to perform similarly in bone healing compared to Bio-Oss® in humans [260]. Nanocrystalline apatites have been shown to improve the synthesis of pro-osteogenic factors, further improving bone healing [116]. These characteristics make nHA a promising material for use in regeneration of periodontal defects, and early studies have shown its potential in this field [260], [262], [263]. However, one drawback is the potential of the particles to mobilise and be transported to a different area of the body [264].

It is possible to tailor and improve the regenerative potential of nHA through modifying its chemical structure and delivery method. The introduction of magnesium has been shown to promote angiogenesis and osteogenesis [248], while nHA in a silica matrix (NanoBone®) is reported to be osteoconductive and biomimetic [250], have good angiogenic properties [139] and show no difference in regeneration to bovine granules [260].

nHA has also been used as a localised BP delivery method, with HA nanocrystals confirmed to have a high affinity for alendronic acid, with a slow release profile [52]. This binding takes place through a two-step reaction involving the substitution of a phosphate and the interaction of the BP with a Ca²⁺ molecule on the surface of the apatite [265]. Pascaud *et al.* [266] found that nanocrystalline apatites adsorbed more of the BPs than regular HA. The adsorption was proven to be irreversible under normal conditions, and it was demonstrated that the BP was only released in the presence of phosphate ions, reversing the ionic exchange process which originally bound the BPs. The affinity and adsorption of three different nanocrystalline apatites were also measured [49]. The apatites were analogues of freshly formed bone material and more mature bone. The study showed that the fresher material analogue had a higher affinity for, and bound more, tiludronic acid *in vitro*.

2.9.1.3 Paste

Aqueous pastes composed of nHA in water are also used in periodontal regenerations. The commercially available Ostim® is common and similar in regenerative potency to Bio Oss® [116], [267]–[270]. Pastes are viscous, bone-mimetic [269] and resorb quickly and completely [270]. In an experimental study by Canuto *et al.* [116] their potential as an extraction socket healing device was shown. In comparison to an unfilled socket in the same patient, Ostim® was evidenced to improve socket healing and epithelialisation, increase VEGF levels and improve the synthesis of pro-osteogenic factors. The Ostim® paste did unfortunately increase pain on day 1 following extraction, however it was suggested this may have been due to an inflammatory response being triggered, and therefore was an indication of the improved healing potential of the material. Conversely, a dorsal skinfold chamber study [269] demonstrated Ostim®'s lack of inflammatory

response *in vivo*. In this study, Ostim® was able to induce angiogenesis, with its degradation forming a scaffold into which cells could invade. While the ability to allow for angiogenesis would be important in a patient taking BPs, the pro-inflammatory response of the material could lead to BRONJ development and therefore confirmation of this effect or lack of it is required to allow for indication as to the use of HA paste as a potential BRONJ treatment device.

2.9.1.4 Bone cement

The use of calcium phosphates in setting bone cements also has a history in extraction socket healing, such as Bone Source™ [259], however they come with certain disadvantages. Once set, the cements have poor mechanical properties in comparison to the native bone and have issues with porosity [271]. The lack of porosity of the set cement inhibits the regeneration of bone, as cells cannot grow into the scaffold. As such, this cement is unlikely to be beneficial in BRONJ treatment.

2.10 Detection and quantification methods

To assess the ability of bone filler materials to bind BPs, the detection of BP concentration in solution is required. Detecting BPs is known to be a difficult process [273], [274]. The lack of a chromophore on several of the BPs has made determination difficult [275]. However, several methods have been developed for the quantitative detection of BPs. These methods are summarised in Table 2.7.

BP detection methods vary in complexity, with some methods available for direct detection, others using chemical agents to increase BP signal, and others using chromatographic processes to separate BPs before detection.

Direct detection of BPs has been performed with ultraviolet-visible (UV-vis) spectroscopy. The R₂ group of certain BPs works as a chromophore to allow detection [265], [276]. This method has successfully been used to determine BP concentration following binding with HA. In three papers from a group at the University of Toulouse, UV-vis spectroscopy was used to determine risedronic acid and tiludronic acid concentration after incubation with HA [49], [265], [266]. The use of this method to examine the BP binding properties of HA suggests a useful mechanism for work in this thesis.

As BP detection is difficult, methods of conjugating the BP to another molecule to allow for greater detection have been tested. Several of these also use UV-vis spectroscopy. One such method uses ninhydrin for the determination of alendronic acid [51], [52], [277]. The primary amine group reacts with the ninhydrin, whereby its colour can be determined using a UV-vis spectrophotometer set at 568 nm for detection, measured against a reagent blank. Cerium (IV) sulphate and copper (II) sulphate have been used to

determine the concentration of BPs with a hydroxyl group at the R₁ position [277], [278]. A novel method devised by Li *et al.* uses quantum dots synthesised from tea, which fluoresce [274]. The quantum dots bind to BPs, whereby their fluorescence is turned off. This allows for a quantitative measure of concentration that was tested in the presence of a variety of metal ions, including calcium. Fluorescence also plays a part in a paper from Gao *et al.* who bound BPs to a guanidinium-modified calix(5)arene molecule that turned on fluorescence, and again was quantifiable [279]. These methods however are novel and not optimised.

A much more well-defined method is chromatography, which separates molecules within a mixture to allow for detection of individual components. High-performance liquid chromatography (HPLC) is commonly used as a BP detection method [280], [281]. However, the polar nature and acidic characteristics of BPs make them difficult to separate and detect with standard measures [282]. Despite this, several ion pair chromatography methods have been defined for a wide range of BPs [273], [282]–[285]. These methods have also shown success in the determination of BP concentration following incubation with both HA and bone cement.

As well as the determination of BPs in solution, some work has been performed detecting BPs bound onto other structures through spectroscopic techniques. Fourier transform infrared spectroscopy (FTIR) has been used to detect the change in structure of a material following soaking in different BP solutions [49]–[51], [265]. The BP itself and the binding material before and after soaking in a BP were tested, and the spectra were compared. The technique was shown to be successful at confirming a change in composition during binding. Raman spectroscopy is a similar method which has also been successful in this task [265], [286]. X-ray photoelectron spectroscopy (XPS) is a technique used to determine the chemical composition of the surface of a material, and has been demonstrated as a method of BP binding determination [46], [51]. The nitrogen found in nBPs provides a simple method for detecting binding. XPS depth profiling can also be used to measure if the BP has diffused through a material, up to 260 nm [46]. This wide range of different BP detection methods suggest the possibility of measuring the binding of BPs to HA.

Table 2.7. Bisphosphonate concentration detection methods. AA = alendronic acid, CA = clodronic acid, EA = etidronic acid, NA, neridronic acid, PA = pamidronic acid, RA = risedronic acid, TA = tiludronic acid, ZA = zoledronic acid. HPLC = high performance liquid chromatography, UV-vis = ultraviolet-visible spectroscopy.

Detection method	BPs detected	Tested with interference?	Limit of Detection	References
Ceric (IV) sulphate with UV-vis	AA, EA, RA	No	2 µg/ml	[277]
Copper (II) sulphate with UV-vis	AA, CA, EA	No	1.55 – 2.13 mg/ml	[278]
Guanidinium-modified calix(5)arene with fluorescence detection	AA, CA, EA, NA, PA, RA, TA, ZA	Yes; artificial urine	0.1 µM	[279]
HPLC with evaporative light scattering detection	AA, EA, PA, ZA	No	15 – 18 µg/ml	[281]
Ion pair HPLC with UV detection	AA, PA, ZA	Yes; HA and bone cement	0.1 µg/ml	[273], [282]–[285]
HPLC with fluorescence detection	PA	Yes; blood and urine	0.1 µg/ml	[280]
Ion chromatography with UV detection	AA, CA, EA, PA, ZA	No	2.5 – 10 µg/ml	[276], [287]
Ion Chromatography with Cu ²⁺ complexation and UV detection	AA, CA, EE, NA, PA	No	0.4 µg/ml (PA)	[288]
Iron (III) chloride + UV-vis	AA, PA	No	2 µg/ml	[289]
Liquid chromatography-mass spectrometry	ZA	Yes; human bone	1 ng/mg	[290]
Ninhydrin with UV-vis	AA, PA	Yes; HA	3.75 µg/ml	[52], [277]
Quantum dots with UV detection	PA, ZA	Yes; metal ions	0.1 µM	[274]
UV-vis	RA, TA	Yes; HA	Not reported	[49], [265], [266]

3. Aims and objectives

The aims of this project were to investigate the effects of two BPs, pamidronic acid (PA) and zoledronic acid (ZA), on the oral mucosa, using a range of *in vitro* cell culture techniques, and to examine whether hydroxyapatite (HA) could be used as a localised BRONJ treatment method.

The main objectives of the work presented within this thesis were:

1. To investigate the 2D effects of PA and ZA on the viability, apoptosis, proliferation, migration and adhesion of human oral fibroblasts and keratinocytes.
2. To use a 3D oral mucosa model to examine BP effects at different stages of epithelial development.
3. To develop a 3D *in vitro* model of the soft tissue component of BRONJ.
4. To investigate whether HA can be used to bind BPs through different spectroscopic techniques.
5. To examine the ability of HA to locally reduce BP concentration in 2D and 3D using biological assays.

4. Materials and methods

4.1 Cell culture

4.1.1 Cell sources and media

All cell culture work took place in Class II laminar flow hoods (Esco), sterilised in 70 % industrial methylated spirit (IMS) (Thermo Fisher Scientific) prior to use. Incubation took place at 37 °C in 5 % CO₂.

Non-tumoral oral fibroblasts derived from the oral cavity (NHS REC ethics #09/H1308/66) were used from passage 2 to 10. They were cultured in Dulbecco's modified Eagle's medium (DMEM) (Sigma-Aldrich) with the supplements described in Table 4.1. Human oral keratinocytes, immortalised through transduction to prevent telomere shortening (OKF6/TERT-2) [179] were used from passage 4 to 25. The medium used for OKF6 cells in 2D was keratinocyte serum free medium (KSFM) (Gibco) supplemented as described in Table 4.2.

Primary human oral keratinocytes (NHS REC ethics #09/H1308/66) were used from passage 1 to passage 3. They were cultured in Green's medium, which is described in Table 4.3. When cultured in 2D, primary keratinocytes were cultured on a feeder layer of irradiated mural fibroblasts (i3T3).

Prior to experimentation, cell seeding densities were optimised for fibroblasts and immortalised keratinocytes (see Chapter 10). Primary keratinocytes were seeded according to a standard density within the laboratory.

Table 4.1. Dulbecco's modified Eagle's medium composition. All components from Sigma-Aldrich, except foetal calf serum, from Biosera.

Solution	Concentration
Dulbecco's modified Eagle's medium	88 %
Foetal calf serum	10 %
L-glutamine	0.01 mg/ml
Penicillin / streptomycin	100 i.u./ml / 100 µg/ml

Table 4.2. Keratinocyte serum free medium composition. All components from Gibco, except penicillin/streptomycin, from Sigma-Aldrich.

Solution	Concentration
Keratinocyte serum free medium	98 %
Bovine pituitary extract	0.05 mg/ml
Penicillin / streptomycin	100 i.u./ml / 100 µg/ml
Human recombinant epithelial growth factor	0.005 µg/ml

Table 4.3. Green's medium composition. All components from Sigma-Aldrich, except foetal calf serum, from Biosera.

Solution	Concentration
Dulbecco's modified Eagle's medium	66 %
Ham's F12 nutrient mixture	21.6 %
Foetal calf serum	10 %
L-glutamine	0.01 mg/ml
Penicillin/Streptomycin	100 i.u./ml / 100 µg/ml
Insulin	5 µg/ml
Hydrocortisone	4 µg/ml
Amphotericin B	0.625 µg/ml
Adenine	0.025 µg/ml
Cholera toxin	8.47 ng/ml
Epidermal growth factor	5 ng/ml
3, 3', 5-Tri-iodothyronine (T3) / Apo-transferrin	1.36 ng/ml T3 / 5 µg/ml apo-transferrin

4.1.2 Cell maintenance

Cells were maintained in T75 flasks (VWR) in an incubator, with media changes occurring at least once weekly. Confluency and viability was monitored using a phase contrast microscope (Motic). Cells were passaged when they were over 75 % confluent. Firstly, the media was removed, and the flasks were washed with phosphate buffered saline (PBS) (Oxoid). Trypsin-EDTA (Sigma-Aldrich), at a concentration of 5 mg/ml trypsin and 2 mg/ml EDTA, was added and cells incubated until detachment, before serum-containing DMEM was added to deactivate the trypsin. The cell-containing media was centrifuged for 5 minutes at 1000 rpm to form a cell pellet. The supernatant was discarded and the cell pellet resuspended in media, counted using a haemocytometer (Hawksley), and divided into flasks as necessary.

Prior to passaging NOKs, the i3T3 feeder layer was first removed with a 5 minute incubation with 0.2 mg/ml EDTA (Sigma-Aldrich). Following this, passaging took place as described above.

4.1.3 Primary cell isolation

Before the isolation of cells, Difco™ trypsin and collagenase A solutions were prepared. Trypsin 1:250 powder (BD Biosciences) was dissolved in 500 ml PBS to create a 0.1 % solution, which was then pH adjusted to 7.4 using an NaOH solution (Sigma-Aldrich) and sterilised with a 0.2 µm filter. This was supplemented with penicillin/streptomycin (0.01 mg/ml) and amphotericin B (0.625 µg/ml) and separated into 10 ml aliquots. Collagenase A (Roche) was prepared in DMEM, supplemented as described in Table 4.1, at a concentration of 0.5 mg/ml. Both solutions were stored at -20 °C and defrosted immediately prior to use.

Primary oral keratinocytes and fibroblasts were isolated from willingly donated sections of human buccal tissue removed by a dentist (NHS REC ethics #09/H1308/66). Samples were placed in Difco™ trypsin overnight to begin cell detachment. The sample was transferred to a petri dish, where forceps and a scalpel were used to gently remove the epithelium containing keratinocytes. The remaining biopsy was transferred to PBS containing penicillin/streptomycin and amphotericin B and refrigerated. The Difco™ trypsin/keratinocyte mixture was transferred to a universal tube. Green's medium was used to wash the petri dish and ensure all keratinocytes were collected, before adding them to the Difco™ mixture. This was then centrifuged for 5 minutes at 1000 rpm. The remaining medium was gently poured away, and the cells resuspended and added to a T75 flask containing an i3T3 feeder layer. Before the end of the day, the remaining biopsy was minced with a sterile scalpel, then placed into the collagenase A solution and incubated overnight in order to isolate the fibroblasts from the extracellular matrix.

The following day, the keratinocyte medium was replaced. Cells were then checked daily, with media changes as necessary until confluent. DMEM, supplemented as described in Table 4.1, was added to the collagenase containing the biopsy to deactivate the enzyme. This mixture was then centrifuged for 10 minutes at 2000 rpm. The medium was gently discarded, then resuspended in DMEM and added to a T25 flask (Thermo Fisher Scientific). Fibroblast growth was then monitored, and media changes performed as required, until confluent. Fibroblasts were then maintained in T75 flasks.

4.1.4 Preparation of de-cellularised dermis (DED)

Split thickness skin samples (NHS Ethics #15/YH/0177) were placed into a sterile 1 M NaCl solution (Sigma-Aldrich) and kept in an incubator at 37 °C for 24 hours, or until

the epithelium separated. Samples were transferred to a petri dish and the epithelium peeled off with forceps. The de-epidermised tissue was washed thrice in PBS and placed in DMEM containing penicillin/streptomycin and amphotericin B and stored at 5 °C.

When patient skin was unavailable, glycerol treated cadaveric skin (Euro Skin Bank) was used. To prepare for use, this was placed in PBS and incubated at 37 °C for up to 1 week, with daily PBS changes, to remove the glycerol. It was then prepared as with donor skin, using NaCl treatment and forceps to remove the epithelium before washing and placing into supplemented DMEM.

4.2 Bisphosphonates

Pamidronate disodium salt hydrate (Sigma-Aldrich) and zoledronic acid monohydrate (Sigma-Aldrich) stock solutions ranging from 1 to 25 mM were made by dissolving the powders individually in sterile distilled water. These solutions were aliquoted and frozen at -20 °C. Aliquots were thawed prior to each experiment.

4.3 Statistics

Prism 7 (GraphPad) was used to perform all statistical analysis, unless otherwise stated. Statistical significance was defined as $P \leq 0.05$. Standard deviation (SD) was used for all error bars. When experiments were performed in triplicate, the mean value of each technical were repeat were averaged and the three values used to give $N = 3$. 'N' is used to denote experimental repeats, while 'n' is used to denote technical repeats throughout.

In most cases, both time and BP concentration were independent variables, and therefore repeated measures two-way analysis of variance (ANOVA) tests were performed to confirm significance between groups. Dunnett's multiple comparison tests were then carried out as post-hoc analysis to investigate the significance between BPs and control medium (0 μM) at each time point. These tests were used except where otherwise noted.

5. The effects of bisphosphonates on human oral fibroblasts and keratinocytes in 2D

5.1 Aim

To examine the effects of pamidronic acid (PA) and zoledronic acid (ZA), two BPs most commonly associated with BRONJ, on cells of the oral mucosa *in vitro* in 2D.

5.2 Introduction

While osteonecrosis is a major part of BRONJ, the soft tissue component of the disease is hypothesised to be key to its development [2]. BRONJ is partly defined as “exposed bone or bone that can be probed through an intraoral or extraoral fistula(e)” [1], [123]. It is clear that the oral mucosa becomes damaged and fails to heal following the dental events leading to most cases of BRONJ, and the exposure through the surrounding mucosa leads to infection and the spread of the disease across the jaw. In cases where BRONJ has been successfully treated, the procedures have involved the closure of the oral mucosa wound through surgery [157]. This is not always possible, however, due to the limited availability of tissue to cover the wound, and the BP effects on the soft tissue. While the BP effect on bone remodelling and wound healing is a clearly defined pathway, the effects on the oral mucosa are less well defined.

Several studies have looked at a variety of BP and their effects on oral mucosa cells, with studies looking at toxicity, apoptosis, migration, proliferation and other processes. However, several different conclusions have been reached. While most studies agree that clinically relevant concentrations of BPs are toxic to oral mucosa cells [57], [144], [168]–[170], [175], there is a lack of consensus on the concentration at which this toxicity occurs, and low levels of BPs have been demonstrated to have a positive effect on keratinocytes [178]. The mechanism by which BPs cause toxicity is also not clear, with keratinocytes reported to undergo apoptosis [142], [175] and senescence [164]. BPs have also been shown to both promote [86], [140] and prevent keratinocyte migration [35]. The large number of different BPs also contribute to the wide-ranging spread of existing data on BPs with a lack of central consensus.

This chapter presents a comprehensive study of the effects of two BPs on the toxicity, proliferation, migration and adhesion effects of BPs on oral mucosa cells. Fibroblasts and keratinocytes derived from human oral tissue were used so as to be physiologically relevant. PA and ZA were used as they are two of the most commonly associated BPs with BRONJ [153], [163]. PA is largely used to treat osteoporosis and is taken both orally and intravenously, while ZA, as the most potent BP, is prescribed for

bone metastases patients and only administered intravenously. The concentrations used ranged from 0.1 to 200 μM , as these are within the expected range found in BRONJ patient mucosa, based on patient saliva and estimated bone concentrations [57], [142], and have previously been shown to effect cells of the oral mucosa.

5.3 Materials and methods

Cell culture was performed as described in section 4.1. BPs were prepared as described in section 4.2. Throughout this chapter, medium containing no BPs (0 μM) was used as a control.

5.3.1 MTT assay

3-(4,5-dimethylthiazol-2-yl)-2,5 diphenyl tetrazolium bromide (MTT) powder (Sigma-Aldrich) was dissolved in PBS at a concentration of 0.5 mg/ml. This took place in a fume cupboard, due to the mutagenic nature of MTT. This was then sterilised with a 0.2 μm filter. The MTT solution was stored at 4 $^{\circ}\text{C}$ for up to two weeks, protected from light. 100 ml isopropanol (Thermo Fisher Scientific) was acidified with 125 μl of 10 M hydrochloric acid (HCl) (AnalaR).

Cells were seeded at the densities described in Table 5.1. All seeding took place in triplicate, with three wells per drug concentration. One plate was seeded per time point as MTT is an endpoint assay. BP stock solutions were diluted in media into concentrations from 0 to 100 μM . At 24 hours after seeding, the media was removed from the cells, and replaced with BP containing media in triplicate, before incubating further.

At 24, 48 and 72 hours after treating, one of the plates was removed from the incubator. Media was removed and replaced with 500 μl of MTT solution (24 well plate) or 100 μl (96 well plate), and incubated depending on cell type in accordance with Table 5.1. Following incubation, the remaining MTT solution was removed, and 125 μl acidified isopropanol was added to elute the stain. 100 μl from each well was transferred to a 96 well plate, and absorbance measured in a plate reader (BioTek ELx800™). Readings were taken at 540 nm, with a reference at 630 nm.

Table 5.1. Seeding densities and incubation times for the MTT assay

Cell Type	Well plate	Seeding density (cells per cm^2)	Incubation time
Fibroblasts	24	1.0×10^4	90 minutes
Immortalised keratinocytes	96	1.67×10^4	40 minutes
Primary keratinocytes/i3T3 fibroblasts	24	$1.0 \times 10^4/5.0 \times 10^3$	60 minutes

5.3.2 Apoptosis and necrosis assay

Fibroblasts were seeded at 5.55×10^3 cells per cm^2 and immortalised keratinocytes at 1.67×10^4 cells per cm^2 in a 6 well plate and left to attach overnight. The media was removed from each well and replaced with BP containing media of a range from 10 to 100 μM PA and 0.5 to 50 μM ZA. PBS containing 1 % saponin (Sigma) was used as a positive control for necrosis and added for 2 hours prior to the staining. As an apoptosis control, 30 % hydrogen peroxide (Sigma) was added and incubated for 5 minutes prior to staining.

At 72 hours, cells were stained using an Annexin V-fluorescein isothiocyanate (FITC) kit (Trevigen). Cell medium was collected from each sample and centrifuged at 6000 rpm for 5 minutes to collect any dead cells. Wells were then trypsinised and centrifuged. All centrifuged samples were resuspended in cold PBS. The pellets from both the medium and trypsinised cells for each sample were combined, and then these suspensions were centrifuged again. Staining took place as per the kit, in 100 μl solution containing 10 μl binding buffer, 10 μl propidium iodide (PI), 1 μl Annexin V-FITC and 79 μl distilled water. Samples were incubated at room temperature, protected from light for 15 minutes, then 400 μl of binding buffer was added. As controls, both unstained and single stained cells were also prepared by the same method.

Cells were analysed using a flow cytometer (BD Biosciences FACSCalibur™), using a 488 nm laser. Annexin V-FITC fluorescence was determined with a 530/30 nm filter, and PI fluorescence using a 650 nm long pass filter. A preliminary gate was set to remove debris and samples were processed so that 10,000 gated cells were analysed per sample. If 10,000 cells were not present due to toxicity, cytometry was performed for 5 minutes at the highest speed setting. Analysis was performed using CellQuest Pro™ (BD Biosciences), where a gate was applied to remove cell debris, and fluorescence gates, set using the single stained cells and positive controls, were applied to separate viable, necrotic and apoptotic cells. Cells were determined to be early apoptotic if they were stained with Annexin V alone, necrotic if they stained with PI alone, and late apoptotic if they were positive for both stains. Unstained cells were determined to be viable.

5.3.3 Mitomycin C optimisation

Mitomycin C (Sigma-Aldrich) was dissolved in distilled water in a fume cupboard at a concentration of 500 $\mu\text{g}/\text{ml}$ and sterilised with a 0.2 μm filter, then aliquoted and snap frozen in liquid nitrogen. It was stored at -80°C , protected from light and thawed prior to each experiment.

Cells were seeded in 6-well plates at densities of 4×10^3 (fibroblasts) or 5×10^3 (immortalised keratinocytes) cells per cm^2 . 24 hours after seeding, the media was removed

and replaced with media containing Mitomycin C at concentrations ranging from 0 µg/ml to 10 µg/ml. After 4 hours, the media was removed, the wells were washed with PBS, and the media replaced.

At time points between 24 to 96 hours, media was removed and wells were washed with PBS. To detach cells, 400 µl of trypsin-EDTA was added to each well and the plate was incubated for 5 minutes (or until cells detached). 400 µl of media was added to the wells to deactivate the trypsin. Three samples were taken from each well, and cell counts were performed using a haemocytometer.

5.3.4 Proliferation assay

CellTrace™ CFSE dye (Thermo Fisher Scientific) was dissolved in dimethyl sulfoxide (DMSO) (Thermo Fisher Scientific) at a concentration of 5 mM and stored at -20 °C. Prior to the assay, this stock was diluted into a 0.1 % bovine serum albumin (BSA) (Sigma-Aldrich) solution in PBS, to a working concentration of 2 µM. Fibroblasts and immortalised keratinocytes were independently trypsinised, counted, and resuspended in the CFSE solution, at a density of 1×10^6 cells per ml, before incubating at 37 °C for 10 minutes. Following this, 10 ml of cold DMEM was added to quench before incubating on ice for 5 minutes. Cells were then centrifuged at 1000 rpm for 5 minutes, the supernatant removed and cells resuspended in the 0.1 % BSA solution twice, before a final centrifugation. Following this, fibroblasts were seeded at 5.55×10^3 cells per cm^2 and keratinocytes at 1.67×10^4 cells per cm^2 in a 6 well plate. Unstained cells were also seeded as a control

The following day, the medium of one well was replaced with mitomycin C containing medium at a concentration of 2 µg/ml for fibroblasts and 0.5 µg/ml for keratinocytes. Plates were incubated for a further 4 hours, before media from all wells was removed, and replaced with BP containing media of a range from 10 to 100 µM PA and 0.1 to 50 µM ZA.

At 24 and 72 hours, cells were trypsinised and resuspended in a 10 % formalin (37 % formaldehyde (Sigma-Aldrich) in PBS) solution and left for 30 minutes to fix. Cells were then centrifuged at 6000 rpm for 5 minutes and resuspended in a 1 % BSA solution in PBS.

Fluorescence intensity was analysed using a flow cytometer, with a 488 nm laser with a 530/30 filter. As before, a preliminary gate was set to remove debris and samples were processed so that 10,000 gated cells were analysed per sample. Analysis was performed using CellQuest Pro™ where a gate was applied to remove cell debris. The mitomycin C treated, non-proliferating cells were used to calculate a proliferation index (I_{pit}), as shown in Equation 5.1.

\tilde{x}_{npf} = no proliferation median \tilde{x} = sample median

$$\frac{\tilde{x}_{npf}}{\tilde{x}} = I_{plf}$$

Equation 5.1. An equation to convert median fluorescence intensity to proliferation index.

5.3.5 Migration assay

Oris™ stoppers (Platypus Technologies), shown in Figure 5.1, were placed into 96 well plates in assumed sterile conditions, using the provided stopper tool. Fibroblasts were seeded in sextuplicate at a density of 5.4×10^4 cells per cm^2 , and immortalised keratinocytes at 1.33×10^5 cells per cm^2 . 24 hours after seeding, media containing mitomycin C was added to the wells to make an overall concentration of $2 \mu\text{g/ml}$ for fibroblasts and $0.5 \mu\text{g/ml}$ for keratinocytes. They were then incubated for 4 hours. Following this, the stoppers were removed and the media replaced with BP containing media at a range of 1 to $30 \mu\text{M}$ for PA, and 0.1 to $10 \mu\text{M}$ for ZA. Fibroblasts were also treated with $30 \mu\text{M}$ PA for 72 hours in a tissue culture flask before seeding by the same process and treating with $30 \mu\text{M}$ PA.

The stopper created a 2 mm circular exclusion zone in the centre of the wells. A phase contrast microscope (Motic AE2000) was used to image the wells at 0, 24, 48 and 72 hours for fibroblasts and 0, 8, 16 and 24 hours for keratinocytes. If the exclusion zone between cells was too large for one image, two images were taken and combined in Photoshop CS2 (Adobe). A diagrammatical representation of the seeding process is shown in Figure 5.2.

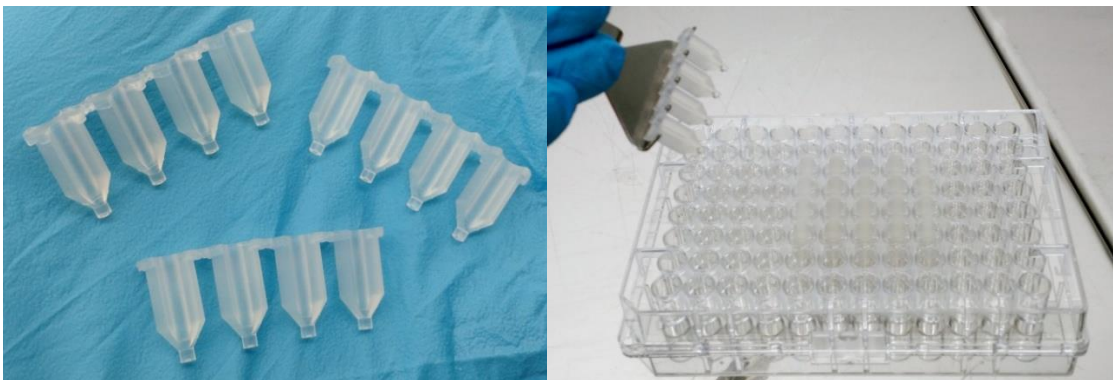


Figure 5.1. Oris™ migration stoppers, and being placed into a 96 well plate.

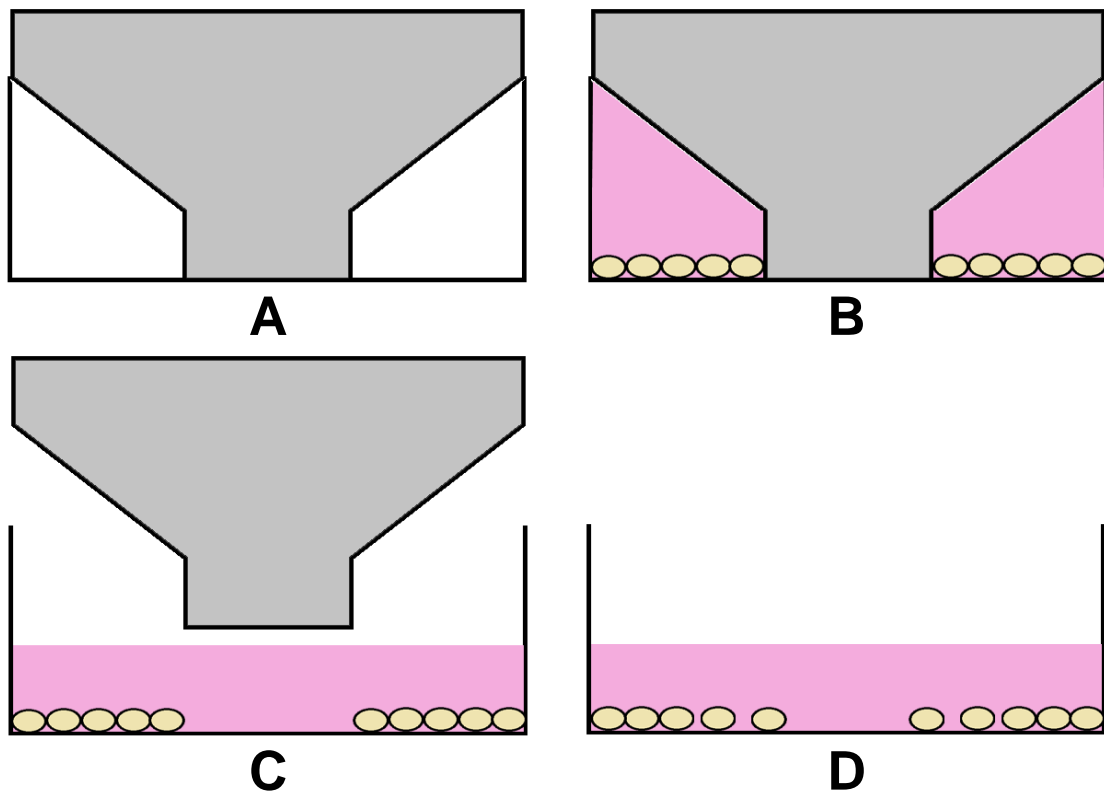


Figure 5.2. Cross sectional diagram of the migration assay setup. (A) Stopper placed into 96 well plate. (B) Cells seeded at high confluence. Mitomycin C is added after cells have adhered. (C) Stopper removed and media replaced. (D) Cell migration tracked.

At each time point the area of the exclusion zone was measured using ImageJ (National Institute of Health). A circle was drawn, as demonstrated in Figure 5.3, and the area of this circle was then calculated by the software. Care was taken to create a circle that best approximated the exclusion zone. Migration rate was calculated by expressing each measurement as a percentage of the area of the original zone. A graphics tablet (Wacom) was used to trace around the edges of the exclusion zone and measure migration more accurately. However, no differences were visible in results, and therefore migration was measured with an approximate circle in the data presented in this thesis. The results of the traced measurements are shown in Figure 10.3 (see Chapter 10).

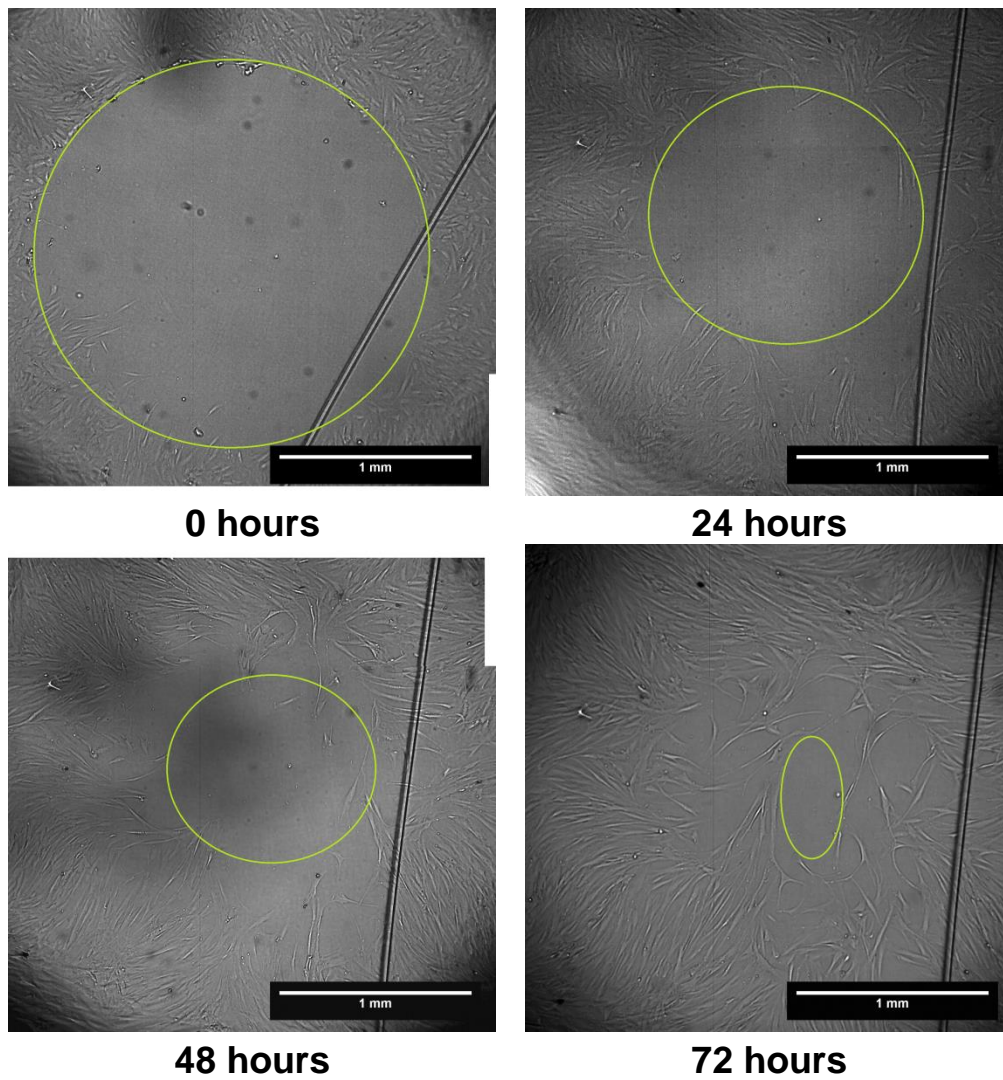


Figure 5.3. Human oral fibroblasts seeded in control medium using the Oris™ migration stoppers, imaged over 72 hours. Using ImageJ, the largest complete circle possible was drawn and the area calculated to estimate migration.

5.3.6 Adhesion assay

The work described in this section was performed in part by an undergraduate MEng student in the Hearnden research group, Jerome Tan Zu Yao. This work formed part of his dissertation research project, of which I was involved in the training and supervision.

To assess the effects of BPs on the adhesion of oral epithelial cells, an adhesion assay was performed. A crystal violet assay was used to measure cell number. A 0.2 % crystal violet (Sigma-Aldrich) solution was made up in 10 % ethanol (Thermo Fisher Scientific) in distilled water. A 10 % acetic acid (Thermo Fisher Scientific) solution in distilled water was also prepared. Cells were fixed by adding a 10 % formalin solution and incubated at room temperature for 30 minutes, before the formalin was removed and the wells washed thrice with PBS. Crystal violet was then added to the fixed cells for 10 minutes at room temperature. This was then removed, and wells were washed with water until all excess crystal violet was removed. The well plates were then left in a fume cupboard to dry out. When the wells were dry, 400 μ l of the acetic acid solution was added to elute the stain. Triplicate samples from each well were transferred to a 96 well plate, which was then read in an absorbance plate reader at 532 nm.

Before performing the assay, the adhesion time for OKF6 cells was examined. Cells were seeded in triplicate in 24 well plates, at a density of 1.5×10^4 cells per cm^2 . At time points ranging from 1 to 24 hours, media was removed, wells were washed thrice with PBS, cells were fixed and the crystal violet assay was performed.

For the adhesion assay, cells were treated with ZA in a well plate for 24 hours, then detached with trypsin and moved to a new well plate. To account for any toxicity effects, a well plate was seeded where the cells were not detached as a control. A diagrammatical representation of the assay is shown in Figure 5.4.

OKF6 cells were again seeded at a density of 1.5×10^4 cells per cm^2 , in two well plates, and left to adhere overnight. The medium was then changed to ZA containing medium from 1 to 30 μ M, or replaced with control medium. Cells were treated in triplicate. Both plates were treated identically up this point.

After 24 hours of treating, the media was removed from both plates. The control plate was washed with PBS thrice and cells fixed as above. For the experimental plate, wells were washed with PBS and trypsin-EDTA was used to detach the cells. After detachment, DMEM was added to deactivate the trypsin, and cells were centrifuged for 5 minutes at 5000 rpm. Cells were then resuspended and seeded into a new well plate in control medium. After 2 hours, the medium was removed, wells were washed with PBS and fixed as described above. A crystal violet assay was then performed on both plates.

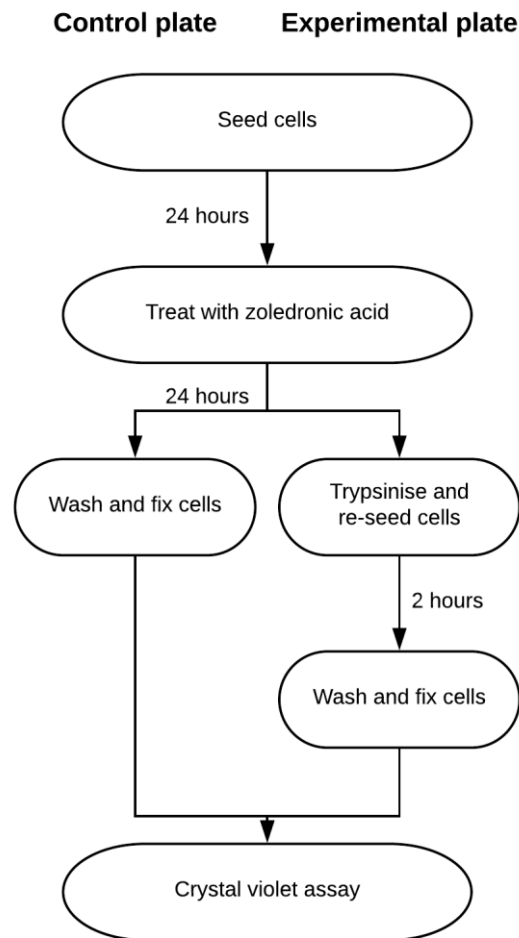


Figure 5.4. A flow diagram of the method for the crystal violet adhesion assay.

5.3.7 120 hour cell viability

To assess adhesion over longer time points, ZA concentration was first tested to ensure enough cells remained viable to assess. Keratinocytes were seeded in a 24 well plate at a density of 1.5×10^4 cells per cm^2 and left to attach overnight. The following day, they were treated with 0.1 to 30 μM ZA and incubated for 120 hours. A crystal violet assay was then performed as described previously in section 5.3.6.

5.3.8 Cytoskeleton staining

To further investigate the effects of BPs on epithelial cell adhesion, immunolabeling of cellular adhesion proteins was performed. Glass coverslips (Thermo Fisher Scientific) were sterilised in 70 % IMS, and placed into a 24 well plate. They were then washed thrice with PBS and left to dry. Once dry, OKF6 cells were seeded at a density of 1.5×10^4 per cm^2 onto the coverslips, left to adhere overnight, then treated with ZA

concentrations from 1 to 30 μM . Cells were then incubated for 24, 48 or 120 hours, then fixed as described previously in section 5.3.6. The 24 and 48 hour experiments were performed by Jerome Tan Zu Yao.

To perform the staining, an Actin Cytoskeleton and Focal Adhesion Staining Kit (Merck-Millipore) was used. This contained three components, tetramethylrhodamine isothiocyanate (TRITC)-conjugated phalloidin, anti-vinculin and 4',6-diamidino-2-phenylindole (DAPI). Phalloidin staining was performed in a 1:300 dilution in PBS. Vinculin staining was performed in a 1:300 dilution in a blocking solution. DAPI was diluted 1:1000 in PBS. Also used for this staining was a FITC-conjugated anti-mouse secondary antibody (Merck-Millipore, #AP124F), diluted 1:100 in PBS. A 1 % BSA blocking solution was prepared in PBS. To permeabilise the cells, a 0.1 % Triton X-100 (Thermo Fisher Scientific) solution in PBS was used. For washing cells, a buffer containing 0.05 % Tween-20 (Sigma-Aldrich) in PBS was used. All staining took place protected from light on a rocking plate (Bibby Scientific), set to 45 rpm to ensure liquid coverage of the whole coverslip.

Firstly, each well was washed twice with the wash buffer, before cells were permeabilised for 5 minutes using the Triton X-100 solution. Wells were then washed twice again. The blocking solution was applied for 30 minutes and removed. Anti-vinculin diluted in blocking solution was then applied for 1 hour. Wells were then washed thrice with the wash buffer, with the buffer left on for 10 minutes each time. The secondary antibody and phalloidin were applied simultaneously for 1 hour. Wells were washed thrice for 10 minutes as before. DAPI was then applied for 5 minutes, before three 10 minute washes. Coverslips were then fixed to glass slides using p-Xylene-bis(N-pyridinium bromide) (DPX) mountant (Merck).

A confocal microscope (Zeiss LSM510 META) with a 543 nm and a 488 nm laser was used to image the samples. Samples were also imaged using a 2-photon 780 nm laser (Chameleon Ultra III, Coherent Inc). Samples were imaged with a Zeiss EC Plan-Neofluar 40x magnification lens and a Zeiss Plan-Apochromat 63x magnification oil immersion lens. For FITC fluorescence excitation and emission wavelengths of $\lambda_{\text{ex}}=488 \text{ nm}/\lambda_{\text{em}}=525 \text{ nm}$ were used. For TRITC, wavelengths of $\lambda_{\text{ex}}=543 \text{ nm}/\lambda_{\text{em}}=576 \text{ nm}$ were used. DAPI stained cell nuclei were visualized at $\lambda_{\text{ex}}=780 \text{ nm}/\lambda_{\text{em}}=480 \text{ nm}$. Images were processed using LSM Image Browser 3.5 (Carl Zeiss Ltd) and ImageJ.

5.3.9 Statistics

Statistics were performed using Prism as described in section 4.3. 'N' is used to denote experimental repeats, while 'n' is used to denote technical repeats throughout. For the MTT results, values were normalised. The mean of the triplicate values for each condition at each time point were calculated. These new values were then calculated as a

percentage of the mean of the control values at 24 hours. One outlying value was removed from the MTT data. This value was identified as a significant outlier ($P \leq 0.001$) using Grubb's test for outliers through Excel (Microsoft). For the full calculation see Figure 10.4 (Chapter 10).

The half maximal inhibitory concentrations (IC_{50}) were calculated as follows. First, values were normalised to the control well at 72 hours. Next, 0 μM was set as 1×10^{-10} μM and concentrations transformed to $\log_{10}(\text{concentration})$. A non-linear fit for the data was calculated using an inhibitor vs. normalised response variable slope curve, using each value as an individual point. The software then generated a curve of best fit and an IC_{50} value.

Certain experiments did not involve time as an independent variable, and therefore other tests were used to determine significance than those described in section 4.3. These were the adhesion assay, 120 hour crystal violet assay, and the apoptosis assay.

Adhesion assay significance was calculated based on Kendall's rank correlation coefficients. These were calculated using SPSS (IBM). Concentration and cell number were set as scale variables. Data was sorted and split based on plate and Kendall's rank correlation coefficient calculated for each plate, using two-tailed significance.

To calculate significance in the 120 hour adhesion assay, a one way ANOVA was performed, again using Dunnett's multiple comparison test to measure significance of each concentration against the control. For the apoptosis assay, these tests were performed individually for viable, early apoptotic, late apoptotic and necrotic cells.

5.4 Results

5.4.1 Pamidronic acid and zoledronic acid were toxic to human oral fibroblasts and keratinocytes over 72 hours

MTT assays give a colorimetric response to metabolic activity, which can be used as an approximation of viability. Figure 5.5 shows the response of oral fibroblasts when cultured in different concentrations of PA over 72 hours, normalised to the control value at 24 hours. At 24 hours there were no significant differences in metabolic activity between cells treated with different doses of PA. Metabolic activity of the control group increased by approximately 50 % between 24 and 72 hours, indicating cell proliferation.

At 48 and 72 hours, a dose dependent response to PA was seen. At 48 hours, 100 μM PA significantly reduced metabolic activity to approximately 40 % of the control cell activity at the same time point, respectively. Both 50 and 100 μM PA significantly lowered fibroblast metabolic activity after 72 hours in culture. No significant difference was seen between the control media and 10 μM PA at any time point.

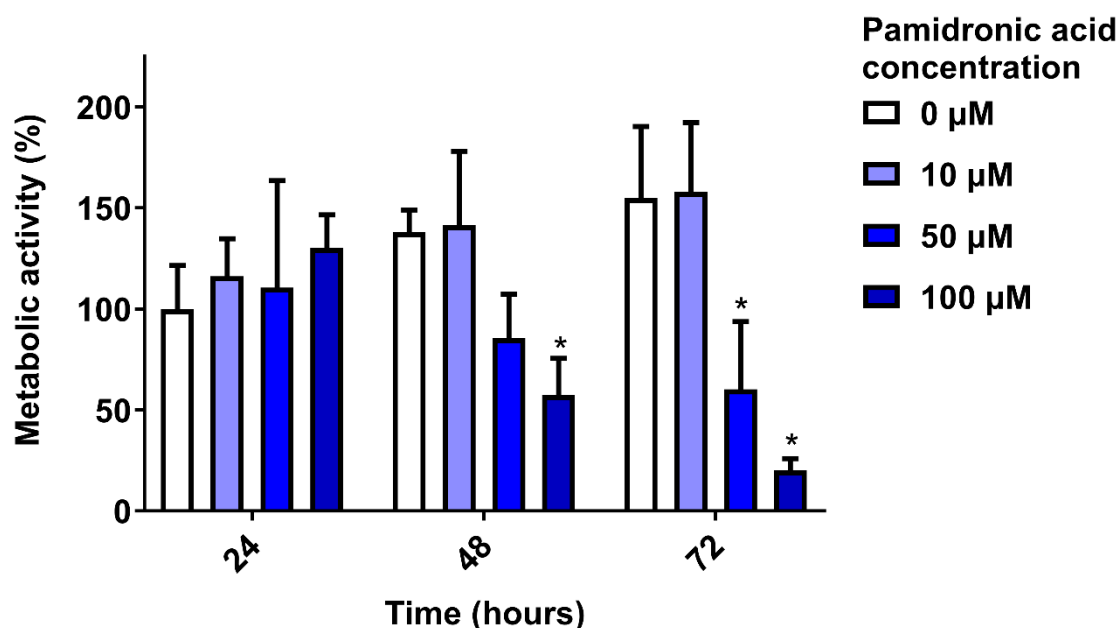


Figure 5.5. Human oral fibroblast metabolic activity over 72 hours in the presence of pamidronic acid. Values normalised to control cells at 24 hours. One outlying value removed. $N=3$, $n=3$. Error bars = SD. Significance against 0 μM at each time point indicated by $*P \leq 0.05$.

When immortalised keratinocytes (OKF6) were cultured in PA, there was no significant difference between metabolic activity for any of the doses tested at 24 hours, as shown in Figure 5.6. Metabolic activity of the control increased between time points at a much higher rate than with fibroblasts, increasing from 100 % to approximately 400 %, although there was high variation, indicated by the error bars. After 48 hours, a dose response was seen, with increasing concentrations of PA causing decreased cell metabolic activity, with 100 μ M reducing metabolic activity by a significant amount in comparison to the control. PA concentrations of 30 μ M and above significantly lowered keratinocyte metabolic activity after 72 hours in culture, in comparison to the control, with a dose dependent response again seen.

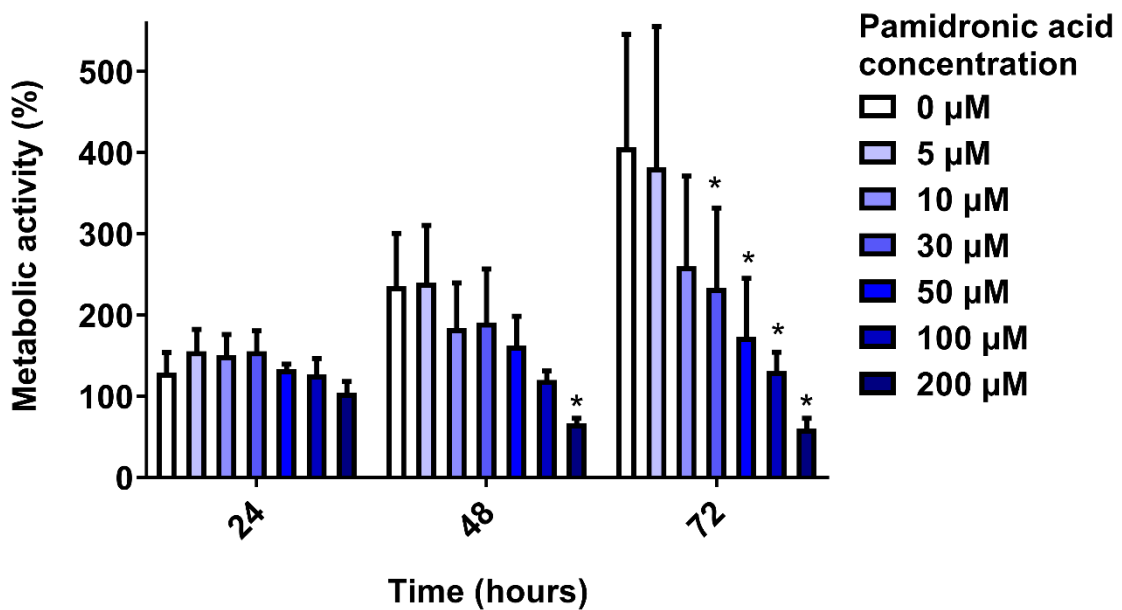


Figure 5.6. Immortalised human oral keratinocyte (OKF6) metabolic activity over 72 hours in the presence of pamidronic acid. Values normalised to control cells at 24 hours. $N=3$, $n=3$. Error bars = SD. Significance against 0 μ M at each time point indicated by $*P\leq 0.05$.

Figure 5.7 shows the metabolic activity of primary oral keratinocytes treated with PA. The metabolic activity of the untreated control cells increased by approximately 25 % between 24 and 48 hours. This was much less than in the immortalised keratinocytes. PA treatment showed a small reduction metabolic activity at 24 and 48 hours, but not significantly, though variation was high. A dose dependent response was seen at 72 hours. However, while the 10, 30 and 50 μM PA treated cells had lower overall values than the control, the values were higher than those at 48 hours. 100 μM PA significantly reduced cell metabolic activity, to approximately 20 %.

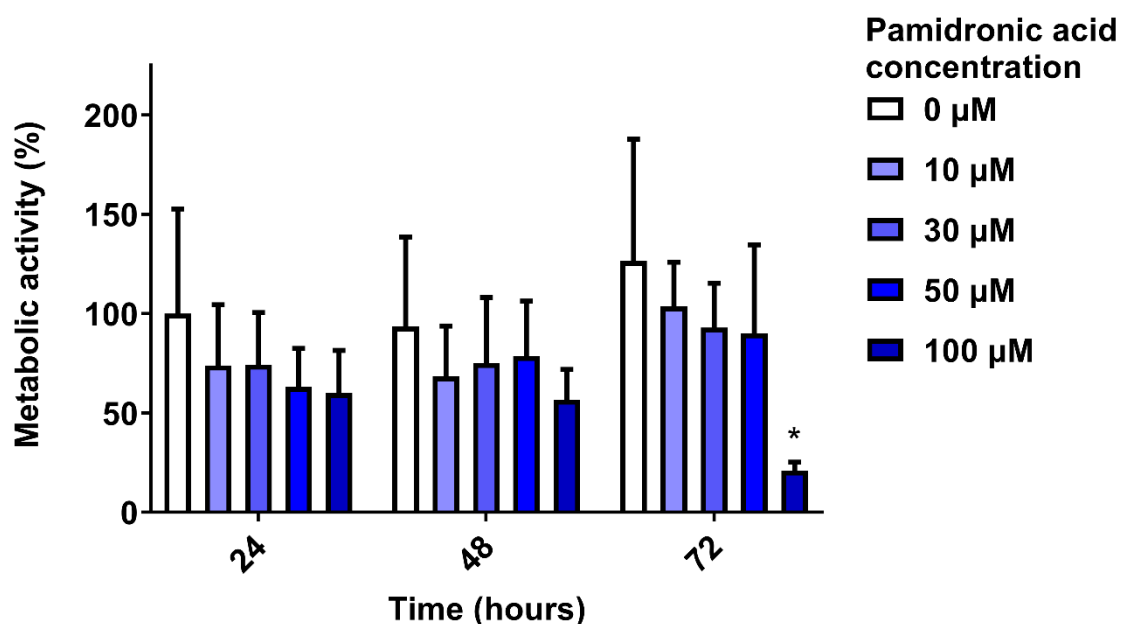


Figure 5.7. Primary human oral keratinocyte metabolic activity over 72 hours in the presence of pamidronic acid. Values normalised to control cells at 24 hours. $N=3$, $n=3$. Error bars = SD. Significance against 0 μM at each time point indicated by $*P \leq 0.05$.

ZA is a more potent anti-resorptive compared to PA, and also proved more toxic to oral mucosa cells. A dose dependent response was seen with fibroblasts in Figure 5.8, with 10 μM significantly reducing metabolic activity following 72 hours culture by around 85 %, in comparison to the control. Metabolic activity of the control remained approximately constant over the time points, with a higher value but greater error at 48 hours.

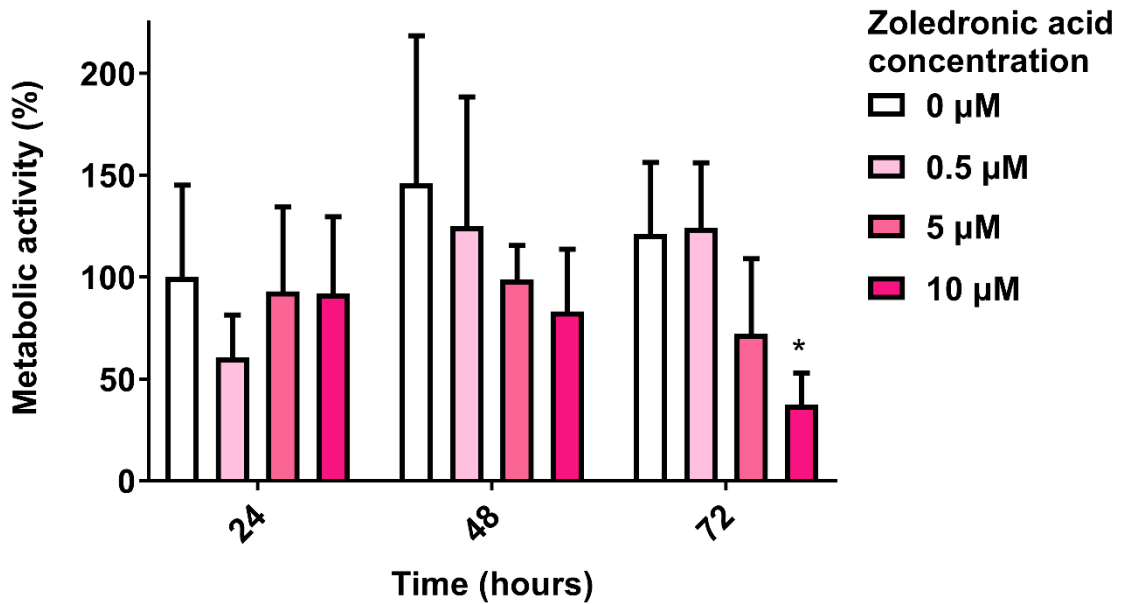


Figure 5.8. Human oral fibroblast metabolic activity over 72 hours in the presence of zoledronic acid. Values normalised to control cells at 24 hours. $N=3$, $n=3$. Error bars = SD. Significance against 0 μM at each time point indicated by $*P\leq 0.05$.

Figure 5.9 shows the response of immortalised keratinocytes to ZA. Again, no significance was found between doses at 24 hours, and a dose response was seen at 48 hours, however this was not significant. At 72 hours, concentrations of 20 and 50 μM significantly reduced cell metabolic activity in comparison to the control.

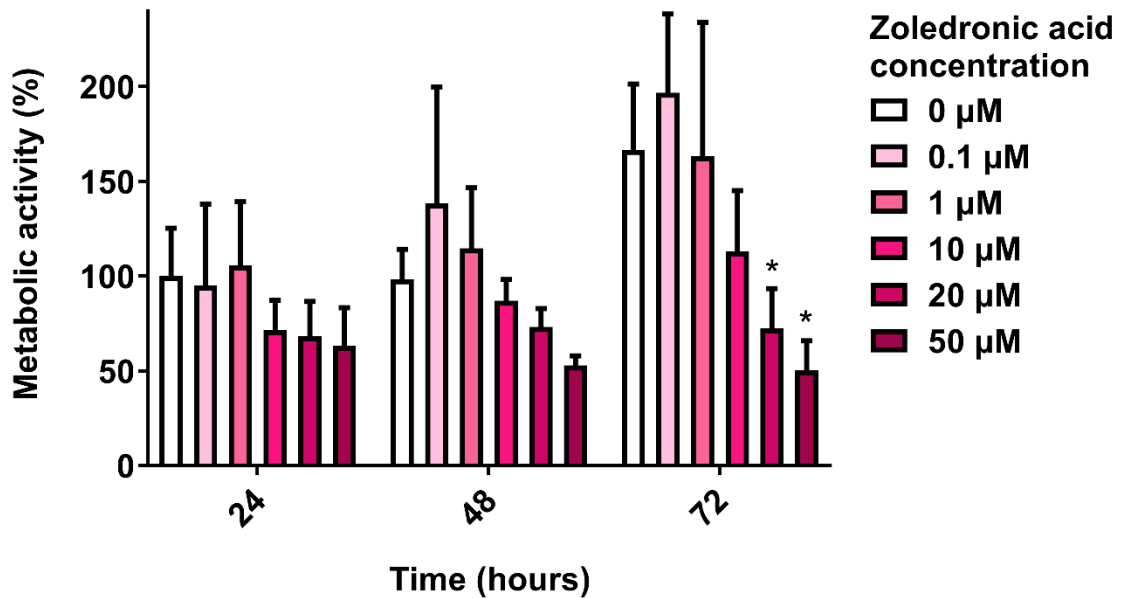


Figure 5.9. Immortalised human oral keratinocyte (OKF6) metabolic activity over 72 hours in the presence of zoledronic acid. Values normalised to control cells at 24 hours. $N=3$, $n=3$. Error bars = SD. Significance against 0 μM at each time point indicated by $*P \leq 0.05$.

ZA caused no significant difference to primary keratinocyte metabolic activity at 24 hours, as shown in Figure 5.10. At 48 hours, a dose dependent response was seen, with a 100 μM concentration reducing metabolic activity significantly. At 72 hours, the metabolic activity of the control cells had increased by approximately 40 % from 24 hours. ZA caused a dose dependent response, with concentrations of 10 μM and above significantly reducing cell metabolic activity.

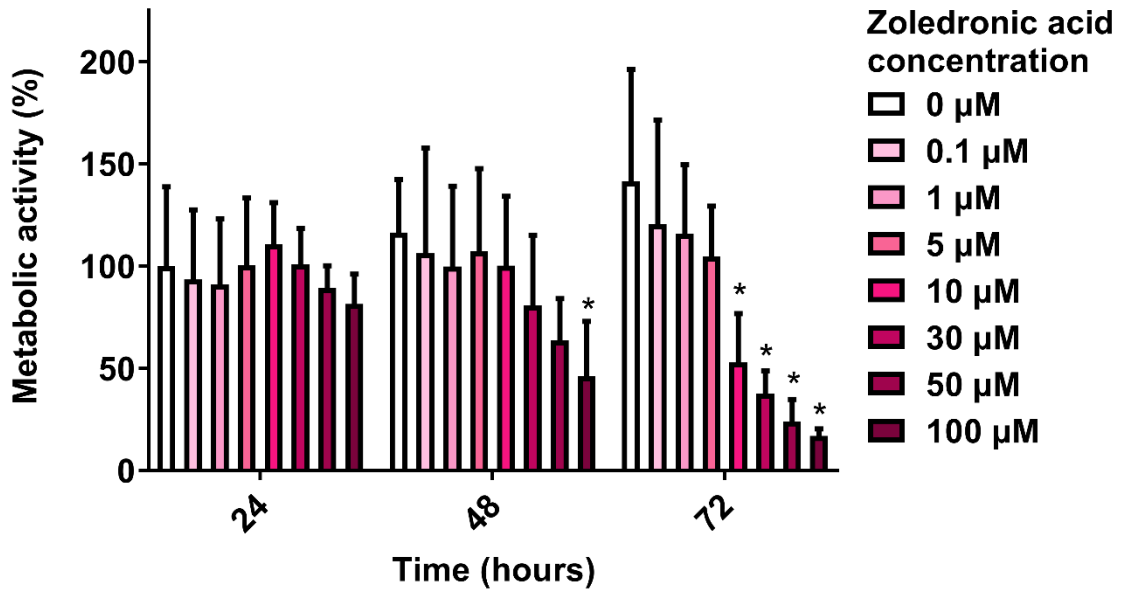


Figure 5.10. Primary human oral keratinocyte metabolic activity over 72 hours in the presence of zoledronic acid. Values normalised to control cells at 24 hours. $N=3$, $n=3$. Error bars = SD. Significance against 0 μM at each time point indicated by $*P\leq 0.05$.

Using the data collected at 72 hours, approximate IC₅₀ values were generated for each drug and cell type, shown in Figure 5.11. ZA was more potent in all cell types, the IC₅₀ approximately 7 times that of PA in fibroblasts and primary keratinocytes, and twice the concentration in immortalised keratinocytes. Immortalised keratinocytes were more resistant to ZA than their primary counterparts, yet less resistant to PA.

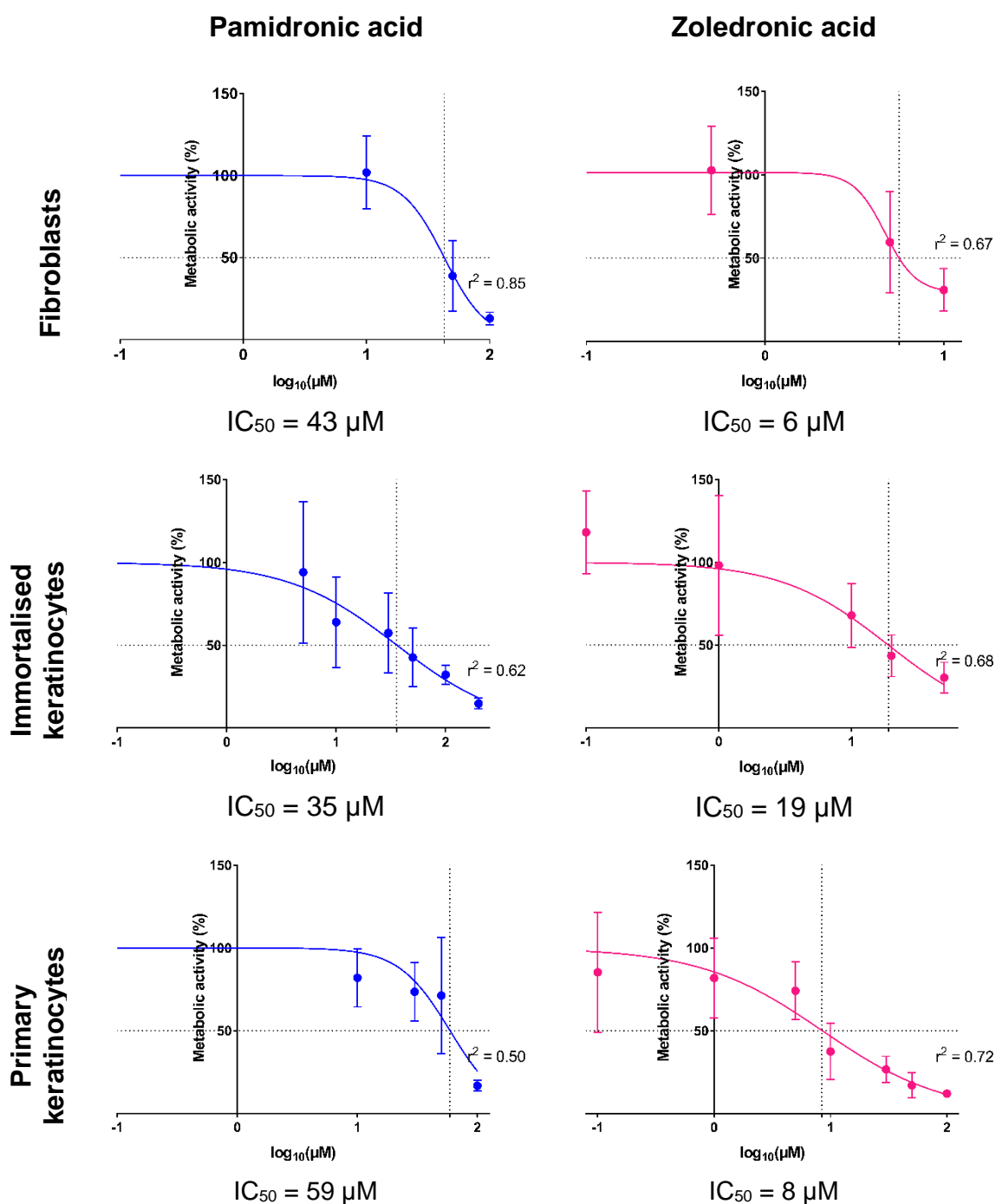


Figure 5.11. IC₅₀ graphs for fibroblasts, immortalised and primary keratinocytes when treated with either pamidronic acid or zoledronic acid for 72 hours. N=3, n=3. Cell metabolic activity normalised to control. 0 μM set as 10⁻¹⁰, data point not shown.

5.4.2 Pamidronic acid and zoledronic acid led to apoptosis in oral mucosa cells

Fibroblasts and keratinocytes were treated with PA and ZA for 72 hours, before staining with Annexin V-FITC and propidium iodide (PI), to assess whether the previously defined BP toxicity was due to apoptosis or necrosis. Annexin V binds to phosphatidylserine, an apoptosis marker. PI is a fluorescent stain that cannot cross a cell membrane, therefore is an indicator of lysed cells. Cells were determined to be early apoptotic if they stained with Annexin V alone, and late apoptotic if they stained with Annexin V and PI. Cells which stained with PI alone were considered necrotic. Cells which did not stain were considered viable.

Figure 5.12 shows the proportion of fibroblasts in each category following 72 hours of treatment with PA and ZA. Approximately 90 % of the untreated control cells were viable after 72 hours, with approximately 7 % cells apoptotic and less than 3 % necrotic. When treated with 10 μ M PA, 0.5 μ M ZA and 10 μ M ZA, no significant differences were seen compared to the untreated cells. When treated with 50 μ M PA the proportion of viable cells was significantly reduced, with only approximately 25 % of cells staining with neither Annexin V nor PI. Of the stained cells, approximately 10 % were early apoptotic and 60 % late apoptotic, both significant increases in comparison to the control.

Approximately 90 % of immortalised keratinocytes were viable after 72 hours, as shown in Figure 5.13, with the remaining 10 % evenly split between apoptotic and necrotic. Following treatment with sub-toxic concentrations of either PA or ZA, no differences were seen compared to the untreated cells. Concentrations above the IC_{50} reduced the number of viable cells. When treated with 100 μ M PA, approximately 10 % of cells became apoptotic, and 10 % became necrotic. When treated with 50 μ M ZA, the amount of viable cells was reduced to approximately 70 %, with approximately 20 % cells apoptotic and 10 % necrotic. The increase in late apoptosis was significant.

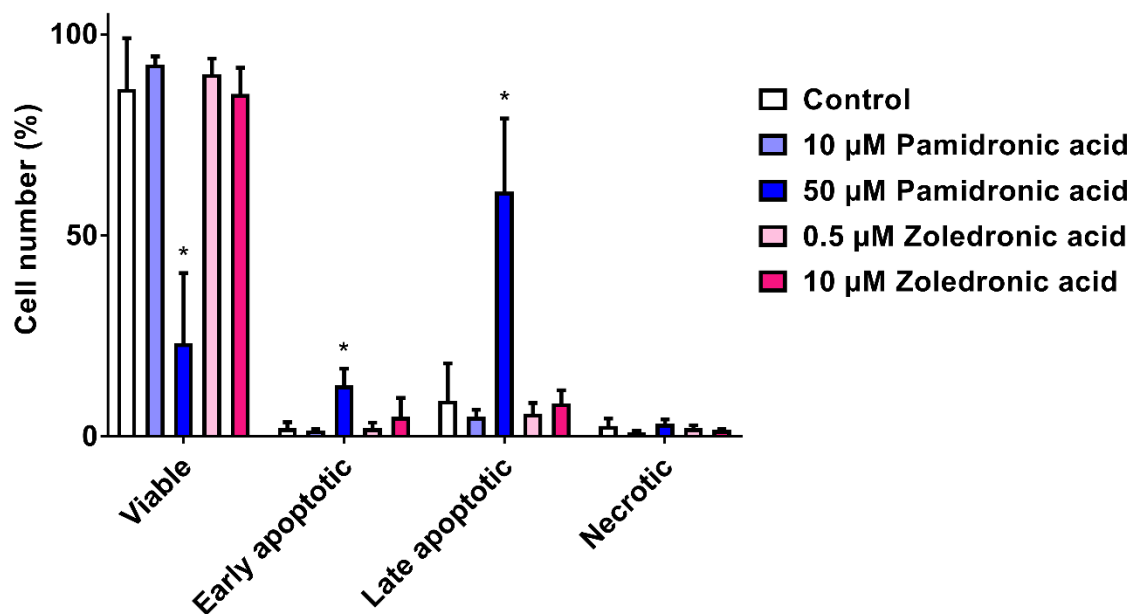


Figure 5.12. Proportion of human oral fibroblasts viable, early apoptotic, late apoptotic or necrotic after 72 hours treatment with pamidronic acid or zoledronic acid. N=3. Error bars = SD. Significance against control indicated by *P≤0.05.

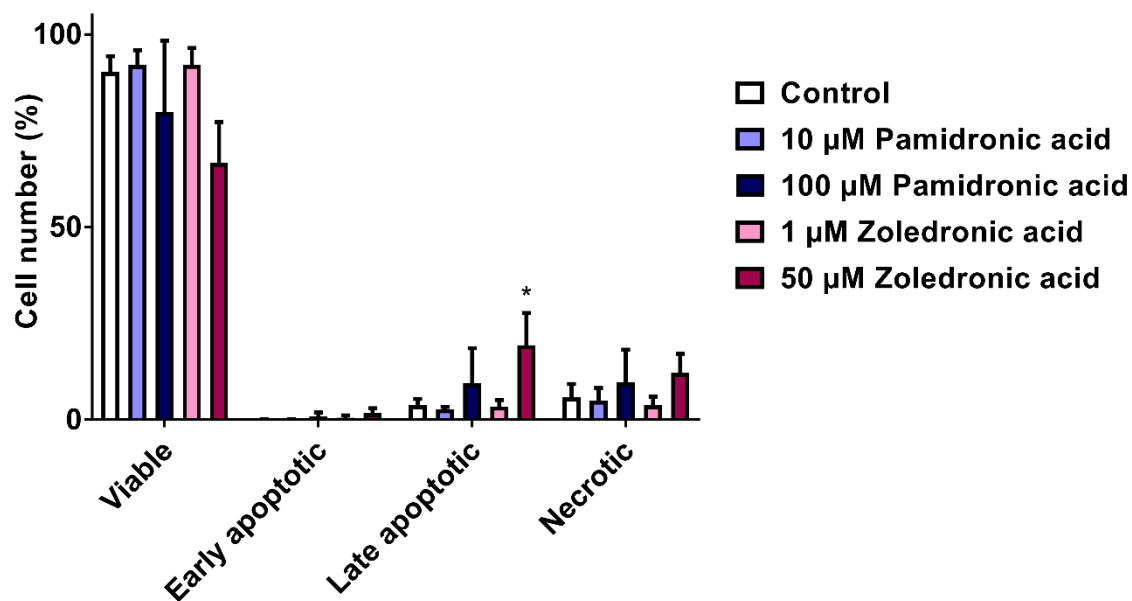


Figure 5.13. Proportion of human oral immortalised keratinocytes viable, early apoptotic, late apoptotic or necrotic after 72 hours treatment with pamidronic acid or zoledronic acid. N=3. Error bars = SD. Significance against control indicated by *P≤0.05.

5.4.3 Mitomycin C prevented proliferation of fibroblasts and immortalised keratinocytes

When performing a migration assay, it is necessary to stop proliferation and ensure that any wound closure seen is due to cell migration alone. Preventing proliferation also is used as a control during a proliferation assay. Mitomycin C is a DNA crosslinker that can be used to arrest the cell cycle, preventing proliferation. It significantly affected the proliferation of fibroblasts at concentrations of 0.625 µg/ml and above, as shown in Figure 5.14. Cells treated with control media tripled in number over 96 hours in culture. Concentrations from 0.625 to 2.5 µg/ml had a near constant cell number over 96 hours. A 5 µg/ml concentration caused a reduction in cell number, highlighting the toxic nature of higher concentrations of mitomycin C. Hence 2 µg/ml concentrations were used going forwards with fibroblasts.

Mitomycin C concentrations from 0.1 to 0.5 µg/ml significantly reduced cell proliferation of keratinocytes over 72 hours in culture, as shown in Figure 5.15. Concentrations of 0.3 µg/ml and 0.5 µg/ml maintained a constant cell number over culture time. Below that concentration cell number increased due to proliferation. Hence we used 0.5 µg/ml concentrations of mitomycin C to arrest cell proliferation in migration studies and to act as a control in proliferation assays with immortalised keratinocytes.

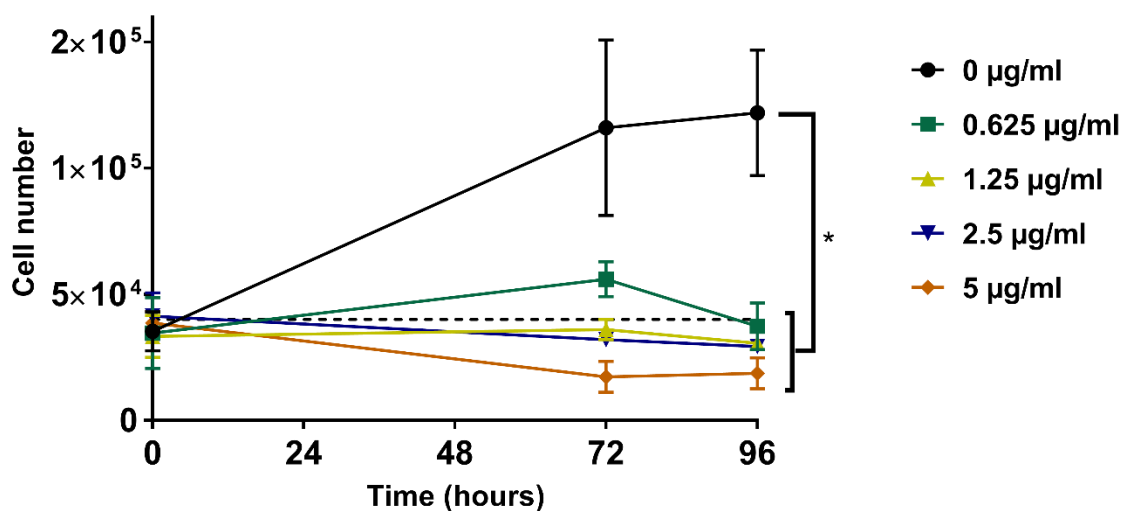


Figure 5.14. Human oral fibroblast cell number over 96 hours in the presence of Mitomycin C. N=1, n=3. Error bars = SD. Significance against 0 µg/ml indicated by *P≤0.05.

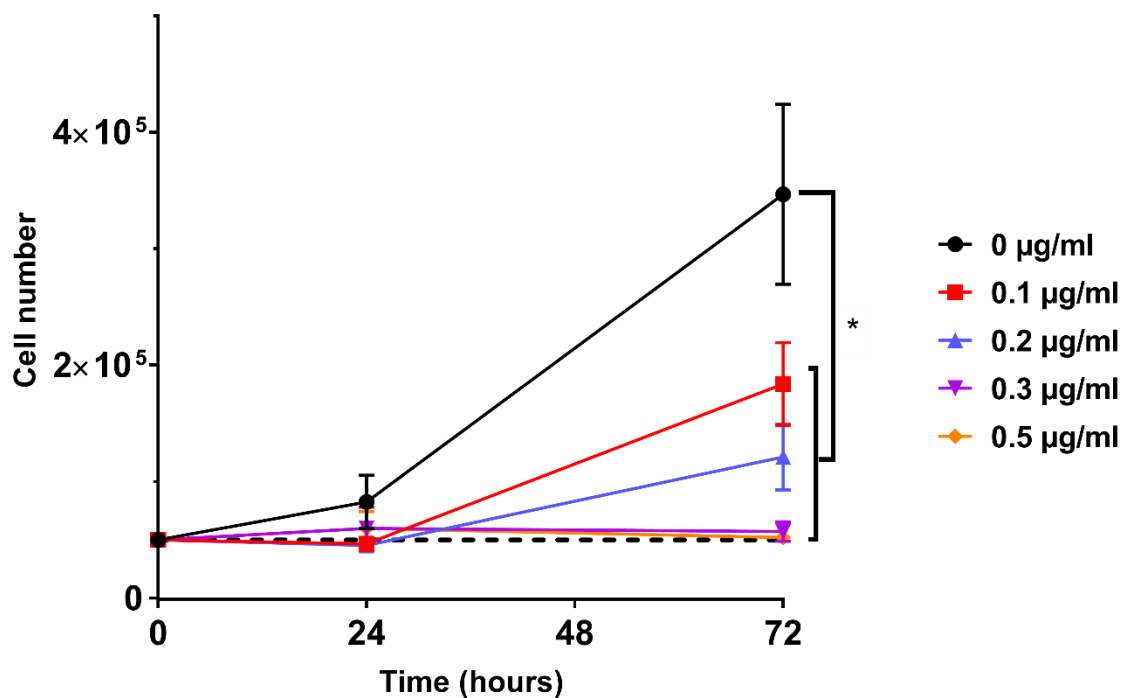


Figure 5.15. Immortalised human oral keratinocyte (OKF6) cell number over 72 hours in the presence of Mitomycin C. N=1, n=3. Error bars = SD. Significance against 0 µg/ml indicated by *P≤0.05.

5.4.4 Pamidronic acid and zoledronic acid prevented fibroblast and immortalised keratinocyte proliferation

Fibroblasts and immortalised keratinocytes were stained with CellTrace™ CFSE before treating with PA and ZA for 72 hours to measure cell proliferation. Flow cytometry was used to measure the median fluorescence intensity of cells at 24 and 72 hours. CellTrace™ CFSE staining allows cell proliferation to be measured, as each time a cell divides, the fluorescence intensity of the two cells formed by that process will be reduced compared to cells which have not divided [291]. By comparing cells treated with mitomycin C that cannot undergo proliferation, it was possible to determine a proliferative index (I_{plif}) as per Equation 2.1. A higher I_{plif} indicated the cells proliferated more and a I_{plif} of 1 indicated no proliferation took place.

Figure 5.16 shows fibroblast proliferation following treatment with PA and ZA. At 24 hours, no significant differences were seen between any treatments. At 72 hours, low concentrations of each drug caused no differences in I_{plif} in comparison to the control. However, 50 μM PA and 10 μM ZA caused a significant reduction in proliferation. PA led to a I_{plif} close to that of the mitomycin C treated cells, indicating proliferation was halted entirely.

Figure 5.17 demonstrates that keratinocyte proliferation was low over 24 hours, with values close to 1 for all treatments and no significant differences seen between the control cells and any of the drug treated cells. At 72 hours, the keratinocyte I_{plif} had increased to approximately 3. When treated with 10 μM and 100 μM PA, proliferation was significantly reduced. ZA also led to a significant reduction in keratinocyte proliferation at both 1 and 50 μM ZA concentrations, compared to untreated control cells. The higher concentrations of both drugs prevented keratinocyte proliferation almost entirely, with the I_{plif} close to 1 in both cases.

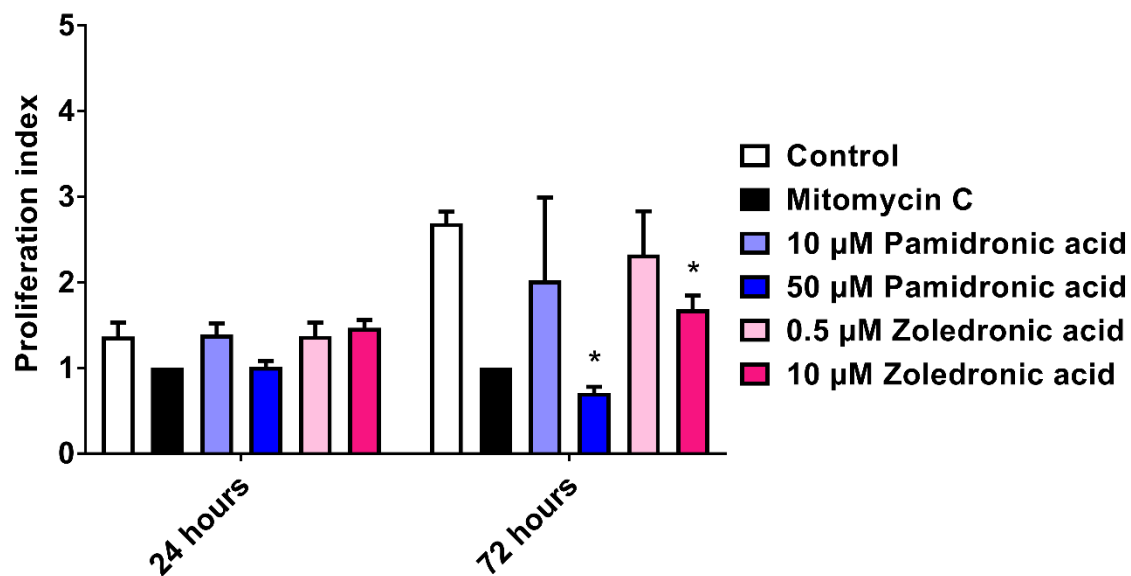


Figure 5.16. Human oral fibroblast proliferation over 72 hours in the presence of pamidronic acid or zoledronic acid. Mitomycin C used as a non-proliferating control. N=3. Error bars = SD. Significance against control indicated by *P≤0.05.

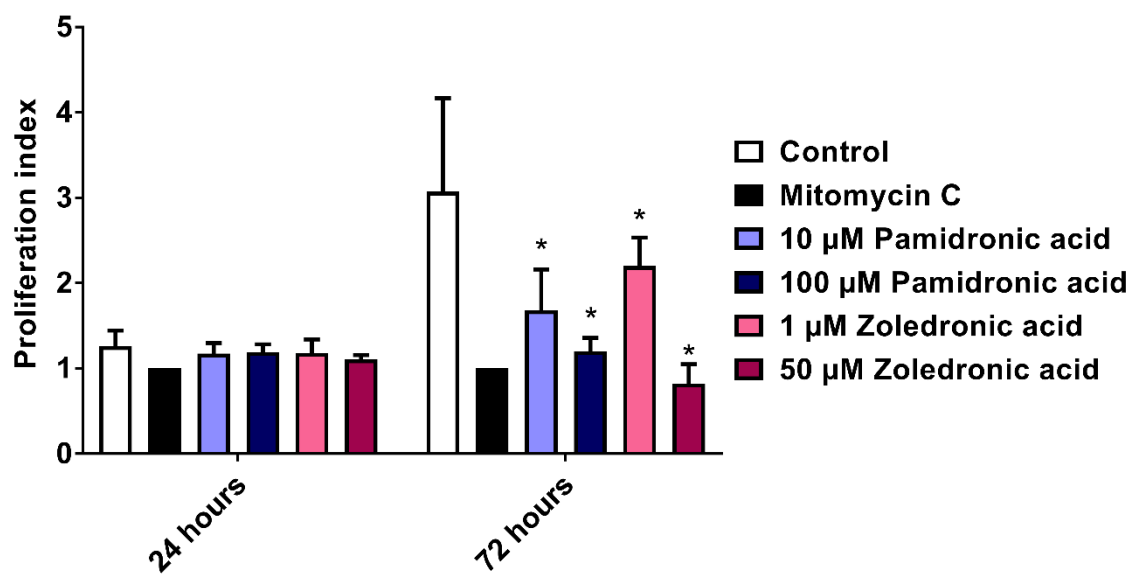


Figure 5.17. Immortalised human oral keratinocyte (OKF6) proliferation over 72 hours in the presence of pamidronic acid or zoledronic acid. Mitomycin C used as a non-proliferating control. N=3. Error bars = SD. Significance against control indicated by *P≤0.05.

5.4.5 Sub-toxic concentrations of pamidronic acid and zoledronic acid did not affect the migration rate of oral mucosa cells

As a key part of BRONJ development is the prevention of oral mucosa wound healing, we next studied cell migration in the presence of BPs. Migration is a key part of wound healing, with both fibroblasts and keratinocytes migrating in the early stages. Sub-toxic concentrations were chosen, to confirm that any effects seen were not due to toxicity, but were BPs affecting the cells by another mechanism.

Figure 5.18 shows representative images of fibroblast migration into an exclusion zone in a well plate over 72 hours when treated with PA. At 0 hours, uniform regions with no cells were seen in all conditions. At 24 and 48 hours, cells had migrated into these regions, and appeared viable at all time points. At 72 hours (not shown), all wells looked uniform and entirely covered by cells. Figure 5.19 shows the migration rate of fibroblasts over the time period. Neither 10 nor 30 μM concentrations showed an effect, with cells migrating into the exclusion zone at a similar rate and no significant difference between any values. By 72 hours, all zones had closed by approximately 95 %.

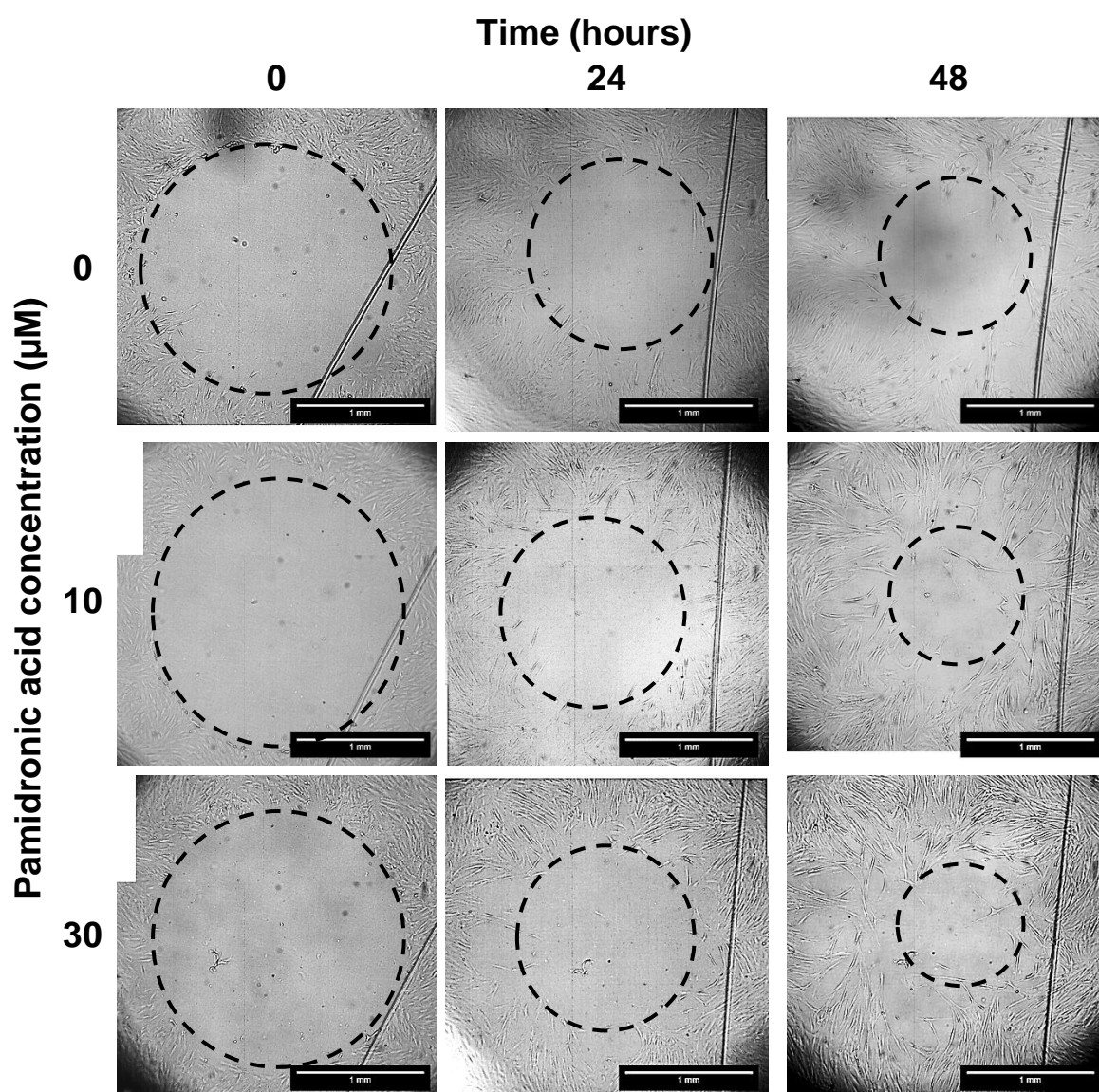


Figure 5.18. Human oral fibroblast migration over 48 hours in the presence of pamidronic acid. Dotted lines indicate approximate exclusion zones. Columns denote each time point, rows denote the concentration of pamidronic acid in μM . One representative well used for each condition. Wells at 72 hours not shown as all exclusion zones were completely closed. Scale bars = 1mm.

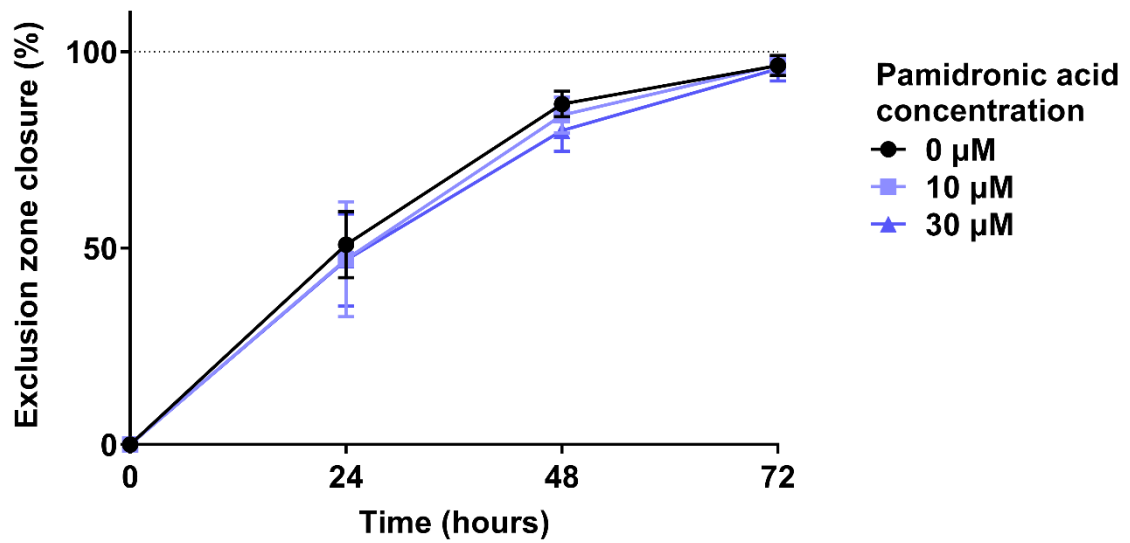


Figure 5.19. Human oral fibroblast migration over 72 hours in the presence of pamidronic acid. $N=3$, $n=6$. Error bars = SD. Statistical tests showed significance ($P \leq 0.05$) between 0 µM and any other concentration.

Fibroblast migration was also unaffected by sub-toxic concentrations of ZA, as shown in Figure 5.20. Again, seeding was uniform at 0 hours, with migration occurring normally over 48 hours and all cells appearing viable at all time points. When treated for 72 hours with ZA concentrations of 0.5, 1 and 5 μM , there were no significant differences between migration at any time points, and all wells closed by approximately 98 % after 72 hours, as shown in Figure 5.21.

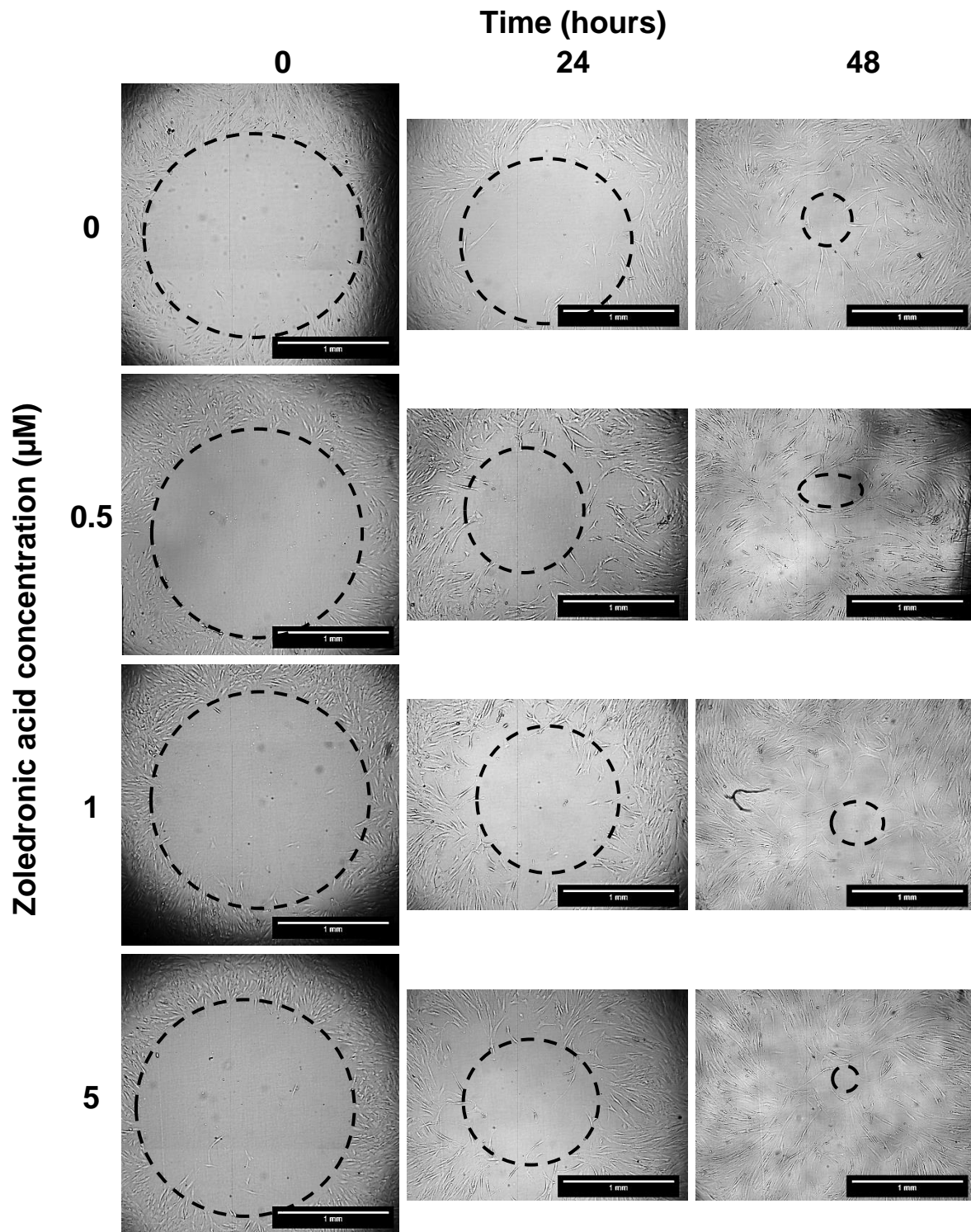


Figure 5.20. Human oral fibroblast migration over 48 hours in the presence of zoledronic acid. Dotted lines indicate approximate exclusion zones. Columns denote each time point, rows denote the concentration of zoledronic acid in μM . One representative well used for each condition. Wells at 72 hours not shown as all exclusion zones were completely closed. Scale bars = 1mm.

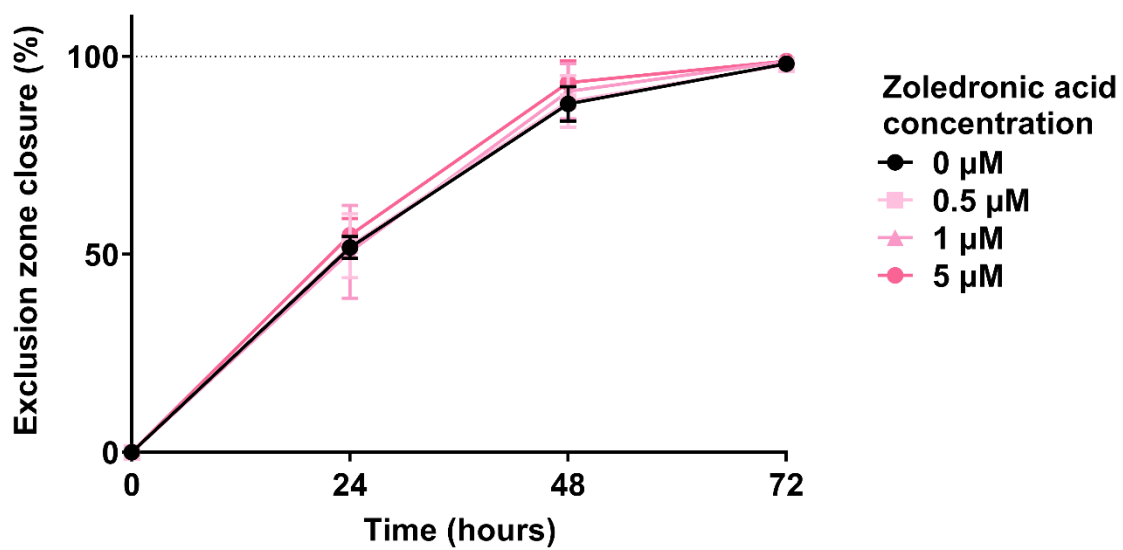


Figure 5.21. Human oral fibroblast migration over 72 hours in the presence of zoledronic acid. $N=3$, $n=6$. Error bars = SD. Statistical tests showed significance ($P \leq 0.05$) between 0 μM and any other concentration.

Immortalised keratinocyte migration occurred at a faster rate, with exclusion zones closing after 24 hours. Concentrations ranging from 0 to 10 μM were used for both PA and ZA, and neither showed any effect on the migration of keratinocytes.

Figure 5.22 shows representative images from each condition at 0, 8 and 16 hours and demonstrates that cells were viable at all time points. The exclusion zones, while similar, were not completely uniform, with a less defined circle than with fibroblasts, as in the 5 μM concentration of PA in Figure 5.22. Figure 5.23 shows that whilst PA treated cells did migrate more quickly, the differences were not statistically significant. All exclusion zones were approximately 95 % closed after 24 hours. The standard deviation, demonstrated as error bars, shows there was high variation between experiments, which was likely due to the variation in exclusion zone size and shape.

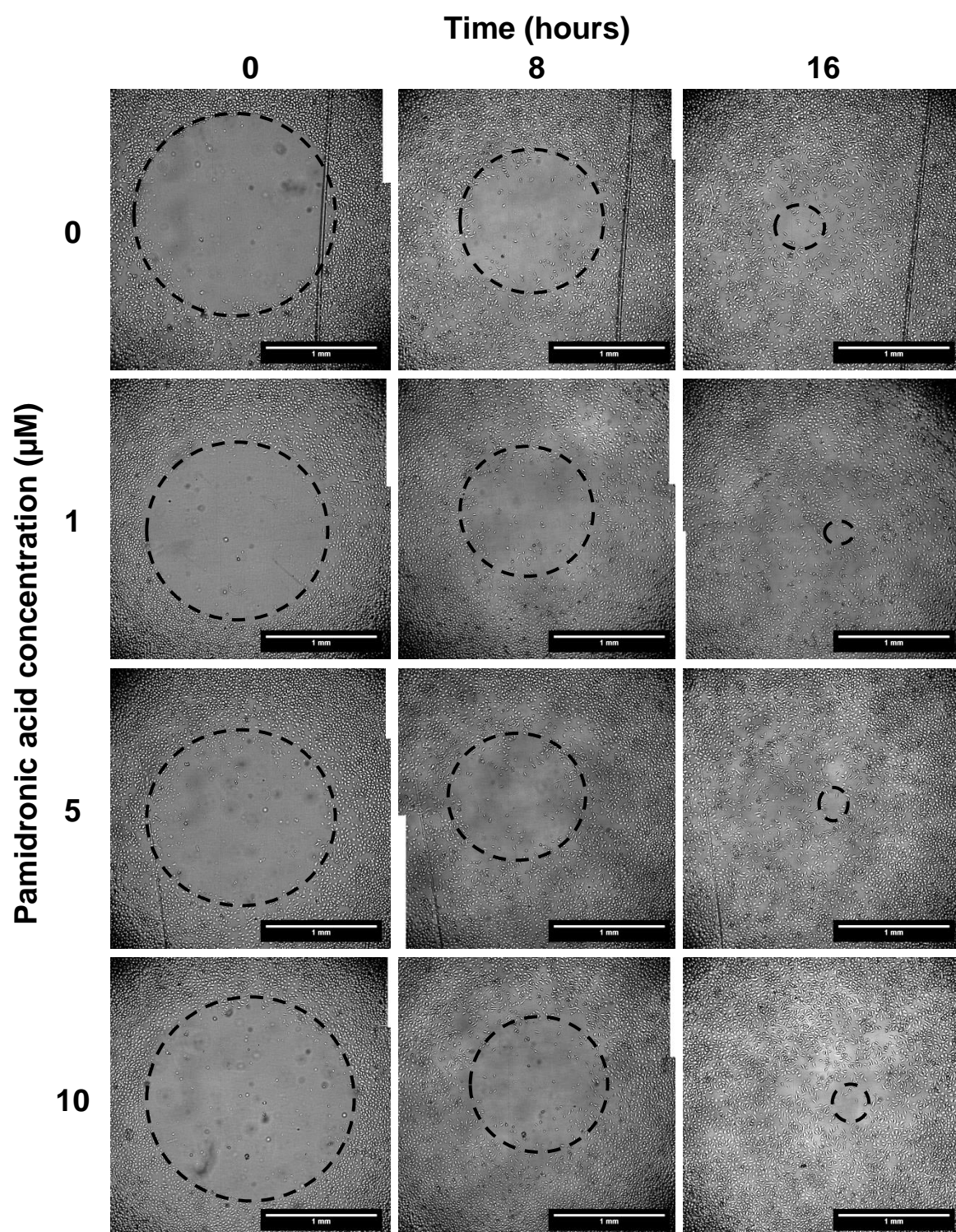


Figure 5.22. Immortalised human oral keratinocyte (OKF6) migration over 16 hours in the presence of pamidronic acid. Dotted lines indicate approximate exclusion zones. Columns denote each time point, rows denote the concentration of pamidronic acid in μM . One representative well used for each condition. Wells at 24 hours not shown as all exclusion zones were completely closed. Scale bars = 1mm.

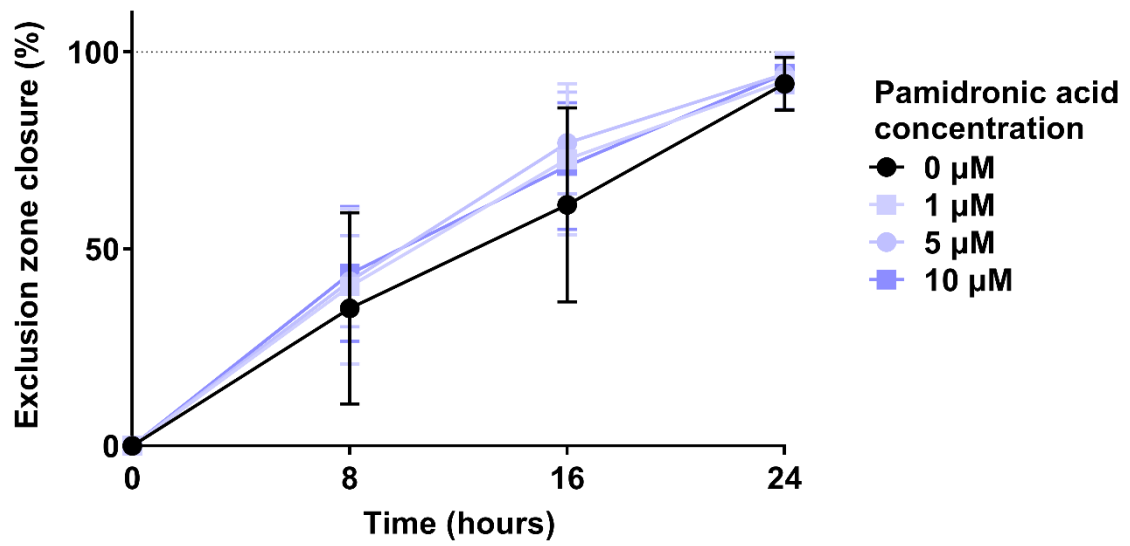


Figure 5.23. Immortalised human oral keratinocyte (OKF6) migration over 24 hours in the presence of pamidronic acid. $N=3$, $n=6$. Error bars = SD. Statistical tests showed significance ($P \leq 0.05$) between 0 μM and any other concentration.

ZA also had no significant effect on the rate of keratinocyte migration, with all wells closing at a similar rate regardless of drug concentration. Figure 5.24 again shows relatively uniform exclusion zones at 0 hours, with migration of viable keratinocytes over 8 and 16 hours in the ZA migration assay. Figure 5.25 highlights that exclusion zones closed at a faster rate, with around 90 % closure at 16 hours and approximately 98 % at 24 hours.

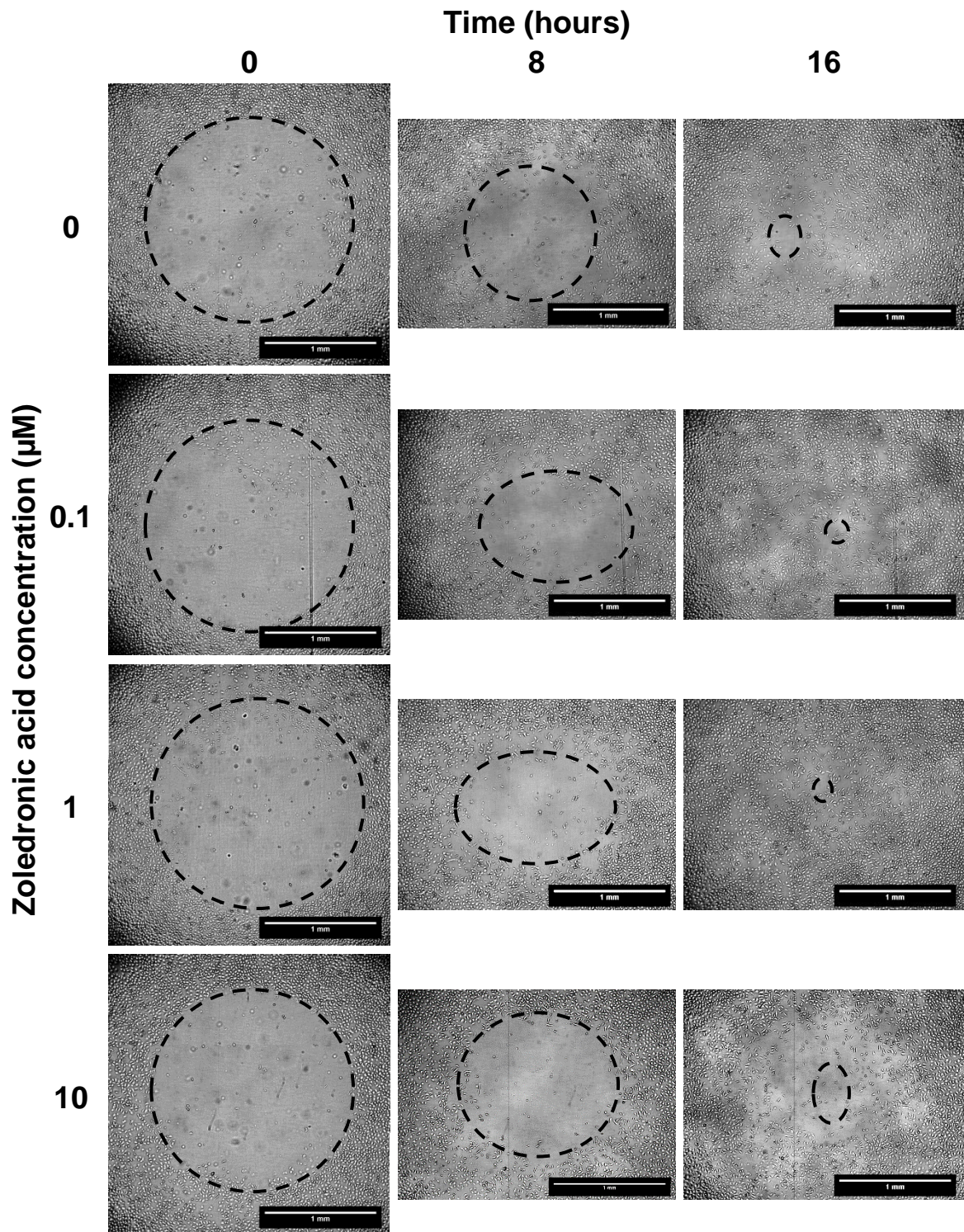


Figure 5.24. Immortalised human oral keratinocyte (OKF6) migration over 16 hours in the presence of zoledronic acid. Dotted lines indicate approximate exclusion zones. Columns denote each time point, rows denote the concentration of zoledronic acid in μM . One representative well used for each condition. Wells at 24 hours not shown as all exclusion zones were completely closed. Scale bars = 1mm.

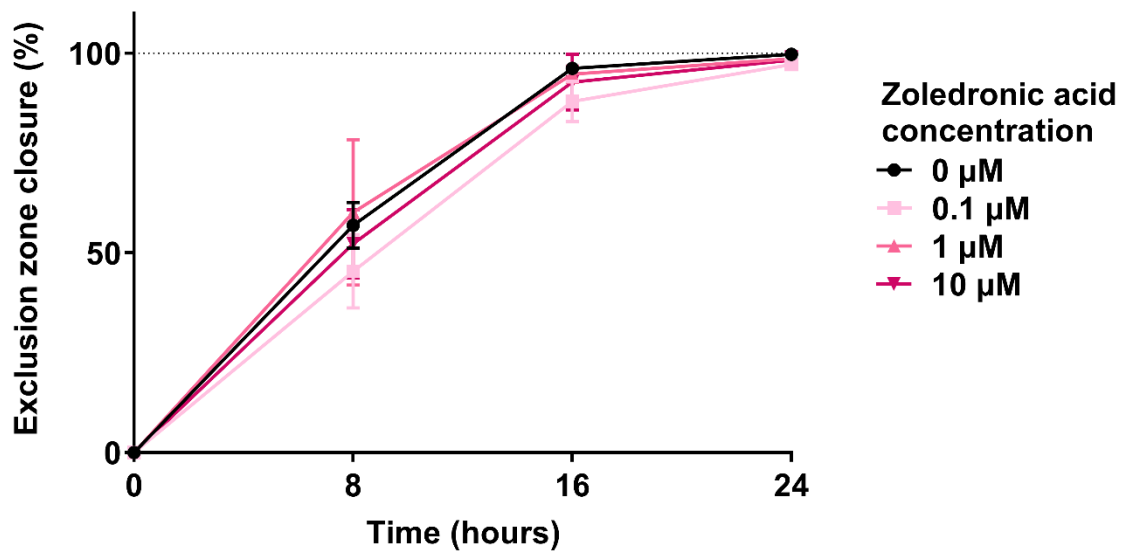


Figure 5.25. Immortalised human oral keratinocyte (OKF6) migration over 24 hours in the presence of zoledronic acid. $N=3$, $n=6$. Error bars = SD. Statistical tests showed significance ($P \leq 0.05$) between $0 \mu\text{M}$ and any other concentration.

5.4.6 Pre-treating fibroblasts with pamidronic acid prevented exclusion zone closure through toxicity

As the oral mucosa of BRONJ patients is potentially exposed to BPs for longer time periods, including before the mucosa is wounded, migration was also examined when cells were treated with PA for 72 hours before seeding until the end of the experiment.

Figure 5.26 shows representative wells during the study, with cells treated with media alone migrating normally. When pre-treated with 30 μ M PA, fewer fibroblasts had migrated into the exclusion zone at 48 hours. By 72 hours, the cells were no longer viable, as shown in Figure 5.27. Treating fibroblasts for a total of 144 hours with 30 μ M PA led to a large number of cells no longer attached to the well plate and caused the remaining cells to no longer retain their distinct morphology, indicating toxicity.

Figure 5.28 shows the migration rate of the pre-treated fibroblasts in comparison to the control. Between 24 and 48 hours, PA led to a reduction in migration rate compared to untreated control cells, however this was not significant. The exclusion zone then re-opened between 48 and 72 hours. The exclusion zone closure in pre-treated fibroblasts at 72 hours was significantly lower compared to the untreated control. However, this effect was due to toxicity following 144 hours total treatment with 30 μ M PA, rather than migration effects.

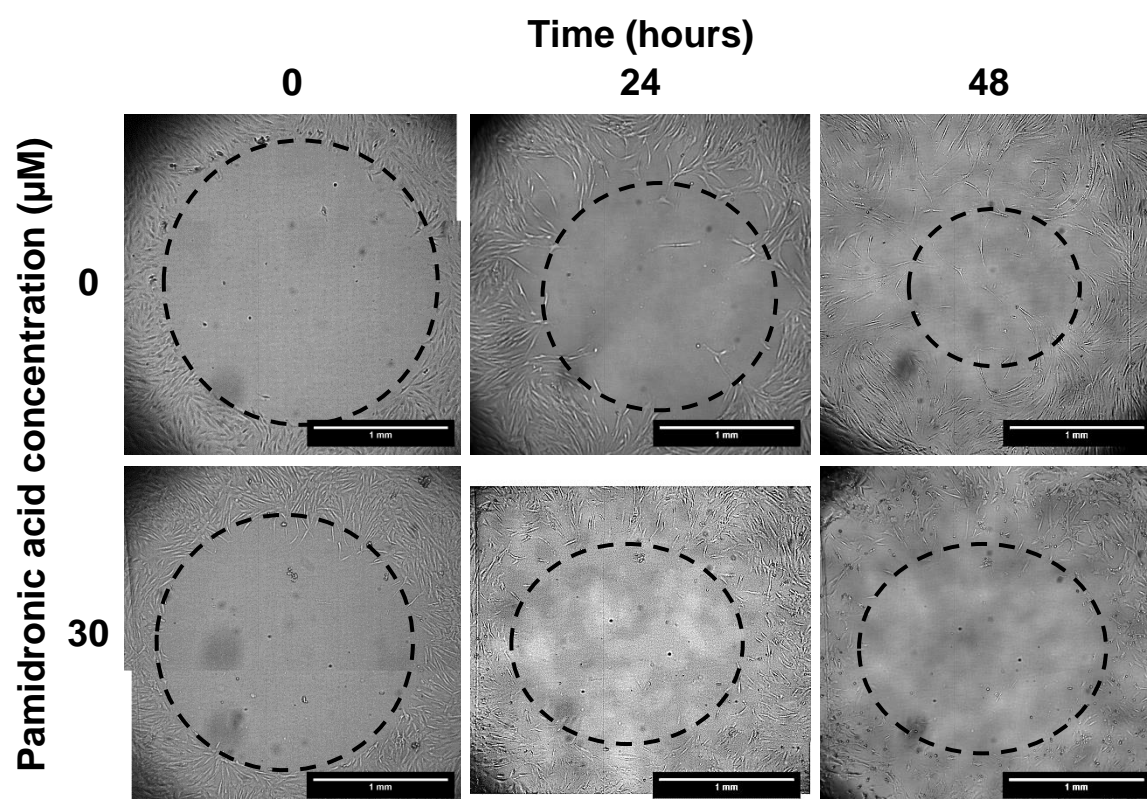


Figure 5.26. Human oral fibroblast migration over 48 hours in the presence of pamidronic acid, following 72 hours pre-treatment. Dotted lines indicate approximate exclusion zones. Columns denote each time point, rows denote the concentration of pamidronic acid in μM . One representative well used for each condition. Scale bars = 1mm.

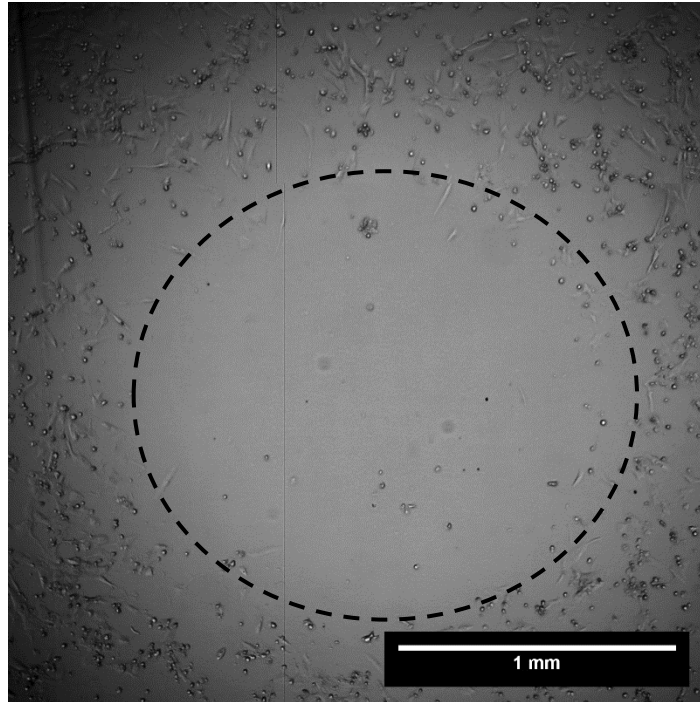


Figure 5.27. Human oral fibroblasts after 72 hours in the presence of 30 μM pamidronic acid, following 72 hours pre-treatment. Dotted line indicates approximate exclusion zone. One representative image used. Scale bar = 1mm.

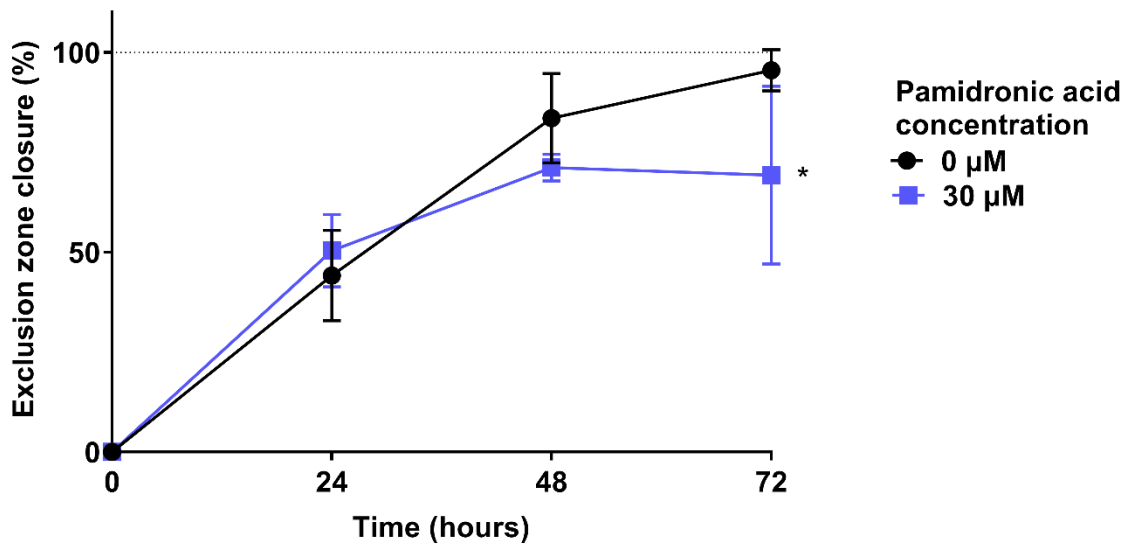


Figure 5.28. Human oral fibroblast migration over 72 hours in the presence of pamidronic acid, following 72 hours pre-treatment. $N=3$, $n=6$. Error bars = SD. Significance against 0 μM indicated by $*P \leq 0.05$.

5.4.7 Zoledronic acid caused a small reduction in immortalised keratinocyte adhesion

BPs have been demonstrated to affect the adhesion of several cell types, including oral fibroblasts, affecting both integrins and the cytoskeleton [82], [144], [181]–[183]. This has never been demonstrated in oral keratinocytes, and presents another potential mechanism through which the oral mucosa could be weakened from BP treatment. If epithelial cells became less adherent this could reduce the thickness and structural strength of the oral mucosa, increasing the risk of damage and thereby increasing the rate of bone exposure. A 2D adhesion assay was performed using immortalised keratinocytes to assess any *in vitro* BP effects on adhesion. To optimise this assay, the adhesion of immortalised keratinocytes was first studied over time through a crystal violet assay.

Figure 5.29 shows the percentage of cells that had adhered to a well plate over 1 to 24 hours, normalised to the 24 hour value, as it can be assumed all cells will have adhered at this time point. Initially, the increase in cell attachment over time was quite steep. Approximately 50 % of cells had adhered 1 hour after seeding. By 2 hours, the adhesion level was approximately 70 %. After this time point, the rate of adhesion began to level off, with around 75 % being adhered at both 4 and 6 hours. Due to the adhesion amount being similar at 2, 4 and 6 hours, 2 hours was chosen as the time point for the adhesion assay, to maximise the ability to see an effect caused by BP treatment.

The results of the adhesion assay are shown in Figure 5.30. The cells of the control plate were not detached, and the crystal violet results show the cell number is largely unaffected by ZA treatment over 72 hours. Although a significant dose dependent reduction is observed, all values remain close to 100 % of the number of the untreated cells. When the cells were detached and allowed to re-attach for 2 hours, approximately 63 % of the untreated cells attached. Again, a dose dependent response is seen when treated with increasing concentrations of ZA, however in this case, the response is more pronounced. Both the control plate and detached plate showed a significant correlation between cell number and ZA concentration. The correlation was stronger for the detached plate, suggesting ZA caused a small reduction on the ability of the immortalised keratinocytes to adhere, over and above toxic effects caused by the ZA.

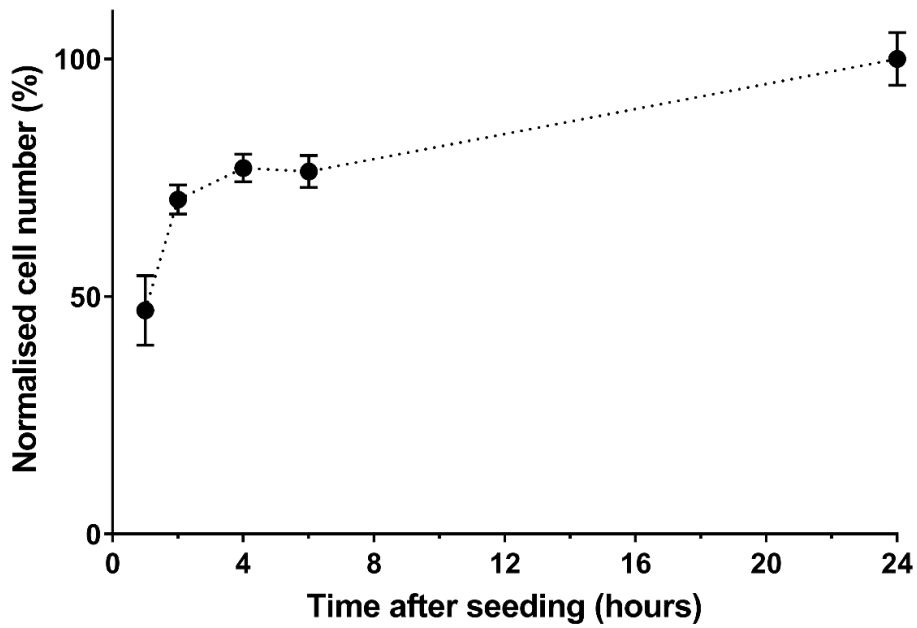


Figure 5.29. Adhesion of immortalised keratinocytes (OKF6) over time measured by crystal violet assay. Values normalised to 24 hours. $N=1$, $n=3$. Error bars = SD.

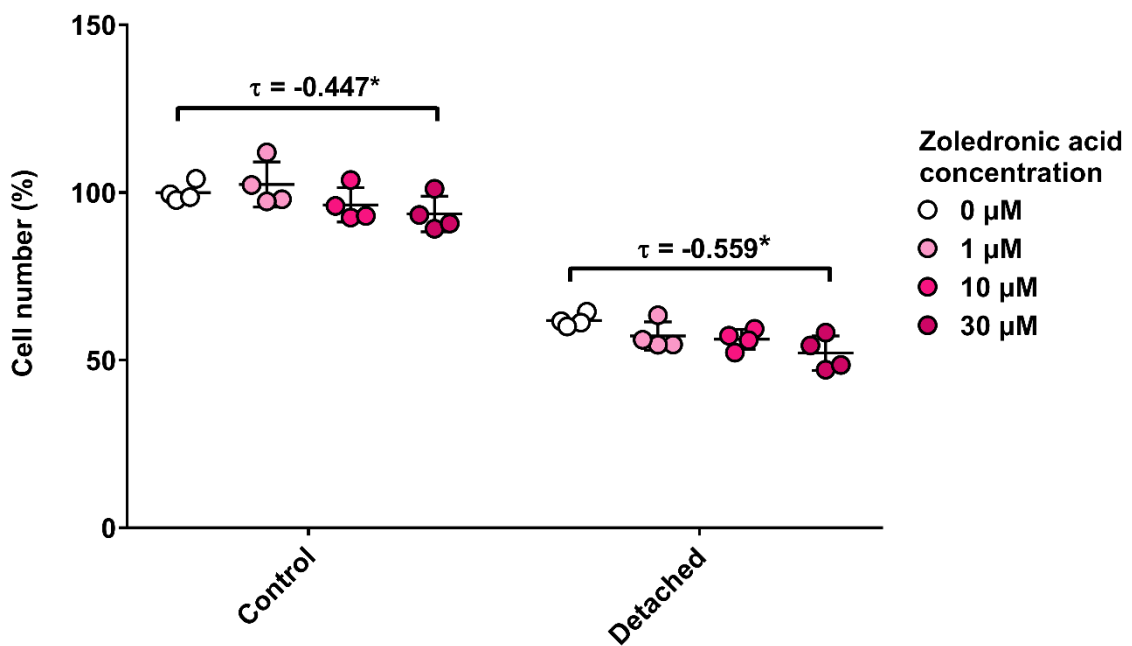


Figure 5.30. Adhesion assay results for immortalised keratinocytes (OKF6) treated with zoledronic acid for 24 hours then fixed (control) or detached, re-seeded and allowed to adhere for 2 hours (detached), measured by crystal violet assay. Values normalised to 0 µM of control plate. $N=4$, $n=3$. Error bars = SD. Kendall rank correlation coefficient for each plate indicated by τ . Significance against 0 µg/ml indicated by $*P \leq 0.05$.

5.4.8 Zoledronic acid did not affect expression of keratinocyte cytoskeleton proteins

Figure 5.31 shows images of immortalised keratinocyte cells stained for cytoskeleton proteins after 24 hours of zoledronic acid treatment. F-actin bundles were stained red, and vinculin was stained green. F-actin bundles appeared present in all images, with no obvious BP effect visible. There was a slight reduction of staining with 10 μM treatment, however this effect is not apparent with 30 μM zoledronic acid. Vinculin staining appears consistent across all concentrations, however is much less specific than would be expected, staining throughout the cell rather than obviously staining focal adhesions.

After 48 hours treatment, staining is again largely consistent across all samples for both vinculin and F-actin, shown in Figure 5.32. The control, 1 μM and 10 μM treated keratinocytes in particular have no noticeable differences. When treated for 48 hours with 30 μM zoledronic acid, there is a slight difference in the F-actin appearance. Fewer obvious bundles appear, with staining appearing more in the cell cortex. Overall vinculin staining was non-specific but had a more diffuse staining pattern in cells treated with 30 μM ZA compared to the other conditions.

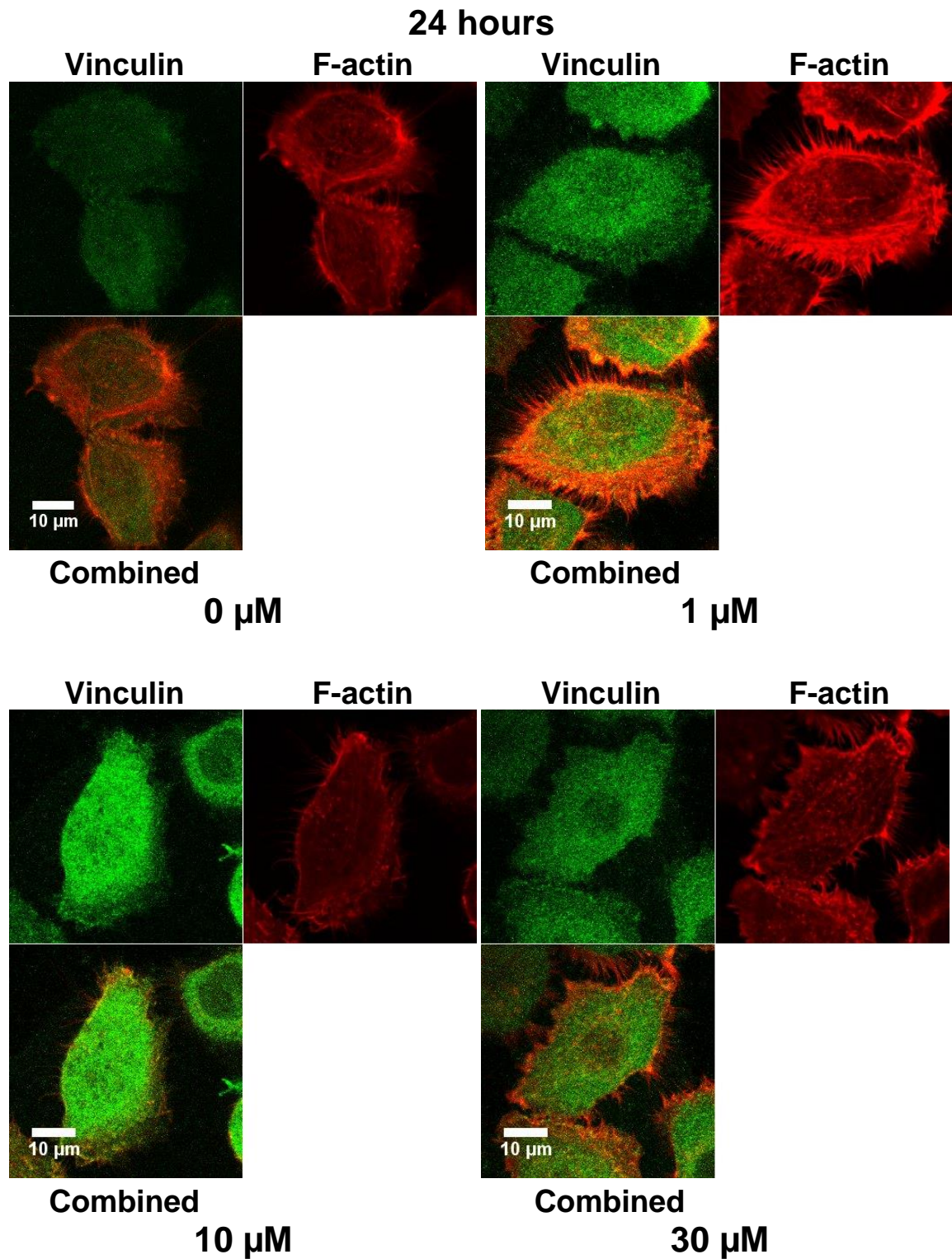


Figure 5.31. Immortalised human oral keratinocytes (OKF6) after treatment with zoledronic acid for 24 hours, stained for F-actin (red) and vinculin (green). Panels show: vinculin staining alone (upper left), F-actin staining alone (upper right) and a combined image (lower left).

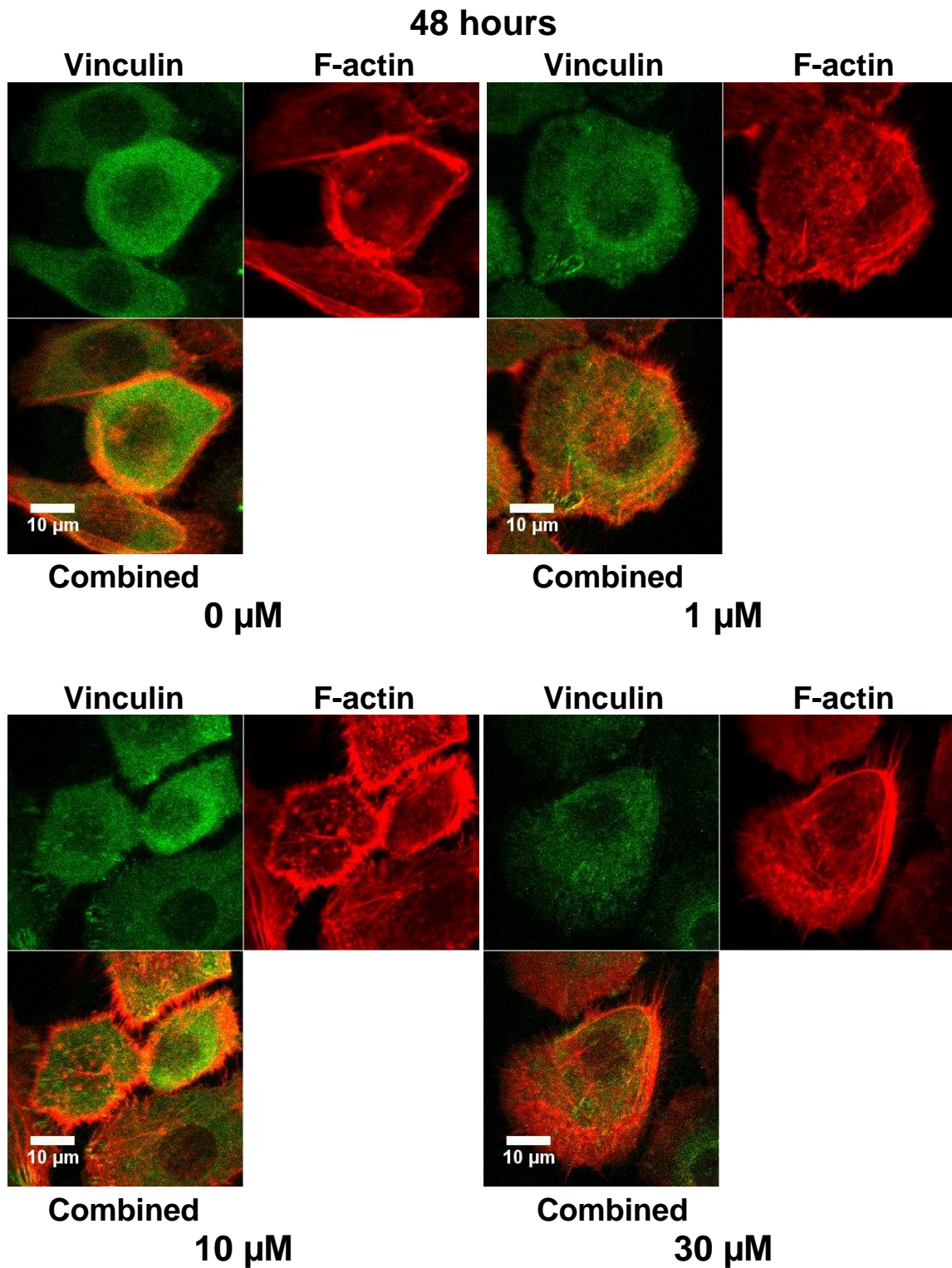


Figure 5.32. Immortalised human oral keratinocytes (OKF6) after treatment with zoledronic acid for 48 hours, stained for F-actin (red) and vinculin (green). Panels show: vinculin staining alone (upper left), F-actin staining alone (upper right) and a combined image (lower left).

Due to there being no clear differences in cytoskeleton staining with ZA treatment over 48 hours, treatment time was increased to 120 hours. Before this, BP toxicity over this time period was measured using a crystal violet assay. Figure 5.33 shows the percentage of cells remaining following treatment with zoledronic acid for 120 hours. A clear dose dependent reduction is apparent. Cells treated with 30 μM zoledronic acid all showed a dramatic reduction in cell number after 120 hours (approximately 80%) meaning this was unsuitable for staining studies. While concentrations from 1 to 10 μM did show a reduction in cell number following 120 hours of treatment, it was anticipated enough cells would remain to allow staining to be performed. There was no difference between cells treated with 0.1 μM and the control cells and this concentration was not used for the 120 hour immunostaining experiment.

Figure 5.33 shows keratinocytes treated for 120 hours with 0, 1, 5 and 10 μM zoledronic acid. F-actin and vinculin were shown in red and green, respectively, and nuclei were stained blue. As expected from the crystal violet results, a reduction in cell number occurred with increasing BP concentration. However, again no obvious differences in staining were apparent. Changes in cell morphology were observed, with cells appearing smaller as ZA concentration is increased, though this was likely due to cytotoxicity, rather than a specific adhesion effect.

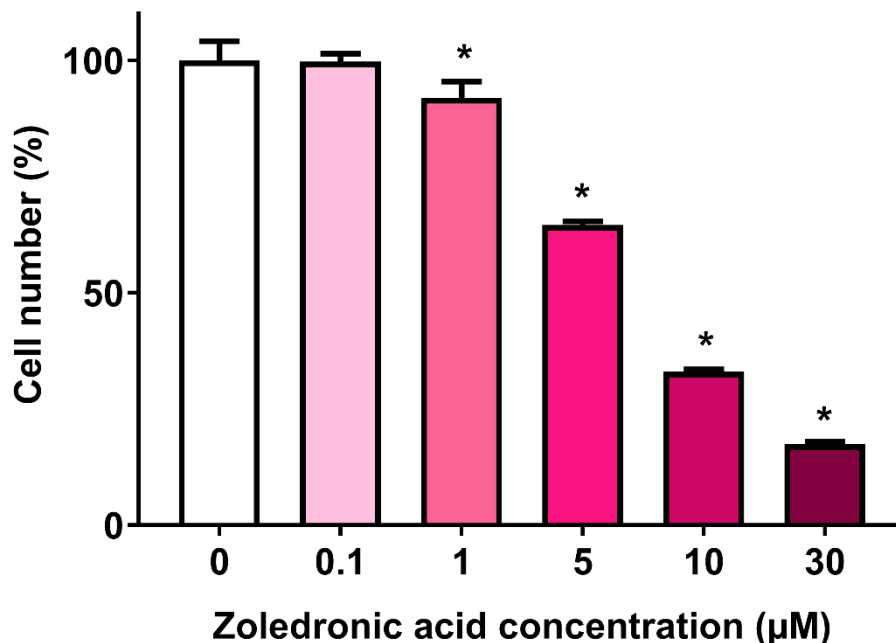


Figure 5.33. Immortalised human oral keratinocyte (OKF6) cell number after treating with zoledronic acid for 120 hours. Cell number measured by crystal violet assay, normalised to 0 μM . $N=1$, $n=3$. Error bars = SD. Significance against 0 μM indicated by * $P\leq 0.05$.

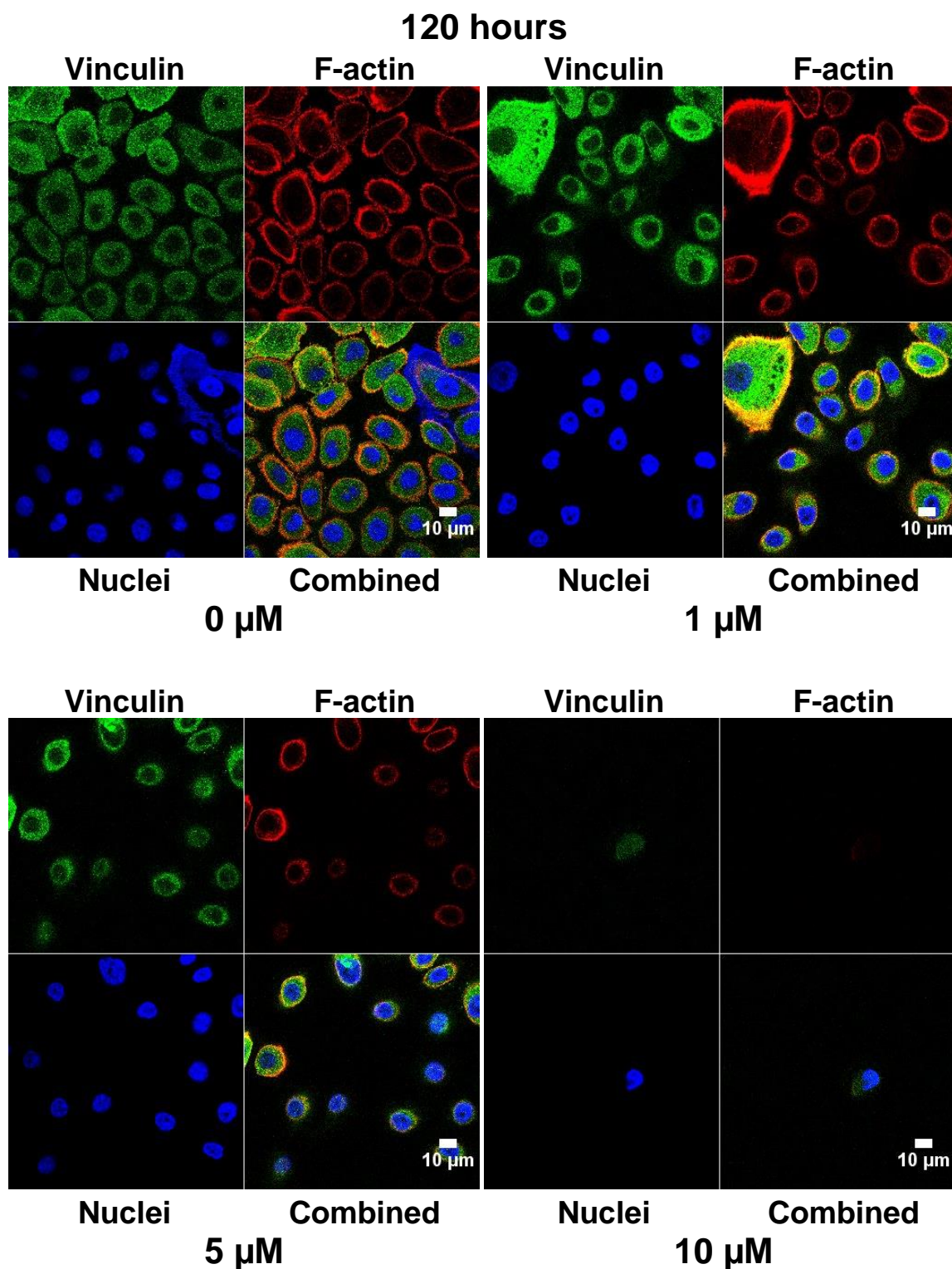


Figure 5.34. Immortalised human oral keratinocytes (OKF6) after treatment with zoledronic acid for 120 hours, stained for F-actin (red), vinculin (green) and nuclei (blue). Panels show: vinculin staining alone (upper left), F-actin staining alone (upper right), DAPI stained nuclei (lower left) and a combined image (lower right).

5.5 Discussion

Toxicity to the oral mucosa is hypothesised to be key to BRONJ development [2]. Following tooth extraction, or other BRONJ precipitating events, the mucosa becomes damaged and does not heal, which exposes the necrotic bone to the surrounding area. This increases the risk of infection and allows BPs bound to the bone to be released into the mouth. However, the mechanisms by which BPs affect the oral mucosa have not been fully elucidated. Investigating the effects of PA and ZA – two BPs which most commonly cause BRONJ – on cells of the oral mucosa is therefore an important step in understanding the condition, as it will allow assessment of how BPs prevent wound healing.

The BP concentration to which the oral mucosa is exposed is not known and difficult to estimate, given the differences in administration method, dosages and length of treatment. The concentration in bone has been estimated to be 2000 μM , assuming a 90 mg monthly infusion of PA for 4 years [56], [57]. The maximum blood serum concentration of ZA following a 4 mg infusion is estimated to be 1.47 μM [55]. The ZA concentration of the saliva of patients with osteonecrosis was measured 5 minutes after an IV 4 mg infusion, and estimated to be between 0.4 and 5 μM [142]. It can hence be assumed that the oral mucosa of BRONJ patients will be subjected to BPs in the concentration range of 0.4 to 2000 μM , and therefore values within this range were used during our work.

We have demonstrated that clinically relevant concentrations of both PA and ZA reduce the metabolic activity of cells from the human oral mucosa in a dose dependent manner over 72 hours of treatment. Our data supports the hypothesis that BP toxicity to the oral mucosa is likely to lead to the development of BRONJ, following dental surgery, with both the epithelium and connective tissue affected.

It is hypothesised that the BPs chelated to the osteonecrotic jaw bone are consistently released into the surrounding environment [48], [175]. We have shown that exposure to concentrations towards the lower limits of those expected will lead to soft tissue cytotoxicity over a relatively short period of time. Our data indicates a clear mechanism by which BPs could prevent soft tissue wound healing and contribute to the prolonged exposure of necrotic bone.

To measure the toxicity of oral mucosa cells, we performed MTT assays. Rather than directly measuring cell viability, these assays measure cell metabolic activity. When cells are subject to adverse conditions, they can occasionally increase their metabolic rate as a stress response and cause a false result, and, as highlighted through our apoptosis assay, metabolic activity can be reduced without a direct effect on viability. However, the assay is currently seen as the gold standard of cytotoxicity assays and we have therefore used it to measure PA and ZA toxicity in this thesis [292].

PA and ZA have previously been demonstrated to be toxic to fibroblasts and keratinocytes [34], [35], [168], [170]–[172], [175]–[177], [57], [86], [142], [144], [164]–[167]. However, these studies used cells from a variety of sources, examined different concentration ranges and treatment lengths, and used different assays to measure viability. Here, we have performed a comprehensive study of the toxicity of two BPs most commonly associated with BRONJ using cells from relevant sources and a broad range of BP concentrations allowing for a more direct comparison between two drugs and three different cell types.

We have also generated IC₅₀s for each cell and drug combination at 72 hours. This is a more precise measure than often used during BP studies and gives a more accurate picture of the toxicity of PA and ZA. Previous literature often features wide ranges and gaps between the highest non-toxic and lowest toxic concentrations (e.g. 30 µM and 100 µM [57]) which makes the determination of the exact toxic level difficult. Our data presents a more accurate measurement which is used worldwide as a standard measure of drug toxicity.

In our study, PA gave a 72 hour IC₅₀ value of 43 µM for fibroblasts. Cozin *et al.* had previously shown toxicity to oral fibroblasts to fall between 30 µM and 60 µM at 72 hours [144]. Our data supports their study and allows for the direct determination of the point at which the BP is toxic. In both our work and theirs, concentrations higher than the IC₅₀ value led to toxicity at 48 hours, and concentrations lower than the IC₅₀ led to toxicity at further time points. While we did not directly measure toxicity past 72 hours, we did treat fibroblasts with 30 µM PA for a total of 144 hours in our migration assay, where there was obvious cell toxicity. This highlights the dangers of prolonged exposure to the drug and suggests that if BP exposure could be limited to short time periods and low doses, the toxicity associated with BRONJ development could be avoided.

ZA has a higher anti-resorptive potency than PA, and has previously been demonstrated to also be more toxic to cells of the oral mucosa [144], [175]. This was also the case in our study, where the 72 hour IC₅₀ for fibroblasts was determined to be 6 µM. Concentrations ranging from 8 to 50 µM ZA have been reported as toxic concentrations for fibroblasts treated with ZA for 72 hours [144], [167], [168], [171], which hold true as they are over the IC₅₀. Our data shows that ZA toxicity occurs at an even lower concentration, and one that is very close to the expected BRONJ patient saliva concentration. This demonstrates one reason why patients taking ZA are more likely to develop BRONJ compared to those taking PA.

We also examined the toxicity of both drugs on two different types of keratinocytes: immortalised OKF6 cells and primary cells derived from human oral mucosa. OKF6 cells were originally sourced from human oral mucosa and modified to achieve immortality [179]. They provide a good model of oral keratinocytes, whilst removing the difficulties that

come with the sourcing and culture of primary human cells. Commonly, in literature, HaCaT cells are used for BP testing [169], [174], [176], [178]. These are highly proliferative immortalised skin cells. While simple to culture, these do not provide an accurate representation of human oral tissue. Murine cells have also been used [57], [140], which have a similar drawback. Our data therefore presents a more representative model of how BPs affect BRONJ patients.

Our work shows that both immortalised and primary keratinocytes are susceptible to BP toxicity. Immortalised cells proved more resistant to ZA toxicity than primaries, but less resistant to PA toxicity. However the toxicity values were all still well within the lower limits of the estimated clinical doses.

Our 72 hour IC₅₀ values for keratinocytes treated with PA were 35 µM and 59 µM for immortalised and primary cells, respectively. Landesberg *et al.* previously showed PA led to keratinocyte toxicity between 30 and 100 µM [57]. Pabst *et al.* indicated toxicity between 50 and 100 µM [175]. Our data supports these values and gives a more accurate suggestion of where the point of toxicity lies. While not mathematically deduced, data from Kim *et al.* suggested a primary keratinocyte IC₅₀ of approximately 50 µM at 96 hours [164], which fits with what is known about BP potency over time. This value, however, is higher than our immortalised keratinocyte IC₅₀ at 72 hours, which suggests that primary keratinocytes may be generally more resistant to PA than the OKF6s.

As with fibroblasts, both types of keratinocytes were more susceptible to ZA toxicity than PA. We generated a 72 hour IC₅₀ value of 19 µM for OKF6 cells and 8 µM for primary cells. Ravosa *et al.* have previously demonstrated that 10 µM concentrations of ZA and above were enough to significantly reduce metabolic activity of OKF6 cells after 48 hours, with 10 µM leading to approximately 20 % toxicity in comparison to untreated cells [35]. In our work, though not significant, 10 µM ZA similarly caused around 15 % toxicity at 48 hours.

Pabst *et al.* demonstrated a dose dependent ZA toxicity to primary human oral keratinocytes after 72 hours treatment in two studies, with a significant viability reduction at 50 µM in the first study, and a small but significant reduction in viability at 5 µM in the second [86], [175]. Whilst 50 µM ZA did cause toxicity to both types of keratinocytes in our work, 5 µM concentrations were not significantly toxic at any time point, and our 72 hour IC₅₀ values are above that value. Due to primary cells coming from different sources with inherent variability, it is to be expected that these differences between toxicity values exist. Due to these inherent differences between primary keratinocytes, as well as the difficulties that come with sourcing and culturing them when compared to immortalised keratinocytes, the rest of the work in this chapter used immortalised keratinocytes.

Immortalised keratinocyte growth took place at a faster rate than with fibroblasts or primary keratinocytes, particularly in Figure 5.6, where the metabolic activity of the control

had increased by around 300 % between 24 and 72 hours. Fibroblasts are metabolically slower than keratinocytes, and primary keratinocytes require an i3T3 feeder layer, so cells were closer to confluence in the well plate to ensure a good reading in the assay, which limited growth. Our proliferation data also indicates that fibroblasts proliferate at a slower rate than OKF6 cells, with the I_{pif} of control keratinocytes higher at 72 hours. Therefore more OKF6 growth between 24 and 72 hours was expected.

In terms of anti-resorptive potency, ZA is approximately 100 times more potent than PA [29]. This potency, however, refers to the ability of the drug to increase bone density in rats in the 'Schenk' model [31], [64]. While ZA was also more toxic than PA in our work, the differences in toxicity were smaller by an order of magnitude compared to anti-resorptive potency.

Based on the IC_{50} s generated, ZA was approximately seven times more toxic to fibroblasts and primary keratinocytes, and two times for immortalised keratinocytes. While the reduced difference in cytotoxic potency is a consistent result within the literature, the reasons for this are yet to be known. It is possible this is due to the mechanisms by which BPs cause their effects.

Nitrogen-containing bisphosphonates (nBPs) prevent resorption by disrupting the mevalonate pathway [31]. This prevents the formation of the osteoclast ruffled border, leading to non-functioning osteoclasts. The BP inhibition of the mevalonate pathway is known to occur at lower concentrations than toxicity [178], [293]. It has been indicated that ZA causes this effect at concentrations orders of magnitude lower than PA [294]. Thereby it follows that ZA would prevent resorption at concentrations at orders of magnitude lower than PA. Toxicity, however occurs through a different mechanism.

To determine the mechanism by which PA and ZA caused toxicity, we used flow cytometry to analyse the number of fibroblasts and immortalised keratinocytes undergoing apoptosis and necrosis, when treated with concentrations both above and below the IC_{50} s for PA and ZA. We found that fibroblast toxicity took place mostly by an apoptotic pathway, while some keratinocyte necrosis also occurred, though not at a significant level.

When treated with 10 μ M PA for 72 hours, there were no differences in the number of viable, apoptotic and necrotic fibroblasts in comparison to the control. This was expected due to our MTT data, where no differences were seen between these groups. Soydan *et al.* previously found approximately 34 % of cells apoptotic after 72 hours treatment with 10 μ M PA, however this work only examined 100 cells. Our assay, which analysed 10,000 cells, therefore, gives a more accurate and statistically robust measure of the proportion of cells undergoing apoptosis. In our work, a 50 μ M PA treatment caused a significant amount of apoptosis, with only around 25 % of cells viable, and approximately 70 % apoptotic. Again, this fits with our MTT data, where at 72 hours the metabolic activity was approximately 30 % of the untreated control. Concentrations of 30 μ M and 50 μ M

have been shown to cause fibroblast apoptosis after 96 hours treatment, with a study by Kim *et al.* indicating 10 μM PA had no effect at this time point [144], [164]. Our data supports this work and indicates that PA leads to apoptosis at an even earlier time point.

ZA did not cause a significant effect on fibroblast apoptosis when compared to the untreated control. Whilst 0.5 μM was not expected to cause a difference, as it led to no effect on metabolic activity in the MTT assay, a 10 μM ZA treatment reduced metabolic activity to approximately 30 % after 72 hours treatment and therefore more apoptosis was expected. Previously, Cozin *et al.* demonstrated ZA concentrations of 10 μM and above led to less fibroblast apoptosis at 7 days than with PA treatment [144], and Zafar *et al.* indicated 30 μM ZA only caused a slight increase in apoptosis at 96 hours [171]. This indicates that although 10 μM ZA is enough to cause an effect on fibroblast metabolism, higher concentrations of the drug are required to induce significant amounts of cell death. These higher concentrations are likely in BRONJ patients, given the estimated range to which the oral mucosa is exposed to.

Keratinocytes were more resistant to BPs when tested by MTT, and this was also the case in the apoptosis assay. Both 10 and 100 μM PA led to less apoptosis than expected based on the MTT data, where metabolic activity was reduced to 65 % and 32 %, respectively, compared to a reduction in viable cells of approximately 10 % and 20 %. Cell death was split evenly between apoptosis and necrosis. PA concentrations ranging from 3 to 100 μM have been shown to not induce apoptosis in keratinocytes before [57], [164]. This suggests the mechanism by which PA has its effect on keratinocytes is through another mechanism than apoptosis or necrosis.

More cell death was seen with ZA treatment, though this was still below the expected level based around the MTT data. When treated with 1 μM ZA, both the MTT and apoptosis assay indicated no differences to the control. However, though 50 μM ZA caused a 66 % metabolic activity reduction, only 30 % of cells had undergone apoptosis or necrosis. When Ravosa *et al.* performed the same assay with OKF6 cells at 48 hours, they found concentrations from 30 to 100 μM ZA to cause less than 10 % apoptosis [35]. We saw a significant level of apoptosis, with approximately 20 % of cells early or late apoptotic, after 72 hours treatment with 50 μM ZA. A longer treatment period would be expected to cause a higher amount of cell death, and therefore our result is expected. Although ZA caused a significant amount of apoptosis, the general low level of cell death indicates another mechanism by which keratinocytes are affected by BPs.

The mechanism by which BPs cause keratinocyte cell death has been examined previously, with different conclusions drawn. After discovering few apoptotic or necrotic cells after PA treatment, when compared to fibroblasts, Kim *et al.* also stained cells for senescence markers [164]. They found that keratinocyte senescence was increased by almost four times, with only a 10 μM PA treatment, while fibroblast senescence was

unaffected. However, Pabst *et al.* have previously indicated over 50 % of human oral keratinocytes underwent apoptosis following 72 hours treatment with 50 μM PA and ZA [86]. Though we saw significant apoptosis with ZA, it was not at the same level as Pabst *et al.*'s work, and twice the concentration of PA caused no effect in our work. This adds to the hypothesis that a different mechanism of cell death may be induced in keratinocytes. The determination of this mechanism presents a route for future examination though was outside the scope of this project.

Oral mucosa wound healing involves two key cellular processes: proliferation and migration. It has been hypothesised that BPs prevent the closure of the soft tissue wound following dental surgery by preventing both of these processes from occurring [2]. We therefore investigated both of these processes to determine the validity of the hypotheses.

We examined concentrations of PA and ZA both above and below the respective IC_{50}s for both fibroblasts and immortalised keratinocytes. High concentrations of PA and ZA caused a reduction in the proliferation rate of both cell types over a 72 hour time period, with low PA and ZA also preventing keratinocyte proliferation. Again, this indicates a mechanism by which BPs lead to the exposure of necrotic bone tissue in a BRONJ patient. Proliferation is normally increased following the creation of an oral mucosa wound so as to provide cells by which to close the wound [89], [115]. If this process is prevented, it follows that the wound would not heal.

PA had a dose dependent effect on fibroblast proliferation, with a 10 μM concentration causing no effect at 24 or 72 hours but 50 μM leading to no proliferation to take place at 72 hours. Soydan *et al.* have previously indicated a dose dependent effect on fibroblast proliferation of concentrations ranging from 0.1 to 1000 μM [165]. This effect was evident at time points from 6 to 72 hours, though only significant above 10 μM . However, they measured this by staining cells for Ki67, a proliferative marker found within cell nuclei. This method is known to be a more sensitive assay by which to measure cellular proliferation, as it can detect changes within more phases of the cell cycle, whereas CFSE staining only detects a reduction in the M phase, where cells divide [295]. This sensitivity would explain the differences seen at earlier time points by Soydan *et al.*, as cells would likely not have completed one cell cycle over 6 hours. As with apoptosis, however, Soydan *et al.* only sampled 100 cells, whereas we sampled up to 10,000, giving a more statistically robust measure of proliferation.

ZA also caused a dose dependent reduction in fibroblast proliferation over 72 hours. A 0.5 μM concentration caused no effect, while 10 μM significantly reduced proliferation in comparison to the control. These values are consistent with literature. Agis *et al.* indicated concentrations of 30 μM and 100 μM reduced proliferation of human gingival fibroblasts (HGFs) [167]. Concentrations between 0.25 and 5 μM have been indicated to reduce the cellular growth rate of human oral fibroblasts over 5 days through

cell counting [169], [173]. However this method is less robust measure of proliferation that does not take into account the amount of cells undergoing cell division [296]. While their data indicates that BPs prevent cell growth, this may be an effect of toxicity. Our data examined viable cells, and therefore indicates that BPs do prevent proliferation, which is therefore an important explanation as to why the mucosa wounds of BRONJ patients fail to heal.

Immortalised human oral keratinocyte proliferation was also reduced following 10 μ M and 100 μ M PA treatment. This study is the first time this has been demonstrated through a proliferation assay. Landesberg *et al.* previously indicated an effect on keratinocyte proliferation, however their study used murine cells and used a 3-(4,5-dimethylthiazol-2-yl)-5-(3-carboxymethoxyphenyl)-2-(4-sulfophenyl)-2H-tetrazolium (MTS) based metabolic activity assay to determine proliferation [57]. While their work suggested a reduction in proliferation, here we can state the cell cycle of keratinocytes is affected and cells do not proliferate when treated with PA for 72 hours.

Keratinocyte proliferation was also reduced by ZA, where 1 and 50 μ M significantly reduced proliferation, with 50 μ M leading to a I_{pif} similar to that of the mitomycin C treated non-proliferating cells. Both 5 μ M and 10 μ M have previously been shown to effect OKF6 proliferation [35], [173]. However both studies used less accurate measurements of proliferation (cell counting or MTS), and the 5 μ M study took place over 5 days, where it would therefore be expected that lower concentrations would have more of an effect. Overall, it is clear that clinically relevant concentrations of the drug reduce OKF6 proliferation and we have demonstrated it takes place at earlier time points and lower concentrations than previously known.

Our results demonstrate that cytotoxicity is not the only mechanism by which BPs lead to the soft tissue effects seen in BRONJ patients. At concentrations above the previously determined IC_{50} s, both PA and ZA caused a significant reduction in proliferation. This combination of effects strongly support the hypothesis that BP effects on soft tissue are key to the development of BRONJ and in particular contribute to the lack of soft tissue regeneration observed in BRONJ patients.

To further assess BP effects on wound healing, we also investigated how PA and ZA affect cell migration. Migration assays provide an *in vitro* approximation of *in vivo* wound healing [180]. Scratch assays are commonly used, where cells are cultured to confluence before a scratch is formed, but have issues with reproducibility and issues relating to cell damage in the creation of the scratch [297]. Using the Oris™ assay removed these issues, by creating uniform exclusion zones in a way which does not damage cells. Although cells are damaged in the development of BRONJ, this test was purely to assess any general effects of BPs on cell migration.

Sub-toxic concentrations of PA and ZA showed no effect on fibroblast or keratinocyte migration. This suggests that the lack of closure of BRONJ wounds is due to toxicity and proliferation effects alone. This counters a commonly reported effect in literature, where BPs have been shown to prevent wound closure in migration assays several times [86], [140], [144], [170], [172], [175]. However, many of the previous studies in this area have limitations. In several cases, literature reports on toxic concentrations of a BP over a certain time period, before then performing a migration assay using the same variables [86], [144], [170], [172], [175]. Often, images are not included. Cozin *et al.*, however, did feature images of their cells following the assay, and they did not appear viable, suggesting a cytotoxic effect is preventing their scratch assays from healing [144].

When performing a migration assay, it is important to ensure only migration is being studied. Concentrations below the IC₅₀ values were chosen so as to ensure any effect seen was a pure migration effect, as it would be expected that over the time periods chosen, concentrations above those levels would lead to cell death and prevent closure of exclusion zones. It has previously been demonstrated that nanomolar concentrations of BPs can affect oral keratinocytes [178], [293], [294], suggesting the concentrations chosen here were high enough that any potential effect could be recorded.

Wound closure is not due to migration alone, as proliferation also plays a part. For this reason, we used mitomycin C to prevent cellular proliferation, and therefore we could be certain any closure of the exclusion zone was due to cells migrating into the exclusion zones, rather than cells proliferating. While this was less representative of the clinical scenario, it allowed the two cell functions to be studied in isolation to further determine specific BP effects. Commonly, these assays are performed with no proliferation control [35], [57], [86], [140], [144], [170], [175], [178]. As we have shown, PA and ZA prevent cellular proliferation, and therefore the often observed literature effect on wound healing is likely due to proliferation differences, rather than the migration which is often reported.

When pre-treated with 30 µM PA for 72 hours, we found exclusion zones did not fully close. However, the cells in that case appeared to be subject to toxicity after 120 hours of BP treatment. This is similar to work from Landesberg *et al.*, who used murine keratinocytes to demonstrate that only pre-treatment with toxic concentrations of PA had any effect on the closure of their scratch assay [57]. This highlights the danger of prolonged exposure of BRONJ wounds to BPs and suggests toxicity plays a greater role than migration in BRONJ wounds. McLeod *et al.* controlled for proliferation in their assay with both OKF6 cells and immortalised human foreskin fibroblasts, and also used sub-toxic BP concentrations and they reported no effect on migration [46]. It therefore appears that, when examined using a more appropriate assay, BP effects on migration are not apparent.

The Oris™ assay did come with some limitations. While fibroblasts routinely formed well defined circles when cultured with the stoppers, keratinocytes were less precise. Cell

exclusion zones were less uniform, with spillage over the line following the removal of the stopper, and due to this more variation was found in the results. This is especially apparent in the data generated when keratinocytes were cultured in the presence of PA. Some cells lose contact inhibition when they are immortalised and begin to form multilayers when cultured to confluence, which could lead to a multi-layered formation of cells near the stopper which would theoretically spill into the exclusion zone when the stopper is removed. However, it has been reported that hTERT immortalised cell lines, such as the OKF6s, maintain contact inhibition which rules this out as a possible reason [298]. Even with this variation within the assay, the data still provided a clear picture of BP effects on migration.

We conclude from our data that PA and ZA do not affect the migration rate of either fibroblasts or keratinocytes. Our data suggests that in previous studies of this nature, both BP reductions in viability and proliferation rate will have contributed directly to the reduced wound closure in the assays performed.

BPs have also been shown to prevent cellular adhesion in different cell types, including oral fibroblasts, cancer cells and endothelial cells [82], [144], [181]–[183]. We have demonstrated for the first time that ZA causes an effect on oral keratinocyte adhesion *in vitro*. Treatment with the drug for 24 hours reduced the ability of cells to adhere to tissue culture plastic in a dose dependent manner. Though a fewer number of cells were expected to be found due to toxicity, the negative correlation between the groups was stronger in the detached and re-seeded cells, which indicates an effect further than just toxicity.

Various methods exist for the determination of cell adhesion effects. Commonly, cells are seeded onto different substrates – collagen, fibronectin, gelatin and vitronectin – as it is known that specific integrins mediate the binding to these substrates [82], [181]–[183]. Through this work it has been demonstrated that BPs effect binding in relation to the α_1 , α_v and $\alpha_v\beta_3$ integrins. BPs have also been shown to reduce the levels of $\alpha_v\beta_6$ and thereby inhibit the re-epithelialisation of oral mucosa wounds [187]. Our work attempted to examine a wider picture, examining keratinocyte adhesion to a tissue culture plastic substrate rather than looking at one specific integrin, however this would be an interesting area for future work and investigation.

We allowed attachment for 2 hours during our adhesion assay. In literature, cells are commonly seeded for 1 hour before the assay [82], [181]–[183]. When we measured keratinocyte adhesion over time, this did not seem suitable, as only approximately 50 % of cells adhered at 24 hours and there was more variation at this time point. Hence, we chose to adhere cells for longer to remove any potential noise from the data. A shorter period was desirable, as the longer the cells were on the substrate, the more time they

had to attach, and thereby overcome any BP effects. A 2 hour adhesion time point allowed for more cell adhesion and less variation.

Adhesion to tissue culture plastic takes place in three phases [299], [300]. Initially, electrostatic attraction draws the cell to the surface. Over the first few hours, integrin binding occurs to attach the cell more strongly, and then focal adhesions form and adhere the cell to the surface, which allows for cell spreading. As our assay is within the expected time frame for the second phase of cellular adhesion, we therefore hypothesise that ZA is affecting the integrin binding ability of oral keratinocytes. However, it is difficult to determine the mechanism by which ZA causes this effect. The integrins which have previously been shown to be affected by BPs in other cell types are mostly not expressed in keratinocytes [188]. Keratinocytes do express $\alpha_v\beta_6$, but only in response to wounding. In future, an integrin array would be a useful tool to determine exactly how BPs affect keratinocyte adhesion.

BP effects on cell adhesion have been reported for several different cell types, including fibroblasts, breast cancer cells, muscle cells and endothelial cells [82], [144], [181]–[183]. Basso *et al.* showed 5 μM ZA reduced the adhesion of HaCaT cells to titanium over 24 hours [174]. They also demonstrated some cellular toxicity with the same concentration but did not draw a link between the two effects. Their keratinocytes were stained for homing cell adhesion molecule, where a reduction of the molecules was seen with increasing BP concentration, confirming an adhesion effect on a titanium substrate. As potential BRONJ sufferers may have titanium implants in their jaws, this information is useful, though not representative of all patients. We have shown here that a more general effect on cell adhesion happens due to ZA treatment.

We saw no clear effect of ZA on the F-actin or focal adhesions of immortalised human keratinocytes. We also saw a much less specific focal adhesion staining than previously observed in similar studies using different cell types. The main effect notable in our staining was the toxicity, with fewer cells appearing at each time point. Cozin *et al.* noted a similar effect in fibroblasts when treated with pamidronic acid, however, they noticed marked differences in their staining following PA treatment [144]. In their work, fewer F-actin bundles were visible and the focal adhesion staining was much less specific. Previous vinculin staining of keratinocytes has appeared similar to our work, with fewer obvious focal adhesions and more general staining [301], [302]. Further, more detailed examinations of binding mechanisms and the effect of BPs on these are needed to draw any firm conclusions, however these were beyond the scope of this study.

BPs have previously been demonstrated to have effects on processes regulating the cytoskeleton [82], [181], [182], [186]. The BP effect on the mevalonate pathway causes the inhibition of rho kinase [144], [183], a protein involved in the assembly and organisation of the cytoskeleton [303]. It also leads to the reduced phosphorylation of focal adhesion

kinase (FAK), which regulates the formation, maintenance and turnover of focal adhesions [184], [304]. This has been reported in several cell types, though not keratinocytes. FAK inhibition is known in keratinocytes to reduce migratory ability, not adhesion, as focal adhesions can still form without phosphorylated FAK, but they cannot disassemble and reassemble [185]. As we have previously shown that BPs do not affect keratinocyte migration, this suggests that phosphorylation of FAK is not affected by zoledronic acid in human oral keratinocytes.

5.6 Summary

In summary, our data demonstrates that both PA and ZA affect a variety of cellular processes in human oral fibroblasts and keratinocytes, at concentrations toward the lower range of expected clinical dose. Both drugs reduced cellular metabolic activity of three different cell types over 72 hours. This toxicity took place through an apoptotic pathway, with higher levels of apoptosis seen in fibroblasts. Concentrations above IC_{50} values also led to a reduction in proliferation over the same time period. Cell migration, however, was not affected by sub-toxic concentrations of PA and ZA. A 24 hour treatment of immortalised keratinocytes with ZA led to a reduction in cellular adhesion to TCP over 2 hours. No clear effects on the keratinocyte cytoskeleton were observed through immunohistochemical staining following 120 hours of treatment.

6. The development of an *in vitro* model of the soft tissue component of BRONJ

6.1 Aim

To investigate the effects of pamidronic acid (PA) and zoledronic acid (ZA) on the oral mucosa at different stages of development using a 3D *in vitro* model, examining newly formed epithelia, established epithelia, and healing epithelia in a wound healing assay.

6.2 Introduction

In chapter 5 we demonstrated that PA and ZA are toxic to oral mucosa cells in 2D, and prevent cell proliferation and adhesion, but have no effects on the rate of migration at sub-toxic concentrations. However, 2D cell culture comes with limitations. It is not truly representative of the *in vivo* setting, and, as such, 3D culture systems have long been used *in vitro* as a way of more closely approximating the *in vivo* scenario.

During BRONJ development, it is clear that BPs prevent the oral mucosa from healing, maintaining exposure of the necrotic bone. It has also been demonstrated that the adhesion and differentiation of the oral mucosa is affected in BP patients with no signs of BRONJ, which increases the risk of BRONJ development [189]. However, this is derived from patient data, and has not been quantified. This chapter studies the effects of BPs on the oral mucosa, modelling three key stages of development. First, models with a single cell epithelial layer, representing the thin oral mucosa formed during re-epithelialisation before stratification occurs. Second, stratified epithelial layers, representing the established, healthy epithelium that exists prior to surgery and surrounding the initial wound. And finally, in a 3D epithelial wound healing model representing the entire soft tissue component of BRONJ. The wound model was one developed for this work, through testing of a variety of different techniques.

Several *in vitro* models of oral mucosal tissue exist [194]. Mostly, these include a scaffold to mimic the lamina propria containing fibroblasts, with a stratified epithelium above. Scaffolds can be made from a wide variety of sources including natural polymers, such as collagen, polymeric blends, or acellular skin [200]. Our work used acellular skin, commonly known as de-epidermised dermis (DED), as it provides a scaffold close to that of the natural environment, and is more mechanically strong than other options, making it easier to wound without compromising the whole model.

Due to the similarities between BP effects on primary and immortalised keratinocytes and ease of culture of immortalised keratinocytes, this work was mostly

performed with immortalised cells. Clinically relevant BP concentrations based on the IC₅₀ values generated from our 2D work were used.

6.3 Materials and methods

Cell culture was performed as described in section 4.1. Bisphosphonates were prepared as described in section 4.2. Throughout this chapter, medium containing no BPs (0 µM) was used as a control.

6.3.1 Seeding of 3D oral mucosa model

DED was cut into squares of approximately 20 x 20 mm using a sterile scalpel and placed into a 6 well plate. Chamfered stainless steel rings with a 10 mm internal diameter were placed onto the DED, and pressed lightly to create a seal. 250,000 fibroblasts in 0.25 ml medium, and 1 million keratinocytes in 0.25 ml medium were seeded into the middle of the ring. DMEM was added outside the ring to prevent the cell solution leaking. The models were placed into an incubator.

After 24 hours, 0.25 ml of media was carefully removed from the middle of the ring, so as not to disturb any unattached cells, and replaced with either KSFM or Green's, depending on the keratinocyte type used. At 48 hours after seeding, the media in the middle of the ring was replaced entirely by 0.5 ml of 1:1 KSFM and Green's for OKF6 models, or Green's alone for primary cell models.

At 72 hours after seeding, the models were lifted to ALI by placing onto a stainless steel grid in Green's medium. The underside of the model was in contact with the liquid medium, while the top was in contact with air, to promote stratification of the epithelium. The seeding process is shown in Figure 6.1.

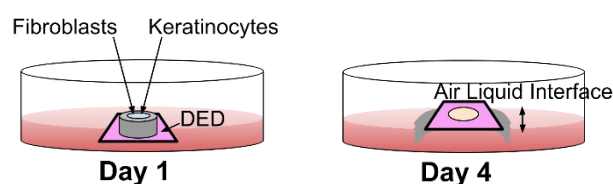


Figure 6.1. The general seeding process for oral mucosa models

6.3.2 DED model epithelium stratification test

To examine the epithelial stratification of the immortalised keratinocyte models, two models were seeded as described in section 6.3.1. Before placing at ALI, they were quartered with a sterile scalpel, forming 8 samples. After 4, 7, 10 and 14 days, two of the

samples were fixed in a 10 % formalin solution in PBS and processed for histological staining.

6.3.3 Resazurin assay

A resazurin assay measures metabolic activity [305]. Resazurin sodium salt (Sigma-Aldrich) was dissolved in distilled water at a concentration of 251 µg/ml and sterilised with a 0.2 µm filter. This was stored at 4 °C, protected from light, for up to two weeks. Before each experiment, the stock solution was diluted 1 in 10 in media. At each time point, samples were moved from ALI to a well plate and incubated in resazurin containing medium for 4 hours. 100 µl samples from each well were taken in triplicate and placed in a 96 well plate. This plate was then read using an absorbance reader. Readings were taken at 562 nm, with a reference at 630 nm. Samples were removed from the resazurin solution, washed with PBS, and either placed back at ALI or fixed overnight in 10 % formalin.

Every resazurin assay included a blank well, which contained only medium and the resazurin salt. This well was run according to experimental conditions, and the value subtracted from the other results to give a no cell value of 0 %. As model to model variation exists in the 3D mucosa models, especially when these models were halved or quartered, the resazurin values were normalised to the earliest time point measured. These time points were set as 100 % to allow comparison between models, and are not displayed in figures.

6.3.4 Oral mucosa models with bisphosphonates

Models were seeded as previously described in section 6.3.1, then quartered, before treating with BPs in one of two different methods. A flow chart of the different regimens for treating the models is shown in Figure 6.2.

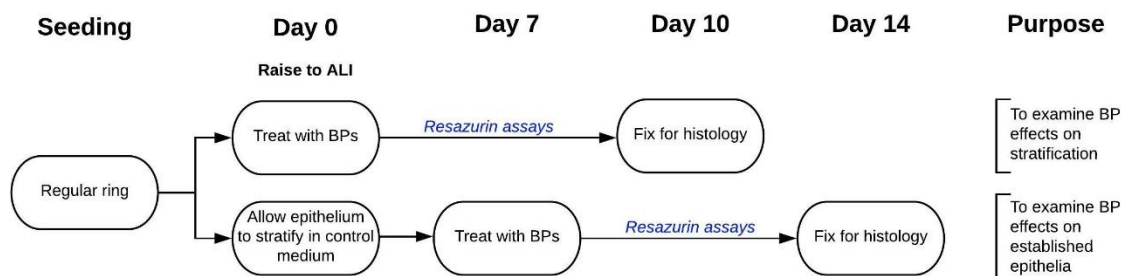


Figure 6.2. A flow diagram to show the different treating regimens for oral mucosa models treated with bisphosphonates.

To examine BP effects on epithelium formation, the models were then put to ALI in triplicate, in media at concentrations of 1 to 30 μM ZA and 50 to 100 μM PA, and control medium. After 4, 7 and 10 days, models were individually transferred to a well plate, where resazurin solution was added. Well plates were protected from light and incubated for 4 hours, when 100 μl was removed from each well in triplicate and read in an absorbance reader, as described previously. Samples were then washed with PBS. At day 4 and 7, models were placed back to ALI and the media replaced. At day 10, samples were fixed. Images were taken of each model directly following each resazurin assay, and resazurin values were individually normalised to day 4 values.

To examine BP effects on established epithelia, models were placed at ALI for 7 days in control medium. Resazurin assays were performed as above and models were placed in BP containing medium. At day 10 and 14, resazurin assays were repeated, before models were either placed back at ALI in fresh medium or fixed, respectively. Values were normalised to those gathered at day 7.

6.3.5 Wounding of oral mucosa models

Models were seeded as before and left whole. Media changes occurred at 4, 7 and 10 days, and following a resazurin assay. Models were cultured at ALI for either 7 or 10 days before wounding. One day prior to wounding, a resazurin assay was performed to establish a value by which to normalise further readings. A soldering iron (Antex) was allowed to reach full temperature, before being pressed to the centre of the model for 1 second. A cauteriser wire (Fine Science) was heated and pressed against the model for 1 second. A biopsy punch (Miltex) was used to manually create a circular wound with a 3.5 mm diameter. Resazurin assays were performed as before. Models were then either fixed, or placed back at ALI for up to 10 days, with resazurin assays performed on days 3, 7 and 10. Following the assay on day 10, models were fixed in 10 % formalin.

6.3.6 3D printed ring design and manufacture

Models were also selectively seeded with keratinocytes to create an in vitro wound equivalent. For this, a bespoke cell culture ring was designed using SketchUp (Trimble Inc.). The design of the ring is shown in Figure 6.3. The model was printed using a stereolithography printer (Form 2, FormLabs) from a photopolymer resin (Grey Resin, FormLabs). After printing, the rings were washed in isopropanol and cured in a UV curer (3D Systems). Rings were then sterilised in 70 % ethanol and rinsed thrice in PBS to remove any ethanol. They were then placed in DMEM in an incubator for 5 days to ensure any uncured polymer was released. After use, rings were rinsed in distilled water and detergent.

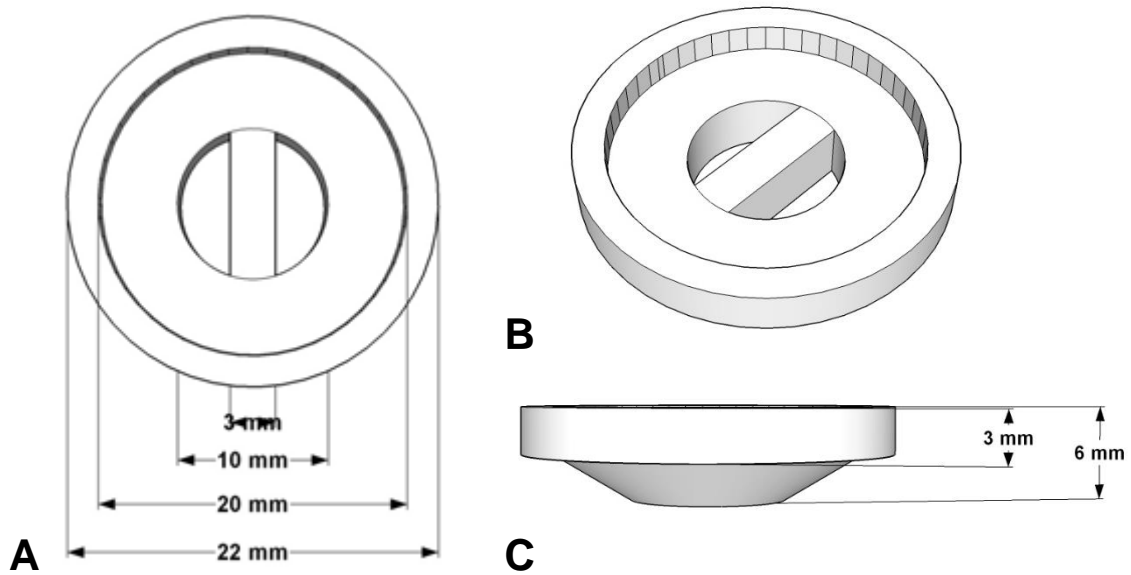


Figure 6.3. The computer-aided design model of a bespoke cell culture ring from (A) top down, (B) isometric and (C) side on view.

6.3.7 3D wound healing assay

Seeding and treating models using the 3D rings took place according to three different regimens. Firstly, models were seeded using the rings then treated immediately when raised to ALI. The rings were sterilised and rinsed as previously described and placed in a petri dish. Sections of DED of approximately 20 x 20 mm were cut as before. The rings were placed, chamfered edge down, onto the DED. To ensure a tight seal was created, a stainless steel ring was placed into the lip of the 3D printed ring to add weight. Cells were then seeded, with 250,000 fibroblasts and 1 million keratinocytes in a total of 0.4 ml media, with media changes taking place over 3 days as in section 6.3.1.

At day 4, models were raised to ALI. Beforehand, the rings were removed and the models transferred to a well plate, where a resazurin assay was performed to visually assess seeding efficacy. This time point was set as day 0. Models were cultured for up to 7 days, with resazurin assays performed at days 1, 4 and 7, at which point samples were fixed.

Models seeded by this method were also cultured in BP containing medium when placed at ALI, in 10 μ M ZA and 50 and 100 μ M PA. Resazurin assays were performed on days 0, 1, 4 and 7, with values normalised against day 0. At day 7, models were fixed and processed for histology.

The second and third seeding regimens were designed to ensure the epithelium of the two sections was stratified. These are represented diagrammatically in Figure 6.4. In both methods, the DED, ring placement and cell seeding was performed as described above. In the first method, the DED was placed onto a stainless steel grid before the rings were applied and pressed into the DED to create a seal. DMEM was then added to the

well, above the level of the DED, and cells seeded. On day 4, media was removed from inside the rings and the liquid level outside the rings lowered to the level of the underside of the DED to create an ALI for the epithelial cells in both sections of the ring. Models were cultured until day 11, with a media change taking place on day 8.

In the second method, DED was placed on the bottom of a well plate and seeded with the 3D printed ring as before. At day 4, media was removed from the inside of the ring, and the liquid level outside of the ring lowered to create an *in situ* ALI. Every 48 hours, media outside of the ring was replaced, and any media inside the ring was removed, until day 11.

After this stage, the procedure for both methods was the same. The rings were removed, ensuring not to remove the epithelial sections. A sterile needle point was used to dislodge the epithelium from the ring for some models. Resazurin assays were performed, as before, with the first resazurin assay being referred to as day 0. Models were then cultured for up to 7 days before fixing and processing for histology. Models seeded by these methods were also treated with BPs.

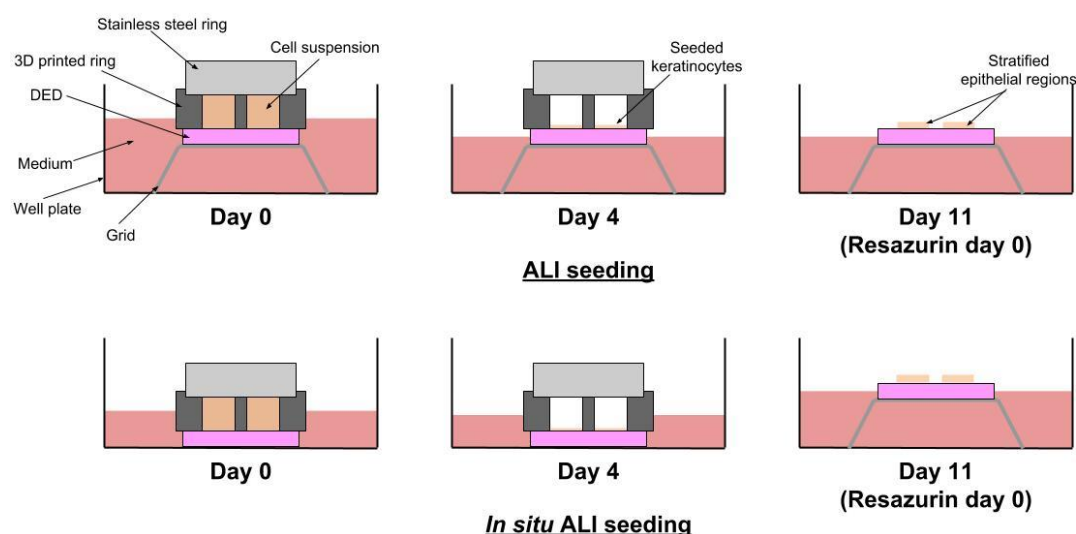


Figure 6.4. Cross sectional diagram of the process for seeding models at air-liquid interface (ALI) or with an *in situ* ALI.

6.3.8 Histology

Models were kept overnight in a 10 % formalin solution in PBS. Samples were bisected with a scalpel to place the area of interest on the outside edge, demonstrated in Figure 6.5. They were then placed in cassettes and ran through a tissue processor (Leica TP 1020), which gradually dehydrated the samples in IMS, cleared them in xylene (Thermo Fisher Scientific) and infiltrated them with paraffin wax (VWR), according to the schedule in Table 6.1.

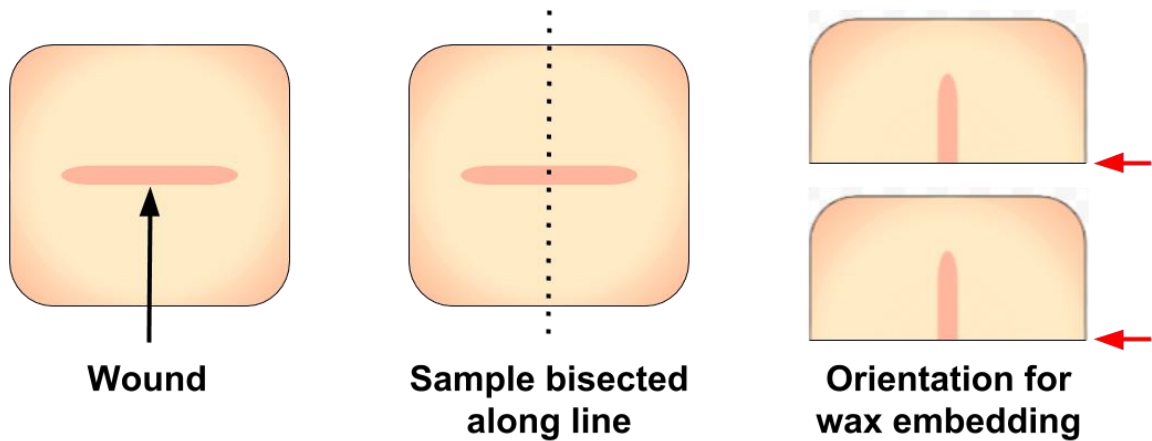


Figure 6.5. A diagrammatical representation of sample preparation for histology, red arrows indicate side used for histological sections.

Table 6.1. The tissue processing schedule

Solution	Time (hours)	Purpose
70 % IMS	1	Gradual dehydration of sample
70 % IMS	1	
80 % IMS	1.5	
85 % IMS	1.5	
90 % IMS	1.5	
95 % IMS	1.5	
100 % IMS	1.5	
100 % IMS	1.5	
Xylene	1.5	To clear the sample and allow for wax infiltration
Xylene	1.5	
Molten paraffin wax	2	Infiltration of wax
Molten paraffin wax	2	

Following processing, samples were embedded in molten paraffin wax using an embedding centre (Leica EG1160). Samples were embedded with the surface of interest placed perpendicular to the bottom of the mould to ensure the right orientation when cutting. Moulds were placed on ice to cool for 1 hour minimum. Samples were then removed from the moulds and transferred to a microtome (Leica RM2145). Samples were initially trimmed in 30 µm slices to expose the full sample, which was then sliced at a thickness of 4 µm. Slices were placed in a 37 °C water bath (Barnstead Electrothermal) to allow them to flatten, then attached to a SuperFrost slide (Thermo Fisher Scientific). Slides were transferred to a 40 °C hot plate to ensure sample attachment to the slide. Slides were

then stained with haematoxylin (Sigma-Aldrich) and eosin (Sigma-Aldrich) in accordance to the protocol in Table 6.2.

Table 6.2. The process for histological staining with haematoxylin and eosin.

Solution	Time	Purpose
Xylene (twice)	3 minutes	To de-wax the sample
100 % alcohol	1 minute	To gradually rehydrate the sample
70 % alcohol	30 seconds	
Distilled water	1 minute	
Haematoxylin	1.5 minutes	To stain basophilic substances such as DNA
Tap water (running)	4 minutes	To 'blue' the stain by neutralizing the acid
Eosin	5 minutes	To stain acidophilic substances
Tap water	1 second	To gradually dehydrate the sample
Tap water	1 second	
70 % alcohol	1 second	
100 % alcohol	30 seconds	
Xylene (twice)	1 second	To clear the sample by removing excess alcohol

After staining, glass coverslips were attached to the slides using DPX mountant and left to dry. Images of the samples were taken using a light microscope (Motic). Images were processed with Photoshop CS2, with images stitched together and backgrounds removed to leave only the sample visible. Scale bars were added using ImageJ.

6.3.9 Statistics

Statistics were performed using Prism as described in section 4.3. 'N' is used to denote experimental repeats, while 'n' is used to denote technical repeats throughout.

6.4 Results

6.4.1 DED models with immortalised keratinocytes were cultured to approximate native tissue

3D models of the oral mucosa were cultured using DED as a scaffold, seeded with established human oral fibroblasts and immortalised human oral keratinocytes. Immortalised cells were used for optimisation of the model as they are easier to culture, in greater supply, and responded to BPs in a similar way to their primary equivalents in our 2D work.

To use these models as close representations of native oral mucosa, it was necessary to determine the length of time the models needed to be at ALI before they contained a stratified epithelium across the whole model. Figure 6.6 shows the stratification of the epithelium over time. As the samples were fixed at each time point, each image is of a different sample. Two samples are included to demonstrate the epithelial consistency. Figure 6.6A & B show that after 4 days culture the epithelium was largely one or two cells thick. By 7 days, the epithelium had become multi-layered in most places with some differentiation between keratinocyte layers shown in Figure 6.6C. However, Figure 6.6D demonstrates there were thinner areas of epithelium at 7 days. After 10 days of culture, the epithelium was multi-layered over the whole sample. Figure 6.6E & F show the morphologies of the keratinocytes change from the basal to top layer of the epithelium, and rete ridges are visible on both samples.

The epithelium after 14 days, shown in Figure 6.6G & H, also has a stratified epithelium across the whole model, however with a thinner epithelium in Figure 6.6H. More haematoxylin staining was evident in the connective tissue in these models.

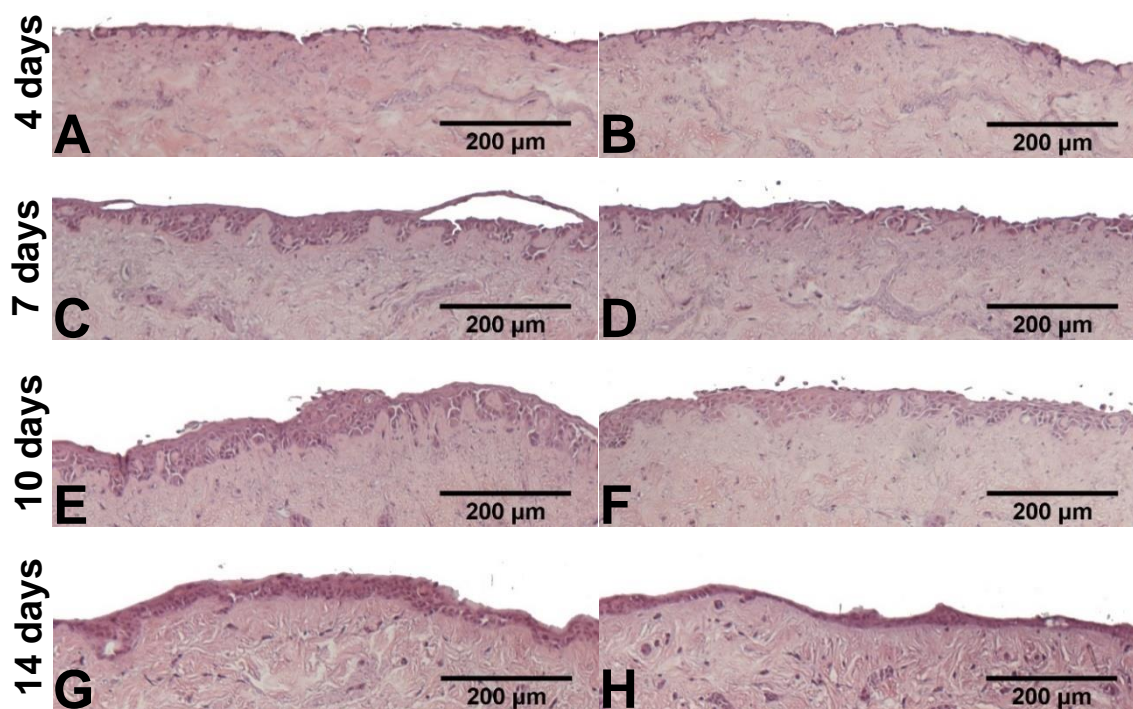


Figure 6.6. H&E stained sections of oral mucosa models seeded with human oral fibroblasts and immortalised human oral keratinocytes cultured at ALI then fixed after (A,B) 4 days, (C,D) 7 days, (E,F) 10 days or (G,H) 14 days. Representative images of two models used.

6.4.2 Bisphosphonates prevented a stratified epithelium from forming

Oral mucosa models were cultured in BP-containing medium immediately when placed at ALI to assess how BPs affected the stratification of the epithelium. Figure 6.7 shows resazurin assay readings as a measure of metabolic activity for the models. When cultured in control medium, the metabolic activity of the models increased at each time point and Figure 6.8A shows a multi-layered, healthy epithelium after 10 days culture. Models cultured in PA showed approximately consistent values over the experiment. However the metabolic activity was significantly reduced in comparison to the control at 10 days. This suggests the BP was preventing growth whilst not toxic. This was confirmed through histology with Figure 6.8B & C showing a thin epithelium largely one or two cells thick following 10 days of treatment with 50 and 75 μM PA, respectively. When treated with 100 μM , a single layer of keratinocytes was present, shown in Figure 6.8D.

ZA showed a more pronounced effect, with a dose dependent reduction of metabolic activity over 10 days. When treated with 1 μM ZA, similar to PA, metabolic activity maintained approximately the same throughout the experiment. However, 10 and 30 μM ZA led to a significant reduction in metabolic activity at days 7 and 10. The 30 μM treated models had metabolic activities of approximately 20 and 10 % of their day 4 reading at days 7 and 10, respectively. The histology again supported the data, with Figure 6.8E demonstrating a thin, disrupted epithelium with a 1 μM ZA treatment, and Figure 6.8F & G demonstrating a lack of epithelium following ZA treatments of 10 and 30 μM .

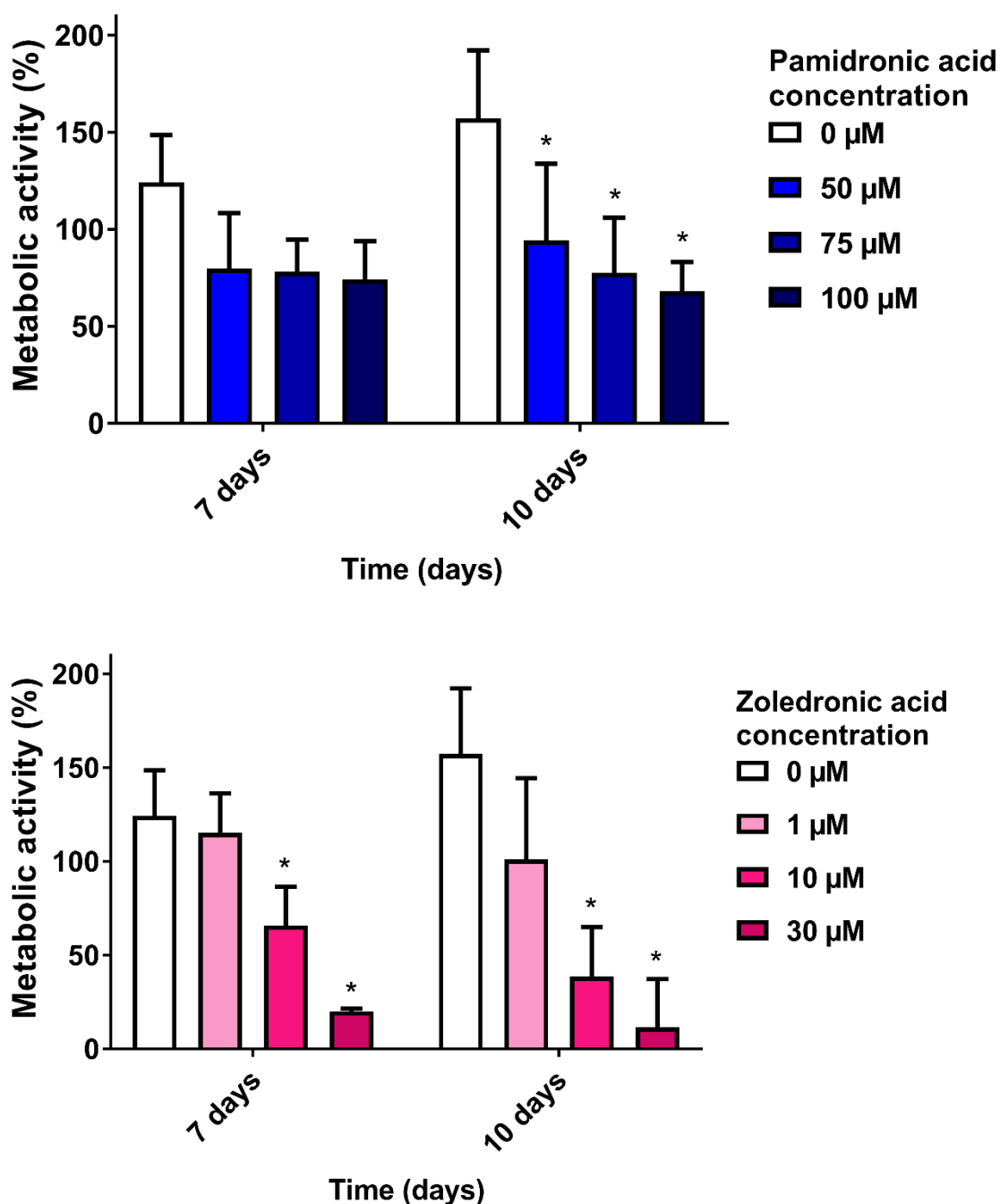


Figure 6.7. Metabolic activity of immortalised keratinocyte oral mucosa models when treated with 50, 75 and 100 µM pamidronic acid and 1, 10 and 30 µM zoledronic acid immediately after placing at ALI, measured with a resazurin assay. Blank well reading subtracted from values before normalising to day 4 values for each model. Day 4 not shown as all values 100%. $N=3$, $n=3$. Error bars = SD. Statistical significance against control at each time point indicated by $*P \leq 0.05$.

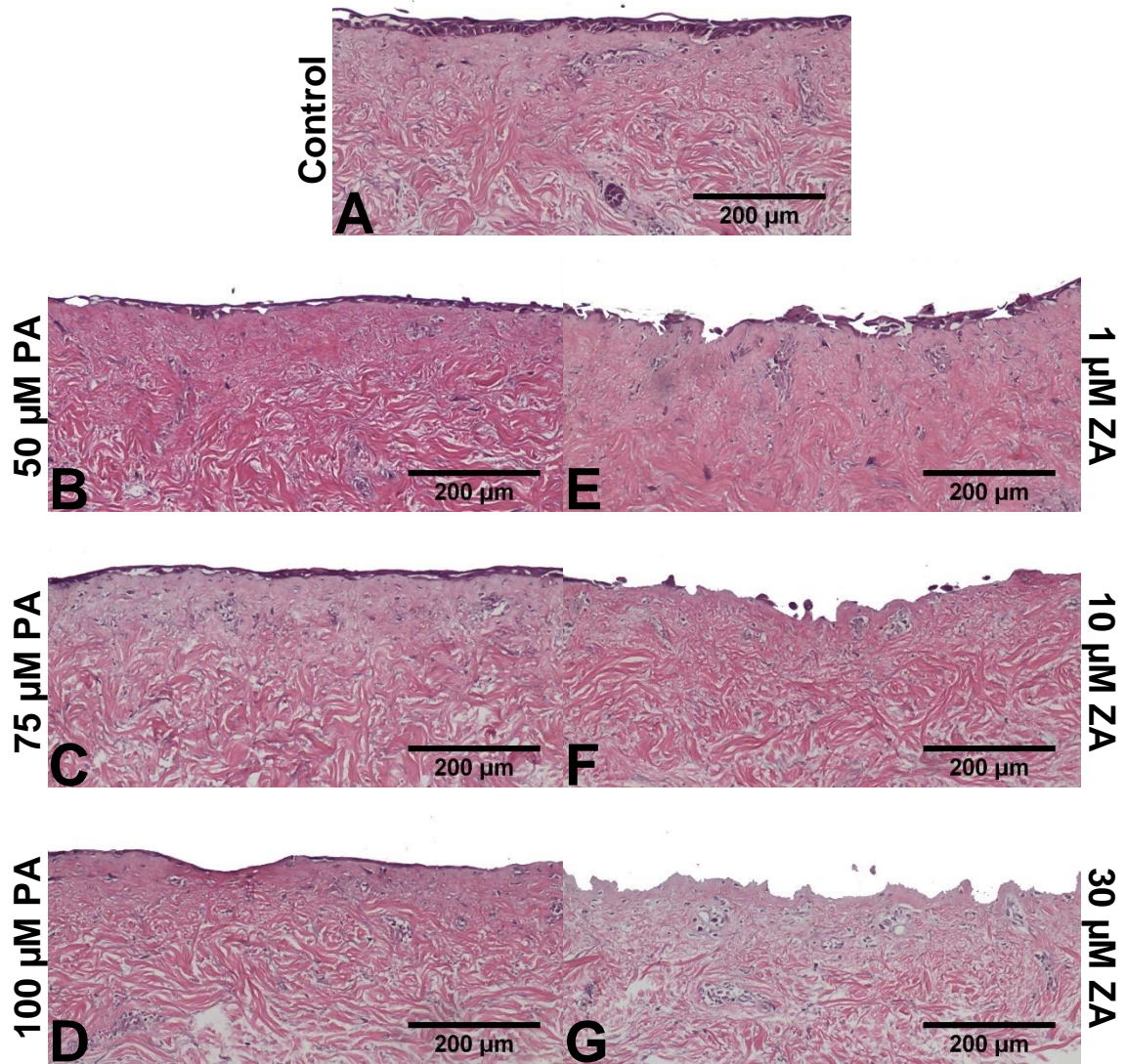


Figure 6.8. H&E stained sections of oral mucosa models seeded with human oral fibroblasts and immortalised human oral keratinocytes cultured at ALI in (A) control medium, (B) 50 μM, (C) 75 μM and (D) 100 μM pamidronic acid, (E) 1 μM, (F) 10 μM and (G) 30 μM zoledronic acid, respectively, for 10 days. Representative images used.

6.4.3 Bisphosphonates reduced the thickness of healthy, established epithelia

In order to study how BPs affected healthy mucosa, models were cultured for 7 days to allow the epithelium to stratify before treatment. This culture time was chosen as the models had previously been shown to be mostly stratified, while allowing for a shorter total culture time and thereby preventing any models from losing their metabolic activity due to length of culture.

Firstly, models were cultured with immortalised keratinocytes. Figure 6.9 shows that PA had no significant effect on the metabolic activity of the models in comparison to the control. Values for all samples, including the control, decreased from day 7 to day 14. Figure 6.10A shows the epithelium of a model cultured for 14 days in control medium, where the epithelium has stratified. Figure 6.10B, C and D demonstrate that while PA had no effect on metabolic activity, it caused a reduction in epithelial thickness. A dose dependent response was seen, with increasing concentration leading to reduced thickness. While these epithelia were thinner, differentiated keratinocytes were still present on the top layer.

ZA again had a more pronounced effect. While 1 and 10 μM concentrations led to no significant reduction, a 30 μM concentration significantly lowered the metabolic activity to approximately 10 % after 7 days of treatment (14 days total culture). Figure 6.10E & F demonstrate 1 and 10 μM concentrations of ZA reduced epithelial thickness in a dose dependent manner. No epithelium was visible on the samples treated with a 30 μM concentration, shown in Figure 6.10G.

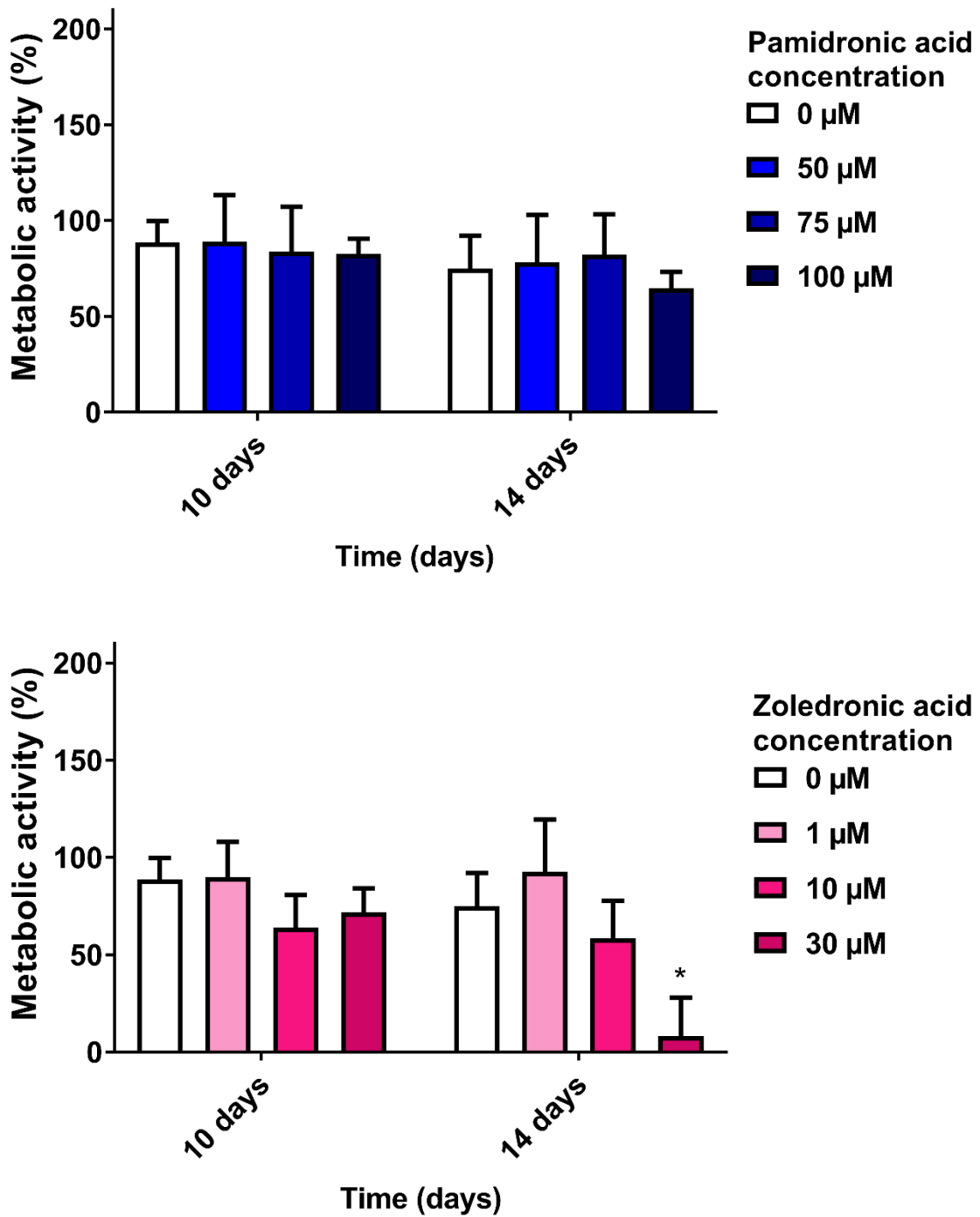


Figure 6.9. Metabolic activity of immortalised keratinocyte oral mucosa models when cultured at ALI for 7 days in control medium, then treated with 50, 75 and 100 µM pamidronic acid and 1, 10 and 30 µM zoledronic acid for 7 days, measured with a resazurin assay. Blank well reading subtracted from values before normalising to day 7 values for each model. Day 7 not shown as all values 100 %. N=3, n=3. Error bars = SD. Statistical significance against control at each time point indicated by *P≤0.05.

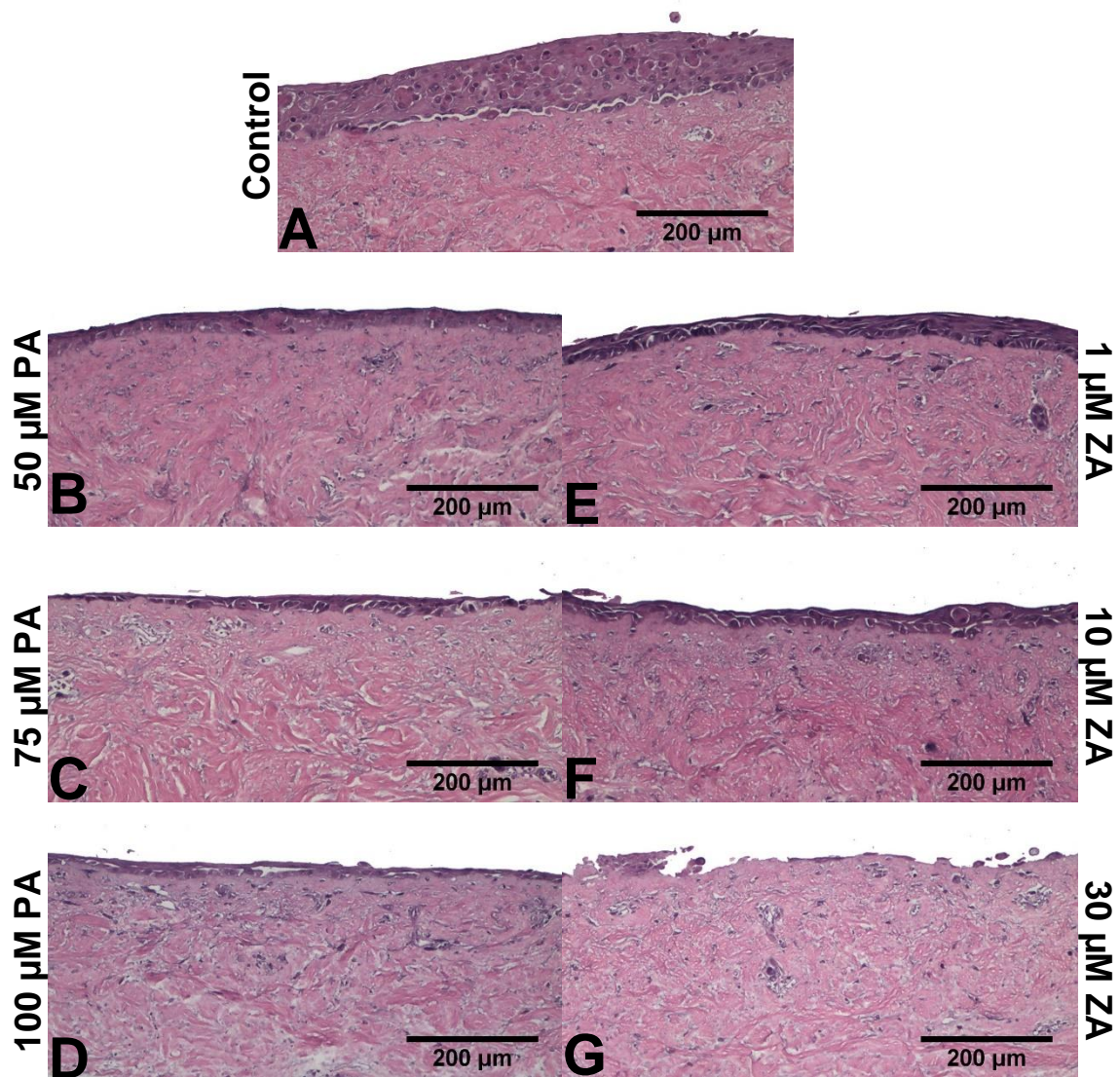


Figure 6.10. H&E stained sections of oral mucosa models seeded with human oral fibroblasts and immortalised human oral keratinocytes cultured at ALI for 7 days in control medium, then treated with (A) control medium, (B) 50 μM , (C) 75 μM and (D) 100 μM pamidronic acid, (E) 1 μM , (F) 10 μM and (G) 30 μM zoledronic acid, respectively, for 7 days. Representative images used.

Models containing primary keratinocytes were also subjected to the same treatment regimen. Figure 6.11 shows the metabolic activity data. PA again showed no significant differences to control medium after 14 days culture. ZA caused no effect at a 1 μM concentration, but was toxic at 10 and 30 μM at day 14, after 7 days treatment, with a dose dependent response seen. In the primary models, the lowest concentration of both BPs caused an increase in metabolic activity at day 10, though this was not significant and variation was high.

Figure 6.12 shows histological sections of primary keratinocytes at day 14, following 7 days BP treatment. After culturing for 14 days in control medium, a complete, stratified epithelium was present on the model, as shown in Figure 6.12A. When treated with PA, though a complete epithelium was present on the models, treatment reduced the thickness of the epithelium in a dose dependent manner. Figure 6.12B shows that 50 μM PA led to an epithelium of a similar thickness to the control model, while 75 and 100 μM PA led to an epithelium that appeared 1 or 2 cells thick and flattened, as shown in Figure 6.12C & D.

A 1 μM ZA treatment led to a multi-layered epithelium, as shown in Figure 6.12E. As expected from the metabolic activity data, 10 μM ZA caused a reduction in epithelial thickness, shown in Figure 6.12F. When treated with 30 μM ZA for 7 days, the epithelium of the models were disrupted, as demonstrated in Figure 6.12G, where the epithelium was not present across the whole sample.

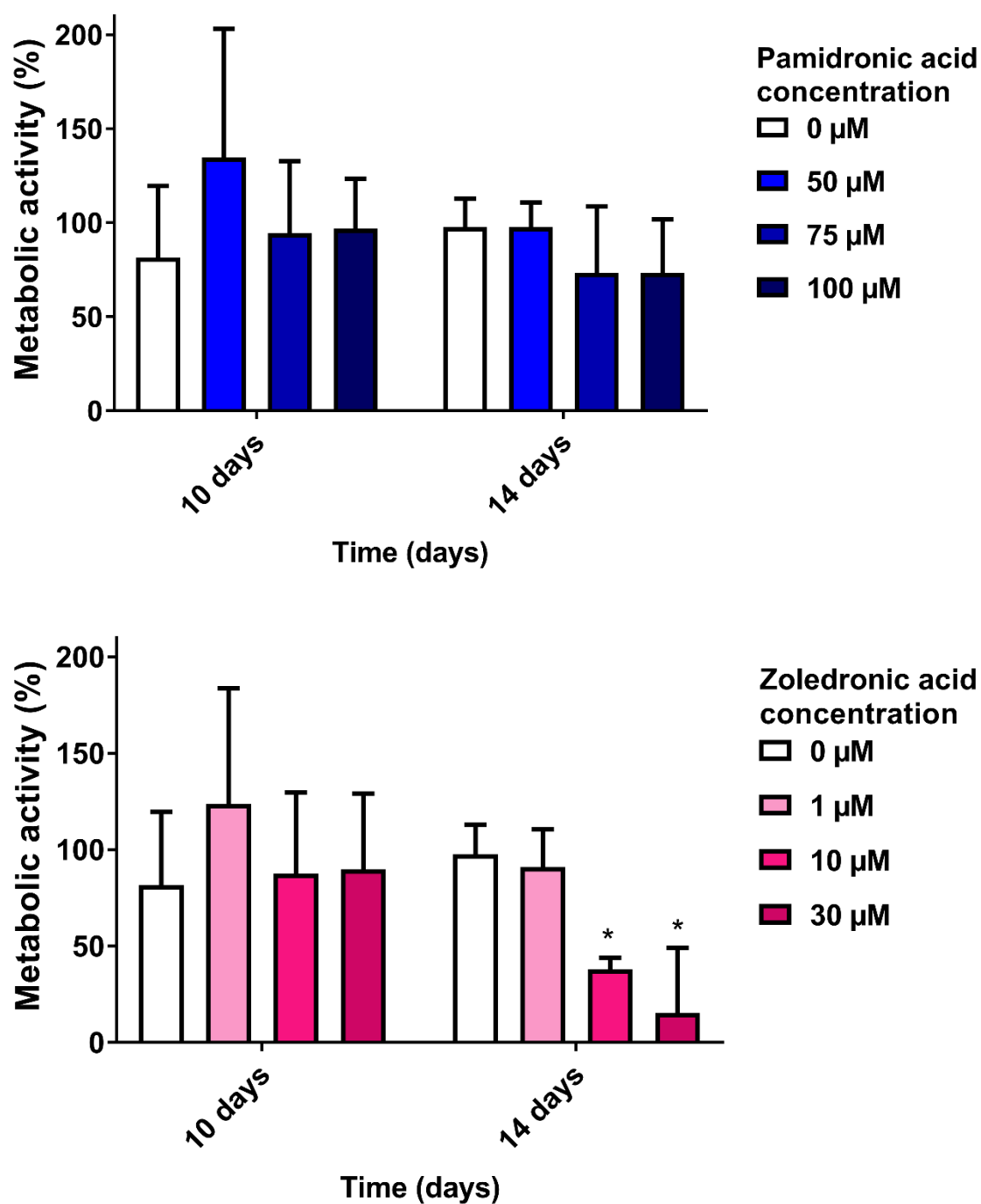


Figure 6.11. Metabolic activity of primary keratinocyte oral mucosa models when cultured at ALI for 7 days in control medium, then treated with 50, 75 and 100 μM pamidronic acid and 1, 10 and 30 μM zoledronic acid for 7 days, measured with a resazurin assay. Blank well reading subtracted from values before normalising to day 7 values for each model. Day 7 not shown as all values 100 %. N=3, n=3. Error bars = SD. Statistical significance against control at each time point indicated by *P≤0.05.

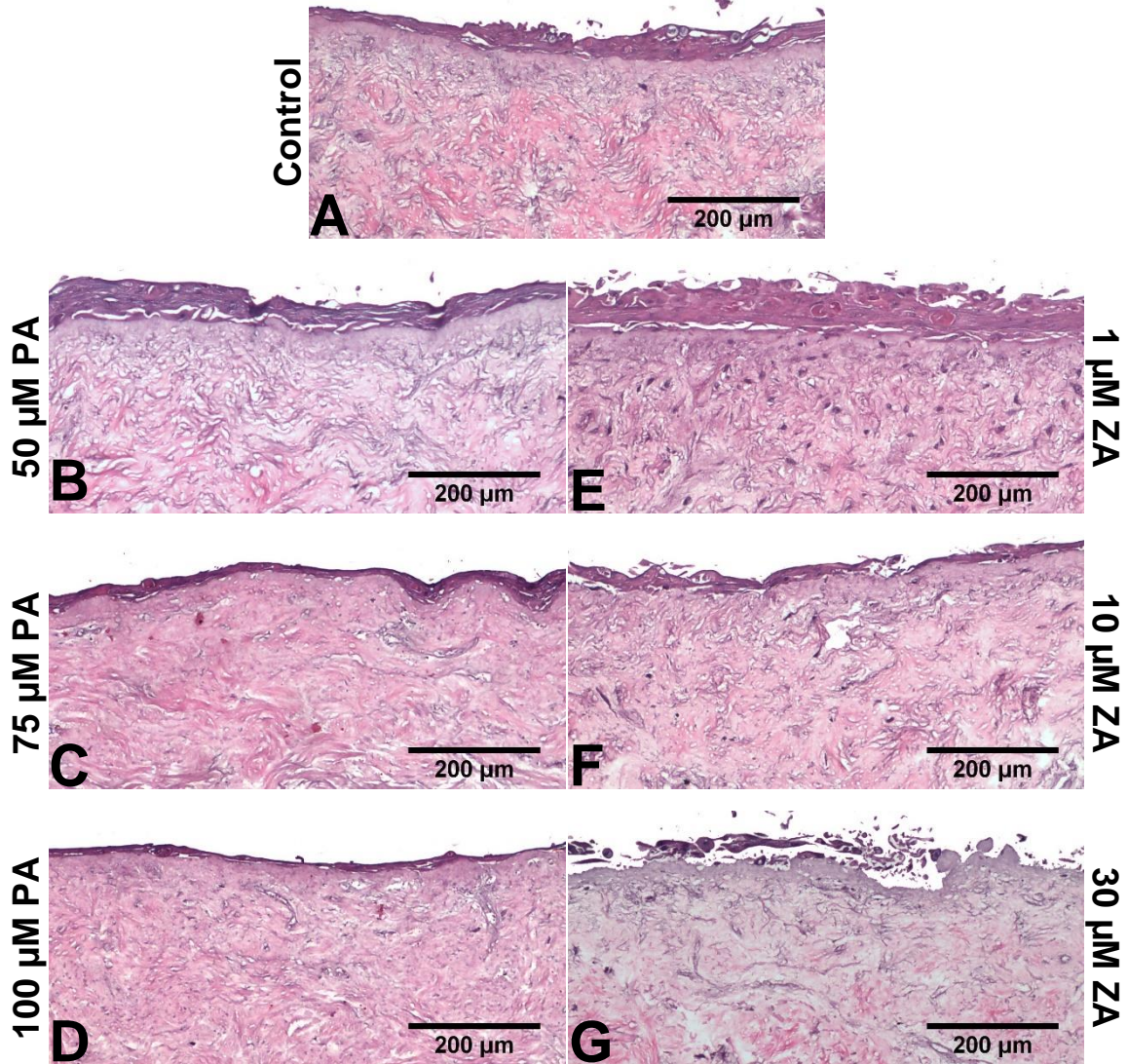


Figure 6.12. H&E stained sections of oral mucosa models seeded with human oral fibroblasts and primary human oral keratinocytes cultured at ALI for 7 days in control medium, then treated with (A) control medium, (B) 50 μM, (C) 75 μM and (D) 100 μM pamidronic acid, (E) 1 μM, (F) 10 μM and (G) 30 μM zoledronic acid, respectively, for 7 days. Representative images used.

6.4.4 Models wounded with biopsy punch showed capacity to regenerate; models wounded with cauteriser and soldering iron did not

Models were cultured with immortalised human oral keratinocytes at ALI for 10 days. At this point, they were wounded with one of three methods – biopsy punch, cauteriser or soldering iron – or left unwounded as a control. Following this, they were cultured at ALI for a further 10 days.

Figure 6.13 shows images of the models immediately after wounding, with the soldering iron causing the most superficial damage, and biopsy punch the least. Metabolic activity was also measured, normalised against values from 1 day prior to wounding, as shown in Figure 6.14. The metabolic activity of the unwounded model continued to increase until day 3, at which point it levelled off at approximately 160 %, indicating the model may still have been stratifying at this point before stabilising by day 3. The level of superficial damage observed matched the reduction of metabolic activity by the wounding method. The model wounded by biopsy punch increased in metabolic activity but only by 5 %. The cauteriser caused metabolic activity to reduce by approximately 5 %, and the soldering iron by around 20 %. Between day 0 and day 3, the metabolic activity of the wounded models increased by approximately 30 %, before levelling off. The metabolic activity of all models had decreased slightly from their maximal points by day 10.

Models were fixed and stained with H&E, both immediately after wounding, and 10 days after wounding. Figure 6.15A shows the unwounded sample had a multi-layered epithelium after 10 days of culture, with differentiated keratinocytes visible. After 10 further days of culture, this was still intact in some places, with differentiated keratinocytes again visible, as seen in Figure 6.15B. However the epithelium was thinner, matching the slight drop in metabolic activity seen following this culture length.

The biopsy punch created a small wound, shown in Figure 6.15C, damaging both the epithelium and the underlying connective tissue. The epithelium healed over 10 days, with a full epithelium visible in Figure 6.15D. However the connective tissue was still indented. The soldering iron caused severe damage to both the epithelium and connective tissue. Figure 6.15E shows burned sections of epithelium above damaged dermis. Figure 6.15F indicates this did not heal at all over 10 days, with thermally damaged epithelial sections still visible. The cauteriser created a wound similar to both the biopsy punch and the soldering iron, with a small wound created in both the epithelium and connective tissue but with burned epithelium at the edges, shown in Figure 6.15G. Again, this did not heal over the 10 day period, with the damaged epithelium still appearing in Figure 6.15H.

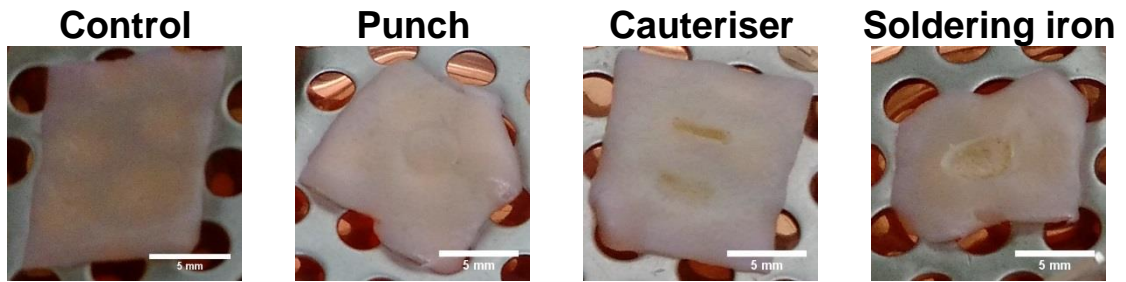


Figure 6.13. Oral mucosa models immediately after wounding. Scale bars = 5 mm.

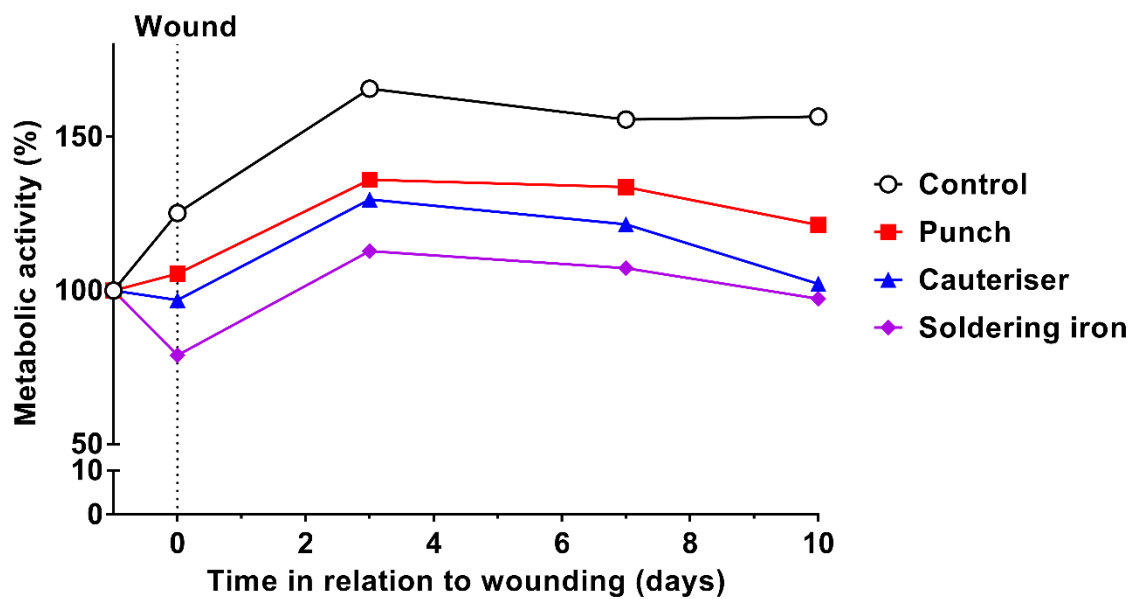


Figure 6.14. Metabolic activity of immortalised keratinocyte DED models wounded after 10 days culture by three different methods – damaged with a biopsy punch, burned with a cauteriser or burned with a soldering iron – or unwounded, measured with a resazurin assay. Blank well reading subtracted from values and values normalised to day prior to wounding (-1). N=1, n=1.

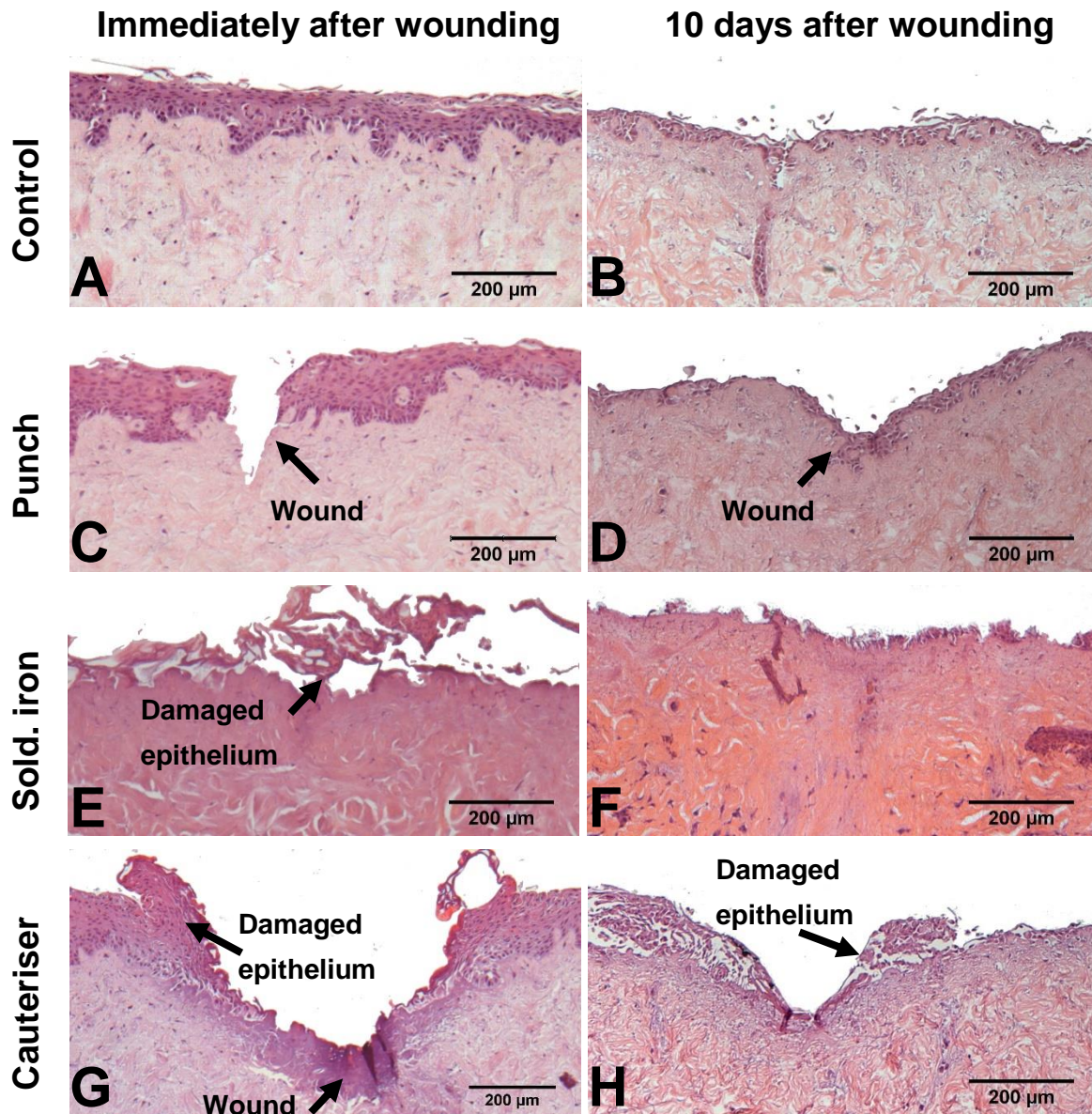


Figure 6.15. H&E stained sections of oral mucosa models seeded with human oral fibroblasts and immortalised human oral keratinocytes cultured at ALI for 10 days. Samples were then (A, B) unwounded, (C, D) damaged with a biopsy punch, (E, F) burned with a soldering iron or (G, H) burned with a cauteriser. Samples A, C, E and G were fixed immediately after wounding. Samples B, D, F and H were cultured for a further 10 days before fixing. Representative images used.

Due to the reduction in metabolic activity after 20 days total culture, a model was wounded with a biopsy punch after 7 days and then cultured for a further 10 to assess healing. The biopsy punch was chosen as models previously wounded with this method demonstrated a capacity to heal. Figure 6.16A shows the full section of a model wounded by biopsy punch at 10 days and fixed immediately, and Figure 6.16B shows a model wounded after 7 days and cultured for a further 10 days before fixing.

As Figure 6.16A is a cross section from the centre of the sample, the circular wound from the biopsy punch is visible as two wounds. The two wounds were not consistent, with one penetrating the dermis and the other only damaging the epithelium. In the post-healing sample in Figure 6.16B, it was possible to locate one of the wound edges due to the superficial damage to the dermis not healing, as before. However the other edge was not readily apparent, suggesting the damage was again only to the epithelium and thereby inconsistent across the wound. Earlier wounding to prevent the model from becoming too old and losing metabolic activity was successful, with the epithelium appearing thicker over the model than the sample wounded at 10 days in Figure 6.15B & D. Whilst the biopsy punch created a wound which then healed over time, the lack of reproducibility within the sample, and the difficulty in identifying the wound area in the healed samples prevent its use when tracking the BP effect on wound healing.

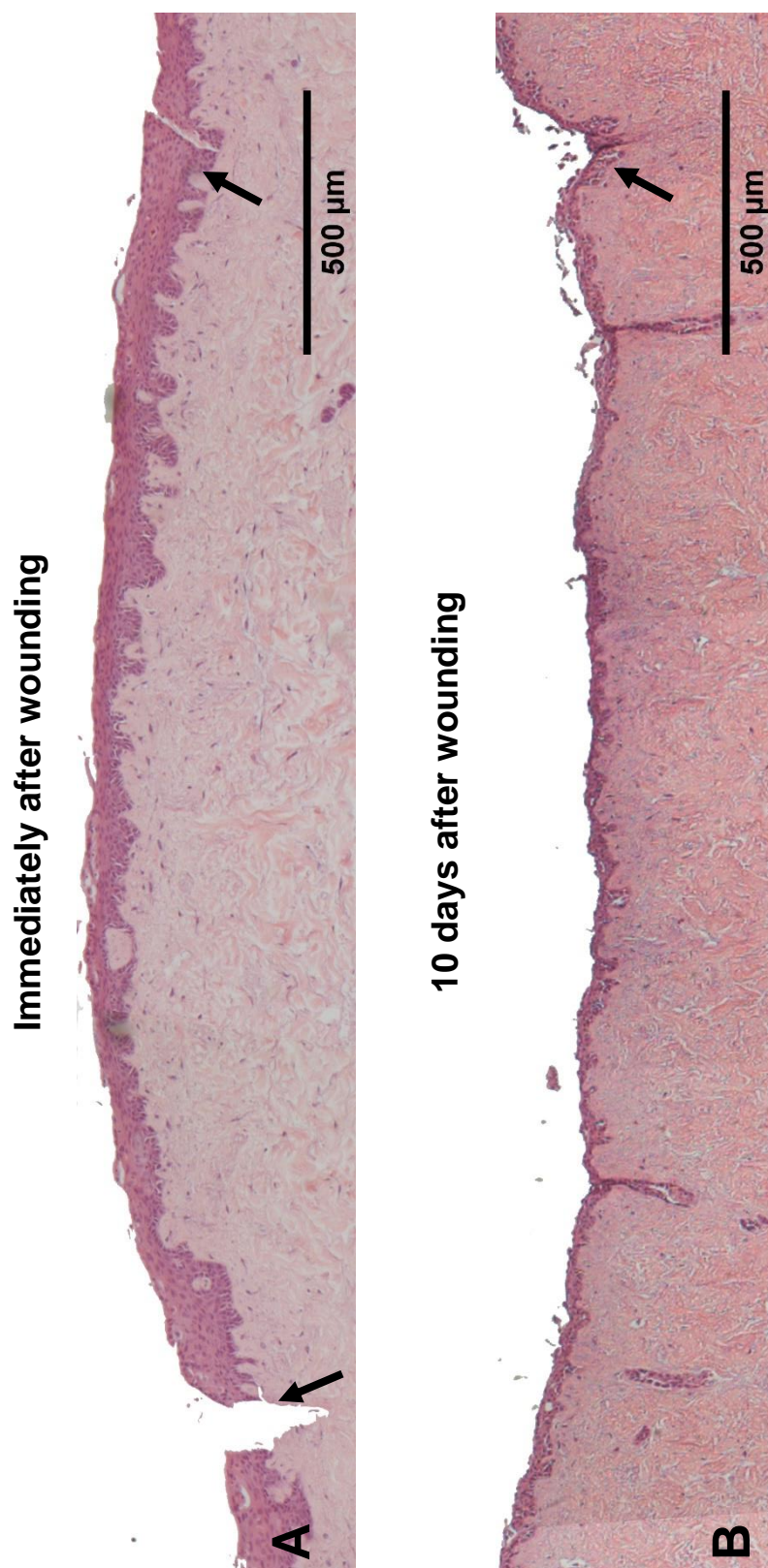


Figure 6.16. H&E stained sections of oral mucosa models seeded with human oral fibroblasts and immortalised human oral keratinocytes, cultured for (A) 10 days, then wounded with a biopsy punch and fixed immediately or (B) cultured for 7 days, wounded with a biopsy punch then cultured for a further 10 days. Arrows indicate wound edges. Representative images used.

6.4.5 Seeding with bespoke 3D printed cell culture rings created a 3D wound healing assay

To overcome the reproducibility issues found with the biopsy punch wounds, cells were instead selectively seeded onto DED using a bespoke cell culture ring made from a 3D printed resin. This created an exclusion zone, similar to the 2D migration work shown in the previous chapter, which allowed the formation of an epithelial wound equivalent of fixed size.

Figure 6.17 shows models seeded in this method, then cultured for 7 days in different BP-containing media, with cell regions visualised through a resazurin reduction assay, whereby cells are coloured pink. At day 0, the areas of keratinocyte seeding were obvious, with a clear exclusion zone in the middle. No difference was seen after 1 day. When cultured in control medium, by day 4 and 7, the cells migrated across the exclusion zone and at day 7 the whole model was entirely coloured pink. Two concentrations of PA were examined, and while migration into the exclusion zone occurred in both cases, the amount was reduced in comparison to the control and a dose dependent response was seen. When treated with 10 μM ZA, the cells began to migrate, with a larger area of pink seen at day 4. At day 7, little pink colour remained.

Figure 6.18 shows resazurin assay results for the same models. All models showed a slight drop in signal between day 0 and day 1, before recovering and increasing between day 1 and 4. At day 7, the metabolic activity of the control and 50 μM PA treated models had increased to around 400 %. The metabolic activity of the models treated with ZA and 100 μM PA stayed constant between day 4 and 7, demonstrating the effect on cell metabolic activity.

A histological section of a model 1 day after removing the ring is shown in Figure 6.19, which indicated the thin nature of the epithelial sections immediately after seeding. Histological sections of these models at day 7 can be seen in Figure 6.20. The control model is shown in Figure 6.20A, where, as before, the epithelium has stratified in the areas of original seeding and migrated across the exclusion zone. The epithelium had begun to stratify in the place of the original wound. When treated with 50 μM PA, a stratified epithelium was visible on one side of the model, and some thinner epithelium is evident in the middle of the model, shown in Figure 6.20B. Figure 6.20C shows the 100 μM PA treated model, which has remnants of a single celled epithelium in some places, but the original seeding areas were no longer apparent. In the ZA treatment model, some epithelial cells are visible on the surface in Figure 6.20D, however, as expected from the resazurin images and data, the drug had largely removed the epithelium

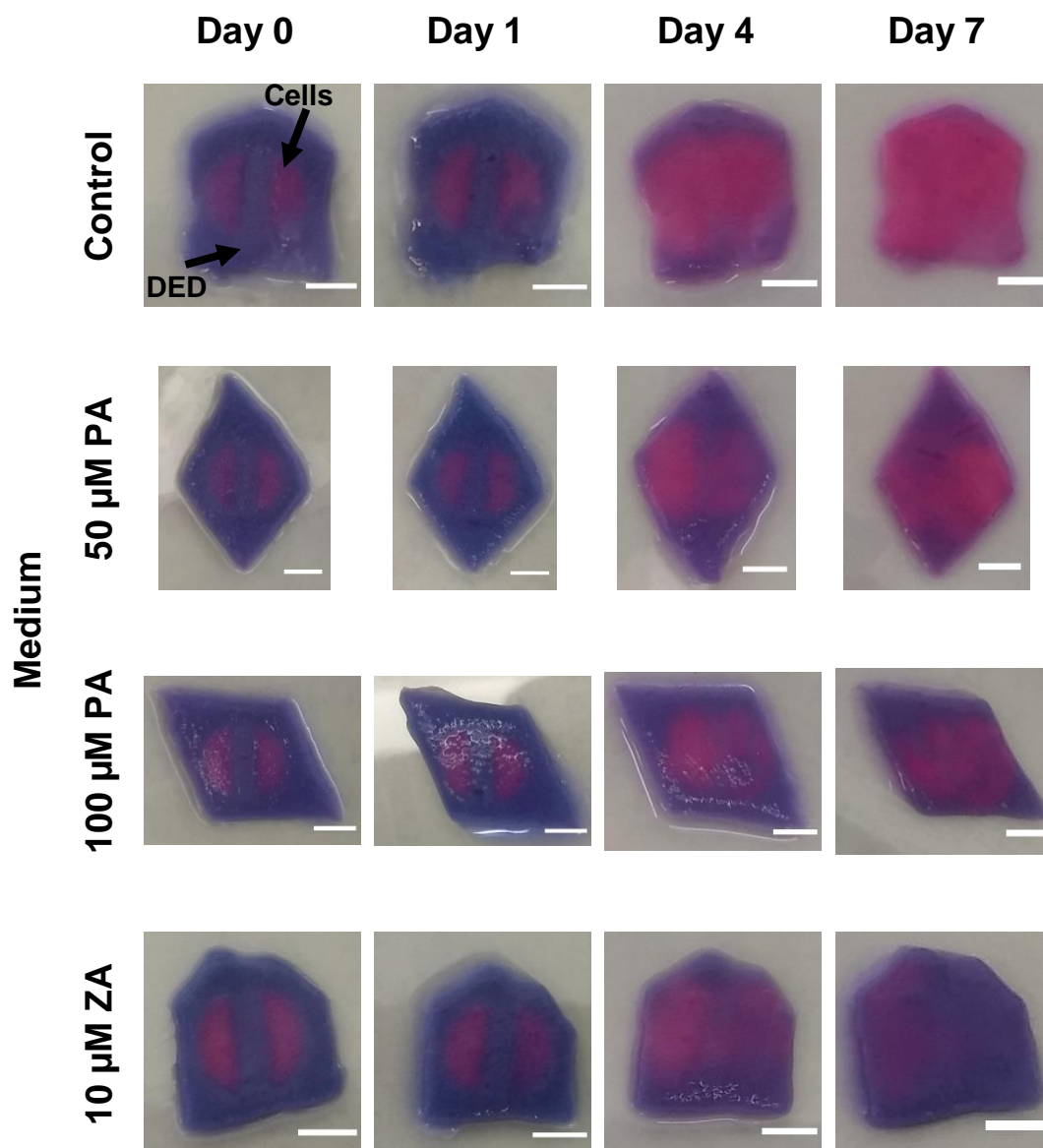


Figure 6.17. Selectively seeded oral mucosa models, cultured for 7 days in control medium, pamidronic acid and zoledronic acid. Imaged immediately following a resazurin assay, pink colour indicates presence of cells. Columns denote length of time, rows denote medium. DED = de-cellularised dermis. Scale bars = 5 mm.

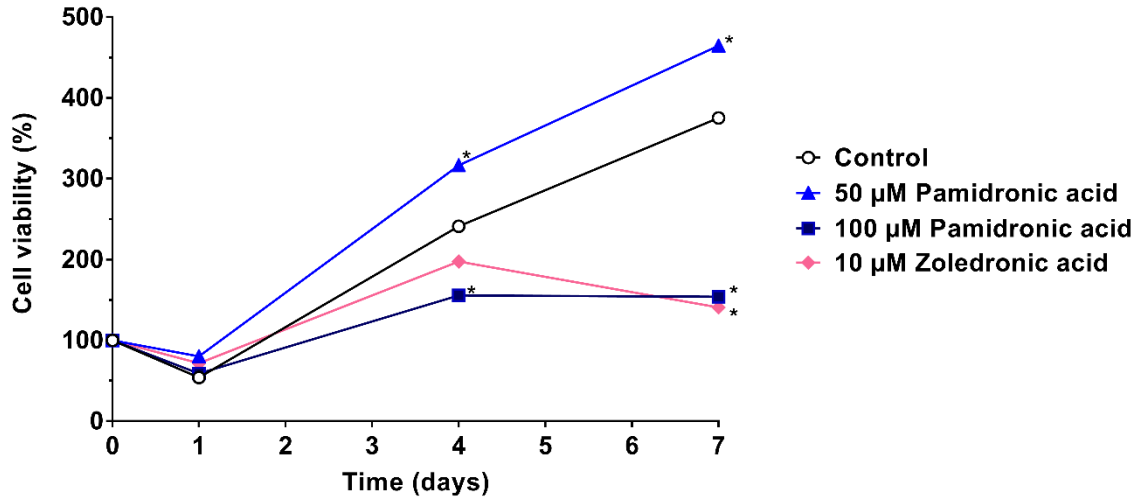


Figure 6.18. Metabolic activity of selectively seeded immortalised keratinocyte DED models cultured for 7 days in pamidronic acid and zoledronic acid, measured by resazurin assay. $N=1$, $n=1$. Values normalised to day 0. Error bars = SD. Statistical significance against control at each time point indicated by $*P \leq 0.05$.

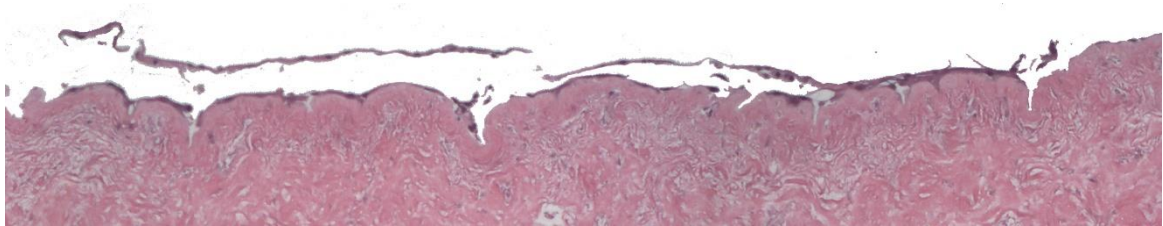


Figure 6.19. H&E stained sections of oral mucosa model selectively seeded with human oral fibroblasts and immortalised human oral keratinocytes, then placed at ALI in control medium for 1 day.



Figure 6.20. H&E stained sections of oral mucosa models selectively seeded with human oral fibroblasts and immortalised human oral keratinocytes, then placed at ALI in (A) control medium, (B) 50 μM pamidronic acid, (C) 100 μM pamidronic acid and (D) 10 μM zoledronic acid for 7 days. Arrows show approximate edges of original seeding area, when apparent. Representative images used.

While the 3D printed rings potentially allowed for a repeatable, successful wound healing model, the epithelial sections were only a single cell thick. While BPs are known to affect the epithelium of a patient before the BRONJ-precipitating event, the epithelial sections either side of a wound will be healthy and multi-layered. Therefore, models were seeded at ALI, with the medium inside the ring removed to allow for the epithelium to stratify, while maintaining the exclusion zone, and thereby more closely represent the *in vivo* scenario.

Models were cultured at ALI for 4 and 7 days, before rings were removed and a resazurin assay was performed to visualise cell seeding, as shown in Figure 6.21. A model with the ring taken off before moving to ALI is included as a control. In all models, the exclusion zone appeared in place, with two sections of pink colour apparent. Figure 6.22 shows models cultured at ALI for 7 days, then cultured in control medium for a further 7 days. By day 4, the exclusion zone had closed and at day 7, the model was completely coloured pink.

Figure 6.23 shows histological sections of models when cultured at ALI for 4 or 7 days with the culture ring in place. After 4 days, in Figure 6.23A, the epithelium was present in two sections, as expected, though largely still single layered. Figure 6.23B shows a model cultured at ALI for 7 days. The epithelium was able to stratify in place, with multi-layered epithelial sections appeared either side of a mostly cell free wound equivalent.

Figure 6.23C, D and E show models cultured at ALI for 7 days, then fixed during the healing process. Figure 6.23C shows two single layered migration fronts had begun to form across the wound. By day 4, these continued further along the model, while stratifying in place. By day 7, the model was covered entirely by a multi-layered epithelium and the areas of original seeding were no longer apparent, indicating successful healing.



Figure 6.21. Selectively seeded oral mucosa models, placed at ALI with the culture ring for 0, 4 or 7 days. Imaged immediately following a resazurin assay, pink colour indicates presence of cells. Scale bars = 5 mm.

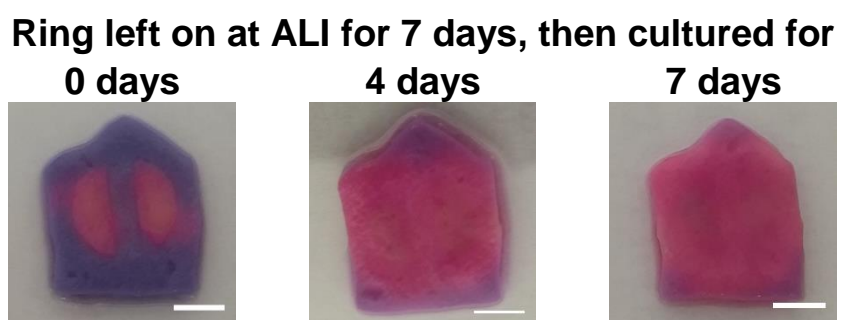


Figure 6.22. Selectively seeded oral mucosa models, cultured at ALI for 7 days before the culture ring was removed, then cultured for 1, 4 or 7 days. Imaged immediately following a resazurin assay, pink colour indicates presence of cells. Scale bars = 5 mm.

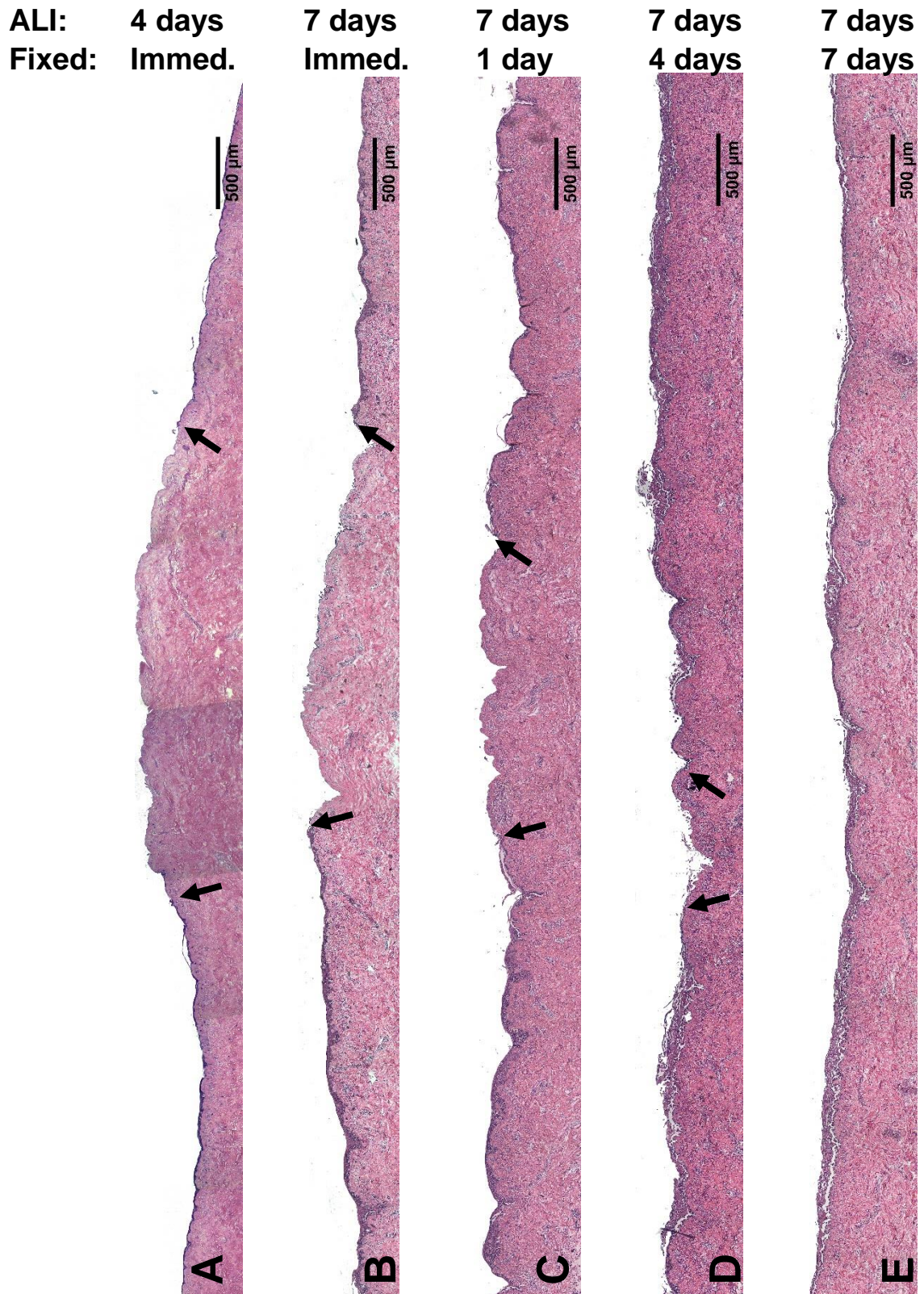


Figure 6.23. H&E stained sections of oral mucosa models selectively seeded with human oral fibroblasts and immortalised human oral keratinocytes, then placed at ALI with a 3D printed cell culture ring preventing migration for (A) 4 days and fixed immediately, or for 7 days and fixed (B) immediately, (C) after 1 day, (D) after 4 days or (E) after 7 days further culture. Arrows indicate approximate edge of seeding area. Representative images used.

6.4.6 Seeding models at air-liquid interface is not reproducible

After initial success in prototyping the wound model when cultured at ALI, more were seeded. A resazurin reduction assay was performed with these models immediately after removing the ring. As Figure 6.24 shows, the seeding process was not successful. While some of the models had two distinct regions of pink colouring, the seeding was not localised to those specific areas as previously. As the model on the bottom centre and bottom right seemed to be most successful and seemingly had an exclusion zone, these models were treated with either 50 μ M PA or control medium for 7 days.

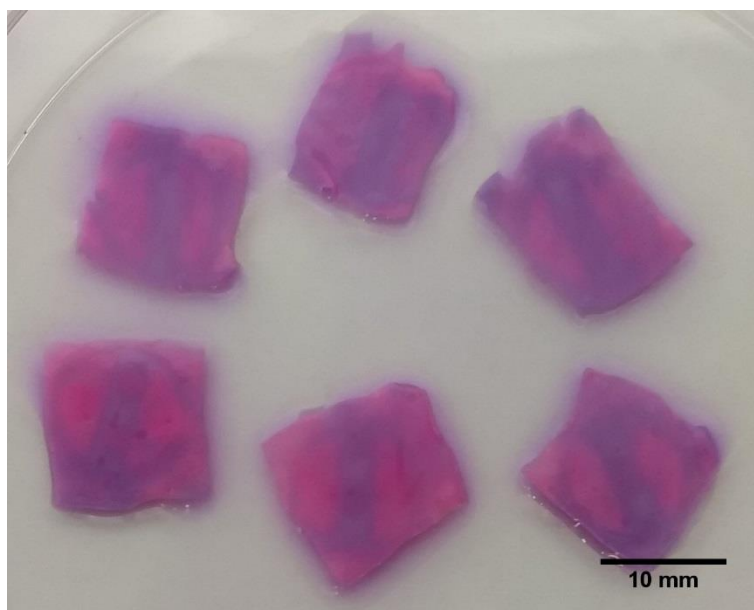


Figure 6.24. Oral mucosa models selectively seeded at ALI with human oral fibroblasts and immortalised human oral keratinocytes. Images taken immediately following a resazurin assay.

6.4.7 Pamidronic acid prevents re-epithelisation of the oral mucosa wound model

Figure 6.25 shows that while clear epithelial regions were seen immediately after removing the ring, by day 4 these regions were impossible to distinguish. At day 7, both models appeared similar, with pink colouration across the whole sample.

Histology, however, showed a clear difference between the samples. When treated with control medium, the models appeared as in Figure 6.23E, with a multi-layered epithelium present over the whole sample. Figure 6.26 shows that while the PA treated model did have a whole epithelium, as suggested from the pink colouring in Figure 6.25, it was not stratified in all areas, while the control sample had a stratified epithelium past the point of original seeding. Figure 6.26A demonstrates that two distinct stratified sections exist, confirming the successful seeding of the model. Figure 6.26B, however, shows that in the original exclusion zone, while cells have migrated, they have not stratified. The epithelium is only 1 or 2 cells thick across the exclusion zone. When treated with control medium, the epithelial region across the exclusion zone was thicker, as shown in Figure 6.26C.

A further set of mucosa models were seeded at ALI, however, in this case, even fewer were successfully seeded, so another seeding method was performed.

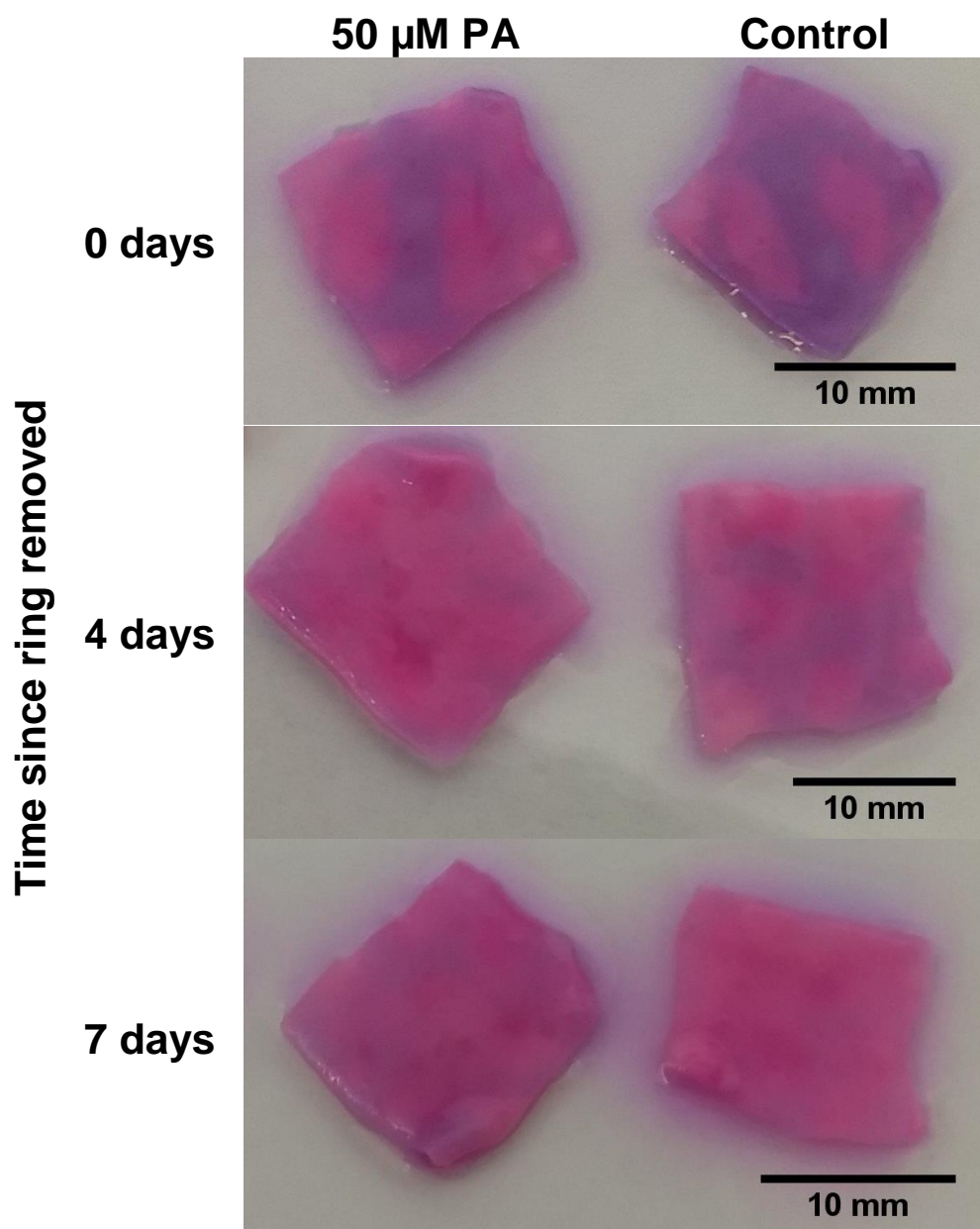


Figure 6.25. Oral mucosa models selectively seeded at ALI with human oral fibroblasts and immortalised human oral keratinocytes, then cultured for 7 days before removing the cell culture ring, and culturing for 7 days in 50 µM pamidronic acid or control medium. Images taken immediately following a resazurin assay, pink colour indicates presence of cells.

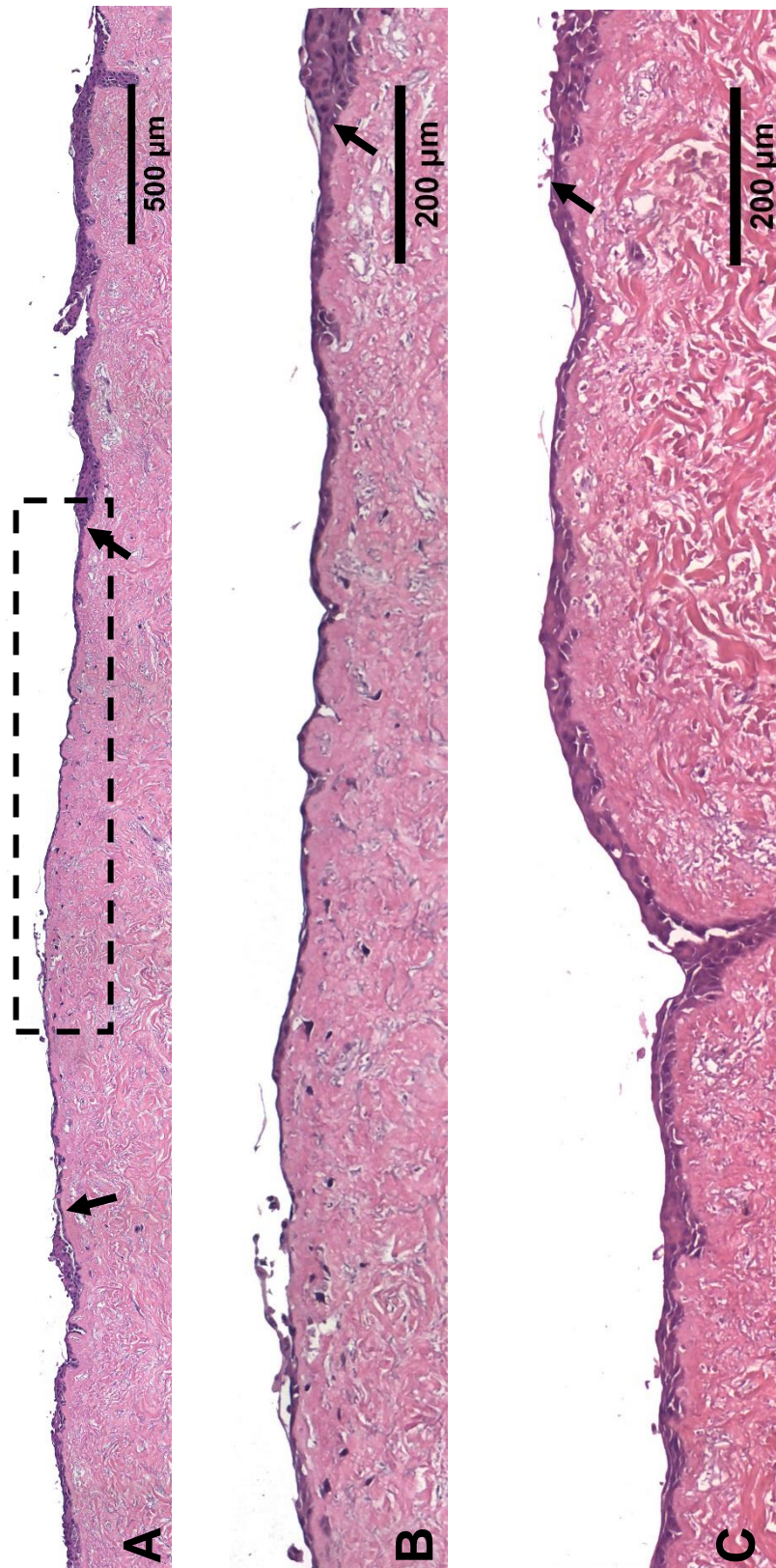


Figure 6.26. H&E stained sections of oral mucosa models selectively seeded at ALI with human oral fibroblasts and immortalised human oral keratinocytes, then treated at ALI with (A, B) 50 µM pamidronic acid or (C) control medium for 7 days. Whole epithelial region shown in (A), dotted line indicates area shown in (B). Arrows show approximate edges of original seeding area, when apparent. Representative images used.

6.4.8 Seeding models with an *in situ* ALI provides a more reproducible wound model

As seeding at ALI proved difficult to reproduce, models were seeded in a well plate, as standard. Rather than removing the rings at day 4, however, the medium inside the rings was removed to create an *in situ* ALI. Models were cultured for 7 days in this state, before removing the ring and performing a resazurin assay. Figure 6.27 demonstrates that this method created much more well defined seeding areas, with two distinct regions of cells present on all models.

Figure 6.28 shows histological sections of a model seeded with an *in situ* ALI. Two distinct epithelial regions were present, with an exclusion zone across the middle of the model, shown in Figure 6.28A. The epithelial sections were stratified, as shown in Figure 6.28B.

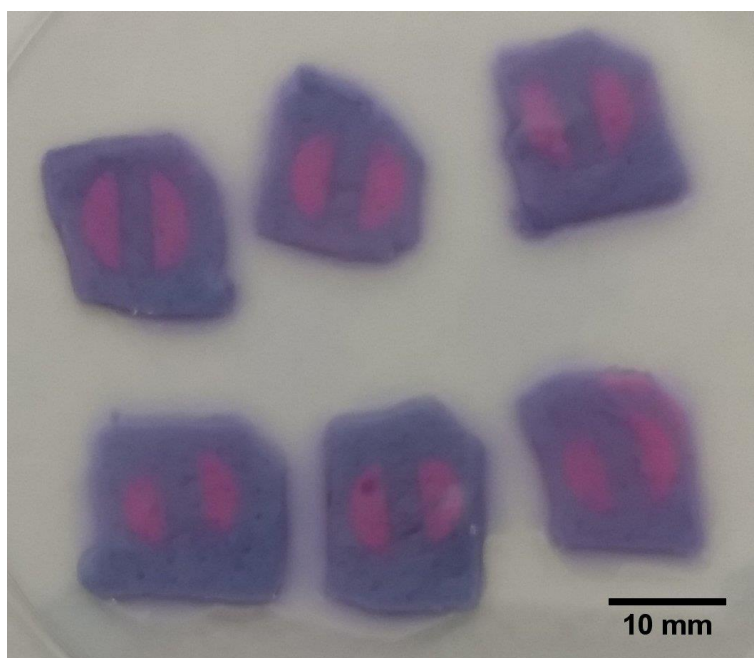


Figure 6.27. Oral mucosa models selectively seeded with human oral fibroblasts and immortalised human oral keratinocytes, before creating an *in situ* ALI and culturing for a further 7 days. Images taken immediately following a resazurin assay, pink colour indicates presence of cells.

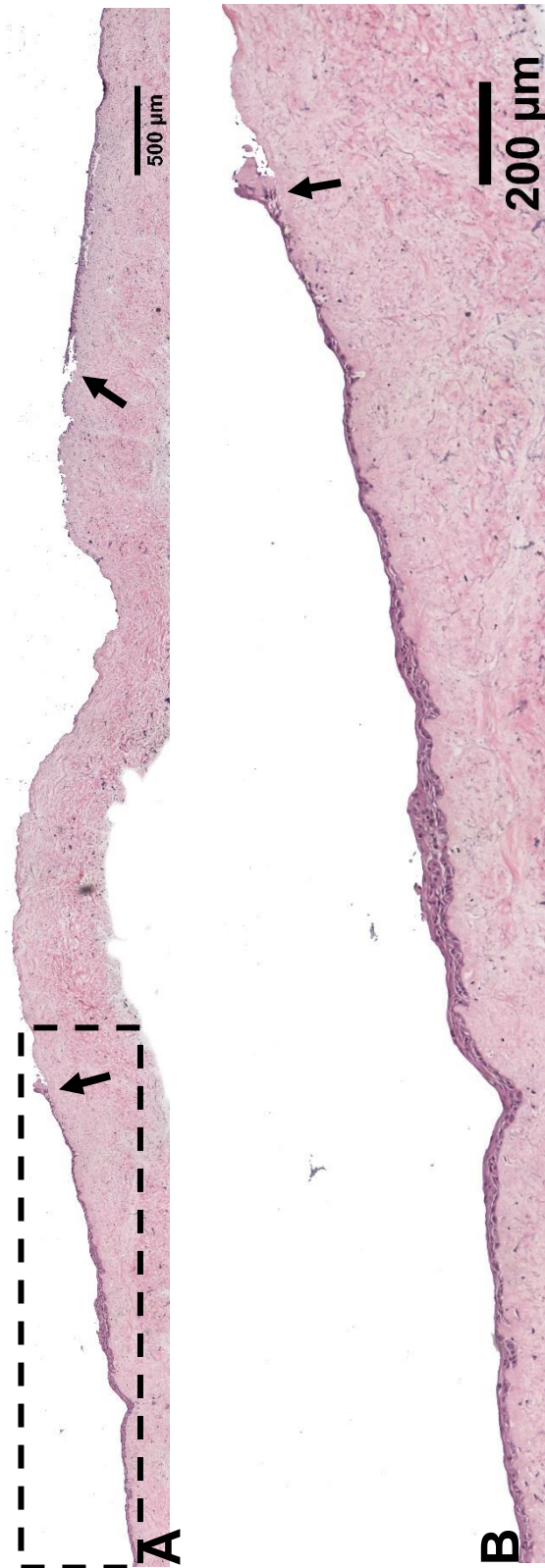


Figure 6.28. H&E stained sections of an oral mucosa model selectively seeded with human oral fibroblasts and immortalised human oral keratinocytes, before creating an *in situ* ALI and culturing for 7 days. Whole epithelial region shown in (A), dotted line indicates area shown in (B). Arrows show approximate edges of original seeding area, when apparent. Representative images used.

6.4.9 Pamidronic acid and zoledronic acid prevented full healing of *in situ* wound model

As seeding with an *in situ* ALI allowed for more consistency, models seeded through this method were treated with BPs. Figure 6.29 shows these models immediately following a resazurin assay after 0, 4 and 7 days of BP treatment. When cultured in control medium, migration of the epithelial regions occurred, and by 7 days the model was entirely pink. Treatment with PA prevented this in a dose dependent manner. When treated with 50 μM PA, some cells had migrated, but the model was not entirely coloured pink by day 7. A 100 μM PA treatment also saw increasing pink colour, suggesting migration, at day 4, but by day 7 the pink colouration was no longer present. A 1 μM ZA treatment had no effect, with a full pink model present at 4 and 7 days. Treating with 10 μM ZA allowed for migration between 0 and 4 days, but by 7 days little pink was seen, suggesting toxicity.

Figure 6.30 shows the metabolic activity of models seeded with an *in situ* ALI and cultured in BPs for 7 days, normalised to day 0. High variation was seen in these models. Control medium allowed for an increase in metabolic activity over the 7 days, rising to approximately 250 %. A 50 μM PA treatment halted growth, with metabolic activity remaining approximately 100 % at all time points, though with an incredibly high amount of variation at day 7. Treating with 100 μM PA reduced metabolic activity, with a significant reduction in comparison to the control at 7 days. When treated with 1 μM ZA, no differences were seen in comparison to the control, with metabolic activity increasing over time. A 10 μM ZA treatment also reduced metabolic activity in comparison to the control at 7 days.

Figure 6.31 shows histological sections of models at day 7, demonstrating one section of original seeding and part of the wound equivalent. Figure 6.31A shows a model cultured in control medium, where a thin epithelium was present across the wound area. When treated with 50 μM PA, shown in Figure 6.31B, a consistent epithelium was again present across the wound. Figure 6.31C shows that, while some keratinocytes remained in the original area of seeding following a 100 μM PA treatment, no epithelium was present across the wound. Treating with 1 μM ZA allowed for re-epithelialisation, with a consistent epithelium seen in Figure 6.31D. No epithelium is seen following a 10 μM ZA treatment, shown in Figure 6.31E.

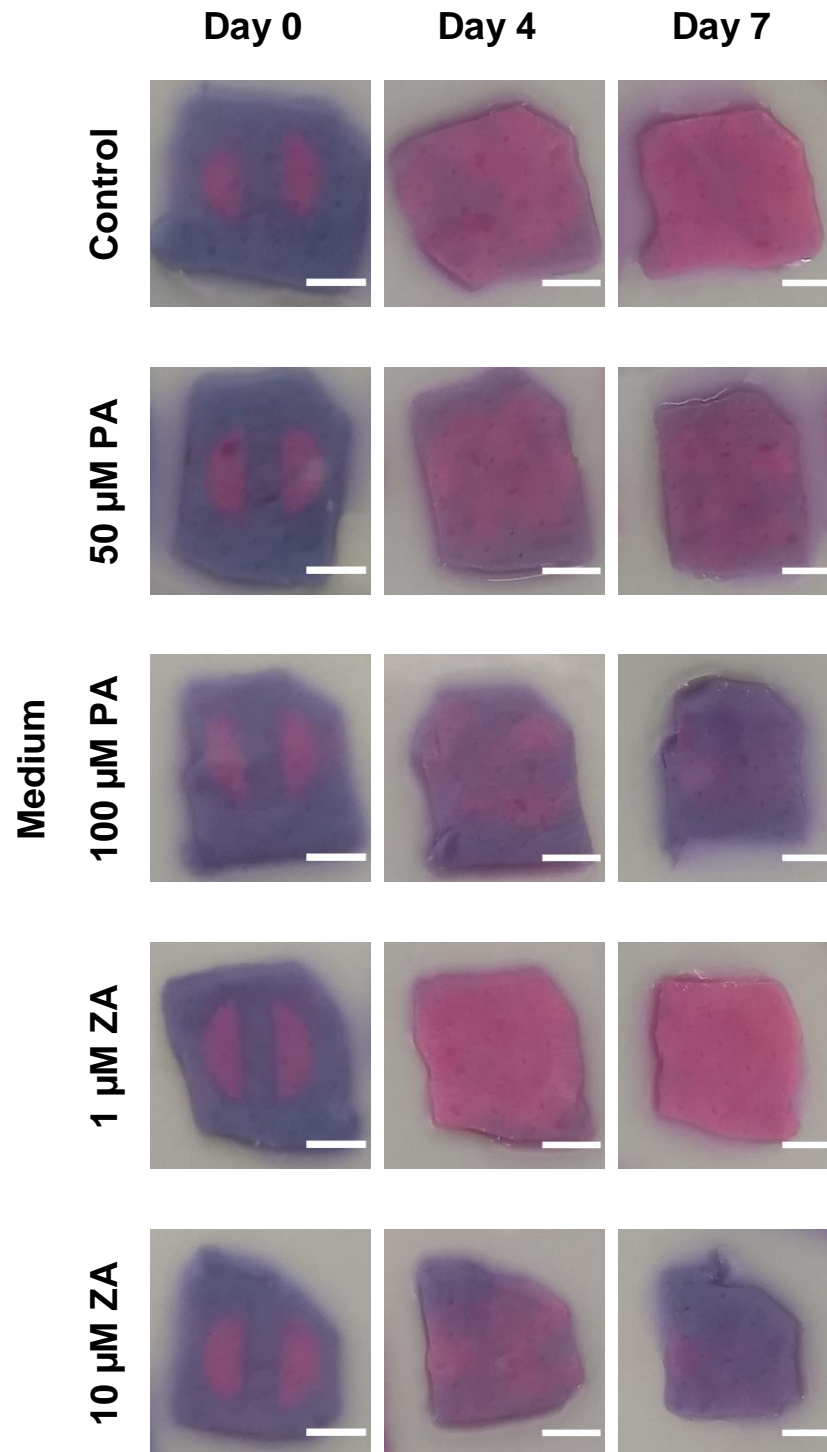


Figure 6.29. Selectively seeded oral mucosa models, cultured with an *in situ* ALI for 7 days, before culturing for 7 days in control medium, pamidronic acid or zoledronic acid. Imaged immediately following a resazurin assay, pink colour indicates presence of cells. Columns denote length of time, rows denote medium. Scale bars = 5 mm.

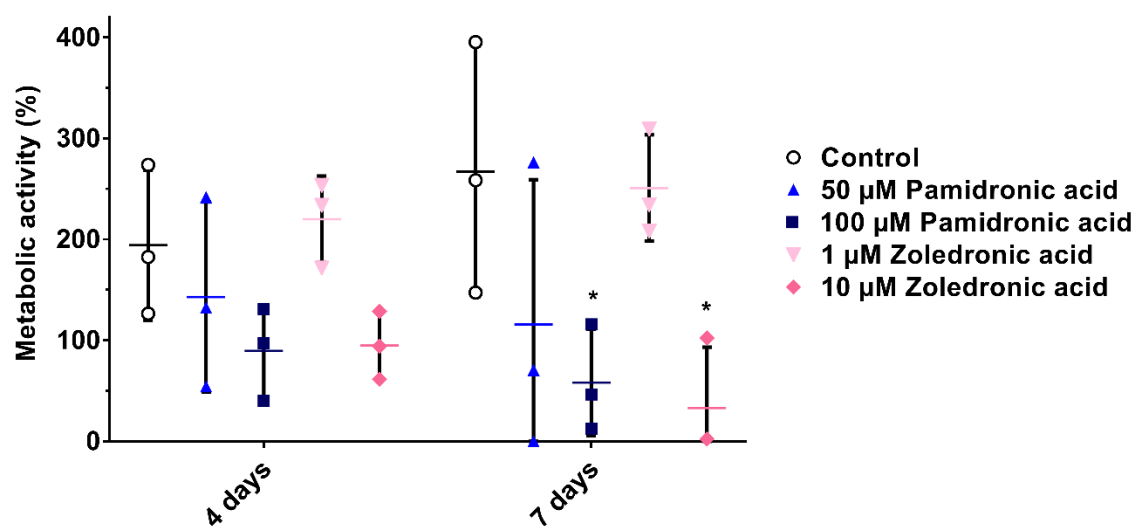


Figure 6.30. Metabolic activity of selectively seeded immortalised keratinocyte DED models using *in situ* ALI, cultured for 7 days in pamidronic acid and zoledronic acid, measured by resazurin assay. $N=3$, $n=1$. Values normalised to day 0. Error bars = SD.

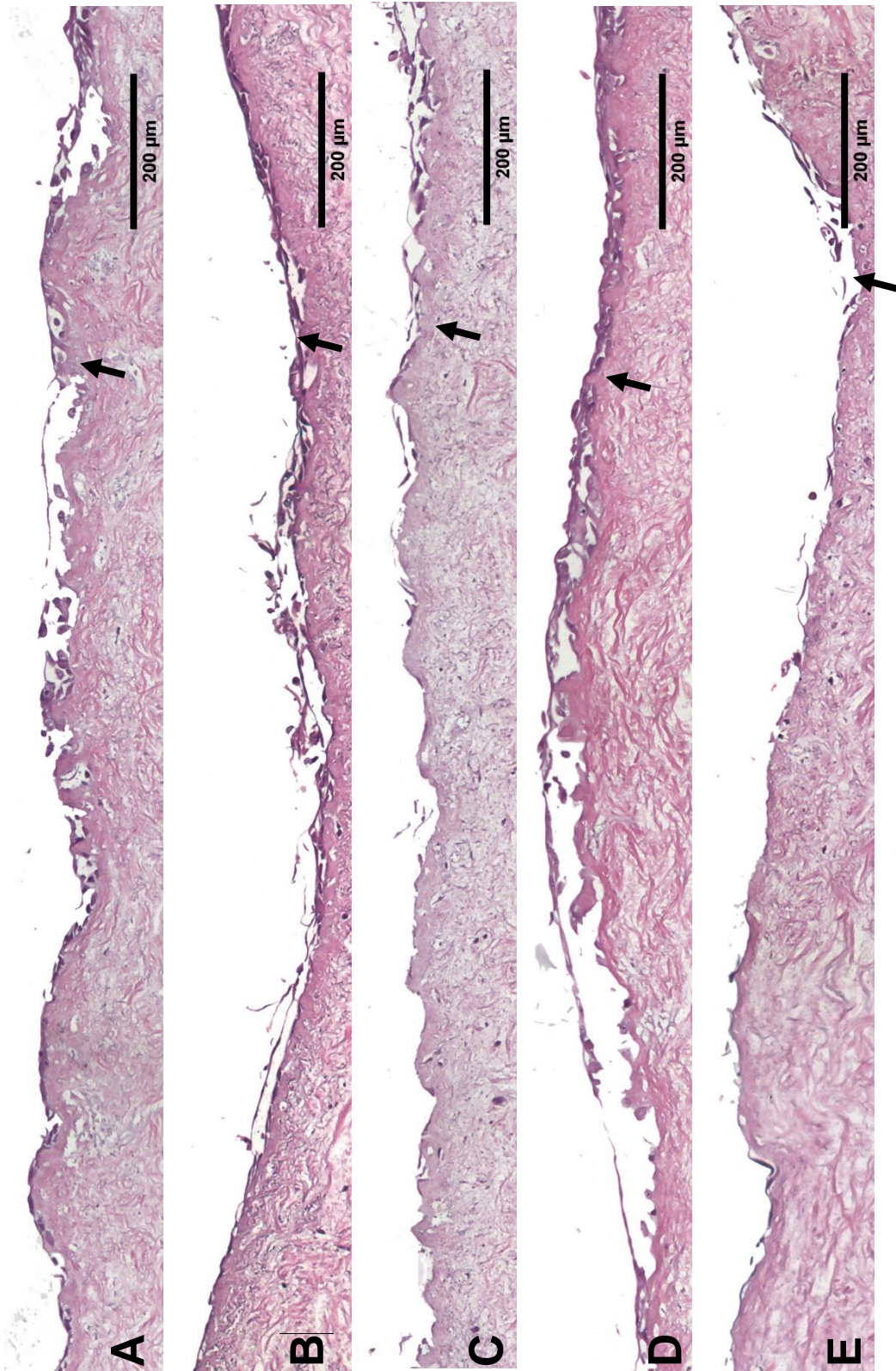


Figure 6.31. H&E stained sections of oral mucosa models selectively seeded with human oral fibroblasts and immortalised human oral keratinocytes, before creating an *in situ* ALI and culturing for 7 days, then placed at ALI in (A) control medium, (B) 50 μ M pamidronic acid, (C) 100 μ M pamidronic acid, (D) 1 μ M zoledronic acid and (E) 10 μ M zoledronic acid for 7 days. Arrows show approximate edges of original seeding area, when apparent. Representative images used.

6.5 Discussion

The epithelium of the oral mucosa in BRONJ patients will exist in several different forms. Firstly, there will be a healthy, stratified epithelium, found before any precipitating event occurs, and surrounding the wounded tissue after the event. As the wounded tissue begins to heal, tissue will exist as two separate sections which migrate to close the wound. When the wound is first closed, the epithelium will exist in a single layer. We have demonstrated that in all these cases, clinically relevant concentrations of PA and ZA negatively affect the epithelium.

To approximate cell viability in 3D, resazurin reduction assays were used. These provide a measure of metabolic activity, however with little cytotoxicity, unlike the MTT assay [292], [305]. This allows for more than one assay to be performed on a model over time, reducing the number of models required per experiment which is beneficial in 3D culture, due to the greater complexity and higher number of cells required. When models were cultured for 7 days before treating with PA and ZA, metabolic activity decreased between day 7 and day 14. This is likely due to the maturation of the models: when a model is stratifying, the metabolic activity will increase as cells proliferate, yet after they become mature, metabolic activity is likely to decrease. Metabolic activity of cells can also increase in response to cellular stresses, and the large variation seen when primary models were treated with low concentrations of PA and ZA is potentially due to this mechanism. The overall trend, however, is clear, with higher concentrations of PA and ZA causing a more pronounced effect and the lower concentrations behaving similarly to the control treatment.

To examine how BPs affect the development of epithelia, we treated models with PA and ZA immediately after placing at ALI. When treated with 50 to 100 μM PA, metabolic activity did not increase and histology showed a dose dependent reduction of epithelial thickness. This is the first time this effect has been demonstrated. ZA proved more toxic to the models than PA, as expected from our 2D work. While 1 μM ZA performed similarly to PA, with no metabolic activity reduction but a thinner epithelium, both 10 and 30 μM ZA led to a reduction in metabolic activity and the removal of the epithelium. Previously, it has been demonstrated 1 μM ZA had no effect on the epithelial formation of oral mucosa models using OKF6 cells [173]. Our results support this, and demonstrate for the first time that higher concentrations of ZA lead to toxicity of newly formed epithelia *in vitro*. As we demonstrated in chapter 5, clinically relevant concentrations of both PA and ZA prevent epithelial cell proliferation, and this has also been demonstrated in 3D [164], [187]. We surmise that the lack of stratification seen is due to this inhibition of proliferation. This indicates a pathway by which necrotic bone exposure could continue over time.

For a BRONJ diagnosis, exposure of necrotic bone must persist for 8 weeks [1]. During oral mucosa wound healing, keratinocytes migrate to close the wound, before cells in the basal layer begin proliferation. This proliferation causes the epithelium to stratify in place to form a new, multi-layered epithelium [99]. In the development of BRONJ, this process is clearly prevented, evidenced by the lack of soft tissue wound closure identified as the key clinical feature of the disease [2]. Our results suggest that PA will cause newly formed tissue to be thinner, and therefore more susceptible to injury, and ZA will be toxic to this newly formed tissue, thereby demonstrating a reason for the persistent soft tissue wound.

The epithelium surrounding a BRONJ wound will exist as a healthy, established epithelium, which will be exposed to BPs following the dental event, such as extraction of a tooth, that precedes the development of the disease. We have demonstrated that clinically relevant concentrations of both PA and ZA cause established epithelia to thin in a dose dependent manner. Kim *et al.* demonstrated PA concentrations of 10 μM reduced the epithelial thickness of established oral mucosa models [164]. We chose concentrations above this value due to the IC_{50} values determined in the previous chapter, however our results show a similar effect. Though no significant change in metabolic activity was seen, the epithelial thickness of both immortalised and primary keratinocyte models was reduced in a dose dependent manner.

ZA treatment not only reduced epithelial thickness, but led to cytotoxicity. A 1 μM ZA treatment caused similar effects to PA, with no metabolic effect seen but epithelial thickness reduced. When treated with 10 μM ZA, immortalised cell models saw no significant metabolic effect, though models seeded with primary cells did. As our IC_{50} s in chapter 5 show, immortalised keratinocytes are more resistant to ZA toxicity than primary keratinocytes, therefore this effect was expected. A 30 μM ZA treatment proved toxic to both immortalised and primary models. Previously ZA concentrations from 4 to 10 μM have been demonstrated to reduce epithelial thickness of *in vitro* oral mucosa models [177], [187], [202]. Our data confirms this effect, while also using metabolic activity data to produce a quantitative measurement of cell viability of these models for the first time, and indicating that a ZA concentration well within the expected range received by the oral mucosa in BRONJ patient will lead to cytotoxicity.

Though it has been demonstrated that BPs reduce epithelial thickness, the mechanism by which this effect happens is not understood. It has been suggested that PA and ZA may increase the speed of the keratinocyte differentiation process, leading to keratinised outer layers, but fewer middle layers [164], [177], [187]. However, Bae *et al.* observed the opposite effect, with fluorescently labelled ZA localising to the outer layers of the epithelium and eventually leading to a reduction in the number of keratinised layers [202]. This effect was suggested to be due to the higher level of calcium present in the

outer layers of the epithelium and supports work from Arai *et al.*, who showed increasing calcium concentration had a synergistic effect on ZA toxicity [176]. No keratinised layers were present in our models, including our controls, however our immortalised keratinocyte models demonstrated fewer middle layers. In the models where no metabolic effect was noted, and therefore no toxicity was seen, the outer layer of the epithelium was consistently flatter than the basal layers. As keratinocytes differentiate through the layers of the epithelium, they flatten [91]. Hence, our immortalised keratinocyte work supports the theory that BPs are affecting differentiation, and further investigation into this mechanism would be useful, particularly investigating the effects on parakeratinised epithelial tissue models, however this was outside the scope of this project.

Our primary keratinocyte models did not show the same effect, with differences in the morphology of the layers seen across the samples. Primary keratinocytes are inherently variable, with variation even within one patient, as epithelial thickness varies across the mouth and even across the gingiva [91], [92], and it is therefore difficult to make strong conclusions based on these histological slides. What is clear, however, is that PA and ZA reduce the thickness of the oral epithelium. ZA led to more toxicity at lower concentrations than PA, which explains why ZA patients are more likely to develop BRONJ.

This data offers both an explanation as to why BRONJ can spread across the jaw with ease, and a reason for BRONJ development in the first place. The epithelium provides a barrier against both mechanical forces and bacterial infection [99]. If the integrity of this barrier is compromised, then the mucosa is more susceptible to injury and infection. BPs are known to promote bacterial adhesion and biofilm formation [58], [148]. Therefore, as clinically relevant concentrations of BPs reduce the integrity of healthy epithelium, it follows that the worsening of the disease is likely.

In terms of disease development, the oral mucosa surrounding the jaw bone is known to be thinner than other areas of the mouth [43], [48]. The oral mucosa is situated directly above the bone with no fat, fascia or muscle tissues between the mucosa and the bone which could potentially prevent exposure, with the gingiva even closer due to the lack of submucosal layer [91], [92], [164]. It has been suggested that oral mucosa exposure to BPs occurs regularly before any dental event or osteonecrosis, through examination of patient tissue [189] and measuring salivary BP concentrations of patients with no clinical BRONJ features [142]. It may be that ZA has an effect on epithelial thickness before the BRONJ preceding dental event, due to the low concentrations at which ZA toxicity occurs. This could also explain the 'spontaneous' cases of the disease. In the development of a treatment for BRONJ, it will be important to investigate whether this thinner epithelium could recover if local BP concentration was reduced. Due to the finite culture length of the oral mucosa models, however, this was not possible in this project.

To further understand BRONJ development, and to examine potential treatment mechanisms, being able to model the soft tissue component of the disease is vital. Following oral surgery, the epithelium will exist in two sections, cleanly separated through a sharp wound [98]. These sections will then migrate to form a complete layer, before stratifying to re-establish a full epithelium. We have begun the development of this soft tissue model, and through its use have demonstrated that PA and ZA both prevent the re-epithelialisation of the oral mucosa.

In optimising the wound healing model, immortalised keratinocytes were used. As with the previous chapter, this is due to the relative ease in the culture of these cells in comparison to their primary equivalents, and the inherent variability that arises from using primary cells. Immortalised cells, including the OKF6 cells used in this thesis, have previously been demonstrated to be successful when culturing epithelial models [94], [173], [202], [203]. Our work again shows this, with models performing well over approximately 18 days of culture. However, following this time point, model viability tended to decrease, with epithelia becoming thinner, and optimisation was required.

In vitro epithelial models have a finite culture time, falling between 14 and 28 days in literature, depending on the cells used and passage number [207]. However, epithelial stratification takes time, and a full epithelium was needed for the model. As 10 days led to a fully stratified epithelium across a whole sample, initially this point was used as a wounding time, but as model viability began to decrease at day 18, and thinner epithelia were present following this time point, wounding time was changed to day 7. While the epithelia at this point were not completely stratified, they were consistent enough to use as a wounding time point.

Different wounding methods were performed, with the aim of finding a wound that could be used to represent that found in a BP patient following oral surgery. Three criteria defined the success of the wound healing assay: reproducibility of the wound, ability to heal, and similarity to the clinical scenario.

The soldering iron did not succeed in any of the criteria. Creating the wound was difficult to perform consistently due to the large amount of damage done to the model, and several models were lost entirely as they contracted around the heated tip. The level of damage was so severe the model seemed to not heal. The burn wound was also unlike those seen in an extraction patients. This method was included in the test as it has been successfully used in literature [203], [204].

The cauteriser created a much more consistent wound, however again, the wound did not heal over time, appearing the same before and after 10 days of culture time. Macroscopically the wound did not change over the time of the experiment, with the burn obvious at all times. These models are limited as they only contain fibroblasts, keratinocytes and connective tissue, therefore do not have the immune response required

for large scale healing. It is likely that the damage to the connective tissue was too great for the model to overcome.

Previously, both hot and cold burn wounds have been used on epithelial models to stimulate wound healing [94], [203], [204]. In these cases, the epithelium alone was damaged and separated from the connective tissue, allowing for migrating keratinocytes to heal below the damaged epithelium. In our work, while some of the epithelium separated in the both the soldering iron and cauteriser wounds, no migration front formed below. Breetveld *et al.* held a soldering iron to their epithelia for 10 seconds and created clean, repeatable epithelial wounds with seemingly no connective tissue damage [204]. In our study, 1 second of contact with the soldering iron caused severe damage. As such, a third method was trialled.

The biopsy punch created a wound that healed consistently, and as a sharp wound it is similar to that found following a tooth extraction. However reproducibility was an issue. Variation was found in single wounds, with one side of the wound often deeper than the other. When the connective tissue was wounded, it was simple to find the original site of wounding as the epithelium migrated into the defect. This is similar to work from Geer *et al.* who found keratinocytes migrated into defects formed when DED models were wounded with a scalpel [198]. When the connective tissue was unaffected in our work, the wound healed completely and undetectably. While in some ways this was a positive, it made assessing the healing process difficult.

None of the tested wound models performed well in all three of the criteria for success. As such, we devised a method for testing epithelial migration similar to the 2D assay used in the previous chapter. While this was less clinically relevant, it allowed for increased reproducibility and a more well-defined wound by which to study BP effects on re-epithelialisation.

The use of selective keratinocyte seeding to study migration has been used before in skin models, with a technique developed by MacNeil *et al.* using two concentric stainless steel rings of different diameters, to create a 'donut' shape of epithelial cells [207]. Whilst this is also applicable for oral mucosa work, the method requires large amounts of cells and dermis, making it more difficult to perform. Collagen models have also been used for similar assays, where smaller devices have been used to prevent keratinocyte seeding in a particular area [208], [209]. These use fewer cells, however they have a much simpler and less representative model of the dermal compartment, with no rete ridges and poor mechanical properties [194], [306].

Here, we have begun the development of an oral mucosa wound model using a combination of these previous methods which removes the main disadvantages of them. Our model retains the use of DED and is thereby more representative of the *in vivo* setting than collagen models, while removing the two main obstructions to the MacNeil model by

requiring fewer cells and smaller pieces of dermis. Creating an ALI with the ring in place for 7 days allowed for a multi-layered epithelium to form on either side of the exclusion zone, approximating the natural scenario for an epithelial wound. A 3 mm wound was created repeatedly, and over 7 days of culture the wound closed, leaving a model with a complete, stratified epithelium.

Our results suggest clinically relevant concentrations of BPs prevent re-epithelialisation. Treatment with 100 μM PA and 10 μM ZA consistently removed any epithelial cells from the wound models, independent of original epithelial thickness. A 50 μM PA treatment allowed for epithelial migration, but prevented stratification, which was particularly evident in our successful ALI seeded model. As we have previously demonstrated, BPs prevent proliferation but do not affect migration, and prevent the stratification of newly formed epithelia. From both the resazurin visualisation and histology, the migration of keratinocytes across the model is consistently evident, even when treated with toxic concentrations of PA or ZA. However, the epithelia formed following this migration were rarely stratified. Epithelial stratification is known as a proliferation effect [99]. Our results thereby suggest that BPs prevent the healing of soft tissue by preventing a full thickness epithelium from forming following surgery.

Previously, both PA and ZA have previously been demonstrated to effect re-epithelialisation in 3D, with proliferation identified as a cause, however only 10 μM concentrations were tested [164], [187]. We chose higher concentrations of PA due to our earlier 3D work and IC_{50} s, and have demonstrated by the first time the clear effect these concentrations have on epithelial wound healing. We have also indicated that 1 μM ZA does not prevent re-epithelialisation. In reducing local BP concentration, this concentration would therefore be a suitable target to prevent BRONJ development.

In their work, Saito *et al.* also identified a further potential pathway by which BPs can affect keratinocyte wound healing – downregulation of the $\alpha_v\beta_6$ integrin [187]. Keratinocytes do not normally express the integrin $\alpha_v\beta_6$, however during wound healing it is upregulated [188], whereby it promotes cell migration and activates TGF β . This presents an interesting area for further study. However, due to our model using immortalised keratinocytes, which behave differently and may not follow this same signalling pathway, this was outside of the scope of the work in this thesis. Following the optimisation of the model, performing the assay with primary keratinocytes and investigating further the mechanisms by which BPs effect the oral mucosa through immunohistochemistry would provide valuable information on BRONJ.

Optimising the model was difficult. The 3D printed ring successfully allowed for the selective seeding of cells onto DED. Resazurin assays allowed for a visual representation of seeding success, which was confirmed through histology. However, when placed immediately at ALI the epithelial sections were single layered, and therefore not a good

representation of the *in vivo* BRONJ scenario. Seeding at ALI gave some success, allowing for the stratification of the epithelium with the ring in place, and in initial tests allowed for a good model of the soft tissue component of BRONJ. However, this was not reproducible. The donor skin which was processed into DED was from a variety of patients, and as such, was inconsistent. The thickness of the skin in particular changed from batch to batch. When the models were seeded at ALI, the DED needed to be thick to allow for a good seal to be created. Due to the seeding process requiring both a 3D printed ring and the heavier stainless steel ring atop it, the structure was top heavy. Therefore, when the well plates were moved, the rings were unsteady and could also move. With thin DED, this movement caused the DED to move and aggregate at the holes of the stainless steel grid, which broke the seal created by the rings and caused the seeded cells to move outside of the sections created by the ring. To achieve distinct epithelial sections but to allow a greater seal, another method was chosen.

Models were seeded on the bottom of a well plate, but media removed from the insides of the ring to create an *in situ* ALI. This created two distinct, multi-layered epithelial sections. Though these sections were not as thick as when models were seeded at ALI, this allowed for greater reproducibility. As such, this mechanism allowed for a wound model that most closely satisfied our three criteria: reproducibility of the wound, healing potential, and similarity to the clinical scenario, and was used for further testing of the BP effect on epithelial wound healing, however still presented with issues.

The final epithelia on the models seeded with an *in situ* ALI were thin, appearing similar to the models originally cultured in the rings with no ALI. The epithelia also appeared discontinuous in places. Though stratified, the keratinocyte areas seeded with the *in situ* ALI were only a few cells thick, as such, it follows that the overall epithelium of these models would be thin at day 7, as fewer keratinocytes were present to proliferate and migrate. To perform the resazurin assays on these models, they had to be transferred between well plates. When transferred, the models often folded and had to be flattened out with forceps. This happened more when the DED used was thinner. This process is likely to have disrupted the epithelium of the models, particularly if the epithelia were thinner to begin with. All this contributed to a model with high variation, indicated by the resazurin results in Figure 6.30. Although these models have provided some results indicative of how BPs contribute to the failure of soft tissue to heal following oral surgery, further optimisation is still required before this is truly a repeatable *in vitro* model of BRONJ.

Re-epithelialisation is not just effected by BPs, and as such, these models have a wide scope for use in the tissue engineering field once fully optimised. Several diseases present with non-healing epithelia, not just in the oral mucosa, but in skin, and several drugs have been tested for their ability to promote re-epithelialisation. For example, a study by Vukelic *et al.* investigated the effects of glucocorticoid receptor on cutaneous wound

healing, whereby they explanted patient tissue and created 3 mm biopsy punch wounds and treated with different drugs [307]. Our wound healing model could potentially allow the consistent creation of a 3 mm epithelial wound by which to study these effects. The models could also be used to generate more data, following optimisation, through the measurement of cytokines and other secreted factors, in order to fully examine the wound healing process of the model. Whilst there is no blood supply in the models, and therefore will be a smaller inflammatory response, studies have previously demonstrated the detection of inflammatory cytokines possible with in vivo models, both through an enzyme-linked immunosorbent assay of the medium [308] and through a polymerase chain reaction following the digestion and homogenisation of the models [309]. These assays would give a much more specific view of the wound healing response, and therefore add to the validity of the model, going forward.

6.6 Summary

In summary, we have demonstrated that clinically relevant concentrations of PA prevent the stratification of newly formed epithelia, and reduce the thickness of healthy epithelia. ZA treatment had the same effect at low concentrations, with higher concentrations leading to toxicity. We have also begun the development of a 3D *in vitro* model of the soft tissue component of BRONJ, and indicated that PA and ZA prevent re-epithelialisation of the oral mucosa.

7. Hydroxyapatite granules prevent bisphosphonate toxicity *in vitro*

7.1 Aim

To assess whether hydroxyapatite (HA) in different forms can bind bisphosphonates (BPs), and thereby reduce BP *in vitro* effects to cells of the oral mucosa.

7.2 Introduction

We have demonstrated in the previous chapters that BP effects on soft tissue have a key role in the development of BRONJ. It is clear these effects must be inhibited in the prevention and treatment of the disease. Due to the severity and complexity of the later stages of BRONJ, and the difficulty that comes with treating them, preventing the disease development entirely would be the most beneficial solution [1], [40]. Most BRONJ cases follow a preceding event, and most of these events are oral surgeries [1], [123]. These therefore offer an obvious point at which to start preventative treatment. As BPs cause a wide variety of different effects, rather than managing each specific effect, reducing the BP level to which the oral mucosa is exposed may be a more elegant and efficient method of treating the condition, and recent literature has indicated potential methods by which to do this – either through using EDTA to chelate calcium or by replacing bound BPs with the less potent etidronic acid [40], [226], [227].

It is well-documented that BPs have a high binding affinity for calcium, and calcium phosphate based materials have previously been used to bind BPs [34], [52], [60], [241], [251]–[253], [266]. Therefore, it may be possible to use this binding affinity to reduce local BP concentration, prevent BP effects, and allow for soft tissue wound closure. This would be particularly advantageous, as calcium phosphate bone filler materials are currently in use in the clinic in the treatment of several different BRONJ-preceding events [242]. However, demonstrating this effect would require the detection of BPs, which is a difficult process [273], [274].

This chapter aims to assess the ability of HA to bind pamidronic acid (PA) and zoledronic acid (ZA). This was first investigated chemically through a variety of spectroscopic techniques, examining both the ability of HA to bind BPs, and retain BPs once bound. Following this, biological tests took place, examining whether HA could be used to counteract the PA and ZA toxicity demonstrated in chapters 5 and 6.

7.3 Materials and methods

7.3.1 Preparation of HA

CAPTAL® 'R' sintering grade, high purity HA powder (Plasma Biotal Limited) was used for the work in this chapter. In order to reliably examine the ability of HA, it was first pressed into uniform discs. Amounts of 0.7 g were weighed and loaded into a 13 mm die (Specac) and pressed under uniaxial pressure in a manual hydraulic press (Specac) with 5 tonnes of pressure held for 30 seconds.

7.3.2 Sintering of HA discs

Discs were sintered to fuse the HA powder. Discs were placed on an alumina boat and into a chamber furnace (Lenton Thermal Designs) where they were sintered in air at 1200 °C with a ramp rate of 5 °C/minute and a dwell time of 2 hours. The final weight of the discs was approximately 0.65 g.

7.3.3 HA granules

ReproBone® 1 to 4 mm HA granules were kindly provided from Ceramisys Limited. Granules were weighed into amounts of 0.65 g to match the final weight of the sintered HA discs.

7.3.4 X-ray diffraction (XRD)

To examine the crystalline phase of the discs, XRD was carried out on a diffractometer (Siemens D5000) with a 2θ angular range of 10 to 60 ° and a step size of 0.05 °. The spectra obtained were compared using the Sleve+ software (ICDD) against the Powder Diffraction Files (PDF) database of the Joint Committee on Powder Diffraction Standards (JCPDS), using reference cards 09-432 (HA) and 09-169 (β -tricalcium phosphate (TCP)).

7.3.5 Brunauer–Emmett–Teller (BET) surface area

In order to calculate the surface area of the discs and granules, nitrogen gas adsorption was performed. The surface area/volume ratio of the 13 mm diameter discs was calculated, before discs were pressed in a 5 mm die (Specac) and sintered, as in sections 7.3.1 and 7.3.2, ensuring the same surface area/volume ratio. The final weight of the discs was approximately 0.03 g.

Nitrogen gas adsorption was performed as a service by Duncan Schofield from the Department of Chemical and Biological Engineering, University of Sheffield. Granules

were measured in duplicate, and 2 discs were analysed together. Firstly, samples were placed in 9 mm diameter test tubes, which were degassed at 30 °C in a degasser (Micrometrics VacPrep 061). Then, nitrogen adsorption isotherms were obtained using a surface area analyser (Micrometrics TriStar II) at -196 °C.

Isotherms were analysed and surface area calculated using 3Flex (Micrometrics). Full isotherms are displayed in Figure 10.5 (see Chapter 10). BET surface area was calculated in the relative pressure region of 0.05 to 0.2, due to the linearity of the measurements in this region.

7.3.6 Ultraviolet-visible (UV-vis) spectroscopy

UV-vis spectroscopy was used to measure BP concentration. All samples were placed in quartz micro-cuvettes with a 0.7 ml capacity (Thor Labs) and measured in a UV-vis spectrophotometer (Unicam UV300) between 200 and 230 nm, referenced against distilled water.

7.3.7 Calibration curves

BPs were prepared as described in section 4.2. BP stock solutions were diluted in distilled water to give PA and ZA solutions of concentrations ranging from 0 to 250 µM. Samples of each concentration were read in triplicate in a UV-vis spectrophotometer, as described above.

7.3.8 Hydroxyapatite binding and release of zoledronic acid

To examine the ZA binding properties of HA discs, they were placed individually into a sterile universal tube containing 200 µM ZA in distilled water and incubated at 37 °C for 14 days. At select time points, a sample of the supernatant was removed and ran through a UV spectrophotometer, as above. When unsintered discs were used, the sample was centrifuged to remove any HA powder. As controls, 200 µM ZA containing no HA was incubated, and HA discs were incubated in distilled water. Three samples were incubated for each condition. To ensure ZA degradation did not take place when incubated, a refrigerated sample of 200 µM ZA in distilled water was also examined at each time point for comparison (not shown).

After the 14 day binding study, the HA discs were removed, dried in air, and placed into new universal tubes. Distilled water was added to each tube before incubation. Over 10 days, samples of this water were examined in the UV-vis spectrophotometer, to assess whether any ZA was released.

7.3.9 Fourier-transform infra red spectroscopy - attenuated total reflectance (FTIR-ATR)

FTIR-ATR was used to examine the chemical structure of the HA before and after BP binding. Samples were crushed to powder with an agate mortar and pestle prior to testing. Spectra were obtained between 4000 and 800 cm^{-1} with a FTIR-ATR spectrometer (Thermo Fisher Scientific Nicolet 380). Powder from HA discs of four different preparations were tested: control sintered HA discs, HA incubated in water for 14 days, HA incubated in 200 μM ZA for 14 days, and HA incubated in 200 μM ZA for 14 days then incubated in water for 10 days.

7.3.10 Raman spectroscopy

The chemical structure of HA discs was also examined through Raman spectroscopy. HA discs were examined using a Raman spectrometer (Thermo Fisher Scientific Nicolet DXR) using a 532 nm laser with a 2 cm^{-1} resolution. Samples were analysed between a spectral range of 4000 and 400 cm^{-1} with a 10 mW power, with exposure times of approximately 300 seconds. The spectra generated were processed using OMNIC™ (Thermo Fisher Scientific).

Discs were tested after no treatment, 14 days incubation in 200 μM ZA, and 14 days incubation in 200 μM ZA then 10 days incubation in water. To assess the ability of Raman spectroscopy to quantify ZA binding, samples were incubated in 100, 200 or 300 μM ZA for 14 days before examination.

7.3.11 Biological binding assays

Discs and granules were sterilised through autoclaving, then added to sterile universal tubes, with one disc or 0.65 g of granules per tube. Empty tubes were used as controls. BP containing medium was added to each tube, ranging from 0 to 100 μM PA and 0 to 50 μM ZA, with a 5 ml volume used.

Cell culture was performed as described in section 4.1. After 48 hours, cells were seeded in preparation for an MTT assay as described in section 5.3.1. The following day, after 72 hours of BP binding, the medium was removed from the cells and replaced with 0.3 ml of HA conditioned media. MTT assays were performed 24, 48 and 72 hours after this step.

Granules were also weighed into smaller amounts, from 0.065 to 0.65 g, to create a calibration curve for granule weight and HA binding ability. Granules were placed into universal tubes and MTT assays performed as before.

Oral mucosa models were seeded as in section 6.3.1, halved with a sterile scalpel and placed at ALI for 7 days, at which point a resazurin assay was performed as in section 6.3.3. Following the assay, models were returned to ALI and treated with either control medium or 30 μM ZA in sextuplicate. Of the six models treated with either medium, two were cultured as normal. Two of the models of each treatment were cultured with a sterile disc placed under the stainless steel grid, and two with 0.65 g of sterile HA granules placed under the grid. At day 10, a resazurin assay was performed and media was replaced. At day 14, another resazurin assay was performed, following which samples were fixed, processed for histology and stained as described in section 6.3.8.

7.3.12 Statistics

Statistics were performed using Prism as described in section 4.3. 'N' is used to denote experimental repeats, while 'n' is used to denote technical repeats throughout. Prism 7 was used to plot linear regressions to create UV-vis calibration curves for PA and ZA. Curves were also plotted for the UV binding and release data. Linear regressions were plotted for each data set, except for when HA was incubated in 200 μM ZA for 14 days, where a one phase exponential decay was plotted.

MTT results were normalised as before in section 5.3.9 and resazurin results were normalised as before in section 6.3.9. In this chapter, a two way ANOVA was again performed, however post-hoc analysis was performed using Tukey's test. To assess the HA effect, significance was calculated between the control group and each HA group; comparing the individual BP concentration of the controls with their corresponding concentration in the HA group (e.g. Control 100 μM PA vs. Granules 100 μM PA).

To create a calibration curve for HA granule weight and 100 μM PA toxicity, metabolic activity values were normalised to the highest weight used (0.65 g) and an exponential growth curve was plotted.

7.4 Results

7.4.1 Hydroxyapatite retains phase purity when sintered at 1200 °C

HA can transform to tricalcium phosphate (TCP) at temperatures above 1200 °C, therefore XRD was performed following sintering to confirm the crystalline phase of the discs. The spectra generated for the sintered discs is shown in Figure 7.1. Also included are Joint Committee on Powder Diffraction Standards (JCPDS) reference cards for HA and β -TCP. The spectra demonstrate that the sintered HA produced was indeed HA, with all peaks found in the sintered disc matching those from the reference card. No unique β -TCP peaks were found. Further peak matching analysis of the data in the software package confirmed the sintered discs were <99% HA.

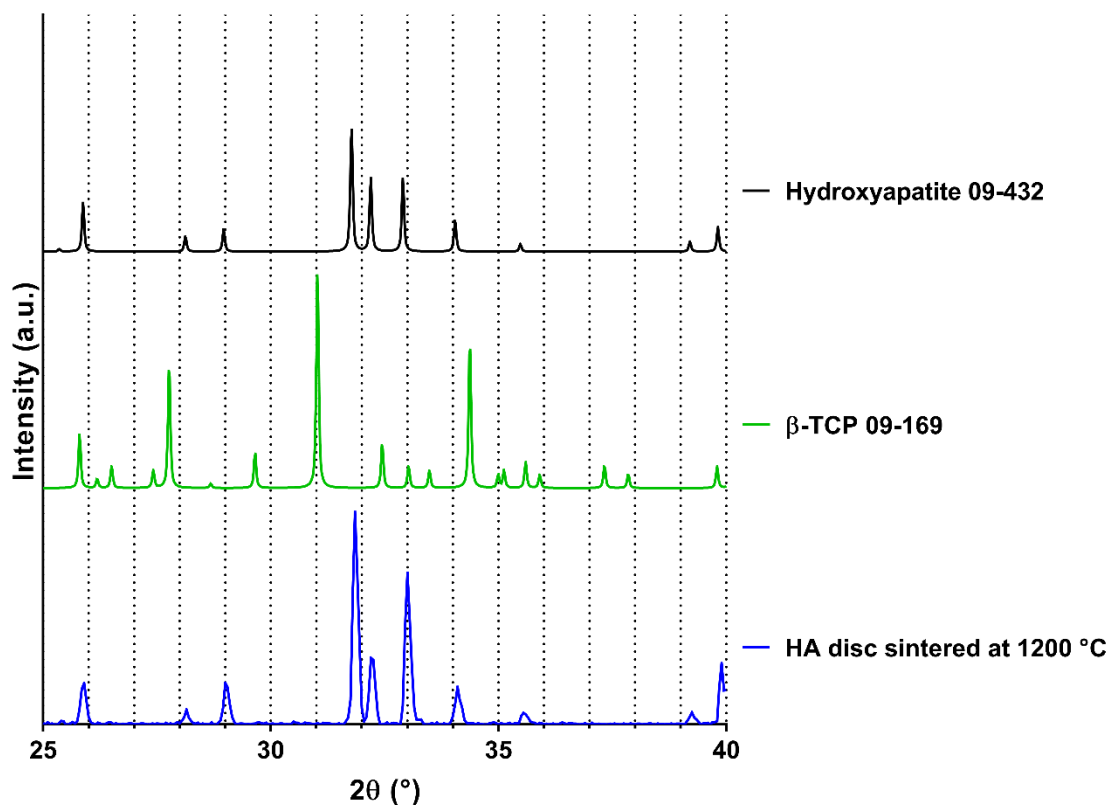


Figure 7.1. X-ray diffraction patterns for hydroxyapatite discs pressed and sintered at 1200 °C, and standard reference cards of β -tricalcium phosphate and hydroxyapatite. $N=1$, $n=1$.

7.4.2 Hydroxyapatite granules have a larger surface area than sintered discs

As surface area is thought to affect the BP binding ability of HA, nitrogen gas adsorption isotherms were generated for HA granules and discs and the surface area calculated using the BET equation. Figure 7.2 shows the surface area of HA granules and discs. The granules had a mean surface area of approximately 345 m²/g. The discs had a surface area of approximately 45 % of that, with a measurement of 160 m²/g.

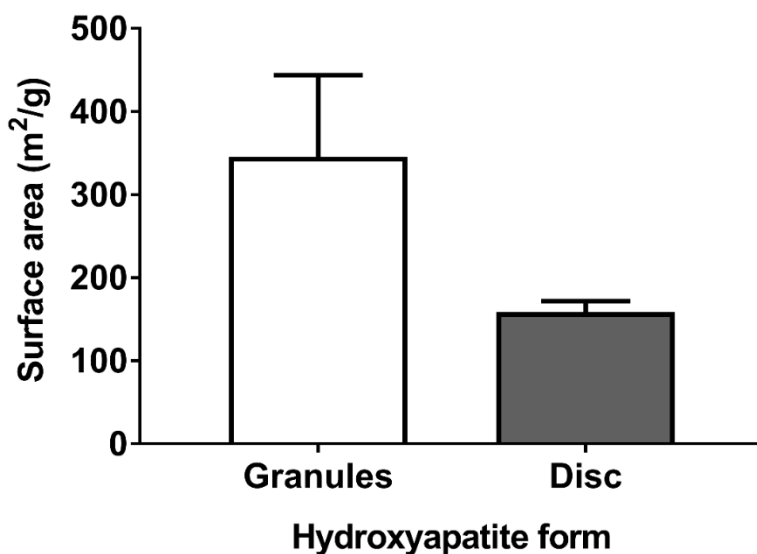


Figure 7.2. BET surface area measurements for hydroxyapatite granules and sintered discs. N=1, n=2. Error bars = mathematical error from BET equation.

7.4.3 Zoledronic acid concentration was quantified using ultraviolet-visible spectroscopy

To assess whether UV-vis spectroscopy could be used to measure BP concentration, samples of ZA and PA were measured in a UV-vis spectrophotometer at a 210 nm wavelength. There was a strong trend between ZA concentration and absorbance for samples from 0 to 250 μM , as shown in Figure 7.3. Samples containing no BP measured approximately 0, as expected. Linear regression was performed with the data to generate a calibration curve, with an r^2 value of 0.99, indicating a strong linear relationship between concentration and absorbance.

PA, however, did not give a strong enough reading through this technique for the determination of unknown concentrations. While there was still a general upward trend and a good linear fit, the standard deviation of each concentration overlapped, indicating this method was unsuitable for the detection of PA concentration.

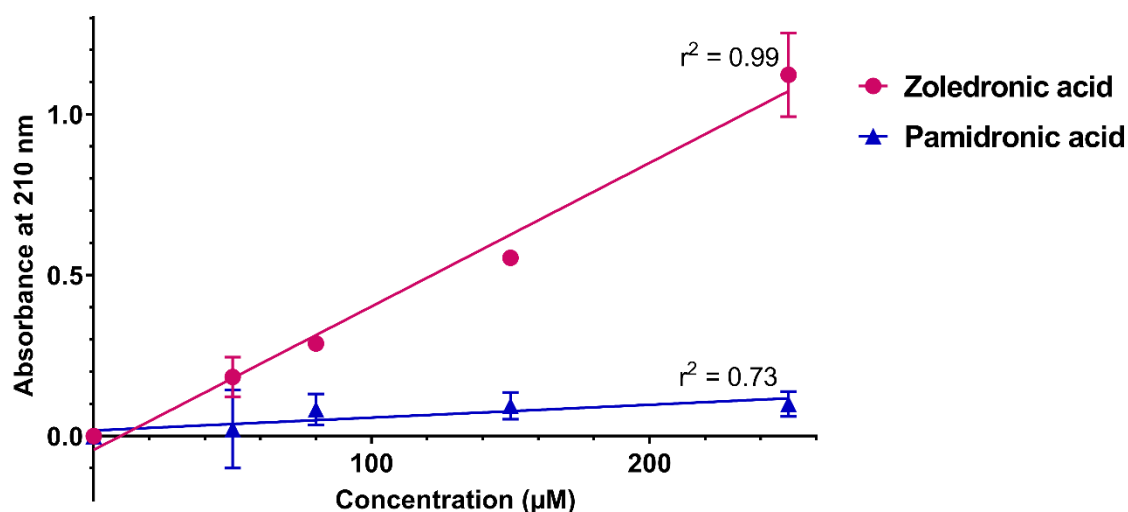


Figure 7.3. Ultraviolet-visible spectroscopy calibration curves for aqueous zoledronic acid and pamidronic acid at 210 nm, from 0 to 250 μM . Distilled water used as a reference blank. $N=1$, $n=3$. Error bars = SD. Linear regressions for each data set shown.

7.4.4 Unsintered hydroxyapatite effected bisphosphonate signal

Initially, unsintered, pressed HA discs were incubated in ZA. Samples of the supernatant were taken periodically, with UV-vis spectroscopy used to assess concentration over time. Samples were centrifuged before reading to remove any HA powder in the samples. Figure 7.4 shows the UV-vis spectroscopy readings for samples taken after 1 day, from 200 to 230 nm, across the region of the ZA peak. While the ZA had a similar value to both that of the calibration curve in Figure 7.3, when HA was present, samples were indistinguishable from one another. No ZA peak was visible. Both readings go above 2, which according to Beer-Lambert Law suggests almost 100% absorbance, and below 210 nm (not shown due to peak height) these values were at the maximum possible value of the spectrophotometer. Sintered discs were therefore used from this point onwards.

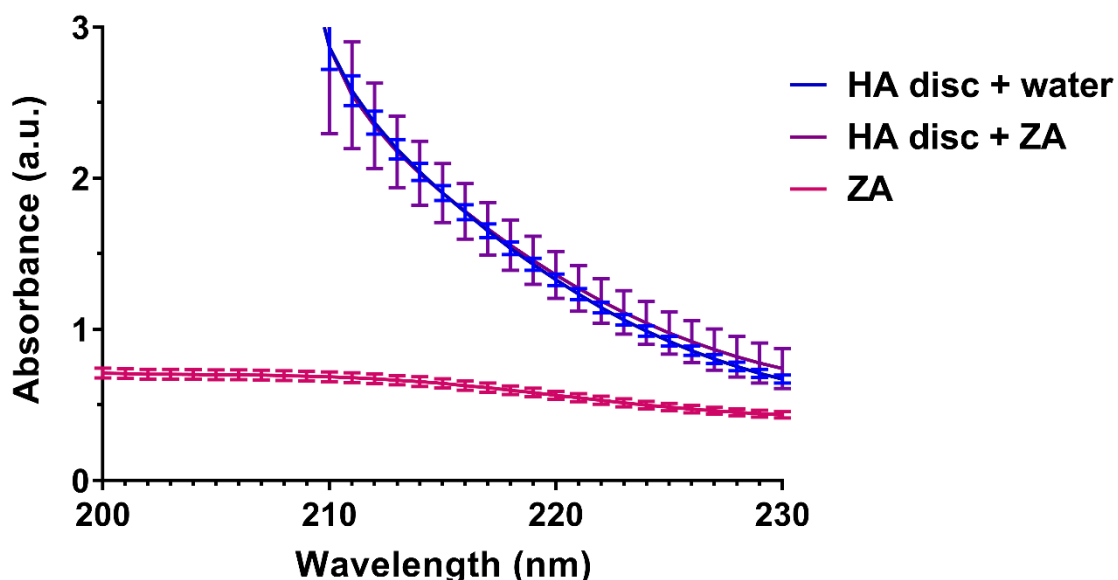


Figure 7.4. Ultraviolet-visible spectroscopy readings for water containing a hydroxyapatite disc, 200 μ M zoledronic acid containing a hydroxyapatite disc, and 200 μ M zoledronic acid alone, incubated at 37 $^{\circ}$ C for 1 day. Samples centrifuged prior to reading. Distilled water used as a reference blank. $N=1$, $n=3$. Error bars = SD.

7.4.5 Sintered hydroxyapatite discs exhibited a potential zoledronic acid binding behaviour

To assess the ZA binding capability of sintered HA discs, they were incubated in 200 μM ZA for 14 days. Figure 7.5 demonstrates that the concentration of the ZA solution reduced over time. Over the first 2 days, the concentration dropped to approximately 140 μM before the reduction steadied, ending at approximately 120 μM . An exponential decay plot indicated binding had levelled off, though with a relatively average fit of the data indicated by the r^2 value.

ZA alone maintained an approximate constant level across the experiment, with a linear regression fitting the data well. The final concentration of this solution was close to 210 μM , however there was a larger amount of error with this value.

When a sintered HA disc was incubated in water alone for 14 days, the absorbance at 210 nm suggested an increase in ZA concentration. This concentration steadily increased over the period of the experiment, in a well-defined linear trend. By day 14, this solution had an absorbance value equivalent to 70 μM , despite no ZA being present in this system, however with a large standard deviation.

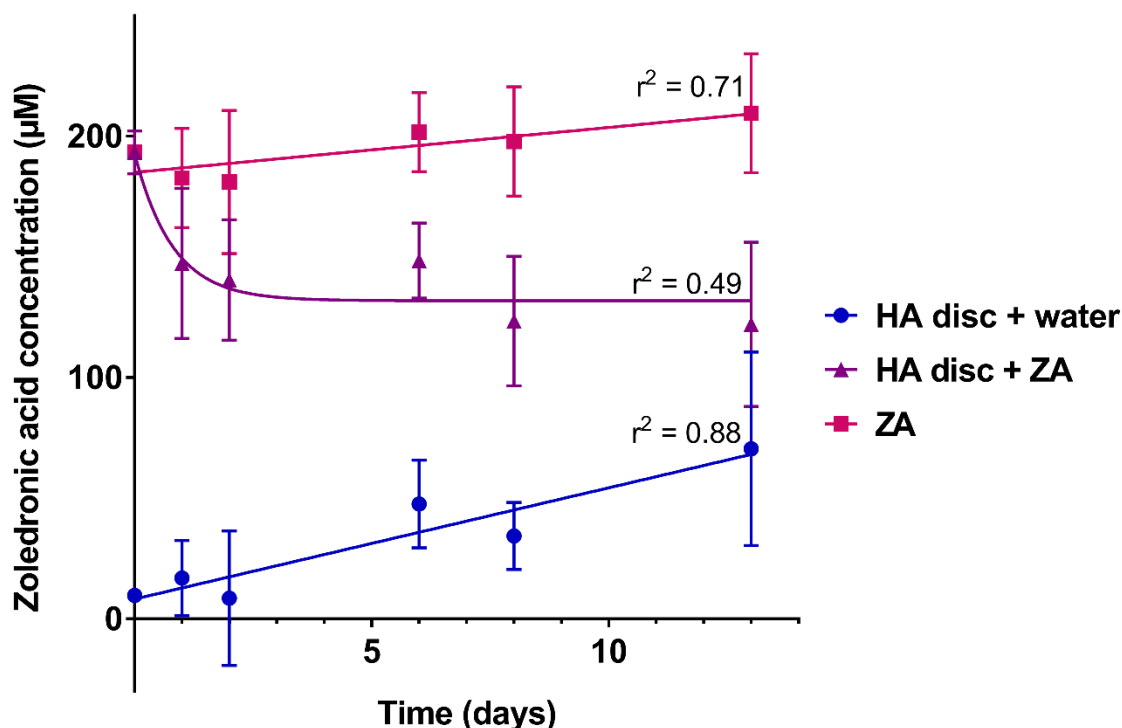


Figure 7.5. Ultraviolet-visible spectroscopy readings for water containing a sintered hydroxyapatite disc, 200 μM zoledronic acid containing a hydroxyapatite disc, and 200 μM zoledronic acid alone, incubated at 37 $^{\circ}\text{C}$ for 14 days. Distilled water used as a reference blank. $N=3$, $n=3$. Error bars = SD. Linear regressions shown, except for zoledronic acid and hydroxyapatite disc, where one phase exponential decay plotted.

7.4.6 Sintered hydroxyapatite may have released previously bound zoledronic acid

The sintered discs which had previously been incubated in either water or 200 μM ZA were dried in air, then incubated in water for 10 days, and UV-vis readings of the supernatants were taken over time, to assess whether any bound BP was being released. Figure 7.6 suggests that previously bound ZA was released from the sintered disc. At 10 days, the solution read as approximately 115 μM ZA, though again with large standard deviation. This was higher than the calculated level of binding from the data in section 7.4.5.

However, when HA was incubated in water, the solution gave a reading suggesting the presence of ZA, which again increased linearly over the duration of the experiment. By day 10 the solution gave a reading that corresponded to approximately 70 μM ZA, though no ZA had been in the system. This again suggested interference of HA with the readings. Linear regressions were performed with each data set, which indicated a strong linear increase in ZA concentration.

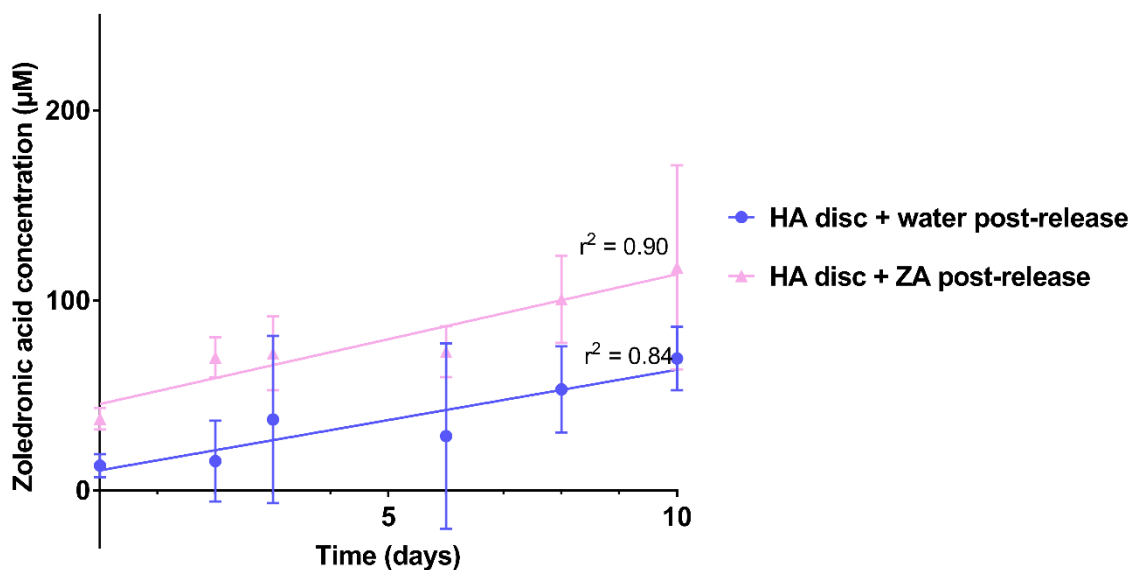


Figure 7.6. Ultraviolet-visible spectroscopy readings for water containing a sintered hydroxyapatite disc incubated at 37 °C for 10 days. Discs had previously been incubated for 14 days in either water or 200 μM zoledronic acid. Distilled water used as a reference blank. $N=3$, $n=3$. Error bars = SD. Linear regressions for each sample shown.

7.4.7 Sintered hydroxyapatite interfered with the ultraviolet-visible spectroscopy signal at 210 nm

Due to the interference in signal exhibited over the experiment, the solutions were examined over a wider spectrum. Figure 7.7 shows the spectra from sintered discs incubated in 200 μM ZA or water for 14 days, before soaking in water for 6 days. The ZA incubated sample showed a small peak close to 210 nm, as expected.

When a sintered HA disc was incubated in water, there was absorbance at 210 nm. As these spectra are referenced against distilled water, a constant value of 0 is the expected reading of the sample. The shape of the absorbance spectra is similar to that of Figure 7.4, though of lower absorbance, which suggested that HA interference caused this reading. It therefore appeared that measuring the concentration of the solutions was not possible, and therefore the chemistry of the discs before and after ZA treatment was investigated.

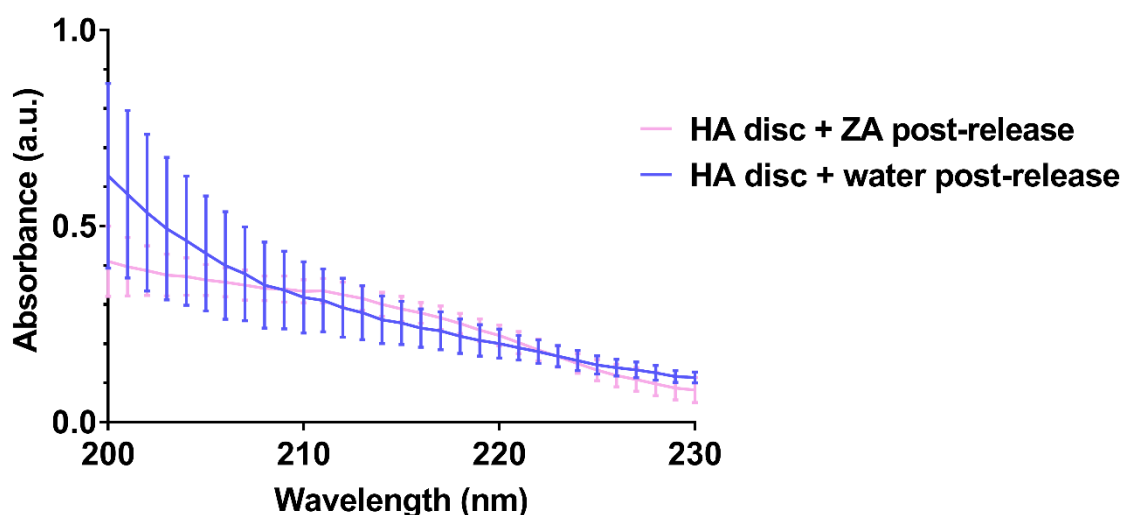


Figure 7.7. Ultraviolet-visible spectroscopy readings for water containing a sintered hydroxyapatite disc incubated at 37 °C for 6 days. Discs had previously been incubated for 14 days in either water or 200 μM zoledronic acid. Distilled water used as a reference blank. $N=1$, $n=3$. Error bars = SD.

7.4.8 FTIR-ATR cannot be used to detect zoledronic acid bound to sintered hydroxyapatite discs

FTIR-ATR spectroscopy can be used to identify compounds based on the excitation of bonds within the compound at certain light wavelengths. As we expected ZA to be bound to the sintered HA discs following the binding and release experiment, discs were analysed with this technique. Sintered HA discs were crushed to powder so as to be able to be loaded onto the FTIR-ATR fully and maintain a complete contact with the IR beam. Figure 7.8 shows the spectra generated for an untreated sintered control disc, a sintered disc incubated in water for 14 days, a sintered disc incubated in 200 μM ZA for 14 days, and a sintered disc incubated in 200 μM ZA for 14 days and then water for a further 10 days.

All samples generated similar spectra, with no obvious regions of difference, except for one area of the control sample. Each sample had a PO_4^{3-} band at approximately 1000 cm^{-1} , characteristic of calcium phosphates. In the control sample, there was a peak at approximately 2360 cm^{-1} . This peak is characteristic of CO_2 , and therefore indicates an incomplete contact of the sample with the beam. ZA peaks were expected at around 1500 cm^{-1} due to the aromatic ring and, due to the phosphorous in ZA, stretches to the PO_4^{3-} band were expected. Neither of these were visible in any sample.

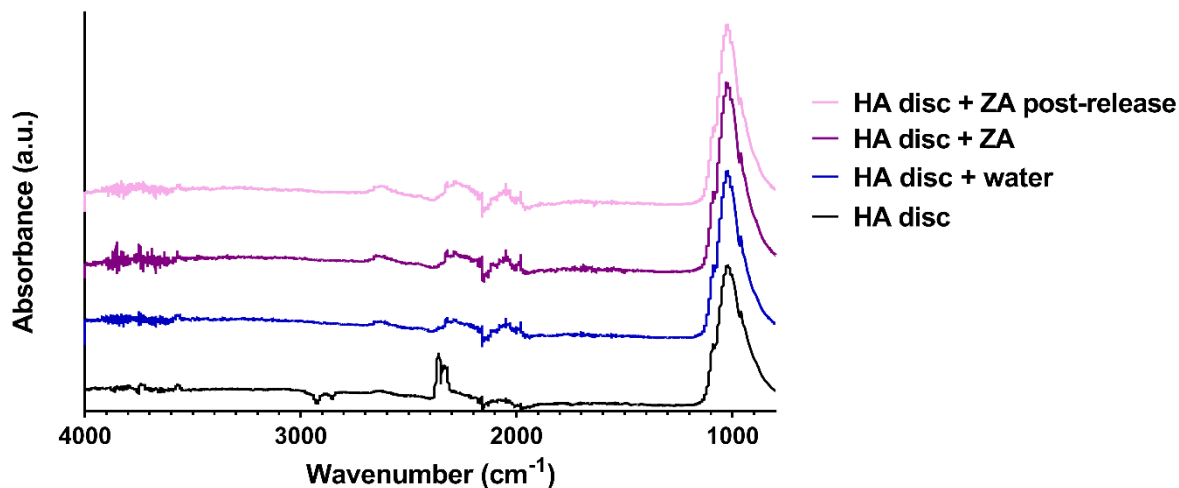


Figure 7.8. FTIR-ATR spectra for sintered hydroxyapatite discs after three different treatments: 14 days incubation in water, 14 days incubation in 200 μM zoledronic acid, and 14 days incubation in 200 μM zoledronic acid followed by 10 days incubation in water. An untreated disc was also measured. $N=1$, $n=1$.

7.4.9 Raman spectroscopy indicated some surface binding of zoledronic acid to sintered hydroxyapatite discs, though not quantitatively

Raman spectroscopy is a similar technique to FTIR, however is performed through the focussing of a laser onto a sample, so could be performed on our sintered discs without the need for crushing to powder.

Figure 7.9 shows Raman spectra of an untreated sintered HA disc, a sintered HA disc incubated in 200 μM ZA for 14 days, and a sintered HA disc incubated in 200 μM ZA for 14 days and then water for a further 10 days. In the region shown in the spectra, no obvious peaks appeared in the control sample. All samples showed the beginning of the characteristic strong PO_4^{3-} band at around 962 cm^{-1} , (not fully shown due to relative height of the peak). In the samples incubated in ZA, small peaks were visible at 906 , 878 , 850 , 824 and 740 cm^{-1} . The peaks at 878 and 850 cm^{-1} indicated carbon bonding, with the 850 cm^{-1} peak indicative of the aromatic ring found in ZA. These peaks were smaller in the sample from the release study, suggesting that previously bound ZA has been released when incubated in water for 10 days.

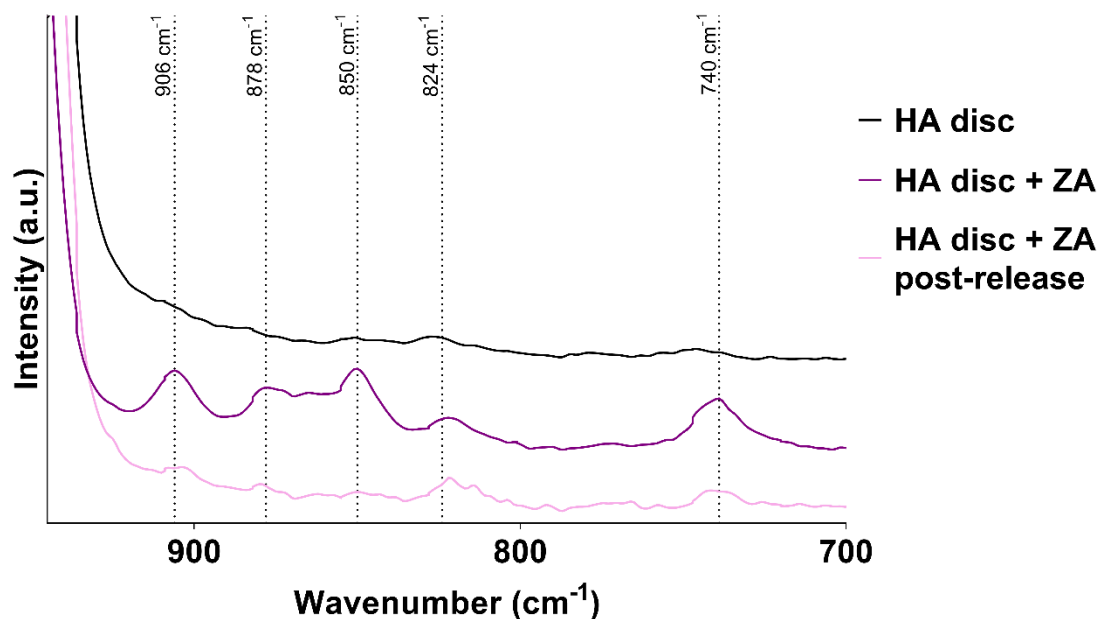


Figure 7.9. Raman spectra for sintered hydroxyapatite discs: untreated as a control, incubated in 200 μM zoledronic acid for 14 days, or incubated in 200 μM zoledronic acid for 14 days and then incubated into water for a further 10 days. $N=1$, $n=1$.

To determine the reliability of this technique in identifying the amount of bound ZA, sintered discs were incubated in three different concentrations for 14 days before analysing. Figure 7.10 shows the Raman spectra for these discs. While the peaks were slightly shifted compared to Figure 7.9, the shift was consistent for all samples indicating this is due to the equipment precision rather than a chemical change in the material. The peaks all appeared as before, however the ratio of the peaks does not follow the concentration of the drug (and thereby the assumed level of binding). While Raman spectroscopy was therefore suitable for the detection of bound ZA, it was not capable of quantitatively measuring the amount.

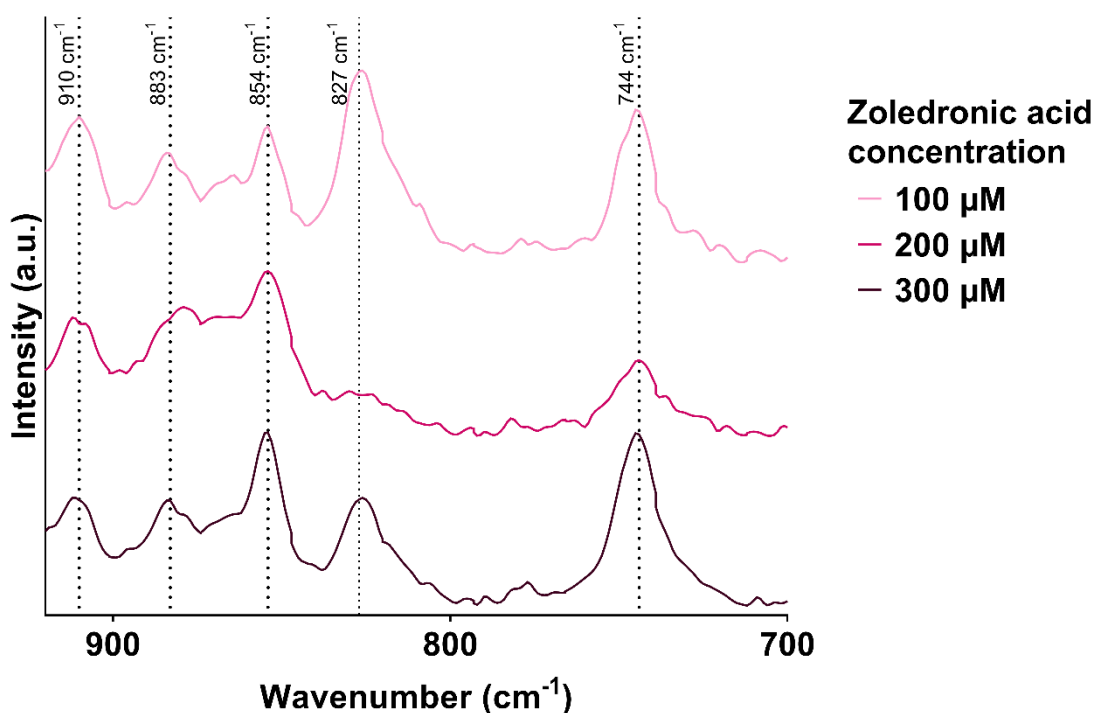


Figure 7.10. Raman spectra for sintered hydroxyapatite discs incubated in 100, 200 or 300 µM zoledronic acid for 14 days. N=1, n=1.

7.4.10 Hydroxyapatite granules prevented bisphosphonate metabolic activity effects in 2D

As our UV and Raman studies suggested that HA had the ability to bind BPs, we tested this biologically. For this, we also included some commercially available HA granules, as these are currently used clinically. A sintered HA disc or an equal weight of granules were incubated for 72 hours in PA and ZA concentrations above the IC₅₀ values defined in chapter 5. PA and ZA incubated with no HA were used as controls.

Figure 7.11 shows metabolic activity for human oral fibroblasts after treating with PA or ZA that had been previously incubated with HA. At 24 hours, no significant differences were seen between any BP concentration of either HA group, compared to the corresponding concentration of the control group.

After 48 hours treatment, both 50 and 100 μ M PA and 50 μ M ZA reduced cell metabolic activity of the control cells. Incubating with a HA disc led to no significant differences to the controls, with the same overall trends seen. Incubating with HA granules prevented the PA reduction in metabolic activity by a significant amount for both concentrations. All conditions had similar levels of metabolic activity to the control, untreated cells.

At 72 hours treatment, PA and ZA were again toxic to cells at both concentrations in the control group. HA discs had no effect, with no significant differences to the control group at any concentration. HA granules prevented the BP toxicity. The untreated cells showed no significant differences to the untreated control cells, indicating the HA granules were not affecting metabolic activity. HA granules showed significantly higher metabolic activity for all four BP treatments, in comparison to the control groups.

Hydroxyapatite granules prevent bisphosphonate toxicity in vitro

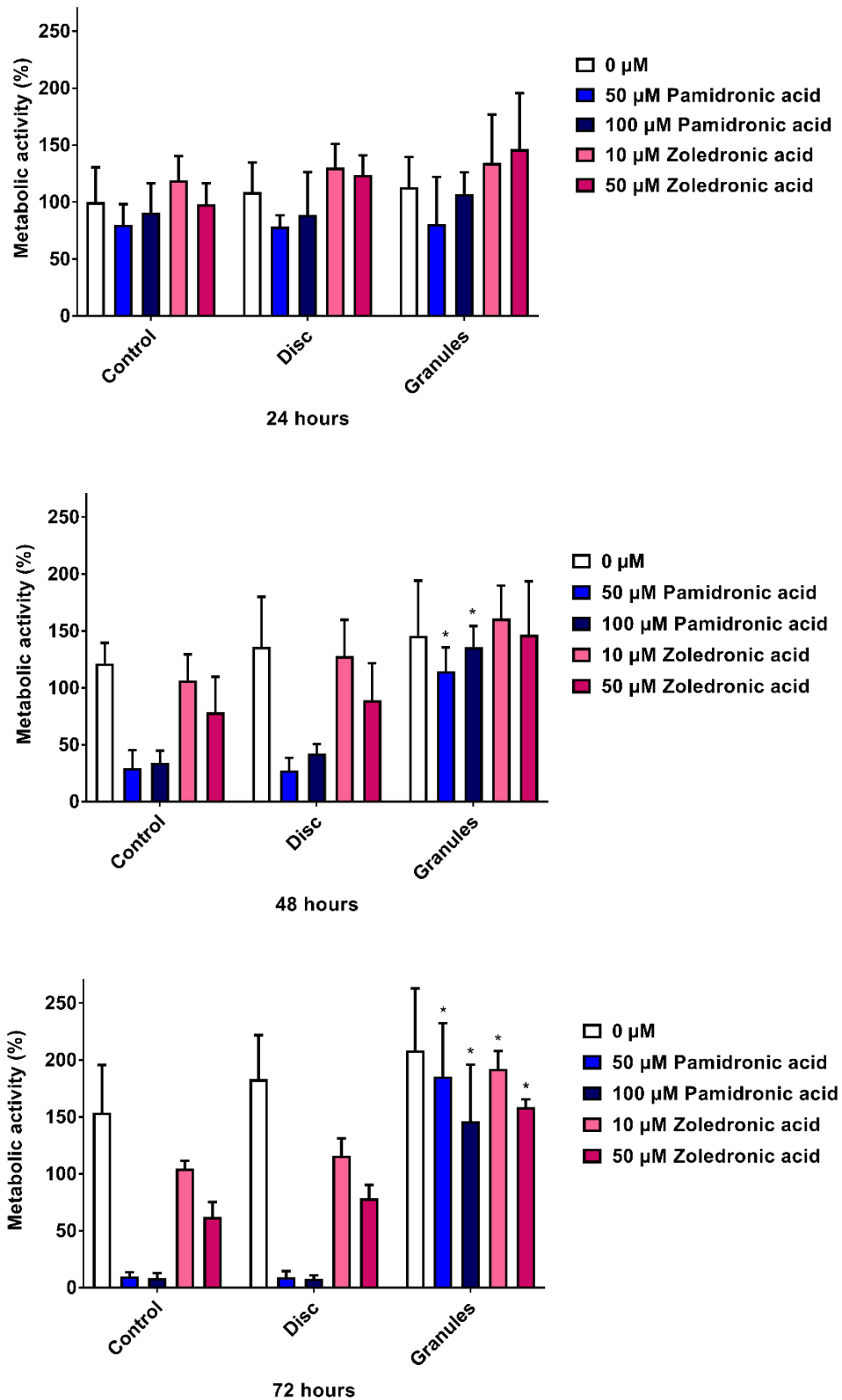


Figure 7.11. Human oral fibroblast metabolic activity over 72 hours in the presence of pamidronic acid and zoledronic acid, incubated prior for 72 hours with hydroxyapatite in sintered disc or granule form. Media incubated with no hydroxyapatite used as a control. Values normalised to control cells at 24 hours. N=3, n=3. Error bars = SD. Significance against control at each time point indicated by *P<0.05.

Immortalised human oral keratinocytes were also used to biologically study the ability of HA to bind PA and ZA. Figure 7.12 shows the metabolic activity over 72 hours. After 24 hours, no significant differences were seen between the control group and either HA group.

At 48 hours, a dose dependent response was seen for both PA and ZA in the control samples. The same trend was seen when PA and ZA were incubated with a HA disc for 72 hours prior to the experiment. This trend was not apparent when granules were used to bind BPs. All values appear similar, though with higher variation. When treated with 20 μM ZA, HA granules led to a significantly higher level of metabolic activity, indicating the HA granules were reducing the level of BP toxicity.

After 72 hours, in the control group a dose dependent toxicity response was seen for both PA and ZA, with both drugs reducing metabolic activity. This was the same in the disc group. HA granules inhibited this reduction, though variation was again high, and no significant differences were seen between any HA granules treated groups and their corresponding control groups.

Hydroxyapatite granules prevent bisphosphonate toxicity in vitro

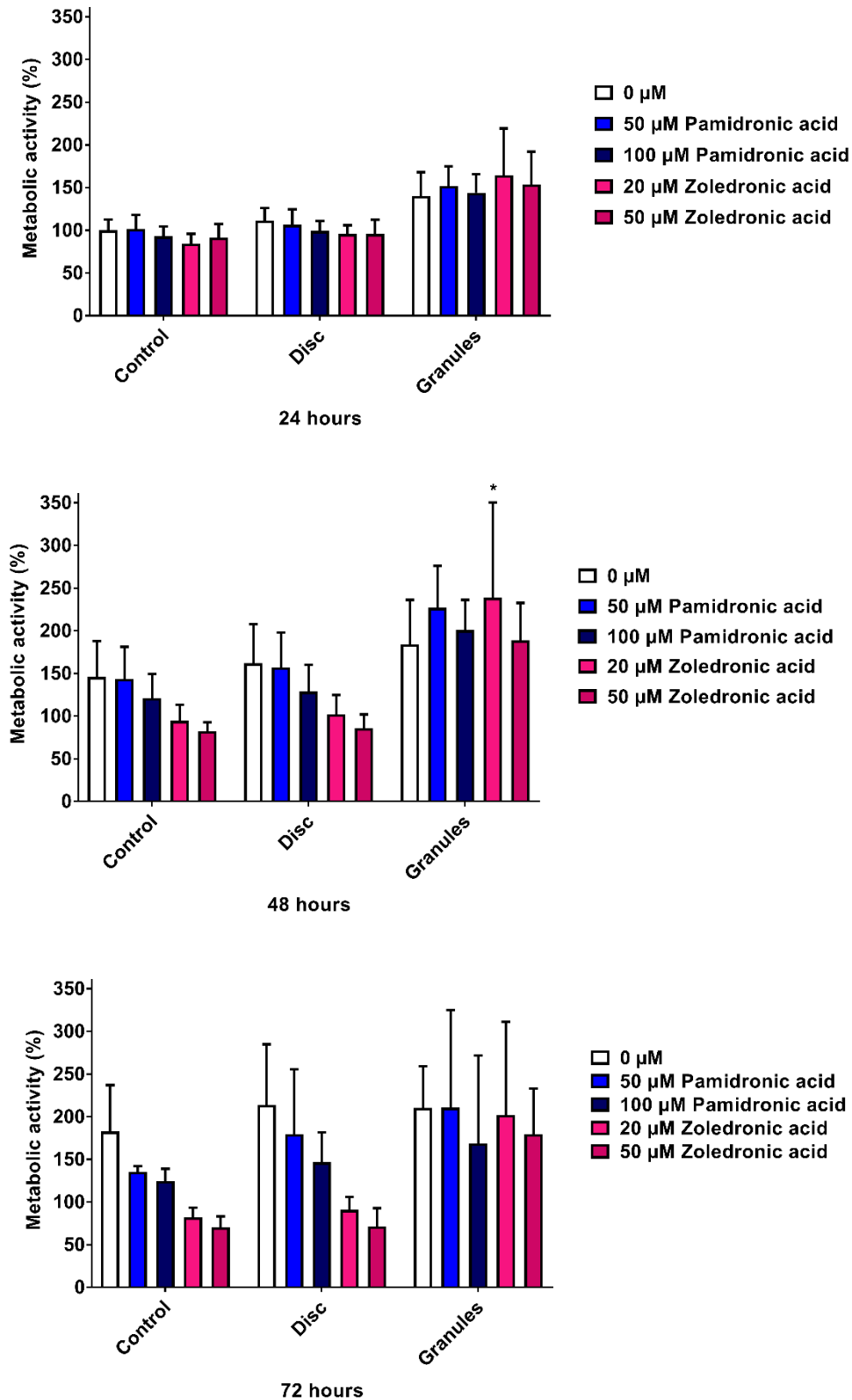


Figure 7.12. Immortalised human oral keratinocyte metabolic activity over 72 hours in the presence of pamidronic acid and zoledronic acid, incubated prior for 72 hours with hydroxyapatite in sintered disc or granule form. Media incubated with no hydroxyapatite used as a control. Values normalised to control cells at 24 hours. $N=3$, $n=3$. Error bars = SD. Significance against control at each time point indicated by $*P \leq 0.05$.

7.4.11 Hydroxyapatite granules prevented zoledronic acid toxicity to oral mucosa models

To assess HA inhibition of BP toxicity in a more representative model, oral mucosa models were raised to ALI and cultured for 7 days. At this time point, a resazurin assay was performed to measure metabolic activity. A HA disc or an equal weight of HA granules were placed below the stainless steel grid, and models were treated with control medium or 30 μ M ZA for 7 days. This concentration was chosen as it caused the greatest reduction in metabolic activity in chapter 6. Models with no HA below the grid were used as controls.

Figure 7.13 demonstrates the effect of HA granules on ZA toxicity, normalised to the day 7 values. With no HA, model metabolic activity was approximately 100 % at day 10 when treated with control medium, while 30 μ M ZA approximately halved this. When cultured in the presence of a HA disc, the same trend was seen, with no significant differences to the control group. When cultured with HA granules, the metabolic activity of both the untreated and treated cells was approximately the same. However, no significant differences were seen compared to the control group.

At day 14, metabolic activity of the control models remained at approximately 100 %. Treatment with 30 μ M ZA reduced metabolic activity to less than 5 %. This was again the case when cultured in the presence of a HA disc. HA granules prevented the toxicity of 30 μ M ZA, with metabolic activity of around 100 % for models cultured in ZA, a significant increase compared to the control group. No significant difference was seen between the untreated models of the control group and granules group, indicating the HA itself caused no effect on metabolic activity when placed in direct contact with the models.

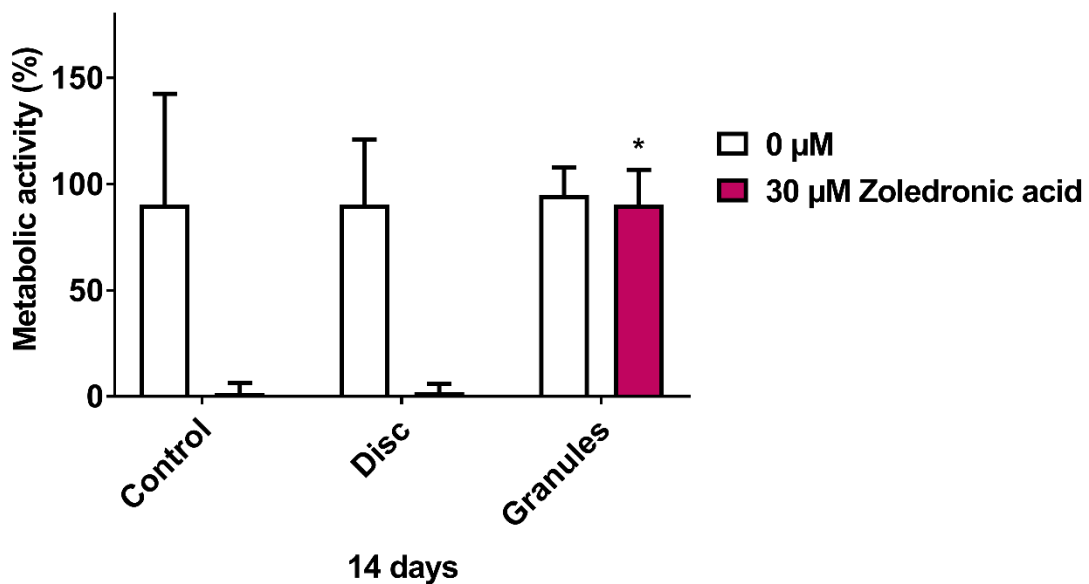
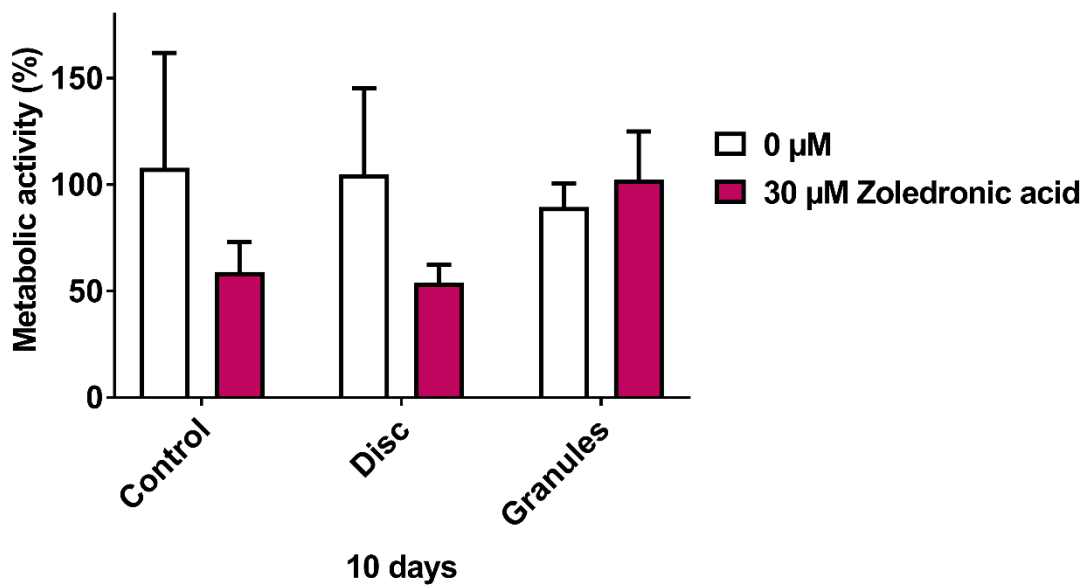


Figure 7.13. Metabolic activity of immortalised keratinocyte oral mucosa models when treated with control medium or 30 μM zoledronic acid, in the presence of a sintered hydroxyapatite disc or granules, after first culturing at ALI in control medium for 7 days. Models cultured with no HA present as controls. Metabolic activity measured with a resazurin assay. Blank well reading subtracted from values before normalising to day 7 values for each model. Day 7 not shown as all values 100 %. $N=3$, $n=2$. Error bars = SD. Statistical significance against control at each time point indicated by $*P\leq 0.05$.

Histological sections from day 14 are shown in Figure 7.14. When treated with control medium from day 7 to day 14, as before, a multi-layered epithelium was visible across the whole model and can be seen in Figure 7.14A. This was also the case when HA was added to the well, both in disc or granule form, with a stratified epithelium present in both Figure 7.14B and Figure 7.14C.

When treated with 30 μM ZA, as before, no epithelium was present on the model, as shown in Figure 7.14D. This was also the case when a disc was present, in Figure 7.14E. However, when treated with 30 μM ZA in the presence of HA granules, a full stratified epithelium was present across the sample, as shown in Figure 7.14F, though with slight disruptions to the outer layer.

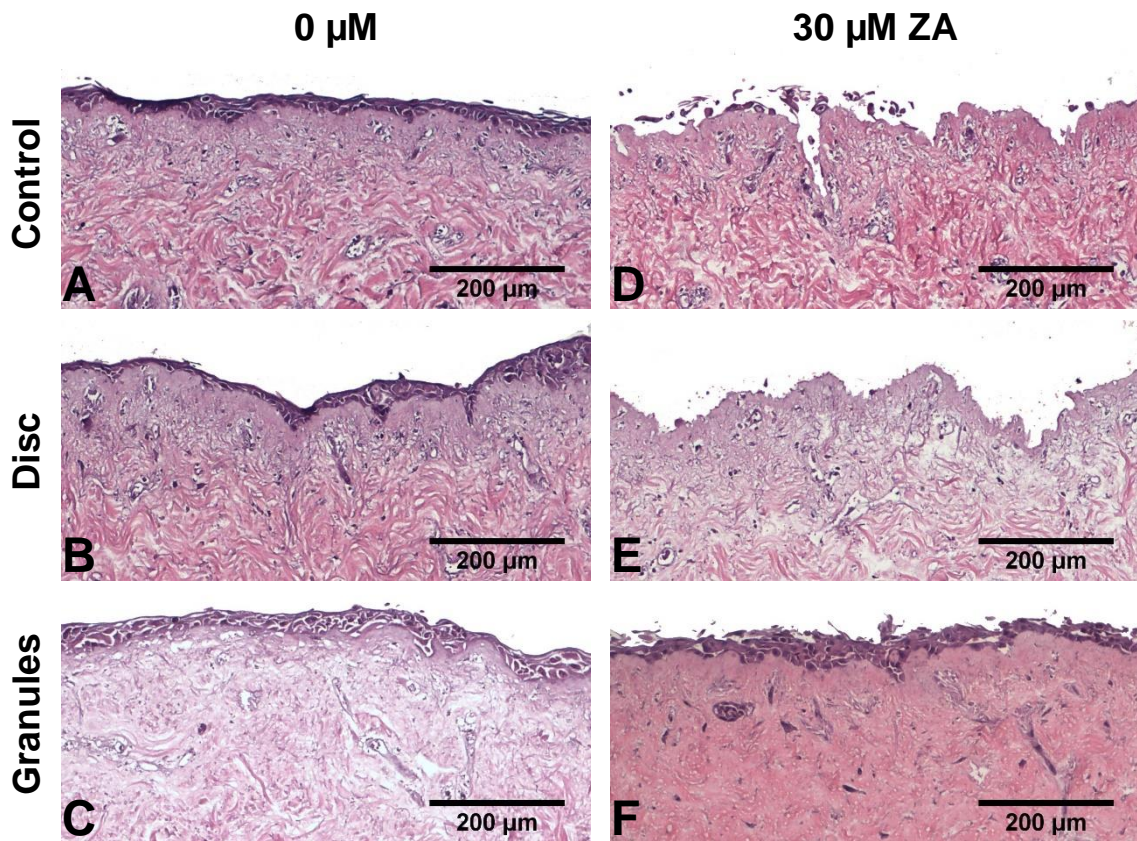


Figure 7.14. H&E stained sections of oral mucosa models seeded with human oral fibroblasts and primary human oral keratinocytes cultured at ALI for 7 days in control medium, then treated with (A) control medium, (B) control medium and a sintered HA disc, (C) control medium and HA granules, (D) 30 μ M zoledronic acid, (E) 30 μ M zoledronic acid and a sintered HA disc, (F) 30 μ M zoledronic acid and HA granules, respectively, for 7 days, with a full media changing occurring at day 3 and day 10. Representative images used.

7.4.12 BP binding was affected by HA surface area

As discs consistently showed no effect in the biological assays, we further examined how HA surface area affected the BP binding ability of HA. Lower weights of granules were incubated in 100 μM PA for 72 hours, before fibroblast cells were treated with this medium. Figure 7.15 shows a calibration curve for granule weight, in comparison to a sintered disc, and metabolic activity, normalised to the metabolic activity of 100 % weight of granules (0.65 g). Increasing weight of granules caused an exponential increase in metabolic activity, with 20 % weight of granules leading to a metabolic activity of less than 10 %, and 50 % weight of granules leading to a metabolic activity of approximately 20 %.

When 100 μM PA was previously incubated for 72 hours with a disc, metabolic activity was approximately 5 % compared to an equal weight of granules. This metabolic activity value was converted using the calibration curve, and suggested a binding ability of approximately 17 %, less than the 45 % expected from the BET data.

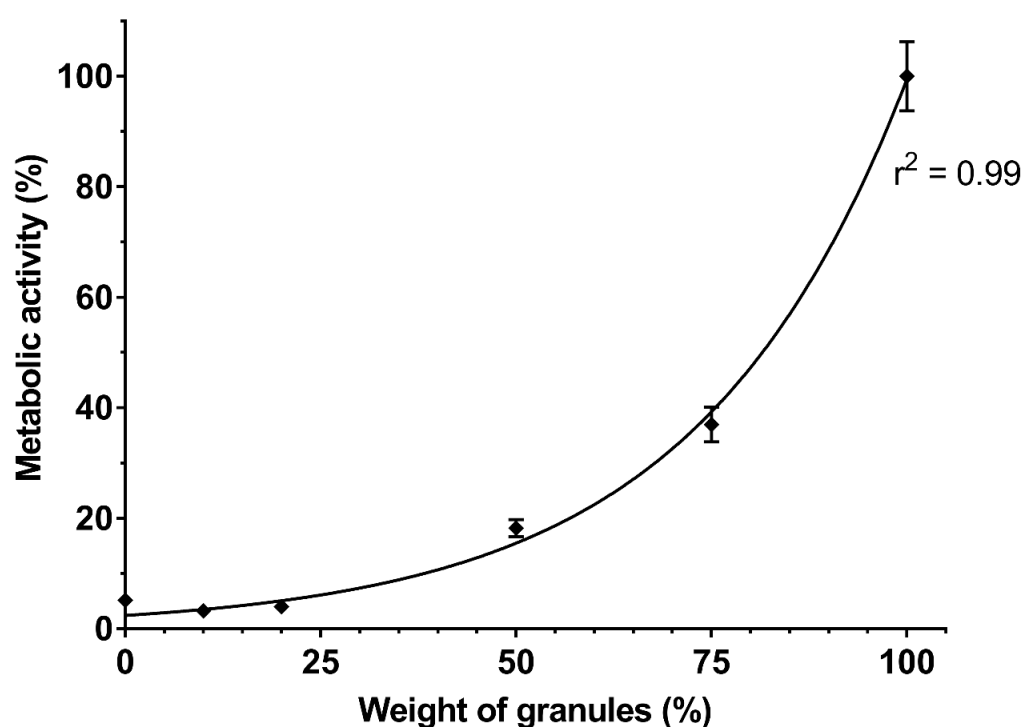


Figure 7.15. Human oral fibroblast metabolic activity after 72 hours in the presence of 100 μM pamidronic acid previously incubated for 72 hours with hydroxyapatite granules. Values normalised to 0.65 g of granules. $N=1$, $n=3$. Error bars = SD. Exponential growth curve fitted.

7.5 Discussion

This chapter has examined the ability of two forms of HA to bind BPs, both commercially available HA granules, and HA powder pressed into discs and sintered. When sintered for 2 hours at 1200 °C, HA did not decompose and remained phase pure. All peaks visible in the XRD spectrum were indexed to HA, with analysis suggesting the discs were made of pure HA. The sintering conditions used were those used by Muralithran and Ramesh, who also found the same result [310]. When sintered above 1200 °C, OH groups in the HA are eliminated due to the HA becoming unstable, through this process TCP is formed [311]. In terms of BP binding properties, it has been demonstrated that the surface Ca:P ratio of calcium phosphates helps define binding properties, with higher calcium increasing binding [52]. Maintaining phase purity is therefore important, as TCP has a lower Ca:P ratio (1.5) than HA (1.67) [312].

In order to examine the BP binding properties of HA, the ability to detect either BP concentration or a quantifiable chemical change to the HA is required. Here we have shown UV-vis spectroscopy alone can be used to detect ZA at concentrations relevant to BRONJ patients. This is the first time ZA concentration has been determined through this method. While UV-vis spectroscopy alone has been used to detect other BPs [265], [266], previous detection of ZA with UV-vis has followed complex HPLC separation methods [273], [275], [283], [284], [287].

Determination of PA was not possible by UV-vis spectroscopy alone as the absorbance was not high enough at the concentrations of interest. Previously, several methods have been performed to detect PA, including a ninhydrin assay, ion-pair HPLC, HPLC with light scattering detection, and a fluorescent assay using carbon dots [273], [274], [277], [281]. These methods should theoretically allow for detection of PA within the concentrations used in this project, however all came with issues that took them outside of the scope of this project. Ninhydrin assays were attempted though required too high a volume of PA to be feasible over long periods. Both HPLC methods were too complex and costly to perform. Though the carbon dot method used is cheap, can also detect zoledronic acid, and was tested with interference from calcium ions, this is a novel method and would require optimisation. For these reasons, the chemical binding experiments were done with ZA alone.

UV detection could not be used to assess the BP binding ability of unsintered HA, due to HA interference. While HA does not have an absorbance peak between 200 and 230 nm, it is known to absorb light of those wavelengths [313], [314]. Using unsintered discs, this caused interference within 24 hours of placing the HA into the solution, even following centrifugation. As such, discs were sintered to convert the powder into a solid mass.

ZA concentration was reduced in the presence of a sintered HA disc over 14 days. The concentration fell rapidly over 24 hours before slowly levelling off. The quick removal of BPs would be highly beneficial for BRONJ patients, potentially preventing the soft tissue from being exposed to BPs entirely. The initial high rate was expected, as binding of ZA has previously been demonstrated at as short a time as 5 minutes [257], and within 24 hours with other BPs [46], [49], [52], [266].

We also saw some ZA released from the HA discs, however due to the interference in the signal it is difficult to conclude much based on this data. In our study, the absorbance peak corresponded to a concentration higher than the amount thought to be bound, indicating the assumed HA signal was contributing to a false reading. Palazzo *et al.* studied the release of alendronic acid bound to nanohydroxyapatite (nHA), and showed only around 20 % of the BP was released [52]. ZA has a similar calcium binding affinity to alendronic acid, as they are two of the highest affinity BPs [42]. High binding affinity BPs are known to have lower desorption rates [45]. Our Raman spectroscopy results also suggest ZA remained bound to the sintered discs following the release study. This indicates the UV-vis release study, which implied that almost all of the previously bound BP was released, may have given a false result due to the HA interference. It may also be that BP binding is dependent on local concentration and placing into fresh water changed the equilibrium and caused release. However, due to the issues with this assay, it was impossible to investigate this effect further.

Sintered discs prevented HA interference to begin with, but over time the absorbance in the region of interest increased, though not to the level of the original powder interference. Our results suggest that there is HA dissolution occurring over the total 24 days of the experiment. This supports what is known about HA dissolution. HA is known to slowly dissolve in distilled water due to an ionic imbalance [315]. The dissolution of HA has been shown to occur as quickly as 15 minutes after being placed in solution when kept at 37 °C [312]. Interestingly, the visibility of a peak and lower variance in Figure 7.7 suggests less HA interference was present in samples containing both ZA and HA. It is known that inorganic pyrophosphate, an analogue of BPs, can delay the dissolution of HA, and this prevention of dissolution contributes to the overall reduction in resorption in bone [31], [316]. Our result suggests that ZA reduces the dissolution of HA over 24 days. Though interesting, the dissolution of HA and therefore the unsuitability of our control in this experiment makes it difficult to draw many strong conclusions about the chemical binding of ZA by HA. As such, methods of detecting changes in the disc before and after ZA incubation were examined.

FTIR-ATR was used to examine the discs after various incubations in ZA and water. This technique requires full contact with the crystal for a good reading with no noise from the atmosphere. When the machine was tightened to ensure contact with the discs,

the brittle nature of the discs caused them to fracture. For this reason, discs were crushed to powder before performing FTIR. No detectable differences were seen by this method, except for a peak in one sample, characteristic of CO₂ and indicating issues with sample contact [317]. Based on previous FTIR studies, ZA peaks corresponding to the aromatic ring were expected at approximately 1500 cm⁻¹ [318], along with stretches to the PO₄³⁻ band at 1000 cm⁻¹ [49]–[51]. These were not visible in our work, which is likely due to the crushing of the discs. High affinity BPs are known to bind to the surface, with low dissolution through the HA [45]. It therefore follows that ZA binding would be at the surface, and through this method little differences should be expected. Therefore a method which did not require the discs to be crushed was performed.

We have demonstrated that it is possible to detect binding of ZA to HA discs using Raman spectroscopy, however not quantifiably. When HA was incubated in ZA, peaks were present at approximately 906, 878, 850, 824 and 740 cm⁻¹. Similar peaks were present when Juillard *et al.* incubated both HA and bone in ZA for 48 hours [286]. While these peak heights were weaker in our release study sample, when incubated with different concentrations of ZA, the peaks did not correlate with concentration. However, due to the issues in measuring BP concentration in liquid, it was impossible to say whether these different concentrations had different binding mechanics. While this offers some use, in order to fully investigate binding mechanics, a more quantifiable method is required. Yet, as previously discussed, these methods are either costly, complex, or newly developed and not optimised, so were outside the scope of this project.

Given the wide range of literature demonstrating the ability of HA and other calcium phosphates to bind BPs [34], [52], [60], [241], [251]–[253], [266], and the suggestion of ZA binding from the UV and Raman studies in our work, we were confident in our hypothesis that HA could be used to reduce local BP concentration. As such, we tested this biologically using assays previously defined in chapters 5 and 6.

We have demonstrated for the first time that HA can be used to reduce toxicity to cells of the oral mucosa, both in 2D with two cell types, and in a 3D model representative of the clinical scenario. This has huge scope to help in the treatment of BRONJ, particularly given there is currently no definitive treatment for the disease [1]. Recent *in vivo* studies have suggested that reduction of the BP concentration to which the oral mucosa is exposed can prevent the development of BRONJ [40], [226], [227], and our work offers a method by which to do that. As HA is currently used in several oral applications relating to BRONJ preceding events [242], our method could be translated to the clinic, following further optimisation.

Several questions must be addressed before granules could be used clinically. For example, when granules are used in oral surgeries, a membrane is normally used to prevent mobilisation [246], [260], which may have an effect both on the exposure of the

granules to BPs and the re-epithelialisation of the oral mucosa. In addition, while the granules may be initially successful in reducing the concentration of BPs, as the jaw regenerates and the granules are resorbed, the bound BPs may be released again. Although the release of BPs through resorption is a normal process in BP patients, the level of BPs released from the granules could potentially be greater than that from bone and this would need to be monitored. It is also unclear as to whether this method could be used in the treatment of already established BRONJ, as there was no bone component including in testing, and reducing BP concentration is unlikely to affect necrotic bone. The well-defined rodent BRONJ model presents an ideal method for investigating this further, following the completion of *in vitro* studies.

HA granules clearly prevented both PA and ZA toxicity to oral fibroblasts and keratinocytes, with concentrations well above the previously defined IC₅₀s leading to metabolic activities similar to those of the non-BP treated cells following incubation in the presence of granules for 72 hours prior to treatment. When immortalised keratinocytes were cultured in medium that had been incubated with HA granules, there was larger variation in the data, particularly in those also treated with PA and ZA. This variation will have contributed to the overall lack of mathematical significance in this data set. It has previously been demonstrated that culturing with HA can inhibit keratinocyte proliferation [319]. It has also been reported that calcium and ZA can have a synergistic effect on keratinocyte viability, with higher cellular calcium increasing the potency of BPs [176]. As such, keratinocytes could have been negatively affected by the HA, which may have contributed to the overall variance in the data. The general trend suggests that HA granules inhibit PA and ZA toxicity to keratinocytes in 2D, however, and therefore this was tested further in an assay more representative of the clinical scenario.

HA granules also reduced toxicity in our 3D mucosa model. This model is much closer to the clinical scenario and supports our hypothesis that HA can be used as a BRONJ preventative treatment. In our study, the models were treated twice, at days 7 and 10. In a long-term BP patient, the local concentration in the mouth is known to spike following receiving a BP dose [142]. Our result indicates that the HA granules would be able to absorb at least one of these dosing spikes. In BRONJ patients, these doses range from monthly to yearly, dependent on BP potency [118]. If BP concentration could be reduced for a month, this would be within the time frame of the full re-epithelialisation of an extraction socket [97]. This mechanism is particularly advantageous due to several calcium phosphate based materials, including the granules used in this study, already being approved and available for clinical use and could be used following the oral surgeries that make up BRONJ-preceding events [242].

When 3D mucosa models were cultured in ZA with HA granules, while an epithelium of full thickness appeared across the model, the top layer appeared disrupted,

similar to an effect seen by Bae *et al.* in their osteomucosal model [202]. The outer layers of the oral mucosa are known to contain more calcium [211]. As previously discussed, ZA and calcium have been shown to have a synergistic relationship [176]. It may be that due to the previously discussed HA dissolution, cellular calcium levels were increasing, causing HA to have a stronger effect on the outer layers of the model. The overall trend, however, was clear, with no effect on metabolic activity and the presence of an epithelium suggesting HA granules can be used to reduce BP toxicity.

The differences in BP binding of the HA discs and granules was in part due to surface area. We have demonstrated that surface area affects BP binding, though the relationship was not linear. Our work indicated that the discs had a surface area of 45 % of the granules, however our metabolic activity data suggested a BP binding ability of only approximately 17 % of an equal weight of granules. Previously, the surface area of HA granules has been demonstrated to affect ZA binding, though again this was not a linear relationship [257]. Further investigations into this are clearly necessary, however, due to the difficulties found in measuring BP binding chemically, this was not possible as part of this thesis.

It is known that high potency BPs mostly bind to the surface of bone, and do not diffuse much into the bone, therefore a surface area effect was expected [45]. PA has previously been demonstrated to cause a surface level binding onto HA through X-ray photoelectron spectroscopy (XPS) analysis [46]. Our results support this and suggest this is also true for ZA. This offers an important consideration for the future of BRONJ treatment. If HA is to be used in the localised reduction of BPs to prevent BRONJ, having a form with a high surface area is likely to be hugely beneficial. The granules used in this study were fairly large, with smaller sizes commercially available, as well as nHA powders and pastes. Investigating this relationship represents a key step in defining a treatment for BRONJ.

7.6 Summary

In summary, we have demonstrated that UV-vis spectroscopy can be used to determine ZA concentration, though not PA. It is not possible, however, to determine ZA binding to HA through this method due to HA interference. We have demonstrated that FTIR-ATR cannot be used to determine HA binding to HA discs, due to sample loading issues. Raman spectroscopy could detect ZA binding, though not quantifiably. Finally, we have demonstrated for the first time that HA granules can be used to reduce BP toxicity to the oral mucosa, *in vitro*, in both 2D and 3D, and retain epithelial stratification, which represents an important step in the development of a preventative treatment for BRONJ.

8. Conclusions

The failure of the soft tissue to heal following oral surgery is hypothesised to be key to the initiation and development of BRONJ [2]. In this thesis, we have demonstrated clear mechanisms by which both PA and ZA, two BPs most commonly associated with BRONJ [153], [163], affect cells of the oral mucosa. We have demonstrated for the first time that PA prevents keratinocyte proliferation, and that ZA reduces keratinocyte adhesion. Clinically relevant concentrations of PA and ZA led to a reduction in both viability and proliferation of fibroblasts and keratinocytes, and in a 3D oral mucosa model caused negative effects in three stages of epithelial development. Our work therefore supports the hypothesis regarding the soft tissue role in BRONJ. Clearly, the BP effects on the oral mucosa are numerous, which indicates why, as of yet, no standardised treatment for BRONJ exists.

In chapters 5 and 6, we looked at the toxicity of PA and ZA, in 2D and 3D, respectively. We performed a methodical examination of BP toxicity to oral fibroblasts and keratinocytes, and calculated IC_{50} values for PA and ZA for these cell types. These values provide a key piece of information on the drugs that was heretofore missing. Due to the soft tissue toxicity associated with BRONJ, it suggests that the oral mucosa is exposed to concentrations at or above those defined in this thesis. There were differences between cytotoxic BP concentration in 2D and 3D. Though similar ZA concentrations caused toxicity to both 2D monolayers and 3D models, models were treated for 7 days while monolayers for 72 hours. PA concentrations higher than the IC_{50} s for all three cell types tested did not lead to toxicity of oral mucosa models. 3D cell culture requires greater cell numbers, and their orientation within the scaffold changes the way tested treatments interact with cells, and therefore differences are expected. 3D cell culture models are known to be more resistant to toxicity than 2D equivalents [320]. The higher concentrations used in 3D were still within the expected dose for BRONJ patient oral mucosa, however [55]–[57], [142], and therefore the prevention of epithelial formation and wound healing, and the reduction in established epithelial thickness seen in chapter 6 indicate why the soft tissue of BRONJ patients does not heal.

We also looked at 2D toxicity in chapter 7. We chose values above the previously defined IC_{50} s, and found slightly different results than those in chapter 5. ZA was less toxic to fibroblasts, and PA to immortalised keratinocytes than we expected based on our earlier work. This highlights the limits of 2D cell culture, where variation can occur over long term projects due to cell passage number and differences in foetal calf serum [321]. Overall, the trends are still clear. PA and ZA cause toxicity to keratinocytes and fibroblasts at clinically relevant concentrations and HA granules can be used to reverse this effect.

The model developed as part of this thesis will, when fully optimised, allow for further investigations into BRONJ treatment methods currently showing potential in the

treatment of the disease, such as GGOH [86], [144], [164], [168], [171] and cell based therapies [237]–[240]. The model would provide a key step between 2D work and the clinic, allowing for the reduction of animal testing in line with the 3Rs [219].

Prevention of BRONJ development is potentially the most effective solution for the disease [1], [40], [159]. We hypothesise that reducing the BP concentration to which the oral mucosa is exposed is the most suitable method by which to do this, as given the multitude of effects caused by BPs, preventing their effects individually would be difficult. The local reduction of BP concentration to prevent BRONJ is the focus of recent literature [40], [227]. We have shown another method by which this can be done, using clinically available materials. We have demonstrated for the first time that HA can be used to reduce BP toxicity to the oral mucosa in both 2D and 3D. The 3D work, in particular, indicates a method to prevent soft tissue toxicity following oral surgery and thereby prevent BRONJ development, while still allowing for the systemic BP effects required for patient quality of life. Further investigations into these materials are clearly warranted, as the potential use of clinically licensed materials to ameliorate a problem with no definitive treatment is highly engaging, and this work could feasibly move towards a clinical trial.

In conclusion, we have demonstrated that both PA and ZA have a wide variety of effects on human oral fibroblasts and keratinocytes *in vitro*, at concentrations well within the expected range for BRONJ patients. This presents a clear picture of how BPs cause the soft tissue toxicity associated with the disease.

We have also begun the development of an *in vitro* approximation of the soft tissue component of BRONJ, in a model that, with more optimisation, could be used further to study both potential BRONJ treatments, and other conditions that present with non-healing epithelia.

We have demonstrated that hydroxyapatite can be used to inhibit BP toxicity to the oral mucosa in 2D and 3D. This is the first time this effect has been demonstrated. This presents a novel strategy for the prevention of BRONJ, and has the advantage that many HA bone filler materials are already licensed for use following many of the dental surgeries that have triggered the development of the disease. However, due to difficulties in the detection of BP binding to HA, we could not confirm this binding chemically. Further work is required to investigate the binding relationship between HA and BPs, and whether other forms of the material could be used to reduce the toxicity further.

9. Future work

This thesis has demonstrated a wide variety of effects of BPs on the oral mucosa and indicated several mechanisms by which soft tissue effects contribute to the development of BRONJ. Clear effects were seen on human oral fibroblasts, keratinocytes, and a 3D oral mucosa model, and methods by which to examine BP effects on the oral mucosa are now well defined. Now these methods are optimised, repeating the 2D work from chapter 5 with primary human oral keratinocytes from a group of different patients would provide valid, more clinically relevant data on BP effects on apoptosis, proliferation, migration and adhesion.

Two interesting pathways for further research were suggested from our 2D data. Firstly, investigating keratinocyte senescence would allow for clarity on the mechanism leading to BP toxicity currently debated in literature [57], [86], [140], [164]. Secondly, the data from our adhesion assay suggested that ZA was causing an effect on integrin binding. Further investigation into the effects of BPs on epithelial adhesion presents an interesting pathway for future work. Well defined assays exist for the detection of integrin binding [82], and a direct assay for this would allow for the confirmation of our hypothesis. This would be a key finding, as BPs had not been shown to affect keratinocyte adhesion before our work. Again, repeating this work with primary cells would also add more clinical relevance. Investigations could also be performed with our 3D models. Desmoglein is known to be affected in BP patients [189], and there may be other potential adhesion pathways. Using immunohistochemistry, it may be possible to gain further information regarding this.

Immunohistochemistry could also provide more information on 3D BP effects in general. While we have demonstrated apoptosis and proliferation effects in 2D, our 3D work was more focussed on developing the *in vitro* representations of BRONJ patient tissue. Now these are defined, confirmation of these effects also appearing in 3D would be useful. This could also help answer the question of how BPs affect the differentiation of keratinocytes, as there is currently no literature consensus [164], [187], [202].

Clearly, our model of the soft tissue of BRONJ requires more development to create consistently thick epithelial sections. Alterations for the seeding process are needed to allow this. Theoretically, producing the rings out of a heavier material would prevent the use of the stainless steel ring as a weight, thereby reducing the fragility of the seeding process. Rather than using a stainless steel grid with large holes that caused the collection of DED and broke the seal, a mesh-like platform would allow the transfer of medium required at ALI but provide a smoother surface. These changes could potentially allow for a highly reproducible seeding method but would require a lengthy design and optimisation process. An alternate solution would be to further reduce the representativeness of the model. Deshayes *et al.* have designed a similar epithelial wound healing model using a

commercially sourced, collagen based dermal compartment and a stainless steel ring to successfully examine drug effects on re-epithelisation [208]. The use of a collagen based dermis allowed for a collagen stain to visualise re-epithelialisation, in the inverse of our work. Though a collagen dermal equivalent is less representative, the thickness and consistency is more repeatable than DED, and may be a useful alternative in the production of a full soft tissue BRONJ model.

Our work focussed on the soft tissue toxicity related to BRONJ, however other mechanisms contribute to its pathophysiology, and adding further complexity to the models could provide key data on BRONJ development. The inclusion of a bone component would provide a full model of the condition, further reducing the need for animal models of the disease. While osteomucosal models exist [201], [202], they are fraught with issues – requiring lengthy seeding or rat calvariae. The optimisation of an experimental treatment regimen with the ability to mimic that found in BRONJ – whereby BPs are bound to bone and left dormant until the creation of a wound – would add further challenges. As infection is known to play a key role in BRONJ development, the introduction of bacterial culture to the BRONJ model could add further details as to how the soft tissue is affected. Models of infected dental tooth tissue have been developed, and could potentially be translated [322]. Adding complexity to this model would provide increased difficulty, however, a fully developed *in vitro* BRONJ model would be a huge leap in the field.

The quantifiable detection of PA and ZA binding to HA is difficult. Though we investigated several techniques, there are others that were outside of the scope of this project. Using fluorescent carbon dots as a sensor has the potential to be a simple, cost effective process and has been tested with the interference of a wide variety of different ions [274], however would require optimisation as it is not a widely used technique. Ion pair HPLC and LC-MS have been used before to detect ZA concentration in systems involving HA and bone, respectively [283], [290]. However these techniques require high specification equipment. BPs modified to be fluorescent have been used to detect BP binding onto calcium phosphates and to determine BP localisation [40], [202]. These BPs are less potent than their non-fluorescent analogues though, and as such make determining the full picture of BP effects difficult. Further investigation into these techniques is evidently required to determine a reproducible way to examine BP binding kinetics both on the bench and *in vitro*. Following this, it would be possible to define the binding properties of calcium-phosphate materials chemically and add clarity to the trends seen biologically in this thesis.

Surface area had an effect on the binding properties of HA. Several different HA based materials exist, all with different surface areas. In the optimisation of a BRONJ treatment method, further investigation into the BP binding affinity of these materials could potentially reveal a material with a greater capacity to inhibit BP toxicity. These tests would

encompass biological assays used previously, tests using the optimised wound model – preferably with a bone component - and a chemical method to confirm binding. Ideally, a treatment regimen to match the clinical scenario would also be used, however, given the difficulties in estimating the concentration of BPs the oral mucosa is exposed to, this may not be possible. These tests would allow for the determination of the ideal amounts of HA to be used, give further indication of how the granules perform over time, and could also investigate how a clinically used membrane would affect bone and soft tissue regeneration. A HA form performing successfully in all these tests would thereby justify its use in an *in vivo* animal model, and going further, a clinical trial in humans.

Our work showed HA has potential as a BRONJ treatment method, however the work was entirely *in vitro*. *In vivo* testing is an important step from the bench to the clinic. As there are several common *in vivo* models of BRONJ, these present a logical step for further examination of the ability of HA to prevent BRONJ development. Though the rodent models are limited in terms of their representation of human bone, their high reproducibility and lower animal welfare concerns, compared to minipigs, offer the most suitable route of testing. These models would allow for the determination of the most suitable application of the granules in this indication and answer questions not able to be answered *in vitro*. As the exact BP concentration to which the oral mucosa is exposed is as yet unknown, as well as the length and release pattern for this exposure, an *in vivo* model would be required to fully assess the suitability of the HA granules in the prevention of BRONJ. These models would also allow for the investigation of longer term effects, such as the clarification of how the resorption of granules which had previously bound HA would affect the soft tissue above them. Following successful animal studies and the determination of the method of administration, a clinical trial in humans using HA as an adjunctive treatment following oral surgery in patients receiving BPs would be feasible.

10. Appendices

10.1 Appendix 1 - Cell seeding densities

Human oral fibroblasts and immortalised human oral keratinocytes were seeded at different densities before culturing for 72 hours in control medium, with cell confluence recorded every 24 hours.

Fibroblast confluence is shown in Figure 10.1. For the apoptosis and necrosis, and proliferation assays, cell confluence was required at 72 hours, and therefore seeding density of 5.55×10^3 cells per cm^2 was chosen. While confluence was also required at 72 hours for the MTT assay, due to the low signal from these cells, a seeding density of 1.0×10^4 cells per cm^2 was chosen. For the migration assay, confluence was required at 24 hours and therefore a seeding density of 5.4×10^4 cells per cm^2 was chosen.

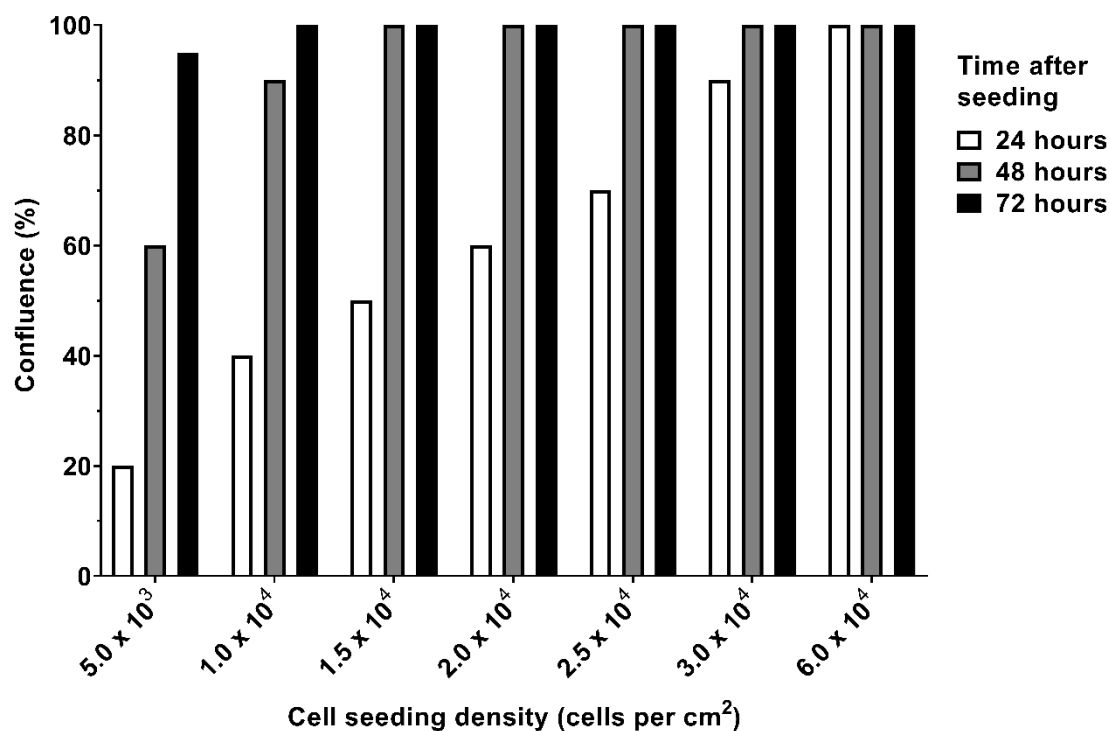


Figure 10.1. Human oral fibroblast confluence over 72 hours at different seeding densities.

Keratinocyte confluence is shown in Figure 10.2. For the MTT, apoptosis and necrosis, and proliferation assays, cell confluence was required at 72 hours, so a seeding density of 1.67×10^4 cells per cm^2 was chosen. One density (1.5×10^4 cells per cm^2) was chosen for both for the adhesion assays and immunohistochemistry, as this was one body of work performed by an MEng student, and this was slightly lower as cells were cultured for up to 120 hours in the immunohistochemistry so required more space for growth. As cell confluence was required at 24 hours for the migration assay, a density of 1.33×10^5 cells per cm^2 was chosen.

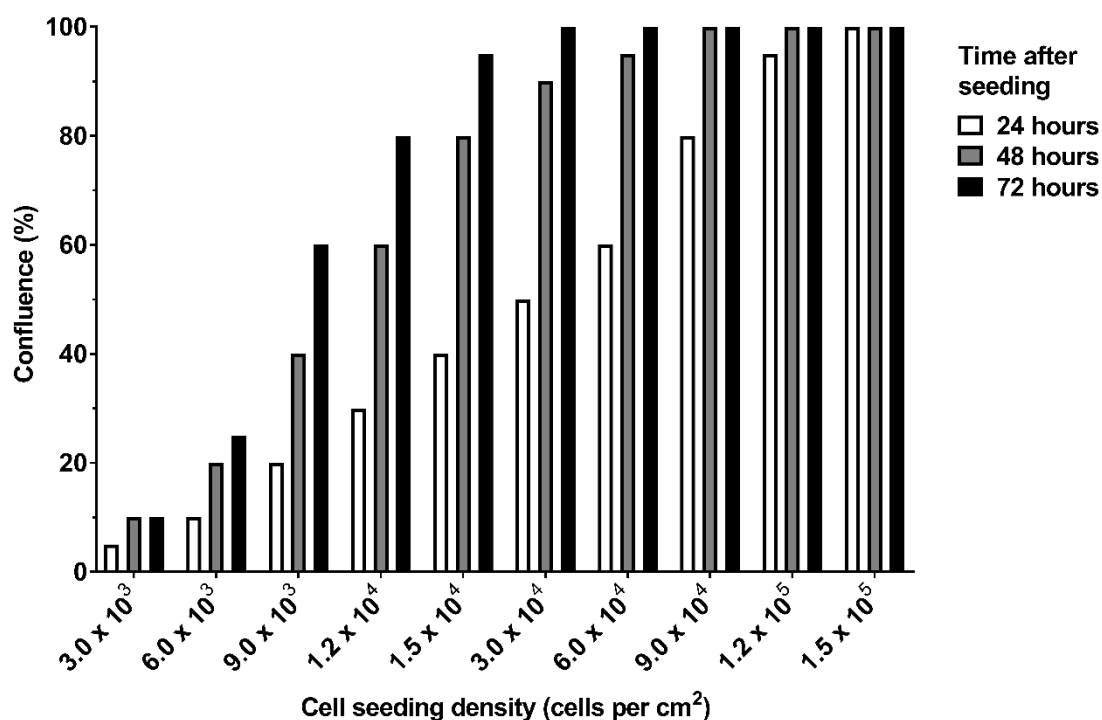


Figure 10.2. Immortalised human oral keratinocyte confluence over 72 hours at different seeding densities.

10.2 Appendix 2 – Migration assay after cell tracing

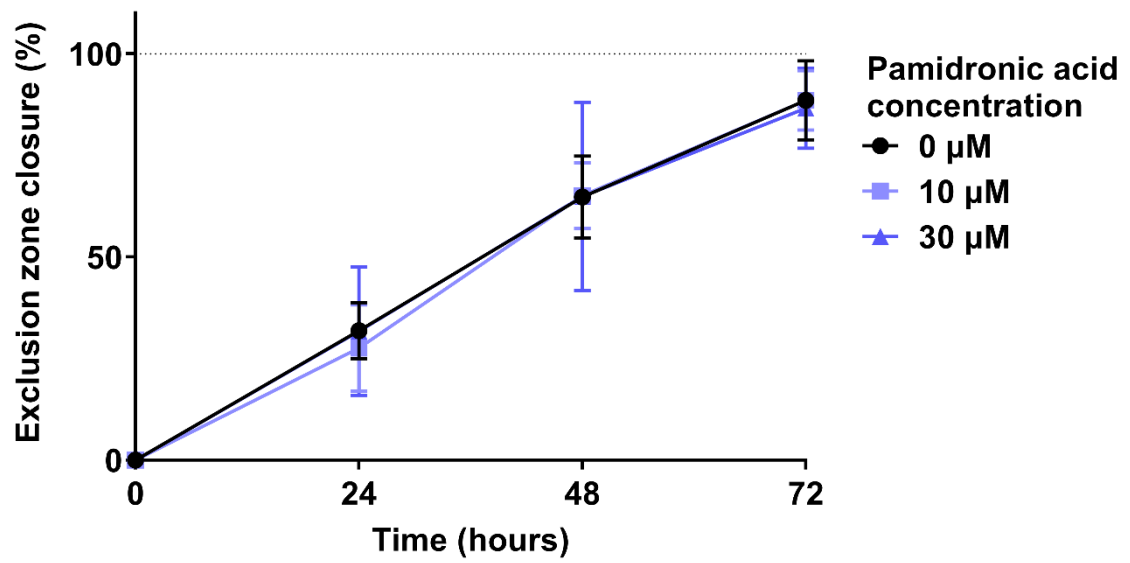


Figure 10.3. Human oral fibroblast migration over 72 hours in the presence of pamidronic acid. $N=3$, $n=3$. Error bars = SD.

10.3 Appendix 3 – Removal of outliers

One outlying value was removed from the MTT data. This value was indicated to be a significant outlier using Grubbs' test for outliers. The equation for this is given in Equation 10.1.

$$G = \frac{|\bar{y} - y|}{n}$$

Equation 10.1. Grubbs' test for outliers.

Grubbs and Beck previously determined critical values for G based on n [323]. For a sample size of 36, $P \leq 0.001$ when $G \leq 3.616$. Figure 10.3 shows the raw data from the assay where an outlier was removed, and the data transformed via Equation 10.1. One value was determined as above the critical limit, and therefore removed.

Raw data

	Pamidronic acid concentration											
	0 μM			10 μM			50 μM			100 μM		
24 hours	0.027	0.033	0.026	0.039	0.033	0.035	0.024	0.029	0.039	0.044	0.038	0.046
48 hours	0.032	0.048	0.051	0.043	0.045	0.043	0.035	0.028	0.037	0.026	0.023	0.025
72 hours	0.045	0.03	0.037	0.043	0.252	0.052	0.017	0.024	0.024	0.006	0.01	0.009

Mean	0.03883	St. dev	0.0383
------	---------	---------	--------

Grubbs' test

	Pamidronic acid concentration											
	0 μM			10 μM			50 μM			100 μM		
24 hours	0.30896	0.1523	0.33507	0.00435	0.1523	0.10009	0.38729	0.25674	0.00435	0.1349	0.02176	0.18712
48 hours	0.17841	0.23933	0.31766	0.10879	0.16101	0.10879	0.10009	0.28285	0.04787	0.33507	0.4134	0.36118
72 hours	0.16101	0.23063	0.04787	0.10879	5.56561	0.34377	0.57005	0.38729	0.38729	0.85725	0.75281	0.77892

Figure 10.4. MTT data for human oral fibroblasts treated with pamidronic acid for 72 hours. Grubbs' test for outliers was performed to indicate outliers. Significant outlier indicated by highlighting in red, $P < 0.001$.

10.4 Appendix 4 – BET isotherms

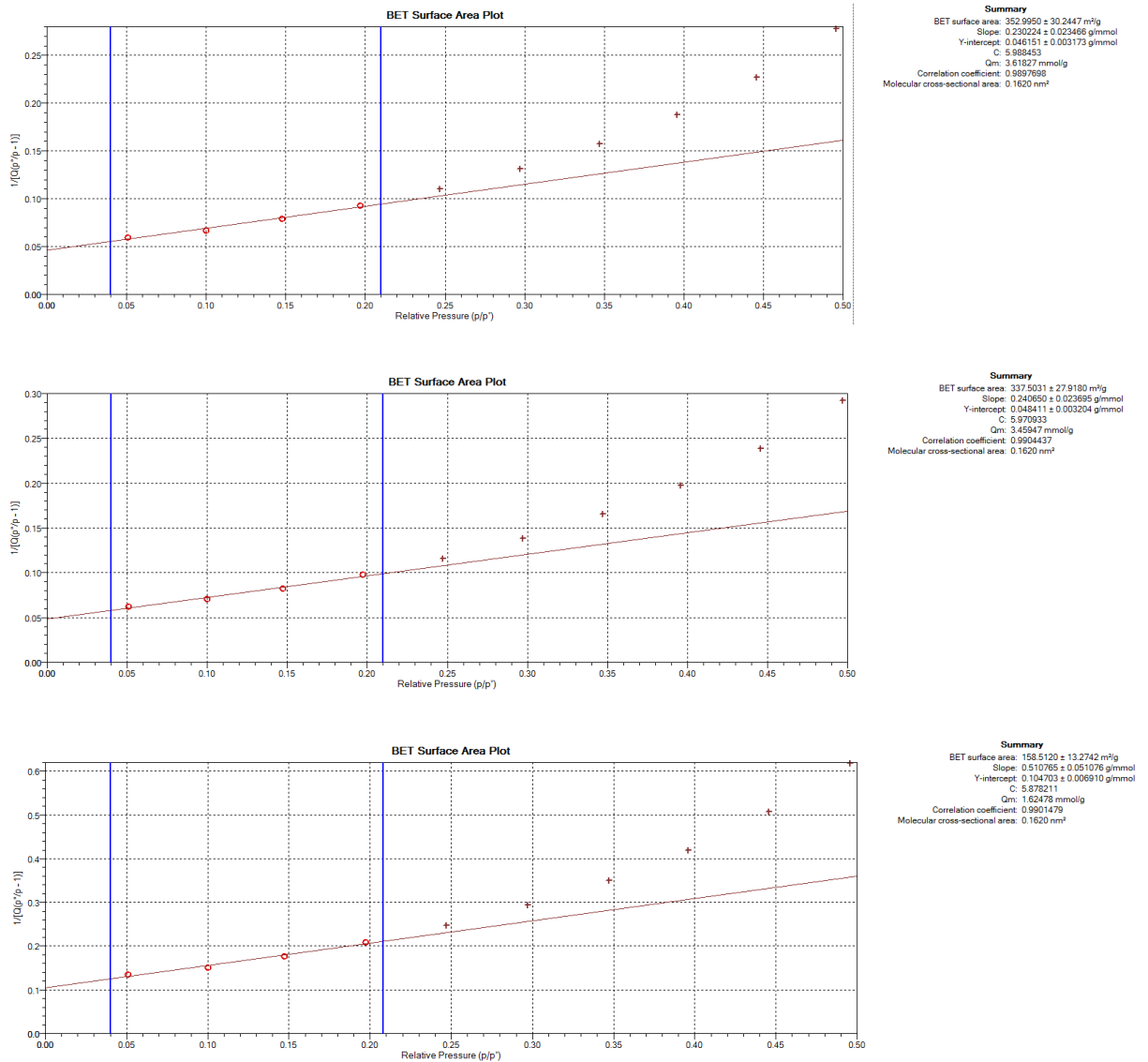


Figure 10.5. Brunauer-Emmett-Teller surface area plots for hydroxyapatite granules, granules and discs, generated by Micrometrics 3Flex.

11. References

- [1] AAOMS, "Medication-Related Osteonecrosis of the Jaw-2014 Update," 2014.
- [2] I. R. Reid, M. J. Bolland, and A. B. Grey, "Is bisphosphonate-associated osteonecrosis of the jaw caused by soft tissue toxicity?," *Bone*, vol. 41, no. 3, Elsevier, pp. 318–320, 01-Sep-2007.
- [3] S. Khosla *et al.*, "Bisphosphonate-associated osteonecrosis of the jaw: report of a task force of the American Society for Bone and Mineral Research.," *J. Bone Miner. Res.*, vol. 22, no. 10, pp. 1479–91, Oct. 2007.
- [4] S.-B. Woo, J. W. Hellstein, and J. R. Kalmar, "Systematic Review: Bisphosphonates and Osteonecrosis of the Jaws.," *Ann. Intern. Med.*, vol. 144, no. 10, pp. 753–761, 2006.
- [5] F. Saad *et al.*, "Incidence, risk factors, and outcomes of osteonecrosis of the jaw: Integrated analysis from three blinded active-controlled phase III trials in cancer patients with bone metastases," *Ann. Oncol.*, vol. 23, no. 5, pp. 1341–1347, May 2012.
- [6] W. J. Boyle, W. S. Simonet, and D. L. Lacey, "Osteoclast differentiation and activation.," *Nature*, vol. 423, no. 6937, pp. 337–42, May 2003.
- [7] A. G. Robling, A. B. Castillo, and C. H. Turner, "BIOMECHANICAL AND MOLECULAR REGULATION OF BONE REMODELING," *Annu. Rev. Biomed. Eng.*, no. 8, pp. 455–98, Jul. 2006.
- [8] M. Zaidi, "Skeletal remodeling in health and disease.," *Nat. Med.*, vol. 13, no. 7, pp. 791–801, Jul. 2007.
- [9] K. S. Saladin, *Human Anatomy*, 2nd ed. McGra-Hill, 2008.
- [10] S. L. Teitelbaum, "Bone Resorption by Osteoclasts," *Science (80-.)*, vol. 289, no. 5484, pp. 1504–1508, Sep. 2000.
- [11] G. D. Roodman, "Mechanisms of bone metastasis.," *N. Engl. J. Med.*, vol. 360, no. 16, pp. 1655–1664, 2004.
- [12] B. F. Boyce and L. Xing, "Functions of RANKL/RANK/OPG in bone modeling and remodeling.," *Arch. Biochem. Biophys.*, vol. 473, no. 2, pp. 139–46, May 2008.
- [13] J. O. Hollinger, T. A. Einhorn, B. A. Doll, and C. Sfeir, *Bone Tissue Engineering*. CRC Press, 2004.
- [14] D. R. Poroca, R. M. Pelis, and V. M. Chappe, "ClC Channels and Transporters: Structure, Physiological Functions, and Implications in Human Chloride Channelopathies," *Front. Pharmacol.*, vol. 8, p. 151, Mar. 2017.
- [15] P. Sambrook and C. Cooper, "Osteoporosis.," *Lancet (London, England)*, vol. 367, no. 9527, pp. 2010–8, Jun. 2006.
- [16] M. T. Drake, B. L. Clarke, and E. M. Lewiecki, "The Pathophysiology and Treatment of Osteoporosis.," *Clin. Ther.*, vol. 37, no. 8, pp. 1837–1850, Jul. 2015.
- [17] R. Morello, "Osteogenesis imperfecta and therapeutics," *Matrix Biol.*, vol. 71–72, pp. 294–312, Oct. 2018.
- [18] F. Rauch and F. H. Glorieux, "Osteogenesis imperfecta," *Lancet*, vol. 363, no. 9418, pp. 1377–1385, Apr. 2004.
- [19] A. G. Feehan, M. R. Zacharin, A. S. Lim, and P. J. Simm, "A comparative study of quality of life, functional and bone outcomes in osteogenesis imperfecta with bisphosphonate therapy initiated in childhood or adulthood," *Bone*, vol. 113, pp. 137–143, Aug. 2018.
- [20] T. Cundy, "Paget's disease of bone," *Metabolism*, vol. 80, pp. 5–14, Mar. 2018.
- [21] I. Kravets, "Paget's Disease of Bone: Diagnosis and Treatment," *Am. J. Med.*, vol. 131, no. 11, pp. 1298–1303, Nov. 2018.
- [22] A. Tan and S. H. Ralston, "Clinical Presentation of Paget's Disease: Evaluation of a Contemporary Cohort and Systematic Review," *Calcif. Tissue Int.*, vol. 95, no. 5, pp. 385–392, Nov. 2014.
- [23] C. L. Chaffer and R. A. Weinberg, "A perspective on cancer cell metastasis.,"

- Science*, vol. 331, no. 6024, pp. 1559–64, Mar. 2011.
- [24] R. E. Coleman, “Skeletal complications of malignancy.,” *Cancer*, vol. 80, no. 8 Suppl, pp. 1588–94, Oct. 1997.
- [25] R. E. Coleman and R. D. Rubens, “The clinical course of bone metastases from breast cancer.,” *Br. J. Cancer*, vol. 55, no. 1, pp. 61–6, Jan. 1987.
- [26] R. E. Coleman, “Metastatic bone disease: clinical features, pathophysiology and treatment strategies,” *Cancer Treat. Rev.*, vol. 27, no. 3, pp. 165–176, Jun. 2001.
- [27] G. R. Mundy, “Metastasis to bone: causes, consequences and therapeutic opportunities.,” *Nat. Rev. Cancer*, vol. 2, no. 8, pp. 584–93, Aug. 2002.
- [28] S. Kachbi Khelfallah, M. Monteil, J. Deschamp, O. Gager, E. Migianu-Griffoni, and M. Lecouvey, “Synthesis of novel polymerizable molecules bearing bisphosphonate,” *Org. Biomol. Chem.*, vol. 13, no. 46, pp. 11382–11392, Nov. 2015.
- [29] M. T. Drake, B. L. Clarke, and S. Khosla, “Bisphosphonates: mechanism of action and role in clinical practice.,” *Mayo Clin. Proc.*, vol. 83, no. 9, pp. 1032–45, Sep. 2008.
- [30] S.-H. Lee *et al.*, “Use of bisphosphonates and the risk of osteonecrosis among cancer patients: a systemic review and meta-analysis of the observational studies.,” *Support. Care Cancer*, vol. 22, no. 2, pp. 553–60, Feb. 2014.
- [31] R. G. G. Russell, “Bisphosphonates: from bench to bedside.,” *Ann. N. Y. Acad. Sci.*, vol. 1068, pp. 367–401, Apr. 2006.
- [32] J. Compston *et al.*, “Diagnosis and management of osteoporosis in postmenopausal women and older men in the UK: National Osteoporosis Guideline Group (NOGG) update 2013,” *Maturitas*, vol. 75, no. 4, pp. 392–396, Aug. 2013.
- [33] N. B. Watts and D. L. Diab, “Long-Term Use of Bisphosphonates in Osteoporosis,” *J. Clin. Endocrinol. Metab.*, vol. 95, no. 4, pp. 1555–1565, Apr. 2010.
- [34] G. F. Draenert, D. O. Huetzen, P. W. Kämmerer, V. Palarie, V. Nacu, and W. Wagner, “Dexrazoxane shows cytoprotective effects in zoledronic acid-treated human cells in vitro and in the rabbit tibia model in vivo.,” *J. Craniomaxillofac. Surg.*, vol. 40, no. 8, pp. e369-74, Dec. 2012.
- [35] M. J. Ravosa, J. Ning, Y. Liu, and M. S. Stack, “Bisphosphonate effects on the behaviour of oral epithelial cells and oral fibroblasts,” *Arch. Oral Biol.*, vol. 56, no. 5, pp. 491–498, 2011.
- [36] L. Cheng *et al.*, “Persistence and Compliance with Osteoporosis Therapies Among Women in a Commercially Insured Population in the United States.,” *J. Manag. Care Spec. Pharm.*, vol. 21, no. 9, pp. 824–33, 2015.
- [37] D. M. Black, D. C. Bauer, A. V. Schwartz, S. R. Cummings, and C. J. Rosen, “Continuing Bisphosphonate Treatment for Osteoporosis - for whom and for how long?,” *N. Engl. J. Med.*, vol. 366, no. 22, pp. 2051–2053, 2012.
- [38] S. C. Kim *et al.*, “Impact of the U.S. Food and Drug Administration’s Safety-Related Announcements on the Use of Bisphosphonates After Hip Fracture,” *J. Bone Miner. Res.*, vol. 31, no. 8, pp. 1536–1540, Aug. 2016.
- [39] S. Khosla and E. Shane, “A Crisis in the Treatment of Osteoporosis,” *J. Bone Miner. Res.*, vol. 31, no. 8, pp. 1485–1487, Aug. 2016.
- [40] R. Elsayed *et al.*, “Removal of matrix-bound zoledronate prevents post-extraction osteonecrosis of the jaw by rescuing osteoclast function,” *Bone*, vol. 110, pp. 141–149, May 2018.
- [41] B. Balkhi, E. Seoane-Vazquez, and R. Rodriguez-Monguio, “Changes in the utilization of osteoporosis drugs after the 2010 FDA bisphosphonate drug safety communication,” *Saudi Pharm. J.*, vol. 26, no. 2, pp. 238–243, Feb. 2018.
- [42] F. H. Ebetino *et al.*, “The relationship between the chemistry and biological activity of the bisphosphonates.,” *Bone*, vol. 49, no. 1, pp. 20–33, Jul. 2011.
- [43] R. E. Marx, “Pamidronate (Aredia) and zoledronate (Zometa) induced avascular necrosis of the jaws: a growing epidemic,” *J. Oral Maxillofac. Surg.*, vol. 61, no. 9, pp. 1115–1117, Sep. 2003.

- [44] P. G. de B. Silva *et al.*, "Effect of different doses of zoledronic acid in establishing of bisphosphonate-related osteonecrosis.," *Arch. Oral Biol.*, vol. 60, no. 9, pp. 1237–45, Sep. 2015.
- [45] G. H. Nancollas *et al.*, "Novel insights into actions of bisphosphonates on bone: differences in interactions with hydroxyapatite.," *Bone*, vol. 38, no. 5, pp. 617–27, May 2006.
- [46] K. McLeod *et al.*, "XPS and bioactivity study of the bisphosphonate pamidronate adsorbed onto plasma sprayed hydroxyapatite coatings," *Appl. Surf. Sci.*, vol. 253, no. 5, pp. 2644–2651, Dec. 2006.
- [47] T. Ikebe, "Pathophysiology of BRONJ: Drug-related osteoclastic disease of the jaw," *Oral Sci. Int.*, vol. 10, no. 1, pp. 1–8, Jan. 2013.
- [48] S. Paulo *et al.*, "Bisphosphonate-related osteonecrosis of the jaw: specificities.," *Oncol. Rev.*, vol. 8, no. 2, p. 254, Sep. 2014.
- [49] P. Pascaud, P. Gras, Y. Coppel, C. Rey, and S. Sarda, "Interaction between a bisphosphonate, tiludronate, and biomimetic nanocrystalline apatites.," *Langmuir*, vol. 29, no. 7, pp. 2224–32, Feb. 2013.
- [50] T. Gong *et al.*, "Preparation, characterization, release kinetics, and in vitro cytotoxicity of calcium silicate cement as a risedronate delivery system.," *J. Biomed. Mater. Res. A*, vol. 102, no. 7, pp. 2295–304, Jul. 2014.
- [51] R. Bosco, M. Iafisco, A. Tampieri, J. A. Jansen, S. C. G. Leeuwenburgh, and J. J. P. van den Beucken, "Hydroxyapatite nanocrystals functionalized with alendronate as bioactive components for bone implant coatings to decrease osteoclastic activity," *Appl. Surf. Sci.*, vol. 328, pp. 516–524, Feb. 2015.
- [52] B. Palazzo *et al.*, "Biomimetic Hydroxyapatite–Drug Nanocrystals as Potential Bone Substitutes with Antitumor Drug Delivery Properties," *Adv. Funct. Mater.*, vol. 17, no. 13, pp. 2180–2188, Sep. 2007.
- [53] M. Mozzati *et al.*, "Oral mucosa produces cytokines and factors influencing osteoclast activity and endothelial cell proliferation, in patients with osteonecrosis of jaw after treatment with zoledronic acid.," *Clin. Oral Investig.*, vol. 17, no. 4, pp. 1259–66, May 2013.
- [54] T. Chen *et al.*, "Pharmacokinetics and Pharmacodynamics of Zoledronic Acid in Cancer Patients with Bone Metastases," *J. Clin. Pharmacol.*, vol. 42, no. 11, pp. 1228–1236, Nov. 2002.
- [55] Y. Komatsu *et al.*, "Zoledronic acid suppresses transforming growth factor-induced fibrogenesis by human gingival fibroblasts," *Int. J. Mol. Med.*, vol. 38, no. 1, pp. 139–147, Jul. 2016.
- [56] D. Marolt, M. Cozin, G. Vunjak-Novakovic, S. Cremers, and R. Landesberg, "Effects of pamidronate on human alveolar osteoblasts in vitro.," *J. Oral Maxillofac. Surg.*, vol. 70, no. 5, pp. 1081–92, May 2012.
- [57] R. Landesberg *et al.*, "Inhibition of Oral Mucosal Cell Wound Healing by Bisphosphonates," *J. Oral Maxillofac. Surg.*, vol. 66, no. 5, pp. 839–847, 2008.
- [58] R. C. Boff, F. G. Salum, M. A. Figueiredo, and K. Cherubini, "Important aspects regarding the role of microorganisms in bisphosphonate-related osteonecrosis of the jaws.," *Arch. Oral Biol.*, vol. 59, no. 8, pp. 790–9, Aug. 2014.
- [59] M. Sato *et al.*, "Bisphosphonate action. Alendronate localization in rat bone and effects on osteoclast ultrastructure.," *J. Clin. Invest.*, vol. 88, no. 6, pp. 2095–105, Dec. 1991.
- [60] H.-C. Kim *et al.*, "Combined effect of bisphosphonate and recombinant human bone morphogenetic protein 2 on bone healing of rat calvarial defects.," *Maxillofac. Plast. Reconstr. Surg.*, vol. 37, no. 1, p. 16, Dec. 2015.
- [61] D. Gatti, M. Rossini, O. Viapiana, L. Idolazzi, and S. Adami, "Clinical development of neridronate: potential for new applications.," *Ther. Clin. Risk Manag.*, vol. 9, pp. 139–47, Jan. 2013.
- [62] M. J. Rogers *et al.*, "Cellular and molecular mechanisms of action of bisphosphonates.," *Cancer*, vol. 88, no. 12 Suppl, pp. 2961–78, Jun. 2000.

- [63] H. . Benford, N. W. . McGowan, M. . Helfrich, M. . Nuttall, and M. . Rogers, "Visualization of bisphosphonate-induced caspase-3 activity in apoptotic osteoclasts in vitro," *Bone*, vol. 28, no. 5, pp. 465–473, May 2001.
- [64] R. Schenk, P. Egli, H. Fleisch, and S. Rosini, "Quantitative morphometric evaluation of the inhibitory activity of new aminobisphosphonates on bone resorption in the rat.," *Calcif. Tissue Int.*, vol. 38, no. 6, pp. 342–349, Jun. 1986.
- [65] B. E. Hillner *et al.*, "American Society of Clinical Oncology Guideline on the Role of Bisphosphonates in Breast Cancer," *J. Clin. Oncol.*, vol. 18, no. 6, pp. 1378–1391, Mar. 2000.
- [66] F. J. Manzano-Moreno, J. Ramos-Torrecillas, E. De Luna-Bertos, C. Reyes-Botella, C. Ruiz, and O. García-Martínez, "Nitrogen-containing bisphosphonates modulate the antigenic profile and inhibit the maturation and biomineralization potential of osteoblast-like cells.," *Clin. Oral Investig.*, vol. 19, no. 4, pp. 895–902, May 2015.
- [67] F. J. Manzano-Moreno, J. Ramos-Torrecillas, L. Melguizo-Rodríguez, R. Illescas-Montes, C. Ruiz, and O. García-Martínez, "Bisphosphonate Modulation of the Gene Expression of Different Markers Involved in Osteoblast Physiology: Possible Implications in Bisphosphonate-Related Osteonecrosis of the Jaw," *Int. J. Med. Sci.*, vol. 15, no. 4, pp. 359–367, 2018.
- [68] J.-B. Park, S.-H. Cho, I. Kim, W. Lee, S.-H. Kang, and H. Kim, "Evaluation of the bisphosphonate effect on stem cells derived from jaw bone and long bone rabbit models: A pilot study," *Arch. Oral Biol.*, vol. 85, pp. 178–182, Jan. 2018.
- [69] H. Hagino *et al.*, "Three years of treatment with minodronate in patients with postmenopausal osteoporosis.," *J. Bone Miner. Metab.*, vol. 30, no. 4, pp. 439–46, Jul. 2012.
- [70] M. R. McClung *et al.*, "Effect of risedronate on the risk of hip fracture in elderly women. Hip Intervention Program Study Group.," *N. Engl. J. Med.*, vol. 344, no. 5, pp. 333–40, Feb. 2001.
- [71] A. Cranney, G. Guyatt, L. Griffith, G. Wells, P. Tugwell, and C. Rosen, "Meta-analyses of therapies for postmenopausal osteoporosis. IX: Summary of meta-analyses of therapies for postmenopausal osteoporosis.," *Endocr. Rev.*, vol. 23, no. 4, pp. 570–8, Aug. 2002.
- [72] D. M. Black *et al.*, "Randomised trial of effect of alendronate on risk of fracture in women with existing vertebral fractures," *Lancet*, vol. 348, no. 9041, pp. 1535–1541, Dec. 1996.
- [73] Ian R. Reid *et al.*, "Intravenous zoledronic acid in postmenopausal women with low bone mineral density.," *N. Engl. J. Med.*, vol. 346, no. 9, pp. 653–661, 2002.
- [74] P. Roschger *et al.*, "Mineralization density distribution of postmenopausal osteoporotic bone is restored to normal after long-term alendronate treatment: qBEI and sSAXS data from the fracture intervention trial long-term extension (FLEX)," *J. Bone Miner. Res.*, vol. 25, no. 1, pp. 48–55, Jan. 2010.
- [75] D. M. Black *et al.*, "Effects of continuing or stopping alendronate after 5 years of treatment: The Fracture Intervention Trial long-term extension (FLEX): A randomized trial," *J. Am. Med. Assoc.*, vol. 296, no. 24, pp. 2927–2938, Dec. 2006.
- [76] A. L. Boskey *et al.*, "Insights into the bisphosphonate holiday: a preliminary FTIRI study," *Osteoporosis International*, vol. 29, no. 3, Springer London, pp. 1–7, 05-Mar-2017.
- [77] M. Rousseau and J.-M. Retrouvey, "Osteogenesis imperfecta: potential therapeutic approaches," *PeerJ*, vol. 6, p. e5464, Aug. 2018.
- [78] J. R. Berenson *et al.*, "The efficacy of pamidronate in reducing skeletal associated events in patients with advanced multiple myeloma," *N. Engl. J. Med.*, vol. 334, no. 8, pp. 488–493, 1996.
- [79] P. Clézardin, F. H. Ebetino, and P. G. J. Fournier, "Bisphosphonates and cancer-induced bone disease: beyond their antiresorptive activity.," *Cancer Res.*, vol. 65, no. 12, pp. 4971–4, Jun. 2005.
- [80] M. Gnant and P. Clézardin, "Direct and indirect anticancer activity of

- bisphosphonates: a brief review of published literature.," *Cancer Treat. Rev.*, vol. 38, no. 5, pp. 407–15, Aug. 2012.
- [81] I. Holen and R. E. Coleman, "Anti-tumour activity of bisphosphonates in preclinical models of breast cancer," *Breast Cancer Res.*, vol. 12, no. 6, p. 214, Dec. 2010.
- [82] M. Wilke *et al.*, "Zoledronic acid and atorvastatin inhibit $\alpha\beta 3$ -mediated adhesion of breast cancer cells," *J. Bone Oncol.*, vol. 3, no. 1, pp. 10–17, 2014.
- [83] D. Santini *et al.*, "Zoledronic acid induces significant and long-lasting modifications of circulating angiogenic factors in cancer patients," *Clin. Cancer Res.*, vol. 9, no. 8, pp. 2893–2897, Aug. 2003.
- [84] B. Yi, P. J. Williams, M. Niewolna, Y. Wang, and T. Yoneda, "Tumor-derived Platelet-derived Growth Factor-BB Plays a Critical Role in Osteosclerotic Bone Metastasis in an Animal Model of Human Breast Cancer," *Cancer Res.*, vol. 62, no. 3, pp. 917–923, Feb. 2002.
- [85] R. G. G. Russell, "Bisphosphonates: The first 40 years," *Bone*, vol. 49, no. 1, pp. 2–19, 2011.
- [86] A. M. Pabst, M. Krüger, T. Ziebart, C. Jacobs, K. Sagheb, and C. Walter, "The influence of geranylgeraniol on human oral keratinocytes after bisphosphonate treatment: An in vitro study," *J. Cranio-Maxillofacial Surg.*, vol. 43, no. 5, pp. 688–695, Jun. 2015.
- [87] S. Di Lorenzo, A. Trapassi, B. Corradino, and A. Cordova, "Histology of the Oral Mucosa in Patients With BRONJ at III Stage: A Microscopic Study Proves the Unsuitability of Local Mucosal Flaps.," *J. Clin. Med. Res.*, vol. 5, no. 1, pp. 22–5, Feb. 2013.
- [88] C. Squier and K. Brodgen, *Human Oral Mucosa: Development, Structure and Function*, Second. John Wiley & Sons, 1976.
- [89] J. E. Glim, M. van Egmond, F. B. Niessen, V. Everts, and R. H. J. Beelen, "Detrimental dermal wound healing: what can we learn from the oral mucosa?," *Wound Repair Regen.*, vol. 21, no. 5, pp. 648–60, Jan. 2013.
- [90] J. D. Smart, "Lectin-mediated drug delivery in the oral cavity.," *Adv. Drug Deliv. Rev.*, vol. 56, no. 4, pp. 481–9, Mar. 2004.
- [91] A. Nanci, *Ten Cate's Oral Histology*, Eighth Edit. Oxford: Mosby Elsevier, 2013.
- [92] B. K. B. Berkovitz, G. R. Holland, and B. J. Moxham, *Oral Anatomy, Histology and Embryology*, Fourth Edi. Oxford: Mosby Elsevier, 2009.
- [93] A. E. Kalinin, A. V. Kajava, and P. M. Steinert, "Epithelial barrier function: Assembly and structural features of the cornified cell envelope," *BioEssays*, vol. 24, no. 9. pp. 789–800, Sep-2002.
- [94] J. K. Buskermolen *et al.*, "Development of a Full Thickness Human Gingiva Equivalent Constructed from Immortalized Keratinocytes and Fibroblasts.," *Tissue Eng. Part C. Methods*, vol. 22, no. September 2015, pp. 1–33, Aug. 2016.
- [95] V. Hearnden *et al.*, "Diffusion studies of nanometer polymersomes across tissue engineered human oral mucosa," *Pharm. Res.*, vol. 26, no. 7, pp. 1718–1728, Jul. 2009.
- [96] A. Sculean, R. Gruber, and D. D. Bosshardt, "Soft tissue wound healing around teeth and dental implants," *Journal of Clinical Periodontology*, vol. 41. Wiley/Blackwell (10.1111), pp. S6–S22, Apr-2014.
- [97] M. H. Amler, "The time sequence of tissue regeneration in human extraction wounds," *Oral Surgery, Oral Med. Oral Pathol.*, vol. 27, no. 3, pp. 309–318, Mar. 1969.
- [98] C. Politis, J. Schoenaers, R. Jacobs, and J. O. Agbaje, "Wound healing problems in the mouth," *Frontiers in Physiology*, vol. 7, no. NOV. Frontiers Media SA, p. 507, 2016.
- [99] I. Pastar *et al.*, "Epithelialization in Wound Healing: A Comprehensive Review," *Adv. Wound Care*, vol. 3, no. 7, pp. 445–464, Jul. 2014.
- [100] E. Fuchs and D. W. Cleveland, "A structural scaffolding of intermediate filaments in health and disease," *Science*, vol. 279, no. 5350. pp. 514–519, 23-Jan-1998.

- [101] S. Werner and R. Grose, "Regulation of Wound Healing by Growth Factors and Cytokines," *Physiol. Rev.*, vol. 83, no. 3, pp. 835–870, Jul. 2003.
- [102] M. Komine *et al.*, "Inflammatory versus proliferative processes epidermis. Tumor necrosis factor α induces K6b keratin synthesis through a transcriptional complex containing NF κ B and C/EBP β ," *J. Biol. Chem.*, vol. 275, no. 41, pp. 32077–32088, Oct. 2000.
- [103] Y. Sogabe, M. Abe, Y. Yokoyama, and O. Ishikawa, "Basic fibroblast growth factor stimulates human keratinocyte motility by Rac activation," *Wound Repair Regen.*, vol. 14, no. 4, pp. 457–462, Jul. 2006.
- [104] T. T. Meckmongkol, R. Harmon, P. McKeown-Longo, and L. Van De Water, "The fibronectin synergy site modulates TGF- β -dependent fibroblast contraction," *Biochem. Biophys. Res. Commun.*, vol. 360, no. 4, pp. 709–714, Sep. 2007.
- [105] A. M. Szpaderska, J. D. Zuckerman, and L. A. DiPietro, "Differential Injury Responses in Oral Mucosal and Cutaneous Wounds," *J. Dent. Res.*, vol. 82, no. 8, pp. 621–626, Aug. 2003.
- [106] A. M. Szpaderska, C. G. Walsh, M. J. Steinberg, and L. A. DiPietro, "Distinct Patterns of Angiogenesis in Oral and Skin Wounds," *J. Dent. Res.*, vol. 84, no. 4, pp. 309–314, Apr. 2005.
- [107] D. T. Graves *et al.*, "IL-1 Plays a Critical Role in Oral, But Not Dermal, Wound Healing," *J. Immunol.*, vol. 167, no. 9, pp. 5316–5320, Oct. 2001.
- [108] M. J. Oudhoff *et al.*, "Histatins Enhance Wound Closure with Oral and Non-oral Cells," *J. Dent. Res.*, vol. 88, no. 9, pp. 846–850, Sep. 2009.
- [109] P. Stephens *et al.*, "Skin and oral fibroblasts exhibit phenotypic differences in extracellular matrix reorganization and matrix metalloproteinase activity," *Br. J. Dermatol.*, vol. 144, no. 2, pp. 229–237, Feb. 2001.
- [110] S. Enoch and P. Stephens, "Scarless healing: oral mucosa as a scientific model," *Wounds UK*, vol. 1, pp. 43–48, 2009.
- [111] M. A. Peake *et al.*, "Identification of a transcriptional signature for the wound healing continuum," *Wound Repair Regen.*, vol. 22, no. 3, pp. 399–405, May 2014.
- [112] S. Enoch *et al.*, "Increased oral fibroblast lifespan is telomerase-independent," *J. Dent. Res.*, vol. 88, no. 10, pp. 916–921, Oct. 2009.
- [113] S. Enoch, R. Moseley, P. Stephens, and D. W. Thomas, "The oral mucosa: A model of wound healing with reduced scarring," *Oral Surg.*, vol. 1, no. 1, pp. 11–21, Feb. 2008.
- [114] S. Meran *et al.*, "Involvement of hyaluronan in regulation of fibroblast phenotype," *J. Biol. Chem.*, vol. 282, no. 35, pp. 25687–25697, Aug. 2007.
- [115] N. Cohen and J. Cohen-Lévy, "Healing processes following tooth extraction in orthodontic cases," *J. Dentofac. Anomalies Orthod.*, vol. 17, no. 3, p. 304, Oct. 2014.
- [116] R. A. Canuto, R. Pol, G. Martinasso, G. Muzio, G. Gallesio, and M. Mozzati, "Hydroxyapatite paste Ostim, without elevation of full-thickness flaps, improves alveolar healing stimulating BMP- and VEGF-mediated signal pathways: an experimental study in humans.," *Clin. Oral Implants Res.*, vol. 24 Suppl A, pp. 42–8, Aug. 2013.
- [117] M. G. Araújo, C. O. Silva, M. Misawa, and F. Sukekava, "Alveolar socket healing: what can we learn?," *Periodontol. 2000*, vol. 68, no. 1, pp. 122–134, Jun. 2015.
- [118] S. L. Ruggiero, B. Mehrotra, T. J. Rosenberg, and S. L. Engroff, "Osteonecrosis of the jaws associated with the use of bisphosphonates: a review of 63 cases," *J. Oral Maxillofac. Surg.*, vol. 62, no. 5, pp. 527–534, May 2004.
- [119] AAOMS, "American Association of Oral and Maxillofacial Surgeons Position Paper on Bisphosphonate-Related Osteonecrosis of the Jaws," *J. Oral Maxillofac. Surg.*, vol. 65, no. 3, pp. 369–376, Mar. 2007.
- [120] S. Fedele *et al.*, "Up to a quarter of patients with osteonecrosis of the jaw associated with antiresorptive agents remain undiagnosed," *Br. J. Oral Maxillofac. Surg.*, vol. 53, no. 1, pp. 13–17, Jan. 2015.

- [121] B. Galis *et al.*, "Is the prevalence of the medication-related osteonecrosis of the jaws underestimated, evaluation in oncological and non-oncological disease," *Bratislava Med. J.*, vol. 118, no. 12, pp. 724–731, 2017.
- [122] S. Köhl, C. Walter, S. Acham, R. Pfeffer, and J. T. Lambrecht, "Bisphosphonate-related osteonecrosis of the jaws--a review.," *Oral Oncol.*, vol. 48, no. 10, pp. 938–47, Oct. 2012.
- [123] S. L. Ruggiero *et al.*, "American Association of Oral and Maxillofacial Surgeons position paper on medication-related osteonecrosis of the jaw--2014 update.," *J. oral Maxillofac. Surg.*, vol. 72, no. 10, pp. 1938–56, 2014.
- [124] R. Kunchur, A. Need, T. Hughes, and A. Goss, "Clinical investigation of C-terminal cross-linking telopeptide test in prevention and management of bisphosphonate-associated osteonecrosis of the jaws.," *J. Oral Maxillofac. Surg.*, vol. 67, no. 6, pp. 1167–73, Jun. 2009.
- [125] T. Yamazaki *et al.*, "Increased incidence of osteonecrosis of the jaw after tooth extraction in patients treated with bisphosphonates: a cohort study.," *Int. J. Oral Maxillofac. Surg.*, vol. 41, no. 11, pp. 1397–403, Nov. 2012.
- [126] J. E. Iglesias, F. G. Salum, M. A. Figueiredo, and K. Cherubini, "Important aspects concerning alendronate-related osteonecrosis of the jaws: a literature review," *Gerodontology*, vol. 32, no. 3, pp. 169–178, Sep. 2015.
- [127] A. Khominsky and M. Lim, "'Spontaneous' medication-related osteonecrosis of the jaw; two case reports and a systematic review," *Aust. Dent. J.*, vol. 63, no. 4, pp. 441–454, Dec. 2018.
- [128] K. Vahtsevanos *et al.*, "Longitudinal cohort study of risk factors in cancer patients of bisphosphonate-related osteonecrosis of the jaw.," *J. Clin. Oncol.*, vol. 27, no. 32, pp. 5356–62, Nov. 2009.
- [129] S. Sivolella, F. Lumachi, E. Stellini, and L. Favero, "Denosumab and anti-angiogenetic drug-related osteonecrosis of the jaw: An uncommon but potentially severe disease," *Anticancer Research*, vol. 33, no. 5, pp. 1793–1798, May-2013.
- [130] T. Yoneda *et al.*, "Antiresorptive agent-related osteonecrosis of the jaw: Position Paper 2017 of the Japanese Allied Committee on Osteonecrosis of the Jaw," *J. Bone Miner. Metab.*, vol. 35, no. 1, pp. 6–19, Jan. 2017.
- [131] Y. Endo *et al.*, "Underlying Mechanisms and Therapeutic Strategies for Bisphosphonate-Related Osteonecrosis of the Jaw (BRONJ).," *Biol. Pharm. Bull.*, vol. 40, no. 6, pp. 739–750, Jun. 2017.
- [132] F. Sulaiman, J. M. Hury, and I. M. Zlotolow, "Dental extractions in the irradiated head and neck patient: a retrospective analysis of memorial sloan-kettering cancer center protocols, criteria, and end results," *J. Oral Maxillofac. Surg.*, vol. 61, no. 10, pp. 1123–1131, Oct. 2003.
- [133] E.-L. Dormand, P. E. Banwell, and T. E. Goodacre, "Radiotherapy and wound healing," *Int. Wound J.*, vol. 2, no. 2, pp. 112–127, Jun. 2005.
- [134] M. Gieringer, J. Gosepath, and R. Naim, "Radiotherapy and wound healing: Principles, management and prospects (Review)," *Oncol. Rep.*, vol. 26, no. 2, pp. 299–307, May 2011.
- [135] K. Rupel *et al.*, "A systematic review of therapeutical approaches in bisphosphonates-related osteonecrosis of the jaw (BRONJ).," *Oral Oncol.*, vol. 50, no. 11, pp. 1049–57, Nov. 2014.
- [136] H. Schell *et al.*, "Osteoclastic activity begins early and increases over the course of bone healing," *Bone*, vol. 38, no. 4, pp. 547–554, Apr. 2006.
- [137] A. Soundia *et al.*, "Zoledronate Impairs Socket Healing after Extraction of Teeth with Experimental Periodontitis," *J. Dent. Res.*, vol. 97, no. 3, pp. 312–320, Mar. 2018.
- [138] V. Patel, M. Kelleher, C. Sproat, J. Kwok, and M. McGurk, "New cancer therapies and jaw necrosis," *Bdj*, vol. 219, no. 5, pp. 203–207, 2015.
- [139] W. Götz, C. Reichert, L. Canullo, A. Jäger, and F. Heinemann, "Coupling of osteogenesis and angiogenesis in bone substitute healing - a brief overview.," *Ann. Anat.*, vol. 194, no. 2, pp. 171–3, Mar. 2012.

- [140] Y. Kobayashi *et al.*, “Zoledronic acid delays wound healing of the tooth extraction socket, inhibits oral epithelial cell migration, and promotes proliferation and adhesion to hydroxyapatite of oral bacteria, without causing osteonecrosis of the jaw, in mice.,” *J. Bone Miner. Metab.*, vol. 28, no. 2, pp. 165–75, Mar. 2010.
- [141] P. Lesclous *et al.*, “Bisphosphonate-associated osteonecrosis of the jaw: a key role of inflammation?,” *Bone*, vol. 45, no. 5, pp. 843–52, Nov. 2009.
- [142] M. A. Scheper *et al.*, “A novel bioassay model to determine clinically significant bisphosphonate levels,” *Support. Care Cancer*, vol. 17, no. 12, pp. 1553–7, 2009.
- [143] S. Otto *et al.*, “Bisphosphonate-Related Osteonecrosis of the Jaw: Is pH the Missing Part in the Pathogenesis Puzzle?,” *J. Oral Maxillofac. Surg.*, vol. 68, no. 5, pp. 1158–1161, May 2010.
- [144] M. Cozin *et al.*, “Novel therapy to reverse the cellular effects of bisphosphonates on primary human oral fibroblasts.,” *J. Oral Maxillofac. Surg.*, vol. 69, no. 10, pp. 2564–78, Oct. 2011.
- [145] S. Pushalkar *et al.*, “Oral microbiota and host innate immune response in bisphosphonate-related osteonecrosis of the jaw,” *Int. J. Oral Sci.*, vol. 6, no. 4, pp. 219–226, Aug. 2014.
- [146] H. Katsarelis, N. P. Shah, D. K. Dhariwal, and M. Pazianas, “Infection and medication-related osteonecrosis of the jaw,” *Journal of Dental Research*, vol. 94, no. 4. SAGE PublicationsSage CA: Los Angeles, CA, pp. 534–539, 20-Apr-2015.
- [147] S. Matsuda, H. Yoshimura, and K. Sano, “Risk factors and treatments for medication-related osteonecrosis of the jaw: A 10-year single-institution experience,” *Journal of Oral and Maxillofacial Surgery, Medicine, and Pathology*, vol. 30, no. 1, Elsevier, pp. 10–16, 01-Jan-2017.
- [148] M. Kos, A. Junka, D. Smutnicka, P. Szymczyk, K. Gluza, and M. Bartoszewicz, “Bisphosphonates enhance bacterial adhesion and biofilm formation on bone hydroxyapatite.,” *J. Craniomaxillofac. Surg.*, vol. 43, no. 6, pp. 863–9, Jul. 2015.
- [149] T. Suzuki, R. Sekiya, Y. Hamada, M. Takahashi, K. Karakida, and H. Sakamoto, “Fatal Bleeding in Conjunction with Mandibular Medication-related Osteonecrosis of the Jaw (MRONJ),” *Bull. Tokyo Dent. Coll.*, vol. 59, no. 1, pp. 27–34, 2018.
- [150] T. Ikeda, J. Kuraguchi, Y. Kogashiwa, H. Yokoi, T. Satomi, and N. Kohno, “Successful treatment of Bisphosphonate-Related Osteonecrosis of the Jaw (BRONJ) patients with sitafloxacin: New strategies for the treatment of BRONJ,” *Bone*, vol. 73, pp. 217–222, Apr. 2015.
- [151] P. Barba-Recreo *et al.*, “Adipose-derived stem cells and platelet-rich plasma for preventive treatment of bisphosphonate-related osteonecrosis of the jaw in a murine model.,” *J. Craniomaxillofac. Surg.*, vol. 43, no. 7, pp. 1161–1168, May 2015.
- [152] P. J. Voss *et al.*, “Surgical treatment of bisphosphonate-associated osteonecrosis of the jaw: technical report and follow up of 21 patients.,” *J. Craniomaxillofac. Surg.*, vol. 40, no. 8, pp. 719–25, Dec. 2012.
- [153] R. Sacco, N. Sacco, U. Hamid, S. H. Ali, M. Singh, and J. S. J. Blythe, “Microsurgical Reconstruction of the Jaws Using Vascularised Free Flap Technique in Patients with Medication-Related Osteonecrosis: A Systematic Review,” *Biomed Res. Int.*, vol. 2018, pp. 1–12, Jun. 2018.
- [154] G. Favia, A. Tempesta, L. Limongelli, V. Crincoli, and E. Maiorano, “Medication-related osteonecrosis of the jaw: Surgical or non-surgical treatment?,” *Oral Dis.*, vol. 24, no. 1–2, pp. 238–242, Mar. 2018.
- [155] S. Caldrony, N. Ghazali, D. Dyalram, and J. E. Lubek, “Surgical resection and vascularized bone reconstruction in advanced stage medication-related osteonecrosis of the jaw,” *Int. J. Oral Maxillofac. Surg.*, vol. 46, no. 7, pp. 871–876, Jul. 2017.
- [156] S. E. C. Pichardo, S. C. C. Kuijpers, and J. P. R. van Merkesteyn, “Bisphosphonate-related osteonecrosis of the jaws: Cohort study of surgical treatment results in seventy-four stage II/III patients,” *J. Cranio-Maxillofacial Surg.*, vol. 44, no. 9, pp. 1216–1220, 2016.

- [157] T. Eguchi, I. Kanai, A. Basugi, Y. Miyata, M. Inoue, and Y. Hamada, "The assessment of surgical and non-surgical treatment of stage II medication-related osteonecrosis of the jaw," *Med. Oral Patol. Oral y Cir. Bucal*, vol. 22, no. 6, pp. 0–0, Nov. 2017.
- [158] M. Nisi *et al.*, "Conservative surgical management of patients with bisphosphonate-related osteonecrosis of the jaws: a series of 120 patients," *Br. J. Oral Maxillofac. Surg.*, vol. 54, no. 8, pp. 930–935, 2016.
- [159] H. Kagami, M. Inoue, A. Kobayashi, A. Taguchi, X. Li, and M. Yoshizawa, "Issues with the surgical treatment of antiresorptive agent-related osteonecrosis of the jaws," *Oral Dis.*, vol. 24, no. 1–2, pp. 52–56, Mar. 2018.
- [160] S. Otto *et al.*, "Fluorescence-guided surgery for the treatment of medication-related osteonecrosis of the jaw: A prospective cohort study," *J. Cranio-Maxillofacial Surg.*, vol. 44, no. 8, pp. 1073–1080, Aug. 2016.
- [161] O. Nicolatou-Galitis *et al.*, "Osteonecrosis of the jaw in oncology patients treated with bisphosphonates: prospective experience of a dental oncology referral center.," *Oral Surg. Oral Med. Oral Pathol. Oral Radiol. Endod.*, vol. 112, no. 2, pp. 195–202, Aug. 2011.
- [162] T. Hasegawa *et al.*, "A multicenter retrospective study of the risk factors associated with medication-related osteonecrosis of the jaw after tooth extraction in patients receiving oral bisphosphonate therapy: can primary wound closure and a drug holiday really prevent MRONJ?," *Osteoporos. Int.*, vol. 28, no. 8, pp. 2465–2473, Aug. 2017.
- [163] K. McGowan, T. McGowan, and S. Ivanovski, "Risk factors for medication-related osteonecrosis of the jaws: A systematic review," *Oral Dis.*, vol. 24, no. 4, pp. 527–536, May 2018.
- [164] R. H. Kim *et al.*, "Bisphosphonates Induce Senescence in Normal Human Oral Keratinocytes.," *J. Dent. Res.*, vol. 90, no. 6, pp. 810–816, Jun. 2011.
- [165] S. S. Soydan *et al.*, "Effects of alendronate and pamidronate on apoptosis and cell proliferation in cultured primary human gingival fibroblasts," *Hum. Exp. Toxicol.*, vol. 34, no. 11, pp. 1073–1082, Nov. 2015.
- [166] Y. Açıl *et al.*, "Cytotoxic and inflammatory effects of alendronate and zoledronate on human osteoblasts, gingival fibroblasts and osteosarcoma cells," *J. Cranio-Maxillofacial Surg.*, vol. 46, no. 4, pp. 538–546, Apr. 2018.
- [167] H. Agis, J. Blei, G. Watzek, and R. Gruber, "Is Zoledronate Toxic to Human Periodontal Fibroblasts?," *J. Dent. Res.*, vol. 89, no. 1, pp. 40–45, Jan. 2010.
- [168] N. Hagelauer, T. Ziebart, A. M. Pabst, and C. Walter, "Bisphosphonates inhibit cell functions of HUVECs, fibroblasts and osteogenic cells via inhibition of protein geranylgeranylation," *Clin. Oral Investig.*, vol. 19, no. 5, pp. 1079–1091, Jun. 2015.
- [169] M. A. Scheper, A. Badros, R. Chaisuparat, K. J. Cullen, and T. F. Meiller, "Effect of zoledronic acid on oral fibroblasts and epithelial cells: A potential mechanism of bisphosphonate-associated osteonecrosis," *Br. J. Haematol.*, vol. 144, no. 5, pp. 667–676, Mar. 2009.
- [170] C. Walter, M. O. Klein, A. Pabst, B. Al-Nawas, H. Duschner, and T. Ziebart, "Influence of bisphosphonates on endothelial cells, fibroblasts, and osteogenic cells," *Clin. Oral Investig.*, vol. 14, no. 1, pp. 35–41, Feb. 2010.
- [171] S. Zafar, D. E. Coates, M. P. Cullinan, B. K. Drummond, T. Milne, and G. J. Seymour, "Zoledronic acid and geranylgeraniol regulate cellular behaviour and angiogenic gene expression in human gingival fibroblasts," *J. Oral Pathol. Med.*, vol. 43, no. 9, pp. 711–721, Oct. 2014.
- [172] J. Jung *et al.*, "Effects of an oral bisphosphonate and three intravenous bisphosphonates on several cell types in vitro," *Clinical Oral Investigations*, vol. 22, no. 7, Springer Berlin Heidelberg, pp. 1–8, 2018.
- [173] N. M. H. McLeod, K. A. Moutasim, P. A. Brennan, G. Thomas, and V. Jenei, "In vitro effect of bisphosphonates on oral keratinocytes and fibroblasts," *J. Oral Maxillofac. Surg.*, vol. 72, no. 3, pp. 503–509, Mar. 2014.

- [174] F. G. Basso, T. N. Pansani, D. G. Soares, L. M. Cardoso, J. Hebling, and C. A. de Souza Costa, "Influence of bisphosphonates on the adherence and metabolism of epithelial cells and gingival fibroblasts to titanium surfaces," *Clin. Oral Investig.*, pp. 1–8, Jul. 2017.
- [175] A. M. Pabst, T. Ziebart, F. P. Koch, K. Y. Taylor, B. Al-Nawas, and C. Walter, "The influence of bisphosphonates on viability, migration, and apoptosis of human oral keratinocytes-in vitro study," *Clin. Oral Investig.*, vol. 16, no. 1, pp. 87–93, Feb. 2012.
- [176] N. Arai, S. Inoue, K. Tomihara, H. Tsuno, and M. Noguchi, "In vitro synergistic effects of zoledronic acid and calcium on viability of human epithelial cells," *Oral Dis.*, vol. 19, no. 2, pp. 200–205, Mar. 2013.
- [177] H. Ohnuki *et al.*, "Zoledronic acid induces S-phase arrest via a DNA damage response in normal human oral keratinocytes," *Arch. Oral Biol.*, vol. 57, no. 7, pp. 906–917, Jul. 2012.
- [178] F. Renò, M. Migliario, M. Rizzi, M. Invernizzi, C. Cisari, and M. Cannas, "Low concentration amino-bisphosphonates stimulate human keratinocyte proliferation and in vitro wound healing," *Int. Wound J.*, vol. 9, no. 4, pp. 442–450, Aug. 2012.
- [179] M. A. Dickson *et al.*, "Human keratinocytes that express hTERT and also bypass a p16(INK4a)-enforced mechanism that limits life span become immortal yet retain normal growth and differentiation characteristics," *Mol. Cell. Biol.*, vol. 20, no. 4, pp. 1436–47, Feb. 2000.
- [180] C. C. Liang, A. Y. Park, and J. L. Guan, "In vitro scratch assay: a convenient and inexpensive method for analysis of cell migration in vitro," *Nat Protoc.*, vol. 2, no. 2, pp. 329–333, Feb. 2007.
- [181] L. Wu, L. Zhu, W.-H. Shi, J. Zhang, D. Ma, and B. Yu, "Zoledronate inhibits the proliferation, adhesion and migration of vascular smooth muscle cells," *Eur. J. Pharmacol.*, vol. 602, no. 1, pp. 124–131, 2009.
- [182] M. Bezzi, M. Hasmim, G. Bieler, O. Dormond, and C. Rüegg, "Zoledronate sensitizes endothelial cells to tumor necrosis factor-induced programmed cell death: evidence for the suppression of sustained activation of focal adhesion kinase and protein kinase B/Akt," *J. Biol. Chem.*, vol. 278, no. 44, pp. 43603–14, Oct. 2003.
- [183] M. Hasmim, G. Bieler, and C. Rüegg, "Zoledronate inhibits endothelial cell adhesion, migration and survival through the suppression of multiple, prenylation-dependent signaling pathways," *J. Thromb. Haemost.*, vol. 5, no. 1, pp. 166–173, Jan. 2007.
- [184] S. K. Mitra, D. A. Hanson, and D. D. Schlaepfer, "Focal adhesion kinase: in command and control of cell motility," *Nat. Rev. Mol. Cell Biol.*, vol. 6, no. 1, pp. 56–68, Jan. 2005.
- [185] M. A. Yurko, E. A. O'Toole, and D. T. Woodley, "Phosphorylation of focal adhesion kinase (pp125FAK) is increased in human keratinocytes induced to migrate by extracellular matrices," *J. Cell. Physiol.*, vol. 188, no. 1, pp. 24–32, Jul. 2001.
- [186] S. Matsunaga, K. Iguchi, S. Usui, and K. Hirano, "Incadronate induces cell detachment and apoptosis in prostatic PC-3 cells," *Anticancer Res.*, vol. 27, no. 2, pp. 927–32, 2007.
- [187] T. Saito *et al.*, "Zoledronic acid impairs re-epithelialization through down-regulation of integrin $\alpha\beta 6$ and transforming growth factor beta signalling in a three-dimensional in vitro wound healing model," *Int. J. Oral Maxillofac. Surg.*, vol. 43, no. 3, pp. 373–380, 2014.
- [188] F. M. Watt, "Role of integrins in regulating epidermal adhesion, growth and differentiation," *EMBO J.*, vol. 21, no. 15, pp. 3919–26, Aug. 2002.
- [189] E. Donetti, A. Gualerzi, A. Sardella, G. Lodi, A. Carrassi, and C. Sforza, "Alendronate impairs epithelial adhesion, differentiation and proliferation in human oral mucosa," *Oral Dis.*, vol. 20, no. 5, pp. 466–472, Jul. 2014.
- [190] A. Dongari-Bagtzoglou and H. Kashleva, "Development of a highly reproducible three-dimensional organotypic model of the oral mucosa," *Nat. Protoc.*, vol. 1, no.

- 4, pp. 2012–8, 2006.
- [191] I. Masuda, “[An in Vitro Oral Mucosal Model Reconstructed From Human Normal Gingival Cells],” *Kokubyo Gakkai Zasshi*, vol. 63, no. 2, pp. 334–353, 1996.
- [192] M. Rouabhia and N. Deslauriers, “Production and characterization of an in vitro engineered human oral mucosa,” *Biochem. Cell Biol.*, vol. 80, no. 2, pp. 189–195, Apr. 2002.
- [193] A. Dongari-Bagtzoglou and H. Kashleva, “Development of a novel three-dimensional in vitro model of oral Candida infection,” *Microb. Pathog.*, vol. 40, no. 6, pp. 271–278, Jun. 2006.
- [194] K. Moharamzadeh, I. M. Brook, R. Van Noort, A. M. Scutt, and M. H. Thornhill, “Tissue-engineered oral mucosa: a review of the scientific literature.,” *J. Dent. Res.*, vol. 86, no. 2, pp. 115–24, Feb. 2007.
- [195] J. S. Mao, H. F. Liu, Y. J. Yin, and K. De Yao, “The properties of chitosan-gelatin membranes and scaffolds modified with hyaluronic acid by different methods,” *Biomaterials*, vol. 24, no. 9, pp. 1621–1629, Apr. 2003.
- [196] L. Ma *et al.*, “Collagen/chitosan porous scaffolds with improved biostability for skin tissue engineering,” *Biomaterials*, vol. 24, no. 26, pp. 4833–4841, Nov. 2003.
- [197] M. M. Ghosh, S. Boyce, C. Layton, E. Freedlander, and S. Mac Neil, “A comparison of methodologies for the preparation of human epidermal-dermal composites.,” *Ann. Plast. Surg.*, vol. 39, no. 4, pp. 390–404, Oct. 1997.
- [198] D. J. Geer, D. D. Swartz, and S. T. Andreadis, “Fibrin promotes migration in a three-dimensional in vitro model of wound regeneration.,” *Tissue Eng.*, vol. 8, no. 5, pp. 787–798, Oct. 2002.
- [199] H. E. Colley *et al.*, “Development of tissue-engineered models of oral dysplasia and early invasive oral squamous cell carcinoma,” *Br. J. Cancer*, vol. 105, no. 10, pp. 1582–1592, Nov. 2011.
- [200] K. Moharamzadeh *et al.*, “Tissue-engineered Oral Mucosa,” pp. 642–650, 2012.
- [201] T. Almela, I. M. Brook, and K. Moharamzadeh, “Development of three-dimensional tissue engineered bone-oral mucosal composite models.,” *J. Mater. Sci. Mater. Med.*, vol. 27, no. 4, p. 65, Apr. 2016.
- [202] S. Bae *et al.*, “Development of oral osteomucosal tissue constructs in vitro and localization of fluorescently-labeled bisphosphonates to hard and soft tissue.,” *Int. J. Mol. Med.*, vol. 34, no. 2, pp. 559–63, Aug. 2014.
- [203] C. M. A. Reijnders, A. van Lier, S. Roffel, D. Kramer, R. J. Scheper, and S. Gibbs, “Development of a Full-Thickness Human Skin Equivalent In Vitro Model Derived from TERT-Immortalized Keratinocytes and Fibroblasts.,” *Tissue Eng. Part A*, vol. 21, no. 17–18, pp. 2448–59, Sep. 2015.
- [204] M. Breetveld, C. D. Richters, T. Rustemeyer, R. J. Scheper, and S. Gibbs, “Comparison of Wound Closure after Burn and Cold Injury in Human Skin Equivalents,” *J. Invest. Dermatol.*, vol. 126, no. 8, pp. 1918–1921, Aug. 2006.
- [205] J. A. Garlick and L. B. Taichman, “Effect of TGF-beta 1 on re-epithelialization of human keratinocytes in vitro: an organotypic model.,” *J. Invest. Dermatol.*, vol. 103, no. 4, pp. 554–559, Oct. 1994.
- [206] A. E. Rizzo, L. A. Beckett, B. S. Baier, and R. R. Isseroff, “The linear excisional wound: An improved model for human ex vivo wound epithelialization studies,” *Ski. Res. Technol.*, vol. 18, no. 1, pp. 125–132, Feb. 2012.
- [207] S. MacNeil, J. Shepherd, and L. Smith, “Production of Tissue-Engineered Skin and Oral Mucosa for Clinical and Experimental Use,” in *3D Cell Culture: Methods and Protocols*, W. J. Haycock, Ed. Totowa, NJ: Humana Press, 2011, pp. 129–153.
- [208] N. Deshayes, F. Bloas, F. Boissout, J. Lecardonnel, and M. Paris, “3D In vitro model of the re-epithelialization phase in the wound-healing process,” *Experimental Dermatology*, vol. 27, no. 5. Wiley/Blackwell (10.1111), pp. 460–462, 01-May-2018.
- [209] T. De Ryck *et al.*, “Development of an oral mucosa model to study host-microbiome interactions during wound healing,” *Appl. Microbiol. Biotechnol.*, vol. 98, no. 15, pp. 6831–6846, Aug. 2014.

- [210] J. D. Bancroft and M. Gamble, Eds., *Theory and Practice of Histological Techniques*, Fifth. Elsevier, 2002.
- [211] E. Proksch, J. M. Brandner, and J. M. Jensen, "The skin: An indispensable barrier," *Exp. Dermatol.*, vol. 17, no. 12, pp. 1063–1072, Dec. 2008.
- [212] V. L. do N. Poubel, C. A. B. Silva, L. A. M. Mezzomo, G. De Luca Canto, and E. R. C. Rivero, "The risk of osteonecrosis on alveolar healing after tooth extraction and systemic administration of antiresorptive drugs in rodents: a systematic review," *Journal of Cranio-Maxillofacial Surgery*, vol. 46, no. 2. Churchill Livingstone, pp. 245–256, 01-Feb-2018.
- [213] P. Barba-Recreo, J. L. Del Castillo Pardo De Vera, M. García-Arranz, L. Yébenes, and M. Burgueño, "Zoledronic acid - Related osteonecrosis of the jaws. Experimental model with dental extractions in rats," *J. Cranio-Maxillofacial Surg.*, vol. 42, no. 6, pp. 744–750, Sep. 2014.
- [214] F. Koneski *et al.*, "In vivo effects of geranylgeraniol on the development of bisphosphonate-related osteonecrosis of the jaws," *J. Cranio-Maxillofacial Surg.*, vol. 46, no. 2, pp. 230–236, Feb. 2018.
- [215] Y. Nagaoka, H. Kajiya, S. Ozeki, T. Ikebe, and K. Okabe, "Mevalonates restore zoledronic acid-induced osteoclastogenesis inhibition.," *J. Dent. Res.*, vol. 94, no. 4, pp. 594–601, Apr. 2015.
- [216] C. Pautke *et al.*, "Bisphosphonate related osteonecrosis of the jaw: A minipig large animal model," *Bone*, vol. 51, no. 3, pp. 592–599, Sep. 2012.
- [217] S. Otto *et al.*, "Further development of the MRONJ minipig large animal model," *J. Cranio-Maxillofacial Surg.*, vol. 45, no. 9, pp. 1503–1514, Sep. 2017.
- [218] M. R. Allen, D. J. Kubek, D. B. Burr, S. L. Ruggiero, and T. M. G. Chu, "Compromised osseous healing of dental extraction sites in zoledronic acid-treated dogs," *Osteoporos. Int.*, vol. 22, no. 2, pp. 693–702, Feb. 2011.
- [219] W. M. S. Russell, R. L. Burch, and C. W. Hume, *The principles of humane experimental technique*. London: Meuthen, 1959.
- [220] H. L. Benford, J. C. Frith, S. Auriola, J. Mönkkönen, and M. J. Rogers, "Farnesol and geranylgeraniol prevent activation of caspases by aminobisphosphonates: biochemical evidence for two distinct pharmacological classes of bisphosphonate drugs.," *Mol. Pharmacol.*, vol. 56, no. 1, pp. 131–40, Jul. 1999.
- [221] J. E. Fisher *et al.*, "Alendronate mechanism of action: geranylgeraniol, an intermediate in the mevalonate pathway, prevents inhibition of osteoclast formation, bone resorption, and kinase activation in vitro.," *Proc. Natl. Acad. Sci. U. S. A.*, vol. 96, no. 1, pp. 133–8, Jan. 1999.
- [222] J. P. Coxon, G. M. Oades, R. S. Kirby, and K. W. Colston, "Zoledronic acid induces apoptosis and inhibits adhesion to mineralized matrix in prostate cancer cells via inhibition of protein prenylation," *BJU Int.*, vol. 94, no. 1, pp. 164–170, Jul. 2004.
- [223] K. Sawada, K. Morishige, and M. Tahara, "Alendronate Inhibits Lysophosphatidic Acid-induced Migration of Human Ovarian Cancer Cells by Attenuating the Activation of Rho Advances in Brief Alendronate Inhibits Lysophosphatidic Acid-induced Migration of Human Ovarian Cancer Cells by Attenuating the," *Cancer Res.*, vol. 62, no. 21, pp. 6015–6020, 2002.
- [224] "2018 Annual Meeting of the American Society for Bone and Mineral Research Palais des congrès de Montréal in Montréal, Québec, Canada September 28 - October 1, 2018," *J. Bone Miner. Res.*, vol. 33, no. S1, pp. S1–S464, Nov. 2018.
- [225] "2017 Annual Meeting of the American Society for Bone and Mineral Research, Colorado Convention Center, Denver, CO, USA - September 8-11, 2017," *J. Bone Miner. Res.*, vol. 32, no. S1, pp. S1–S432, Dec. 2017.
- [226] T. Oizumi *et al.*, "Inhibition of Necrotic Actions of Nitrogen-Containing Bisphosphonates (NBPs) and Their Elimination From Bone by Etidronate (a Non-NBP): A Proposal for Possible Utilization of Etidronate as a Substitution Drug for NBPs," *J. Oral Maxillofac. Surg.*, vol. 68, no. 5, pp. 1043–1054, May 2010.
- [227] T. Oizumi *et al.*, "A Strategy against the Osteonecrosis of the Jaw Associated with

- Nitrogen-Containing Bisphosphonates (N-BPs): Attempts to Replace N-BPs with the Non-N-BP Etidronate," *Biol. Pharm. Bull. Pharm. Bull.*, vol. 39, no. 9, pp. 1549–1554, Sep. 2016.
- [228] P. P. Poli, F. Á. Souza, and C. Maiorana, "Adjunctive use of antimicrobial photodynamic therapy in the treatment of medication-related osteonecrosis of the jaws: A case report," *Photodiagnosis Photodyn. Ther.*, vol. 23, pp. 99–101, Sep. 2018.
- [229] G. A. C. Momesso *et al.*, "Successful use of lower-level laser therapy in the treatment of medication-related osteonecrosis of the jaw," *J. Lasers Med. Sci.*, vol. 8, no. 4, pp. 201–203, 2017.
- [230] J. Abtahi, F. Agholme, and P. Aspenberg, "Prevention of osteonecrosis of the jaw by mucoperiosteal coverage in a rat model.," *Int. J. Oral Maxillofac. Surg.*, vol. 42, no. 5, pp. 632–6, May 2013.
- [231] M. Ragazzo, D. Trojan, L. Spagnol, A. Paolin, and L. Guarda Nardini, "Use of amniotic membrane in the treatment of patients with BRONJ: two case reports," *J. Surg. Case Reports*, vol. 2018, no. 4, Apr. 2018.
- [232] S. Hafner, M. Ehrenfeld, E. Storz, and A. Wieser, "Photodynamic Inactivation of *Actinomyces naeslundii* in Comparison With Chlorhexidine and Polyhexanide—A New Approach for Antiseptic Treatment of Medication-Related Osteonecrosis of the Jaw?," *J. Oral Maxillofac. Surg.*, vol. 74, no. 3, pp. 516–522, Mar. 2016.
- [233] M. S. de Castro, N. V. Ribeiro, M. L. de Carli, A. A. C. Pereira, F. F. Sperandio, and J. A. C. Hanemann, "Photodynamically dealing with bisphosphonate-related osteonecrosis of the jaw: Successful case reports," *Photodiagnosis Photodyn. Ther.*, vol. 16, pp. 72–75, Dec. 2016.
- [234] S. Rajesh, E. Koshi, K. Philip, and A. Mohan, "Antimicrobial photodynamic therapy: An overview.," *J. Indian Soc. Periodontol.*, vol. 15, no. 4, pp. 323–7, Oct. 2011.
- [235] H. Chung, T. Dai, S. K. Sharma, Y.-Y. Huang, J. D. Carroll, and M. R. Hamblin, "The Nuts and Bolts of Low-level Laser (Light) Therapy," *Ann. Biomed. Eng.*, vol. 40, no. 2, pp. 516–533, Feb. 2012.
- [236] C. Pautke *et al.*, "Tetracycline Bone Fluorescence: A Valuable Marker for Osteonecrosis Characterization and Therapy," *J. Oral Maxillofac. Surg.*, vol. 68, no. 1, pp. 125–129, Jan. 2010.
- [237] M. González-García *et al.*, "Cell therapy in bisphosphonate-related osteonecrosis of the jaw.," *J. Craniofac. Surg.*, vol. 24, no. 3, pp. e226-8, May 2013.
- [238] L. Cella *et al.*, "Autologous bone marrow stem cell intralesional transplantation repairing bisphosphonate related osteonecrosis of the jaw," *Head Face Med.*, vol. 7, no. 1, p. 16, Dec. 2011.
- [239] T. Kikuri *et al.*, "Cell-based immunotherapy with mesenchymal stem cells cures bisphosphonate-related osteonecrosis of the jaw-like disease in mice," *J. Bone Miner. Res.*, vol. 25, no. 7, pp. 1668–1679, Jan. 2010.
- [240] Y. Li *et al.*, "Allogeneic Mesenchymal Stem Cell Therapy for Bisphosphonate-Related Jaw Osteonecrosis in Swine," *Stem Cells Dev.*, vol. 22, no. 14, pp. 2047–2056, Jul. 2013.
- [241] A. Bigi and E. Boanini, "Calcium phosphates as delivery systems for Bisphosphonates," *Journal of Functional Biomaterials*, vol. 9, no. 1. Multidisciplinary Digital Publishing Institute (MDPI), 13-Jan-2018.
- [242] V. S. Kattimani, S. Kondaka, and K. P. Lingamaneni, "Hydroxyapatite—Past, Present, and Future in Bone Regeneration," *Bone Tissue Regen. Insights*, vol. 7, p. BTRI.S36138, Jan. 2016.
- [243] F. A. Santos, M. T. Pochapski, M. C. Martins, E. G. Zenóbio, L. C. Spolidoro, and E. Marcantonio, "Comparison of biomaterial implants in the dental socket: histological analysis in dogs.," *Clin. Implant Dent. Relat. Res.*, vol. 12, no. 1, pp. 18–25, Mar. 2010.
- [244] Z. Schwartz *et al.*, "Ability of Commercial Demineralized Freeze-Dried Bone Allograft to Induce New Bone Formation," *J. Periodontol.*, vol. 67, no. 9, pp. 918–

- 926, 1996.
- [245] A. Figueiredo, P. Coimbra, A. Cabrita, F. Guerra, and M. Figueiredo, "Comparison of a xenogeneic and an alloplastic material used in dental implants in terms of physico-chemical characteristics and in vivo inflammatory response," *Mater. Sci. Eng. C*, vol. 33, no. 6, pp. 3506–3513, 2013.
- [246] P. Hanseler *et al.*, "Delivery of BMP-2 by two clinically available apatite materials: In vitro and in vivo comparison," *J. Biomed. Mater. Res. - Part A*, vol. 103, no. 2, pp. 628–638, Feb. 2015.
- [247] L. L. Hench, "Bioceramics: From Concept to Clinic," *J. Am. Ceram. Soc.*, vol. 74, no. 7, pp. 1487–1510, Jul. 1991.
- [248] L. Canullo, F. Heinemann, T. Gedrange, R. Biffar, and C. Kunert-Keil, "Histological evaluation at different times after augmentation of extraction sites grafted with a magnesium-enriched hydroxyapatite: Double-blinded randomized controlled trial," *Clin. Oral Implants Res.*, vol. 24, no. 4, pp. 398–406, 2013.
- [249] J. E. Maté Sanchez de Val, J. L. Calvo-Guirado, G. Gomez-Moreno, C. Pérez-Albacete Martinez, P. Mazon, and P. N. De Aza, "Influence of hydroxyapatite granule size, porosity, and crystallinity on tissue reaction in vivo. Part A: Synthesis, characterization of the materials, and SEM analysis," *Clin. Oral Implants Res.*, vol. 0, pp. 1–8, Jun. 2015.
- [250] W. Götz, T. Gerber, B. Michel, S. Lossdörfer, K.-O. Henkel, and F. Heinemann, "Immunohistochemical characterization of nanocrystalline hydroxyapatite silica gel (NanoBone(r)) osteogenesis: a study on biopsies from human jaws.," *Clin. Oral Implants Res.*, vol. 19, no. 10, pp. 1016–26, Oct. 2008.
- [251] S. Josse *et al.*, "Novel biomaterials for bisphosphonate delivery.," *Biomaterials*, vol. 26, no. 14, pp. 2073–80, May 2005.
- [252] B. Möller, J. Wiltfang, Y. Acil, M. Gierloff, S. Lippross, and H. Terheyden, "Prevention of the surface resorption of bone grafts by topical application of bisphosphonate on different carrier materials.," *Clin. Oral Investig.*, vol. 18, no. 9, pp. 2203–11, Dec. 2014.
- [253] B. Houshmand, H. Rahimi, F. Ghanavati, A. Alisadr, and B. Eslami, "Boosting effect of bisphosphonates on osteoconductive materials: a histologic in vivo evaluation.," *J. Periodontal Res.*, vol. 42, no. 2, pp. 119–23, Apr. 2007.
- [254] J. P. D'Lima, J. Paul, P. Palathingal, B. R. R. Varma, M. Bhat, and M. Mohanty, "Histological and histometrical evaluation of two synthetic hydroxyapatite based biomaterials in the experimental periodontal defects in dogs," *J. Clin. Diagnostic Res.*, vol. 8, no. 9, pp. ZC52–ZC55, Sep. 2014.
- [255] M. Nevins, M. L. Nevins, P. Schupbach, S.-W. Kim, Z. Lin, and D. M. Kim, "A prospective, randomized controlled preclinical trial to evaluate different formulations of biphasic calcium phosphate in combination with a hydroxyapatite collagen membrane to reconstruct deficient alveolar ridges.," *J. Oral Implantol.*, vol. 39, no. 2, pp. 133–9, 2013.
- [256] J. Kolmas, S. Krukowski, A. Laskus, and M. Jurkitewicz, "Synthetic hydroxyapatite in pharmaceutical applications," *Ceram. Int.*, vol. 42, no. 2, pp. 2472–2487, 2016.
- [257] T. C. Sörensen, J. Arnoldi, P. Procter, B. Robioneck, and H. Steckel, "Bone substitute materials delivering zoledronic acid: physicochemical characterization, drug load, and release properties.," *J. Biomater. Appl.*, vol. 27, no. 6, pp. 727–38, Feb. 2013.
- [258] M. Piattelli, G. Favero, A. Scarano, G. Orsini, and A. Piattelli, "Bone reactions to anorganic bovine bone (Bio-Oss) used in sinus augmentation procedures: a histologic long-term report of 20 cases in humans," *Int J Oral Maxillofac Implant.*, vol. 14, no. 6, pp. 835–40, 1999.
- [259] A. Indovina and M. S. Block, "Comparison of 3 bone substitutes in canine extraction sites," *J. Oral Maxillofac. Surg.*, vol. 60, no. 1, pp. 53–58, Jan. 2002.
- [260] G. A. Gholami, B. Najafi, F. Mashhadiabbas, W. Goetz, and S. Najafi, "Clinical, histologic and histomorphometric evaluation of socket preservation using a

- synthetic nanocrystalline hydroxyapatite in comparison with a bovine xenograft: A randomized clinical trial," *Clin. Oral Implants Res.*, vol. 23, no. 10, pp. 1198–1204, Oct. 2012.
- [261] J. Huang, J. Xiong, J. Liu, W. Zhu, and D. Wang, "Investigation of the in vitro degradation of a novel polylactide/ nanohydroxyapatite composite for artificial bone," *J. Nanomater.*, vol. 2013, no. Figure 1, 2013.
- [262] A. Horváth, A. Stavropoulos, P. Windisch, L. Lukács, I. Gera, and A. Sculean, "Histological evaluation of human intrabony periodontal defects treated with an unsintered nanocrystalline hydroxyapatite paste.," *Clin. Oral Investig.*, vol. 17, no. 2, pp. 423–30, Mar. 2013.
- [263] A. Pilloni *et al.*, "Clinical evaluation of the regenerative potential of EMD and NanoHA in periodontal infrabony defects: a 2-year follow-up.," *Biomed Res. Int.*, vol. 2014, p. 492725, Jan. 2014.
- [264] S. J. Kalita, A. Bhardwaj, and H. A. Bhatt, "Nanocrystalline calcium phosphate ceramics in biomedical engineering," *Mater. Sci. Eng. C*, vol. 27, no. 3, pp. 441–449, 2007.
- [265] F. Errassifi, S. Sarda, A. Barroug, A. Legrouri, H. Sfihi, and C. Rey, "Infrared, Raman and NMR investigations of risedronate adsorption on nanocrystalline apatites.," *J. Colloid Interface Sci.*, vol. 420, pp. 101–11, Apr. 2014.
- [266] P. Pascaud *et al.*, "Adsorption on apatitic calcium phosphates for drug delivery: interaction with bisphosphonate molecules.," *J. Mater. Sci. Mater. Med.*, vol. 25, no. 10, pp. 2373–81, Oct. 2014.
- [267] D. Busenlechner *et al.*, "Simultaneous in vivo comparison of bone substitutes in a guided bone regeneration model," *Biomaterials*, vol. 29, no. 22, pp. 3195–3200, 2008.
- [268] D. Rothamel *et al.*, "Dimensional ridge alterations following socket preservation using a nanocrystalline hydroxyapatite paste. A histomorphometrical study in dogs," *Int. J. Oral Maxillofac. Surg.*, vol. 37, no. 8, pp. 741–747, 2008.
- [269] M. W. Laschke, K. Witt, T. Pohlemann, and M. D. Menger, "Injectable Nanocrystalline Hydroxyapatite Paste for Bone Substitution: In Vivo Analysis of Biocompatibility and Vascularization," *J. Biomed. Mater. Res.*, vol. 82, no. 2, pp. 494–505, 2007.
- [270] D. Carmagnola, S. Abati, S. Celestino, M. Chiapasco, D. Bosshardt, and N. P. Lang, "Oral implants placed in bone defects treated with Bio-Oss, Ostim-Paste or PerioGlas: an experimental study in the rabbit tibiae.," *Clin. Oral Implants Res.*, vol. 19, no. 12, pp. 1246–53, Dec. 2008.
- [271] H. H. K. Xu and C. G. Simon, "Fast setting calcium phosphate-chitosan scaffold: mechanical properties and biocompatibility.," *Biomaterials*, vol. 26, no. 12, pp. 1337–48, Apr. 2005.
- [272] S. V. Dorozhkin, "Nanodimensional and nanocrystalline apatites and other calcium orthophosphates in biomedical engineering, biology and medicine," *Materials*, vol. 2, no. 4. Molecular Diversity Preservation International, pp. 1975–2045, 27-Nov-2009.
- [273] Ł. Matuszewski, A. Matuszewska, and T. Mazurkiewicz, "Determination of Bisphosphonates by Ion – pair HPLC," vol. 56, no. 2, pp. 213–216, 2011.
- [274] P. Li and Y. Hu, "'Turn-Off' Fluorescent Sensor for Pamidronate Disodium and Zoledronic Acid Based on Newly Synthesized Carbon Dots from Black Tea," *J. Anal. Methods Chem.*, vol. 2018, pp. 1–7, Mar. 2018.
- [275] C. K. Zacharis and P. D. Tzanavaras, "Determination of bisphosphonate active pharmaceutical ingredients in pharmaceuticals and biological material: a review of analytical methods.," *J. Pharm. Biomed. Anal.*, vol. 48, no. 3, pp. 483–96, Nov. 2008.
- [276] C. Fernandes, R. S. Leite, and F. M. Lancas, "Rapid Determination of Bisphosphonates by Ion Chromatography with Indirect UV Detection," *J. Chromatogr. Sci.*, vol. 45, no. 5, pp. 236–241, May 2007.

- [277] E. A. Taha and N. F. Youssef, "Spectrophotometric determination of some drugs for osteoporosis.," *Chem. Pharm. Bull. (Tokyo)*, vol. 51, no. 12, pp. 1444–1447, 2003.
- [278] M. Koba, K. Koba, and L. Przyborowski, "Application of UV-derivative spectrophotometry for determination of some bisphosphonates drugs in pharmaceutical formulations.," *Acta Pol. Pharm.*, vol. 65, no. 3, pp. 289–94, Jan. 2008.
- [279] J. Gao, Z. Zheng, L. Shi, S.-Q. Wu, H. Sun, and D.-S. Guo, "Strong binding and fluorescence sensing of bisphosphonates by guanidinium-modified calix[5]arene," *Beilstein J. Org. Chem.*, vol. 14, no. 1, pp. 1840–1845, Jul. 2018.
- [280] J. A. Wong, K. W. Renton, J. F. S. Crocker, P. A. O'Regan, and P. D. Acott, "Determination of pamidronate in human whole blood and urine by reversed-phase HPLC with fluorescence detection," *Biomed. Chromatogr.*, vol. 18, no. 2, pp. 98–101, Mar. 2004.
- [281] Z. Xie, Y. Jiang, and D.-Q. Zhang, "Simple analysis of four bisphosphonates simultaneously by reverse phase liquid chromatography using n-amylamine as volatile ion-pairing agent.," *J. Chromatogr. A*, vol. 1104, no. 1–2, pp. 173–8, Feb. 2006.
- [282] N. S. Raghu, "A new analytical method for estimation of zoledronic acid in commercial pharmaceutical injections by ion-exchange (IEC) high performance liquid chromatography," *J. Liq. Chromatogr. Relat. Technol.*, vol. 34, no. 6, pp. 476–489, Mar. 2011.
- [283] D. K. Khajuria and R. Razdan, "Sensitive and Rapid RP-HPLC Quantification of Zoledronic Acid in a Hydroxyapatite-based Nanoparticles," *Indian J. Pharm. Sci.*, vol. 79, no. 4, 2017.
- [284] L. Matuszewski *et al.*, "Determination of pamidronate in bisphosphonate-enriched bone cement by ion-pair HPLC and capillary electrophoresis," *Bull. Vet. Inst. Pulawy*, vol. 57, no. 2, pp. 257–262, 2013.
- [285] B. M. Rao *et al.*, "A validated stability indicating ion-pair RP-LC method for zoledronic acid," *J. Pharm. Biomed. Anal.*, vol. 39, no. 3–4, pp. 781–790, Sep. 2005.
- [286] A. Juillard *et al.*, "Molecular interactions between zoledronic acid and bone: An in vitro Raman microspectroscopic study," *Bone*, vol. 47, no. 5, pp. 895–904, Nov. 2010.
- [287] J. Zirojevic, Z. Jovic, A. Djurdjevic, A. Ciric, and P. Djurdjevic, "Chemometric-assisted determination of some bisphosphonates and their related substances in pharmaceutical forms by ion chromatography with inverse UV detection," *Acta Chromatogr.*, vol. 27, no. 2, pp. 215–237, Jun. 2015.
- [288] R. W. Sparidans, J. den Hartigh, and P. Vermeij, "High-performance ion-exchange chromatography with in-line complexation of bisphosphonates and their quality control in pharmaceutical preparations," *J. Pharm. Biomed. Anal.*, vol. 13, no. 12, pp. 1545–1550, Nov. 1995.
- [289] J. Kuljanin, I. Janković, J. Nedeljković, D. Prstojević, and V. Marinković, "Spectrophotometric determination of alendronate in pharmaceutical formulations via complex formation with Fe(III) ions," *J. Pharm. Biomed. Anal.*, vol. 28, no. 6, pp. 1215–1220, Jun. 2002.
- [290] A. F. Lo Faro *et al.*, "Development and validation of a method using ultra performance liquid chromatography coupled to tandem mass spectrometry for determination of zoledronic acid concentration in human bone," *J. Pharm. Biomed. Anal.*, vol. 162, pp. 286–290, Jan. 2019.
- [291] J. D. Tario, K. Humphrey, A. D. Bantly, K. A. Muirhead, J. S. Moore, and P. K. Wallace, "Optimized Staining and Proliferation Modeling Methods for Cell Division Monitoring using Cell Tracking Dyes," *J. Vis. Exp.*, no. 70, p. e4287, Dec. 2012.
- [292] A. van Tonder, A. M. Joubert, and A. D. Cromarty, "Limitations of the 3-(4,5-dimethylthiazol-2-yl)-2,5-diphenyl-2H-tetrazolium bromide (MTT) assay when compared to three commonly used cell enumeration assays.," *BMC Res. Notes*, vol. 8, p. 47, 2015.

- [293] L. Sinigaglia, M. Varena, and S. Casari, "Pharmacokinetic profile of bisphosphonates in the treatment of metabolic bone disorders," *Clinical Cases in Mineral and Bone Metabolism*, vol. 4, no. 1. CIC Edizioni Internazionali, pp. 30–36, Jan-2007.
- [294] J. E. Dunford *et al.*, "Structure-Activity Relationships for Inhibition of Farnesyl Diphosphate Synthase in Vitro and Inhibition of Bone Resorption in Vivo by Nitrogen-Containing Bisphosphonates," *J. Pharmacol. Exp. Ther.*, vol. 296, no. 2, pp. 235–242, 2001.
- [295] J. Lašovička, M. Rataj, and J. Bartůňková, "Assessment of lymphocyte proliferation for diagnostic purpose: Comparison of CFSE staining, Ki-67 expression and 3H-thymidine incorporation," *Hum. Immunol.*, vol. 77, no. 12, pp. 1215–1222, Dec. 2016.
- [296] M. Roederer, "Interpretation of cellular proliferation data: Avoid the panglossian," *Cytometry Part A*, vol. 79 A, no. 2. Wiley-Blackwell, pp. 95–101, 01-Feb-2011.
- [297] W. Gough *et al.*, "A quantitative, facile, and high-throughput image-based cell migration method is a robust alternative to the scratch assay," *J. Biomol. Screen. Off. J. Soc. Biomol. Screen.*, vol. 16, no. 2, pp. 155–163, Feb. 2011.
- [298] M. Choi and C. Lee, "Immortalization of primary keratinocytes and its application to skin research," *Biomol. Ther.*, vol. 23, no. 5, pp. 391–399, Sep. 2015.
- [299] S. Hong, E. Ergezen, R. Lec, and K. A. Barbee, "Real-time analysis of cell–surface adhesive interactions using thickness shear mode resonator," *Biomaterials*, vol. 27, no. 34, pp. 5813–5820, Dec. 2006.
- [300] A. A. Khalili and M. R. Ahmad, "A Review of Cell Adhesion Studies for Biomedical and Biological Applications.," *Int. J. Mol. Sci.*, vol. 16, no. 8, pp. 18149–84, Aug. 2015.
- [301] M. J. Wheelock and P. J. Jensen, "Regulation of keratinocyte intercellular junction organization and epidermal morphogenesis by E-cadherin," *J. Cell Biol.*, vol. 117, no. 2, pp. 415–425, Apr. 1992.
- [302] D. Lü *et al.*, "β1 integrin signaling in asymmetric migration of keratinocytes under mechanical stretch in a co-cultured wound repair model," *Biomed. Eng. Online*, vol. 15, no. S2, p. 130, Dec. 2016.
- [303] A. Hall, "Rho GTPases and the actin cytoskeleton.," *Science*, vol. 279, no. 5350, pp. 509–14, Jan. 1998.
- [304] J. T. Parsons, K. H. Martin, J. K. Slack, J. M. Taylor, and S. A. Weed, "Focal Adhesion Kinase: A regulator of focal adhesion dynamics and cell movement," *Oncogene*, vol. 19, no. 49. Nature Publishing Group, pp. 5606–5613, 20-Nov-2000.
- [305] J. O'Brien, I. Wilson, T. Orton, and F. Pognan, "Investigation of the Alamar Blue (resazurin) fluorescent dye for the assessment of mammalian cell cytotoxicity," *Eur. J. Biochem.*, vol. 267, no. 17, pp. 5421–5426, Sep. 2000.
- [306] Z. Zhang and B. B. Michniak-Kohn, "Tissue engineered human skin equivalents," *Pharmaceutics*, vol. 4, no. 1. Multidisciplinary Digital Publishing Institute (MDPI), pp. 26–41, 06-Jan-2012.
- [307] S. Vukelic *et al.*, "Farnesyl pyrophosphate inhibits epithelialization and wound healing through the glucocorticoid receptor.," *J. Biol. Chem.*, vol. 285, no. 3, pp. 1980–8, Jan. 2010.
- [308] A. J. Sloan *et al.*, "A novel ex vivo culture model for inflammatory bone destruction," *J. Dent. Res.*, vol. 92, no. 8, pp. 728–734, Aug. 2013.
- [309] J. L. Roberts, J. Y. Maillard, R. J. Waddington, S. P. Denyer, C. D. Lynch, and A. J. Sloan, "Development of an ex vivo coculture system to model pulpal infection by streptococcus anginosus group bacteria," *J. Endod.*, vol. 39, no. 1, pp. 49–56, Jan. 2013.
- [310] G. Muralithran and S. Ramesh, "Effects of sintering temperature on the properties of hydroxyapatite," *Ceram. Int.*, vol. 26, no. 2, pp. 221–230, 2000.
- [311] A. Tampieri, G. Celotti, F. Szontagh, and E. Landi, "Sintering and characterization of HA and TCP bioceramics with control of their strength and phase purity," *J. Mater.*

- Sci. Mater. Med.*, vol. 8, no. 1, pp. 29–37, 1997.
- [312] P. Ducheyne, S. Radin, and L. King, “THE EFFECT OF CALCIUM-PHOSPHATE CERAMIC COMPOSITION AND STRUCTURE ON INVITRO BEHAVIOR .1. DISSOLUTION,” *J. Biomed. Mater. Res.*, vol. 27, no. 1, pp. 25–34, Jan. 1993.
- [313] B. Cem, “Biomedical Optics and Lasers,” in *A Roadmap of Biomedical Engineers and Milestones*, S. Kara, Ed. InTech, 2012.
- [314] M. Vukomanović *et al.*, “Hydroxyapatite/platinum bio-photocatalyst: A biomaterial approach to self-cleaning,” *J. Mater. Chem.*, vol. 22, no. 21, pp. 10571–10580, May 2012.
- [315] C. Dawes, “What is the critical pH and why does a tooth dissolve in acid?,” *J. Can. Dent. Assoc.*, vol. 69, no. 11, pp. 722–724, 2003.
- [316] R. G. G. Russell, R. C. Mühlbauer, S. Bisaz, D. A. Williams, and H. Fleisch, “The influence of pyrophosphate, condensed phosphates, phosphonates and other phosphate compounds on the dissolution of hydroxyapatite in vitro and on bone resorption induced by parathyroid hormone in tissue culture and in thyroparathyroidectomised rats,” *Calcif. Tissue Res.*, vol. 6, no. 1, pp. 183–196, Dec. 1970.
- [317] P. A. Gerakines, W. A. Schutte, J. M. Greenberg, and E. F. Van Dishoeck, “The infrared band strengths of H₂O, CO and CO₂ in laboratory simulations of astrophysical ice mixtures,” 1995.
- [318] J. L. Paris, J. Román, M. Manzano, M. V. Cabañas, and M. Vallet-Regí, “Tuning dual-drug release from composite scaffolds for bone regeneration,” *Int. J. Pharm.*, vol. 486, no. 1–2, pp. 30–37, May 2015.
- [319] Y. Han *et al.*, “Different Inhibitory Effect and Mechanism of Hydroxyapatite Nanoparticles on Normal Cells and Cancer Cells In Vitro and In Vivo,” *Sci. Rep.*, vol. 4, no. 1, p. 7134, May 2015.
- [320] S. Breslin and L. O’Driscoll, “The relevance of using 3D cell cultures, in addition to 2D monolayer cultures, when evaluating breast cancer drug sensitivity and resistance.,” *Oncotarget*, vol. 7, no. 29, pp. 45745–45756, Jul. 2016.
- [321] C. Castells-Sala, J. Martorell, and M. Balcells, “A human plasma derived supplement preserves function of human vascular cells in absence of fetal bovine serum.,” *Cell Biosci.*, vol. 7, p. 41, 2017.
- [322] A. J. Sloan, J. Colombo, J. Roberts, R. J. Waddington, and W. N. Ayre, “Tissue culture models and approaches for dental tissue regeneration,” in *Tissue Engineering and Regeneration in Dentistry*, Chichester, UK: John Wiley & Sons, Ltd, 2016, pp. 96–109.
- [323] F. E. Grubbs and G. Beck, “Extension of Sample Sizes and Percentage Points for Significance Tests of Outlying Observations,” *Technometrics*, vol. 14, no. 4, pp. 847–854, Nov. 1972.